Universitat Autònoma de Barcelona

Nanovesicle-bioactive conjugates to be used as nanomedicines, prepared by a one-step scalable method using CO_2-expanded solvents

Ingrid Cabrera Puig

Tesi doctoral

Programa de Doctorat de Ciència dels Materials

Directores

Nora Ventosa Rull

Jaume Veciana Miró

Tutora

Adelina Vallribera Massó

Departament de Química

Facultat de Ciències

2013

Memòria presentada per aspirar al Grau de doctor per:

Ingrid Cabrera Puig

Vist i plau:

Nora Ventosa
(Director 1)

Jaume Veciana
(Director 2)

Adelina Vallribera
(Tutora)

a Bellaterra, 26 de Octubre de 2013

Agradecimientos

Quiero agradecer primeramente al Prof. Jaume Veciana y a la Dr. Nora Ventosa por la oportunidad para realizar esta tesis doctoral en el grupo NMMO. También al CSIC por el apoyo económico a través de la beca predoctoral JAE.

A todos los grupos de investigación que forman parte del proyecto NanoFabry y a los miembros del CIGB por la excelente colaboración mantenida durante este tiempo. A Sandrine Sagan por la oportunidad de hacer la estancia breve en su Laboratoire des biomolecules UMR7-203.

A todos mis compañeros de grupo NANOMOL, es especial a las supercríticas por el buen ambiente de trabajo y por todo el apoyo.

Quiero agradecer en general a todas las personas que durante estos años de doctorado me han ayudado, apoyado y hecho sentir como en casa.

CONTENTS

Introduction

The application of innovative nanotechnologies to medicine has shown a great potential to significantly benefit clinical practice, offering solutions to many of the current limitations in diagnosis, treatment and management of human diseases[1-5]. Among the various approaches for exploiting developments in nanotechnology for biomedical applications, drug delivery systems (DDS) have already had an enormous impact on medical technology, improving the performance of many existing drugs and enabling the use of entirely new therapies[6-9]. The fact that DDSs can protect sensitive biomolecules, such as enzymes and proteins, from degradation and the *in vivo* attack of the immune system providing longer blood circulation times, have been used to improve the effectiveness and delivery of these drugs[10-12]. Although nanoparticulate carriers can be made from a variety of organic and inorganic materials, vesicle and polymer based-nanocarriers are perhaps the most widely used for drug delivery purposes[13-15]. Particularly vesicles have served as convenient delivery vehicles for biologically active compounds because they are non-toxic, biodegradable and non immunogenic[16-19]. Contrary to products where the active substance is in simple solution, the pharmacological properties of vesicle-based delivery systems strongly depend on the structural characteristics of the conjugates[20]. Indeed, a high degree of structural homogeneity regarding size, morphology and lipid organization in the membrane is crucial, for their optimum performance as functional entities[21,22] (Figure 1).

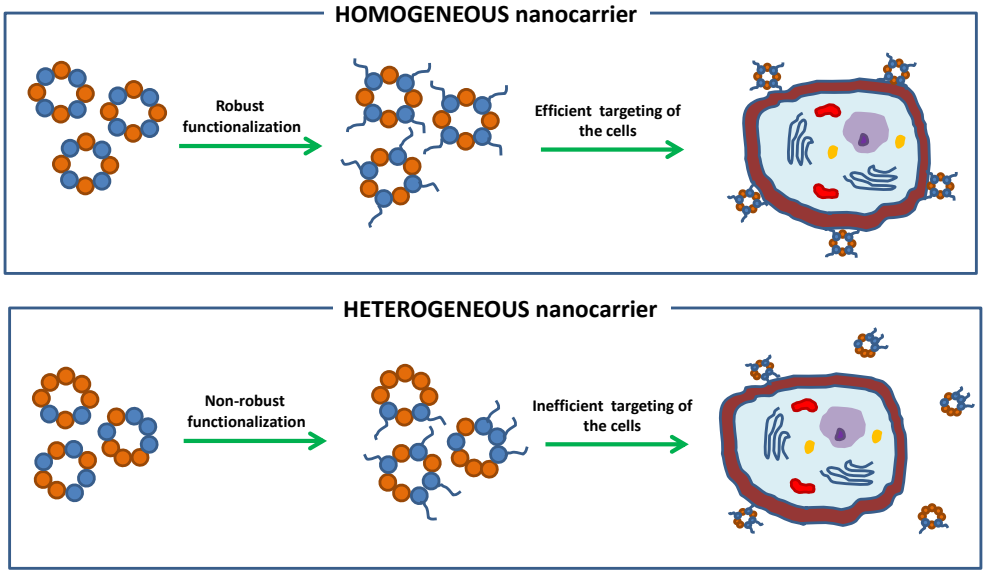

Figure 1. Influence of the structural homogeneity in the performance of the vesicles as DDS.

These nanocarriers are commonly prepared following a "bottom-up" strategy where a nanomaterial is built from their constituent units (macromolecules, molecules, atoms) by synthetic or self-assembly procedures. The potential of "bottom-up" approach is enormous regarding material engineering. For instance, with a well-controlled "bottom-up" process, the design and control of particle size, morphology and internal structure, should be possible. Conventional methodologies to produce nanocarriers, such as vesicles, usually present difficulties in controlling the self-assembling of the molecules constituting the system, leading to materials with high structural heterogeneity[23,24]. Therefore additional operations are needed in order to achieve the desired structures. In order to be able to commercially exploit the enormous potential of these DDS as nanomedicines, it is necessary the development of new, efficient and environmentally respectful methodologies that allow the manufacturing of these materials with control nanostructure, and that are amenable to be scalable.

Compressed fluid (CFs)-based methodologies have been gaining ground during the last 20 years as promising alternative to conventional methodologies for the preparation of nanostructured materials[25-29]. CFs are defined as a substance that at normal conditions of pressure (P) and temperature (T) exist as gases but with increased P can be converted into liquids or supercritical fluids. The supercritical region is achieved when the substance is exposed to conditions above its critical pressure (P_c) and temperature (T_c). The most important feature, within the supercritical region, is that there is no phase boundary between the gas and liquid phases. The consequence is that supercritical fluids have properties which are "hybrids" of those normally associated with liquids and gases and which are continuously adjustable from gas to liquid with small pressure and temperature variations (Figure 2). Thus, the viscosities and diffusivities are similar to those of the gas phase while the density is closer to that of a liquid one. The possibility of obtaining such special behavior at conditions below or near the critical point (subcritical region), allow working at mild conditions of T and P, reducing the cost related to the use of elevated pressures and decreasing the risk of damaging the structure and properties of the molecules to be processed.

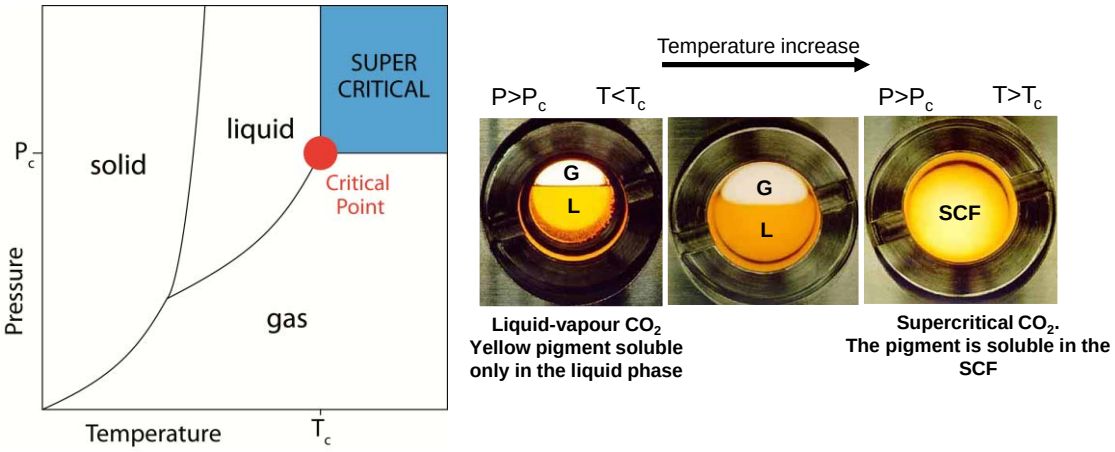

Figure 2. Phase diagram of a compressed fluid

The solvent power of a CF, either in the liquid or supercritical state, is proportional to its density, which is extremely responsive to changes in temperature and pressure around the critical point. Solvation power can therefore be tuned by pressure changes, which propagates much more quickly than temperature and composition solvent changes. This can offer a better control over the morphology of the materials on the microscopic scale than most of conventional processing techniques. This combination of properties makes compressed or supercritical fluids particularly attractive and has led to the current scientific and industrial interests on them for material processing[30,31]. The most widely used dense gas is carbon dioxide since it is non-flammable, non-toxic, non-corrosive, inexpensive, non-polluting and has easily accessible critical parameters of 31.1°C and 73.8 bar[32]. The solvent can be easily recovered after processing by simply returning to atmospheric pressure. This is why it has gained great attention as a "green substitute" to organic solvents in the preparation of lipid-based nanocarriers such as liposomes. Several methodologies involving compressed CO_2 have been under intensive research for several years to improve the production of liposomal formulations, especially to reduce the organic residual solvents, which is an essential issue for all the conventional production methods[33-35]. CF-based procedures are nowadays a development platform for producing vesicle–based DDS[36].

Despite all these advantages, the way from bench to pharmaceutical industry has not been as fast as expected and the number of industrial successes is to date still very low. This could be attributed, among other reasons, to the stringent regulatory requirements that pharmaceutical companies have to satisfy for changing their production procedures. Apart from regulatory requirements and related to the fact that the field is still relatively

young, another reasons of the low translation are the few examples of biomolecule-vesicle conjugates prepared with these technologies and the limited studies on their reproducibility and scalability. There are also scarce studies on the preparation route impact on the structure and activity of the nanoconjugates as well as limited examples of Nanomedicine candidates presently tested on preclinical cascades.

This is why a continuous effort toward the application and acceptance of these novel technologies is been carried out by the compressed fluid scientific community. The present Thesis is part of this effort.

In order to demonstrate the enormous potential of CFs methodologies in the drug delivery field the main objectives of this PhD Thesis were:

- Development of new methodologies based on the DELOS-SUP process for the direct, robust and scalable encapsulation of biomolecules in cholesterol-rich vesicles.
- Development of reproducible and scalable methodologies in order to functionalize those vesicles with targeting/protective units enabling greater selectivity of the therapeutic targets and therefore more effective treatments.
- Use of the biomolecules-vesicles conjugates prepared by DELOS-SUSP in the treatment of different diseases.

References

1 Malam, Y., Loizidou, M. & Seifalian, A. M. Liposomes and nanoparticles: nanosized vehicles for drug delivery in cancer. *Trends Pharmacol. Sci.* **30**, 592-599 (2009).

2 Hubbell, J. A. Enhancing drug function. *Science* **300**, 595-596 (2003).

3 Zhang, L. & Webster, T. J. Nanotechnology and nanomaterials: Promises for improved tissue regeneration. *Nano Today* **4**, 66-80 (2009).

4 Yokoyama, M. Drug targeting with nano-sized carrier systems. *Journal of Artificial Organs* **8**, 77-84 (2005).

5 Farokhzad, O. C. & Langer, R. Impact of Nanotechnology on Drug Delivery. *ACS Nano* **3**, 16-20, doi:10.1021/nn900002m (2009).

6 LaVan, D. A., McGuire, T. & Langer, R. Small-scale systems for in vivo drug delivery. *Nature Biotechnology* **21**, 1184-1191 (2003).

7 Ganta, S., Devalapally, H., Shahiwala, A. & Amiji, M. A review of stimuli-responsive nanocarriers for drug and gene delivery. *Journal of Controlled Release* **126**, 187-204 (2008).

8 Davis, M. E., Chen, Z. G. & Shin, D. M. Nanoparticle therapeutics: an emerging treatment modality for cancer. *Nature reviews. Drug discovery* **7**, 771-782 (2008).

9 Lim, S. B., Banerjee, A. & Önyüksel, H. Improvement of drug safety by the use of lipid-based nanocarriers. *Journal of Controlled Release* **163**, 34-45 (2012).

10 Lee, K. Y. & Yuk, S. H. Polymeric protein delivery systems. *Progress in Polymer Science (Oxford)* **32**, 669-697 (2007).

11 Jiang, M., Wu, Y., He, Y. & Nie, J. Micelles formed by self-assembly of hyperbranched poly[(amine-ester)-co-(D,L-lactide)] (HPAE-co-PLA) copolymers for protein drug delivery. *Polymer International* **58**, 31-39 (2009).

12 Dai, C., Wang, B., Zhao, H., Li, B. & Wang, J. Preparation and characterization of liposomes-in-alginate (LIA) for protein delivery system. *Colloids and Surfaces B: Biointerfaces* **47**, 205-210 (2006).

13 McAllister, K. *et al.* Polymeric nanogels produced via inverse microemulsion polymerization as potential gene and antisense delivery agents. *Journal of the American Chemical Society* **124**, 15198-15207 (2002).

14 Howse, J. R. *et al.* Templated formation of giant polymer vesicles with controlled size distributions. *Nature Materials* **8**, 507-511 (2009).

15 Sawant, R. R. & Torchilin, V. P. Liposomes as 'smart' pharmaceutical nanocarriers. *Soft Matter* **6**, 4026, (2010).

16 Sawant, R. R. & Torchilin, V. P. Challenges in development of targeted liposomal therapeutics. *AAPS Journal* **14**, 303-315 (2012).

17 Koudelka, Š. & Turánek, J. Liposomal paclitaxel formulations. *Journal of Controlled Release* **163**, 322-334 (2012).

18 Li, C. *et al.* Encapsulation of mitoxantrone into pegylated SUVs enhances its antineoplastic efficacy. *European Journal of Pharmaceutics and Biopharmaceutics* **70**, 657-665 (2008).

19 Chopra, S., Venkatesan, N. & Betageri, G. V. Liposomes as nanocarriers for anti-HIV therapy. *Drug Delivery and Translational Research* **3**, 471-478 (2013).

20 Reflection paper on the data requirements for intraveneous liposomal products developed with reference to an innovation liposomal product. *European MedicinesAgency,*

http://www.ema.europa.eu/ema/index.jsp?curl=pages/regulation/general/general_content_000564.jsp&mid=WC0b01ac05806403e0 (2013).

21 Davis, M. E., Chen, Z. & Shin, D. M. Nanoparticle therapeutics: An emerging treatment modality for cancer. *Nature Reviews Drug Discovery* **7**, 771-782 (2008).

22 Ventosa, N. Materiales moleculares nanoestructurados en el desarrollo de nuevos fármacos. *SEBBM* **168** (2011).

23 Liang, M. T., Davies, N. M. & Toth, I. Encapsulation of lipopeptides within liposomes: Effect of number of lipid chains, chain length and method of liposome preparation. *International Journal of Pharmaceutics* **301**, 247-254 (2005).

24 Cortesi, R. *et al.* Preparation of liposomes by reverse-phase evaporation using alternative organic solvents. *J. Microencapsul.* **16**, 251-256 (1999).

25 Jennings, J. *et al.* One-pot synthesis of block copolymers in supercritical carbon dioxide: A simple versatile route to nanostructured microparticles. *Journal of the American Chemical Society* **134**, 4772-4781 (2012).

26 Pasquali, I. & Bettini, R. Are pharmaceutics really going supercritical? *International Journal of Pharmaceutics* **364**, 176-187 (2008).

27 Reverchon, E. & Adami, R. Nanomaterials and supercritical fluids. *The Journal of Supercritical Fluids* **37**, 1-22 (2006).

28 Eckert, C. A., Knutson, B. L. & Debenedetti, P. G. Supercritical fluids as solvents for chemical and materials processing. *Nature* **383**, 313-318 (1996).

29 Elizondo, E., Veciana, J. & Ventosa, N. Nanostructuring molecular materials as particles and vesicles for drug delivery, using compressed and supercritical fluids. *Nanomedicine* **7**, 1391-1408 (2012).

30 Cansell, F. & Aymonier, C. Design of functional nanostructured materials using supercritical fluids. *The Journal of Supercritical Fluids* **47**, 508-516, (2009).

31 Reverchon, E., Adami, R., Cardea, S. & Della Porta, G. Supercritical fluids processing of polymers for pharmaceutical and medical applications. *J. Supercrit. Fluids* **47**, 484-492 (2009).

32 Perrut, M. & Clavier, J. Y. Supercritical fluid formulation: Process choice and scale-up. *Ind. Eng. Chem. Res.* **42**, 6375-6383, doi:10.1021/ie030144x (2003).

33 Otake, K. *et al.* Preparation of liposomes using an improved supercritical reverse phase evaporation method. *Langmuir* **22**, 2543-2550 (2006).

34 Meure, L. A., Knott, R., Foster, N. R. & Dehghani, F. The depressurization of an expanded solution into aqueous media for the bulk production of liposomes. *Langmuir* **25**, 326-337 (2009).

35 Lesoin, L., Crampon, C., Boutin, O. & Badens, E. Development of a continuous dense gas process for the production of liposomes. *J. Supercrit. Fluids* **60**, 51-62 (2011).

36 Beh, C. C., Mammucari, R. & Foster, N. R. Lipids-based drug carrier systems by dense gas technology: A review. *Chemical Engineering Journal* **188**, 1-14, (2012).

Chapter 1. Nanovesicle-bioactive conjugates prepared by a one-step procedure using CO_2-expanded solvents

1.1 Introduction

1.1.1Vesicles as promising nanocarriers for drug delivery

In the past two decades, several therapeutics based on drug delivery systems have been successfully introduced for the treatment and diagnosis of human diseases. Many problems exhibited by free active pharmaceutical ingredients (APIs), such as poor solubility, toxicity, rapid *in vivo* breakdown, unfavorable pharmacokinetics, poor biodistribution and lack of selectivity for target tissues, can be ameliorated by the use of DDS[1]. Although a whole range of delivery agents exist nowadays, the main components typically include a nanocarrier, a targeting moiety conjugated to the nanocarrier, and a cargo, such as the desired API[2] (Figure 1.1).

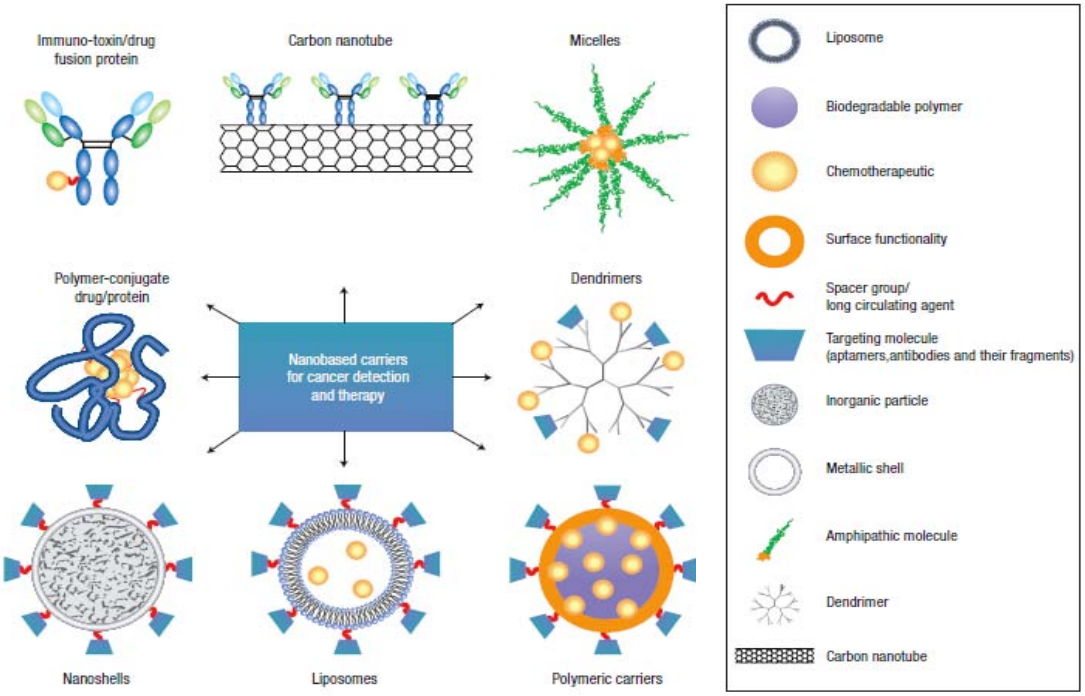

Figure 1.1.. Examples of nanocarriers for drug delivery and diagnosis purposes. *Adapted from ref. 2*.

Nanocarriers can be either unimolecular (i.e: dendrimers, carbon nanotubes, polymer-congugate drug/protein, etc) or multimolecular carries, based on molecular self-assemblies (micelles, nanoshells, vesicles, etc). Their major constituents are either lipids or polymers and they all have in common that the final arrangement is governed by the nature of the initial components and the methodology used in their preparation[3]. Some

of the advantages that APIs conjugation to nanocarriers can offer over the free drug is the protection from premature degradation, a higher stability, an enhance permeability through biological membranes, a higher control of the pharmacokinetics, a better drug tissue distribution profile, and an improvement of intracellular penetration[4,5]

Liposomes, and in general vesicles, are undoubtedly one of the most promising nanocarriers in nanomedicine. They are particularly important in the pharmaceutical field due to their great versatility respect to size, composition, surface characteristics, biocompatibility, biodegradability, low toxicity, capacity for entrapping and/or integrating hydrophilic and/or hydrophobic molecules and possibility of surface functionalization[6] (Figure 1.2).Vesicles are spherical objects enclosing a liquid compartment, with a diameter ranging from 20 nm to a few thousand of nanometers, separated from its surroundings by at least one thin membrane consisting of a bilayer (unilamellar) or several layers (multilamellar) of amphiphilic molecules. Sometimes the terms liposome and vesicle are used interchangeably, alhtough a liposome is a type of vesicle composed mainly by phospholipids while vesicles can be formed also by non-lipid building blocks, such as block co-polymers or surfactants[7].

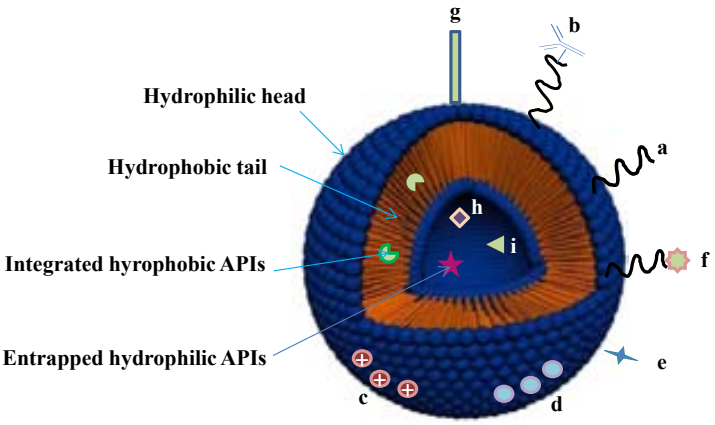

Figure 1.2. Schematic representation of a vesicle. Lipid-soluble drugs can be integrated into the lipid bilayer while hydrophilic drugs can be entrapped in the aqueous lumen. The outer surface of vesicles can be modified in different ways. Some of these modifications include the attachment of a protective polymer (**a**) or a targeting ligand, such as an antibody (**b**); the incorporation of positively charged lipids (**c**); the incorporation of stimuli-sensitive lipids (d); the attachment of stimuli-sensitive polymer (e); the attachment of peptides (**f**) and the incorporation of viral components (**g**). In addition to a drug, vesicles can be loaded with magnetic particles (**h**) for magnetic targeting and/or with colloidal gold or silver particles (**i**) for improving images obtained by electron microscopy. *Adapted from ref. 6*

The building blocks of vesicles are normally amphiphilic molecules which have a hydrophobic tail and a hydrophilic or polar head. In the presence of water, this dual

hydrophilic-hydrophobic character promotes their association through weak, non-covalent interactions to form closed bilayers. Depending on the number of bilayers formed (lamellarity) and the size of the vesicles, they are broadly classified into small unilamellar vesicles (SUVs, size≤ 200 nm and single bilayer), large unilamellar vesicles (LUVs, size ranging from 200-800 nm and single bilayer), multilamellar vesicles (MLVs, size from 500-5000 nm consisting of several concentric bilayers) and multivesicular vesicles (MVVs, composed by several small vesicles entrapped into larger ones)[6] (Figure 1.3).

Size and lamellarity are important structural parameters that need to be controlled, since they are crucial factors affecting the properties and performance of vesicles, for instance, as pharmaceutical carriers[8].

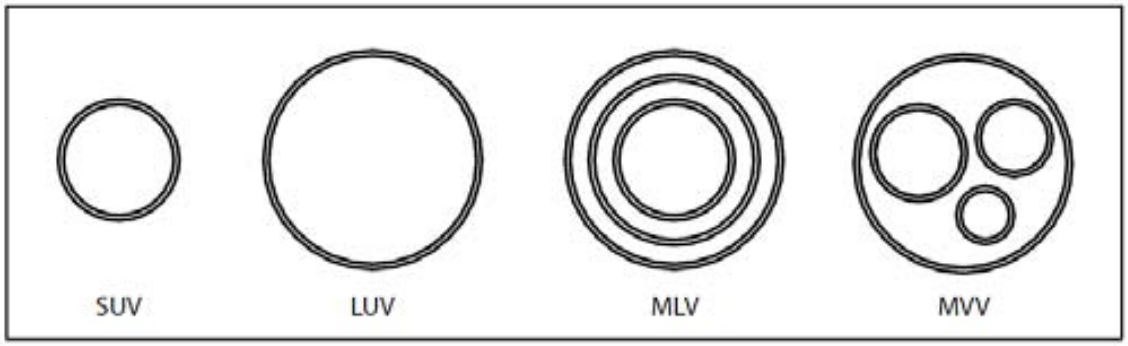

Figure 1.3. Classification of vesicles regarding size and lamellarity.

The diversity in the design of the composition, structure, and size of vesicles makes possible to tailor vesicle-based systems for different applications in drug delivery and for diagnosis purpose (Figure 1.2). Vesicle membranes can be modified with different targeting or protective units, that promote specific and increased accumulation of the drug or the bioactive molecule in the target cells. For example the incorporation of polyethyleneglycol (PEG) units to the bilayer membrane results in an increased blood circulation half-life by sterically stabilizing the liposomes against their clearance by the mononuclear phagocytic system (MPS)[9,10]. The membrane functionalization with targeting ligands (e.g. peptides) is envisioned to facilitate not only the targeting to specific cells that overexpress certain antigens but also the drug retention at the site of action[11]. More recent trends in liposomal technology in nanomedicine include designing 'smart' liposomal carriers for site-specific triggered release of their contents. These so-called 'smart' stimuli-sensitive liposomes will go through structural changes in response

to certain internal or external stimuli, such as pH, temperature or redox potential changes, or the presence of an external magnetic field[12]. The great potential and felicitous properties of liposomes has prompted their use in the treatment of some major health threats for humans including cancer, infections, metabolic and autoimmune diseases, and has even led to first marketed products[13]. For example liposomal formulations of anticancer drugs have already been approved for human use. This is the case of Doxil®, a liposomal formulation of doxorubicin, which is anthracycline drug, used to treat cancer in AIDS-related Karposi sarcoma, multiple myeloma and ovarian cancer. Its advantages over the free doxorubicin are a greater efficacy and lower cardio toxicity[14].

Important pharmacological specifications like stability, loading capability and leakage kinetics of entrapped substances, are determined by the structural characteristics (e.g. size, morphology, supramolecular organization, structural homogeneity) of these nanocarriers[4]. This is why the control of their structural features is a very important issue for drug delivery purposes. For instance small unilamellar vesicles have attracted great attention in the drug delivery field since these vesicles are large enough to avoid the first-pass elimination through the kidneys but sufficiently small to present a minimal uptake by the MPS, facilitating their longer circulation lifetime in the body and hence a higher possibility to reach the target cells[15]. Moreover, due to their nano-scale size SUVs can accumulate within tumours through the so-called enhanced permeability and retention (EPR) effect and thereby be applied in cancer therapy[1,16] (Figure 1.4). This latter effect is produce by the anomalous enhancement of vascularisation around the tumours and the weakening of vascular endothelial cells.

Current methodologies for vesicle formation such as the lipid thin-film hydration[17,18] or the reverse-phase evaporation[19,20], render systems with low structural homogeinity. For instance, the thin-film hydration of vesicle-bioactive conjugates, yields vesicles with large heterogeneity in terms of sizes and lamellarity. For this reason modifications after production are required in order to obtain a vesicle population with specific characteristics and properties. When preparing SUVs using these methodologies, post-formation steps such as sonication[21,22], extrusion[23,24] and freeze-thawing[25] are necessary for their size reduction and homogenization (Figure 1.5).

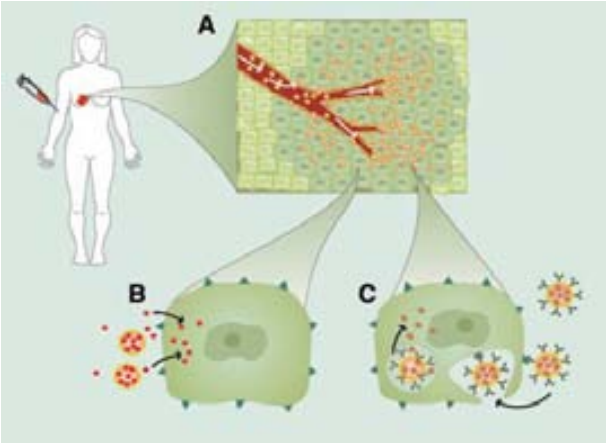

Figure 1.4. A schematic diagram depicting the passive or ligand-targeted accumulation of liposomal DDS in breast cancer tumors through the enhance permeability (EPR) effect. (**A**) Liposomes containing an anticancer drug extravasate from the blood through gaps in vascular endothelial cells and accumulate in tumor tissue (dark green), but not into normal tissues (light green). (**B**) Drug is released from the liposomes in the vicinity of the tumor cells and taken up into the cells. (**C**) Ligand-targeted liposomes containing anticancer drugs, or nucleic acid–based therapeutics, such as plasmid DNA or antisense oligonucleotides, bind to cell surface receptors (dark green triangles), which triggers the internalization of the DDS. *Adapted from ref 1*

The use of large amounts of organic solvents, which are toxic in many cases, and particularly its incomplete post processing removal are other major issues not only at lab scale but also at large scale production[26]. In addition these multi-step and time-consuming procedures have a high risk of damaging the functionality of bioactive molecules and of oxidizing vesicle membrane components, such as phospholipids. All these drawbacks are particularly relevant for the preparation of colloidal bioconjugates with expensive and/or fragile active biomolecules such as proteins, peptides, enzymes or hormones. Thus, it is crucial to develop simple and mild processes for controlling the structure at the micro-, nano- and supramolecular levels that are also amenable to be scalable[27].

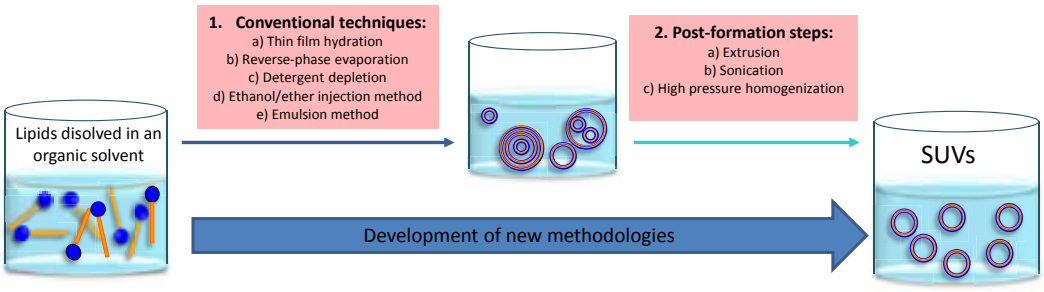

Figure 1.5. Conventional methodologies for the preparation of vesicles-bioactive conjugates and the most common post-formation steps for their homogenization.

1.1.2 Compressed fluids (CFs)-based technologies to produce vesicles

Compressed fluid-based methodologies, also named as dense gas technologies, are attracting an increasing interest for the production of lipid-based drug carrier systems with structural characteristics not reachable by already existing procedures using liquid organic solvents[26]. These techniques have recently been investigated to improve the processing of vesicles because they provide the potential to reduce the amount of organic solvent required by conventional methods and allow a better control over the final vesicle structural characteristics. Moreover compressed fluid processing offers sterile operating conditions and the potential for one-step production processes, which is convenient in transferring the technology to larger scale operations[28].

Several CFs methodologies have been used to generate vesicles, some of them already existed and others were developed for this specific application. Most of the methods involve a mixture between the compressed CO_2, the vesicle membrane constituents and an organic solvent for producing the vesicles upon contact with an aqueous phase. However, changes in the experimental procedures and equipments result in vesicular systems with differentiated characteristics. The processes can also be distinguished by the latter hydration step that can occur either during the pressurization or the depressurization step. Depending on the role of the compressed CO_2 used in each method, they can be classified as: i) Process involving the use of CO_2 as a solvent (e.g. *Supercritical Liposome Method and Rapid Expansion of Supercritical Solutions*), ii) Processes involving the use of CO_2 as an anti-solvent (e.g. *Gas Antisolvent Precipitation and Aerosol Solvent Extraction System*) and iii) Processes involving the use of CO_2 as a co-solvent or a processing aid (e.g. *Depressurization of an Expanded Liquid Organic Solution-Suspension and Supercritical Reverse Phase Evaporation*). Model hydrophilic and hydrophobic compounds, such as fluorescent dyes, sugars and cholesterol, have been encapsulated into vesicles using these methodologies whereas biomolecules like proteins, anticancer drugs and antibiotic, have been integrated in less extent[28].

Compressed fluid technology is a developing platform for producing lipid-based drug carrier systems that can address most of the limitations of conventional methods. This is reflected in the increasing research activity related to the production of drug carrier systems by CFs technology in the last years. Major advantages of the CFs technology are that sterile and stable liposomal formulations can be produced with minimum amounts of organic solvents. However, some problems related with the elevated

pressures and temperatures required during the processing are still a drawback for some of the methods described above.

1.1.3 DELOS-SUSP method for the preparation of cholesterol-rich vesicles

In the year 2000 the NANOMOL group developed a new procedure based on the use of compressed CO_2 called DELOS (Depressurization of an Expanded Organic Solution) for the production of micron-sized and submicron-sized crystalline particles from an organic solution. As novelty the process used the CO_2 as co-solvent being completely miscible at a given pressure and temperature with a specific solution of an organic solvent containing the solute to be crystallized[29]. In order to take full advantage of compressed fluid processing without using severe working conditions a novel and improved procedure based on DELOS process was developed latter on. This method, named as DELOS-SUSP (Depressurization of an Expanded Organic Solution-Suspension), enabled the preparation of rich-cholesterol vesicles[30]. The process uses milder conditions of pressure (< 10 MPa) and temperature (< 308 K) than the previously described methodologies based on CFs, allowing the processing of heat labile compounds and reducing the investment cost of a high pressure plant when the process is scale-up. Using this procedure, homogeneous nanovesicles composed of cholesterol and the cationic surfactant CTAB, in a molar ratio 1:1, were prepared by depressurizing a volumetric expanded organic solution containing the cholesterol over a flow of an aqueous solution containing the CTAB surfactant (Figure 1.6).

During the depressurization step, the expanded organic solution experiences a large, abrupt and extremely homogenous temperature decrease produced by the CO_2 evaporation from the expanded solution. This is probably the reason that explains the obtaining of homogenous vesicles regarding size, lamellarity and morphology compared with the same system but prepared by a conventional mixing method (Figure 1.7).

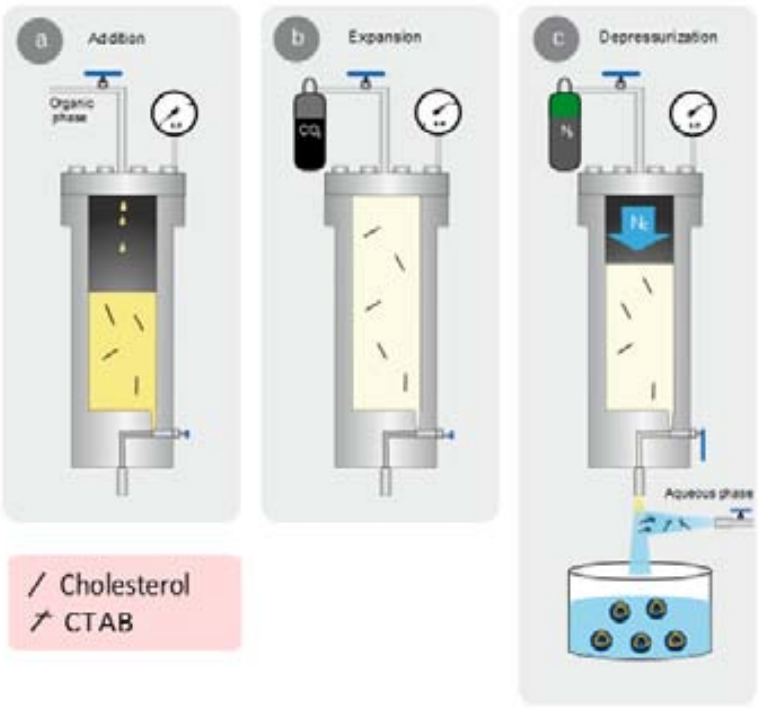

Figure 1.6. Schematic representation of the DELOS-SUSP method for the preparation of vesicles composed of cholesterol and CTAB. The procedure includes the loading stage (a) of an organic solution containing cholesterol into an autoclave at a working temperature (T_w) and atmospheric pressure; the stage of theaddition of CO_2 (b) to produce a CO_2-expanded solution, at a given X_{CO2}, working pressure (P_w) and T_w, where the cholesterol remains dissolved and finally, the depressurization stage (c) of the expanded solution over an aqueous solution containing the cationic surfactant CTAB.

In order to prepare any vesicular system using DELOS-SUSP is necessary that the lipids forming the membrane are completely soluble in the CO_2-expanded organic solvent, presenting one phase at the working conditions of pressure, P_w, temperature, T_w and CO_2 molar fraction, X_2. Therefore for the preparation of rich-cholesterol vesicles by DELOS-SUSP method is always necessary to analyze the solubility behavior of the used sterol in CO_2-expanded solvents, by means of a detailed phase diagram study, like the one showed in Figure 1.8.

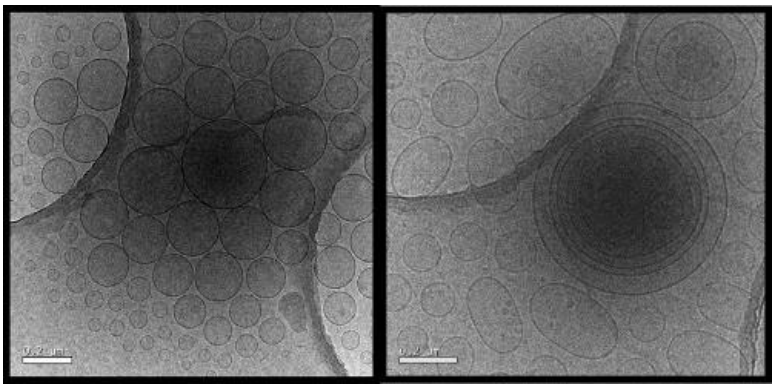

Figure 1.7. Cryo-TEM micrograph images of cholesterol:CTAB (1:1 mol:mol) vesicles obtained through the DELOS-SUSP method (left) and the conventional mixing method (right). *Adapted from ref. 30*

Figure 1.8 shows the solubility curve of cholesterol in CO_2-expanded ethanol. A co-solvent behavior of CO_2 is observed until X_i=0.76, which means that below this molar fraction one single phase is obtained when the CO_2 is added over a saturated solution of cholesterol in pure ethanol. This also means that a DELOS-SUSP process can only be applied for preparing cholesterol-CTAB vesicles in the range of molar fractions of CO_2 between 0-0.76.

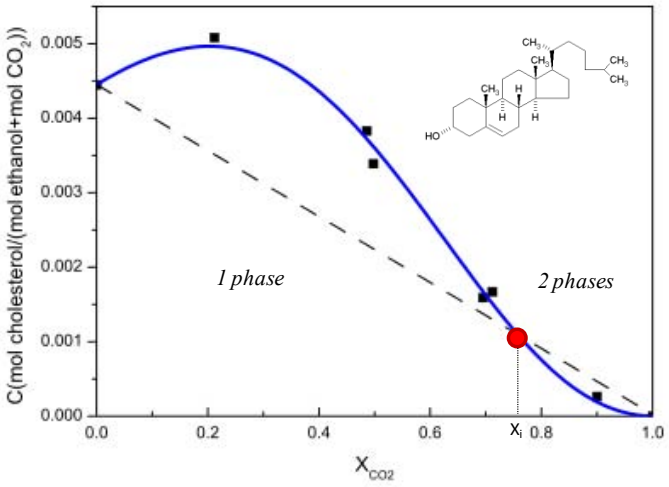

Figure 1.8. Solubility curve of cholesterol in ethanol/CO_2 at 10 MPa and 308 K (blue curve). The dashed line represents the solubility variation of a three component system, in which no interaction among the components exist, in an ideal process. X_i is the intersection point between the ideal solution line and de real solubility curve. *Adapted from ref. 35*

An important prerequisite for the effective use of liposomes as a drug carrier is to control their stability, which can be defined as the extent to which the carrier retains its drug contents either *in vitro* or *in vivo* studies. One of the major disadvantages when using classical liposomes based on phospholipids, is the leakage of the encapsulated

drug during their storage. One variant that can enhance the retention of drugs and promote the stability of liposomes is the presence of cholesterol in the formulation[7]. Another variant is the preparation of liposomes from non-phospholipid amphiphiles, such as surfactants[31] or polymers[32]. This kind of vesicular formulations show low passive leakage in comparison to liposomal systems based only on phospholipids and therefore a higher retention of the encapsulated materials, as for example therapeutically active molecules. Cano et al. used DELOS-SUSP for the preparation of positively charged vesicles composed by cholesterol and the cationic surfactant hexadecyltrimethylammonium bromide (CTAB). More recently nanoscopic vesicles, composed by different sterols and other quaternary ammonium surfactants have been also successfully prepared. This is why it was decided to name this kind of formulations as "quatsomes®".

Quatsomes are stable for periods as long as several years, their morphology do not change upon rising the temperature or by dilution and they show a great homogeneity regarding size and morphology. Studies at molecular level of the self-assembling of cholesterol and CTAB molecule in aqueous medium showed that a pure vesicular phase is only formed at equimolar ratios of both components. Moreover molecular dynamic (MD) simulations revealed that the cholesterol and the CTAB self-assemble in a unique bimolecular synthon that can be considered as a single entity which further self-assembles in particularly stable vesicles (Figure 1.9). Moreover, MD simulations have provided a theoretical support to justify the experimental high thermal stability and the exceptional morphological properties attributed to cholesterol/CTAB vesicles at 1:1 molar ratio[33].

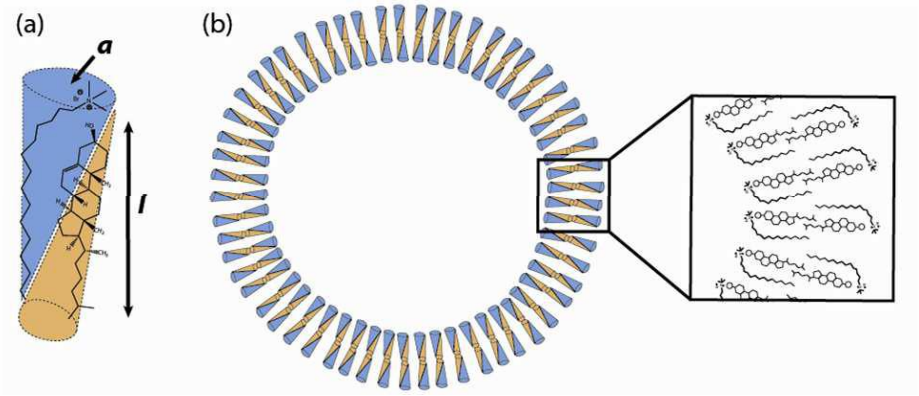

Figure 1.9. Schematic illustration of the formation of (a) the cholesterol/CTAB bimolecular amphiphile and (b) their self-assembling into bilayer vesicles based on the packing parameter concept. *Adapted from ref. 33.*

A confocal fluorescence microscopy-based assay was used to study the influence of the preparation route on the supramolecular organization of lipids forming the membrane in quatsomes[34]. The results revealed that a more homogeneous arrangement of lipids in the membranes was found when DELOS-SUSP methodology was used to prepare vesicles composed of cholesterol and CTAB. The authors explained this fact based on the lipid demixing process of some lipid mixtures (ex: cholesterol and CTAB) during the thin film formation in the lipid film hydration methodology, that involves a free-solvent step. With DELOS-SUSP the solvent-free step is avoided and thereby a more homogeneous lipid supramolecular organization can be obtained (Figure 1.10). The outstanding thermodynamic stability of quatsomes, as well as their high vesicle to vesicle homogeneity regarding size, lamellarity and membrane supramolecular organization, renders them as promising nanocarriers in the development of new nanomedicines.

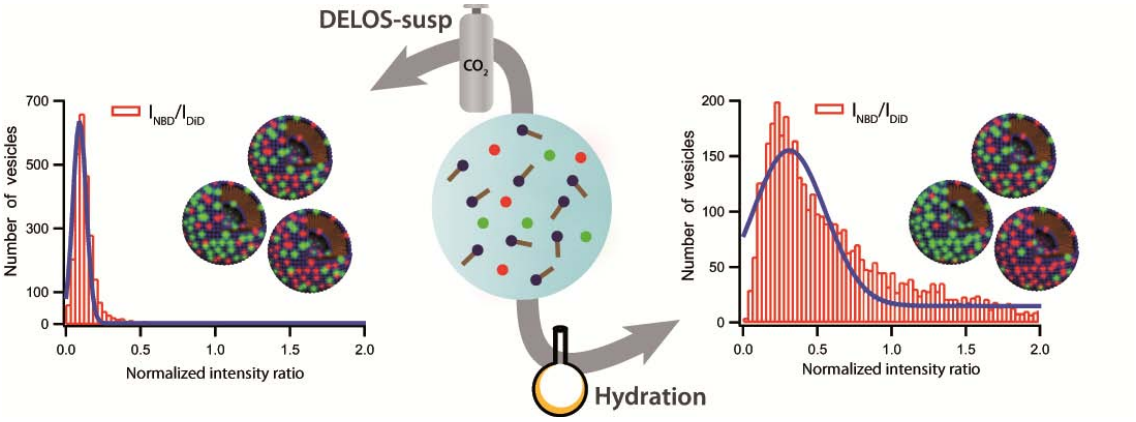

Figure 1.10. Histograms of vesicular samples prepared by DELOS-SUSP (left) and the hydration method (right). In each histogram the distribution of the ratio of the two integrated intensities, I_{NBD}/I_{DiD}, of two dyes is represented. Each integrated intensity belongs to the NBD and DiD dyes that are located in the vesicle membrane and mimic their components. The I_{NBD}/I_{DiD} ratio should be constant if all the individual vesicles had the same membrane composition and identical supramolecular organization; so the narrower the distribution is, the higher the homogeneity in the supramolecular arrangement of lipids in the membranes. *Adapted from ref. 34*

The goodness of DELOS-SUSP for the encapsulation of an active compound was tested for the first time by Dr. E. Elizondo in her PhD thesis work[35]. Gentamicin sulfate (GS) was used as a model hydrophilic drug which was dissolved in the aqueous phase for its entrapment in cholesterol/CTAB quatsomes. DELOS-SUSP allowed the one-step

encapsulation of gentamicin sulfate into small unilamellar vesicles with an encapsulation efficiency (EE) percentage around 1%, independently of the GS/lipid ratio used in the encapsulation experiments. The low EE was explained by two main reasons: a) the existence of electrostatic repulsions between the positively charged membrane of quatsomes and the cationic GS molecule, and b) the small volume of aqueous phase that was entrapped into the SUVs. Although the EE achieved was low, the values were still comparable to those obtained by some conventional methods for vesicle production[36]. It is important to remark here the good reproducibility of the method regarding both the structural and encapsulating properties of the different samples prepared at each GS/lipid molar ratio, which is very important for the implementation of any liposome producing process at industrial scale.

In this Thesis, and for the first time, the suitability of DELOS-SUSP method to prepare different examples of vesicle-biomolecule conjugates for applications in Nanomedicine as drug delivery systems was developed and studied in detail constituting the main objective of this research work.

1.2 Preparation of multifunctional nanovesicle-bioactive conjugates using DELOS-SUSP.

Taken into consideration the advantages offered by DELOS-SUSP as a one-step, simple, robust and scalable method to produce SUVs, the development of methodologies based on this process to prepare a variety of vesicle-based conjugates was investigated and the results obtained are presented in this Chapter. Indeed, the versatility and adaptability of the method allowed the synthesis of different nanovesicle-bioactive conjugates demonstrating that it functions as a general platform for the preparation of vesicle-based conjugates of biomolecules (Figure 1.11).

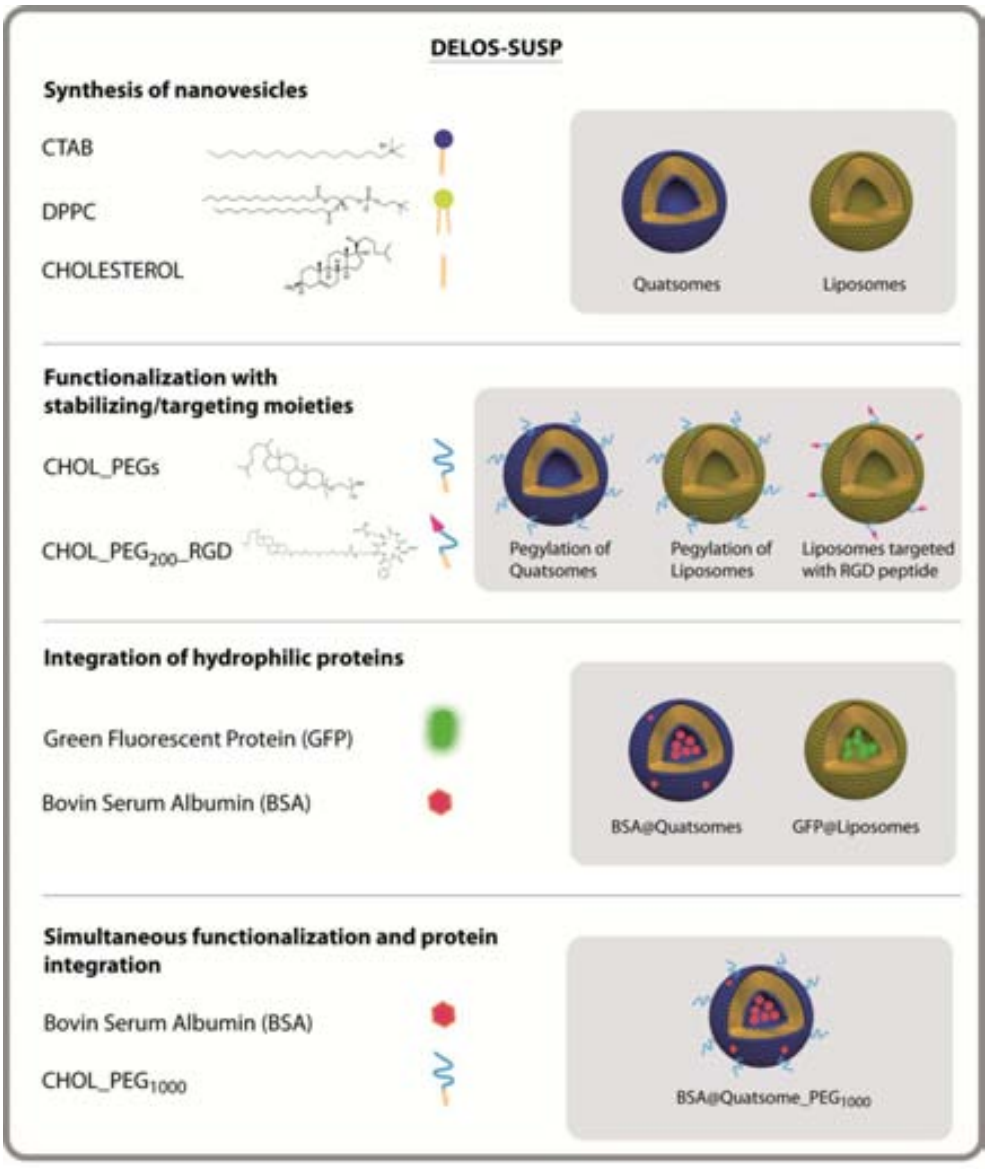

Figure 1.11. Schematic representation of the different nanovesicle-bioactive conjugates prepared in this Chapter by DELOS-SUSP method and the molecular structure of their components.

The methodology was adapted for the direct functionalization of vesicle membranes with stabilizing/targeting moieties. As stabilizing unit we used the hydrophilic poly(ethylene glycol) (PEG) polymer, a stealth agent widely employed to prolong circulation time by protecting the vesicles against phagocytosis. This is one of the most spread strategies to avoid the fast clearance of vesicles by opsonisation and to increase the blood circulation time in the body. It is well known that the so-called long-circulating or stealth liposomes can experience a "passive" accumulation in tumours and inflammations, enhancing the drug delivery in these affected parts[9,10,37].

DELOS-SUSP methodology was also adapted for the obtaining of vesicles functionalized with targeting units. As targeting unit, cyclic RGD peptides were incorporated to the vesicle membrane in order to promote the "active targeting" of specific cells. RGD-peptides have become a popular tool for the labelling of drug delivery systems due to its capacity of binding to integrins, which behave as cell surface receptors that mediate adhesion between cells and the extracellular matrix by binding to ligands with an exposed arginine-glycine-aspartate (RGD) sequence[11,38,39].

Other signalling units were incorporated to vesicles made by DELOS-SUSP method since they are useful for labeling studies in Nanomedicine. Indeed the labeling of cellular membranes and/or organelles with fluorescent probes, together with the use of microscopic techniques have contributed in the last years to a better understanding of cellular processes and functions. For example organelle stains can be used as counterstains to help identify the location of specific proteins and targets of interest within the cell. On the other hand florescent labeling of vesicle membrane allow different types of studies such as in vivo tumor targeting, cellular uptake experiments and the monitoring of single vesicles within a population to extract unique information on heterogeneous properties of the membranes[34]. For these reasons different strategies to label the vesicles produced by DELOS-SUSP were developed. Two molecules were used for this purpose: a) the molecular probe 1,1'-dioctadecyl-3.3.3'.3'-tetramethylindodicarbocyanine perchlorate (DiD) widely used in biological studies involving cell membrane labelling, and the fluorescein sodium salt, a water soluble fluorescent dye widely used for labeling nanoparticles, liposomes, etc. The latter dye has also been utilized in permeability studies due to its small molecular radius as well as a model of small drugs.

The capability of DELOS-SUSP to encapsulate/integrate different proteins was also studied since such biomolecules have attractive applications in Nanomedicine. Therapeutic proteins, also known as "pharmaceutical proteins", are defined as 'proteins or polypeptides which by reason of their native functions in the human body are *(potentially)* suitable as "therapeutic substances" [40]. Nowadays, therapeutic proteins are attracting the attention of clinicians for the treatment of many diseases. They are well tolerated by the body and have the ability to perform specific functions without interfering with normal biological processes[41]. However, the inherent lability associated with proteins, including thermal instability, degradation by proteolysis, rapid body excretion and low solubility, hinder the rapid progression of this field. Some drug delivery systems such as polymeric nanoparticles or liposomes have been used to overcome these limitations[42]. Indeed, there are several examples of enzymes and hormones, among other biomolecules,' encapsulated into vesicles which show a considerable increase of their therapeutic activities. For instance, the entrapment of superoxide dismutase enzyme into liposomes has proven to prolong its circulation time in blood and increase the therapeutic activity[43]. Moreover, insulin encapsulated in liposomes formed by dipalmitoylphosphatidylcholine (DPPC) and dipalmitoylphosphatidylethanol (DPPE), substantially decreased the plasma glucose levels in rats after oral administration[44].

Vesicles containing proteins are generally prepared using methodologies that might involve the use of organic solvents which can lead to a rapid denaturation of the enzyme with the consequent loss in the functionality[17]. Furthermore in many cases further post-formation steps are necesary to achieve the desired size and to reduce the multilamellarity of the vesicles. These steps may sometimes affect the final protein-to-lipid ratio and reduce the drug activity in the resulting formulation[45]. In order to overcome such drawbacks and to prove the suitability of DELOS-SUSP for encapsulating of hydrophilic biomolecules, two proteins were chosen as model biomolecules: 1) the green fluorescence protein (GFP) and 2) the bovine serum albumin (BSA).

1.2.1 General methodology for the preparation of nanovesicle-bioactive conjugates using the DELOS-SUSP process.

All nanovesicle-bioactive conjugates synthesized at lab-scale in the present Thesis were prepared in a small volume (7.5 mL) reactor, following the procedure schematically represented in Figure 1. 12, operating always under mild conditions to preserve the activity of the labile biomolecules. The general method consists in loading a solution of the membrane lipid components and the desired hydrophobic bioactives in an organic solvent (e.g. ethanol), into the high-pressure reactor previously driven to the working temperature (Figure 1.12 a). The reactor is then pressurized, in a second stage, with a large amount of compressed CO_2 until reach the working pressure (10 MPa) (Figure 1.12 b). Finally in the third stage, the vesicular conjugates are formed by depressurizing the resulting CO_2-expanded solution over an aqueous phase, which might contain water soluble surfactants and hydrophilic bioactives (Figure 1.12 c). In this step a flow of N_2 at the working pressure is used in order to push down the CO_2−expanded solution and to keep constant the pressure inside the reactor.

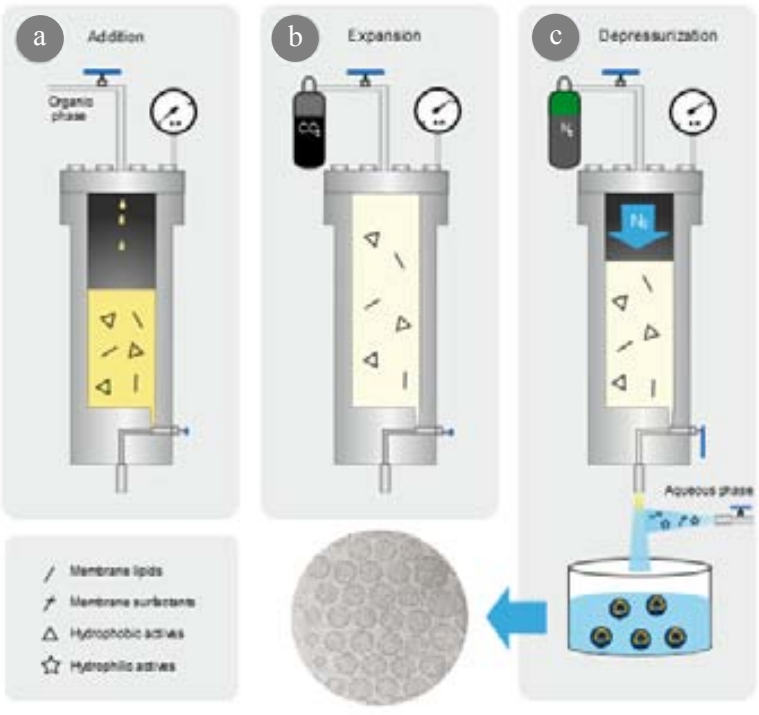

Figure 1.12. Schematic representation of the three stages of DELOS-SUSP method for the preparation of nanovesicle-bioactive conjugates.

It is worth to note that no further energy input is required for achieving the desired SUVs structural characteristics, neither for increasing the loading or functionalization

efficiencies. The CO_2 here acts as a co-solvent and its evaporation from the organic expanded solution during the depressurization stage produces a fast, large and homogeneous cooling which is responsible of the high vesicle-to-vesicle structural homogeneity. It should be pointed out, that lipids, such as cholesterol, have a great sensitivity to solvent media variations. Therefore, homogeneous vesicle formation paths are required to guarantee a high degree of structural homogeneity. Details of the experimental procedure and the equipment used are given in the Experimental Section 2.1.1.

All the biomolecule-vesicle conjugates were storaged at 4 ^{0}C after their preparation. The physical stability of the systems was evaluated by means of the Z potential and the particle size evolution. Following the size, the formation of vesicles aggregates or the vesicles growing can be detected. Details of the size evolution with time for all systems are shown in Experimental section 3.4.1. On the other hand, Z potential is an important and useful indicator of particle surface charges, which can be used to predict and control the stability of colloidal suspensions. The higher the Z potentials, the more stable a suspension becomes since the system is stabilized by mean of electrostatic repulsions[46].

1.3 Quatsomes-based conjugates as a platform for drug delivery

Quatsomes formed by cholesterol and CTAB, have been specially studied and characterized by the NANOMOL group in the last years due to its outstanding properties. Their great stability along time together with their homogeneity regarding size, lamellarity, and membrane supra-molecular organization make them excellent carriers for the development of new nanomedicines.

1.3.1 Study of the physico-chemical stability of quatsomes with temperature

The physico-chemical stability of a nanocarrier is an important parameter for drug release. The homogeneity of a nanocarrier during its administration does not depends only on the homogeneity of the initial product but also on their thermal stability. Thus if precipitation occurs during storage, the quantity of drug delivery for each administration would be unknown and this situation must be absolutely avoided[47]. Therefore the setting of the right storage temperature and the maximum storage time are crucial for every system. For such a reason the stability of quatsomes, prepared under the conditions given in Table 1.1 was studied under different storage temperatures by placing a

solution of plain quatsomes at different temperatures: 253, 277, 298 and 310 K. In order to check the influence of the temperature in the stability of the vesicles, the size and the Z potential were measured after 1, 2, 3, 7 and 15 days of storage. The tendency followed by the size and the Z potential with time and under different temperatures is shown in Figure 1.13. After the first 24 hours, the vesicles kept at 253 K increases their size more than two times the initial value (Figure 1.13, left panel), probably because during the freezing/thawing process the vesicles fuse forming bigger structures. Hence this temperature was discarded since the beginning for the stability study. At 310 K the size remains constant during a week, and then increases five times. The best behaviors were found at 277 and 298 K although there was a slightly increment in the size at 298 K. Regarding the Z potential, the values at 277 and 298 K remain constants during the time of the experiment meanwhile there was a drop of the value at 310 K which indicates certain degree of colloidal destabilization (Figure 1.13, right panel). In short, the vesicles keep their physico-chemical properties under 277 and 298 K, preserving their properties better at 277 K. After this study, the later temperature was established as the optimum storage temperature for quatsomes and quatsomes-bioactive conjugates.

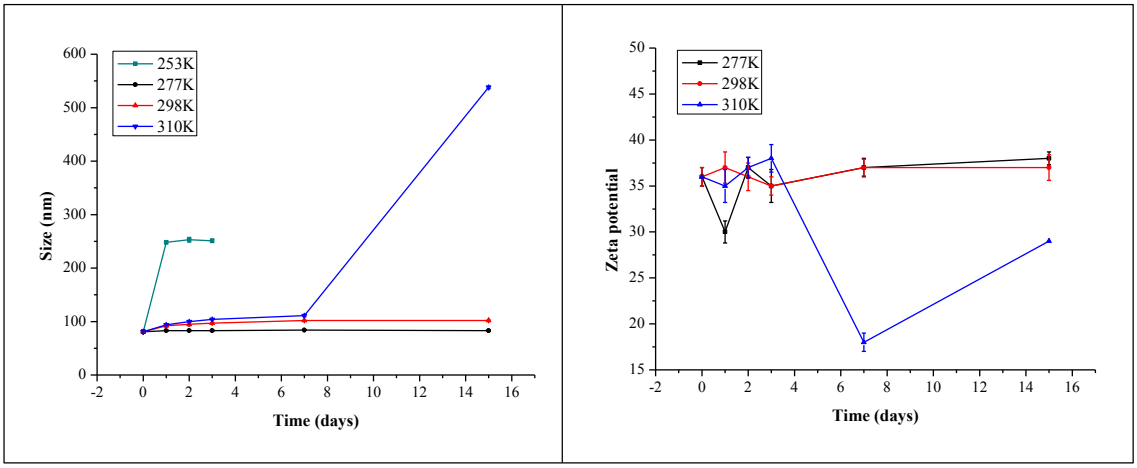

Figure 1.13. Evolution of size and Z potential of plain quatsomes with time, at different temperatures. The Z potential was not measure for the vesicles storage at 253 K because the first measurement of size provided undesirable morphological changes.

1.3.2 Study of the sterility and cytotoxicity of quatsomes

Drug delivery vehicles are usually administrated through different routes, especially parenteral. Therefore in addition to good physico-chemical characteristics, like

homogenous morphology and stability, the vesicles should also fulfill other requirements such as being sterile, non-cytotoxic and non-hemolitic, among others[47]. The sterility of quatsomes was studied in collaboration with the group of Prof. A.Villaverde from the Institut de Biotecnologia y Biomedicina (IBB-UAB), by measuring the vesicle capacity to produce microorganism colonies upon contact with different media. In the assay tested a sample of plain quatsomes were mixed with certain volume of water, PBS and cellular culture media in a 6 well plate and incubated overnight at 310 K (Experimental Section 9.1). After 24 hours the presence of microorganism colonies in the plate was not visually detected. So, in order to confirm this result a drop of the samples in the different media were placed into a glass slide and analyzed using an optical microscope with a coupled camera. No evidence of microorganism colonies were observed, with levels lower than 100 CFU/mL being therefore possible to conclude that plain quatsomes obtained by DELOS-SUSP were sterile (Figure 1.14).

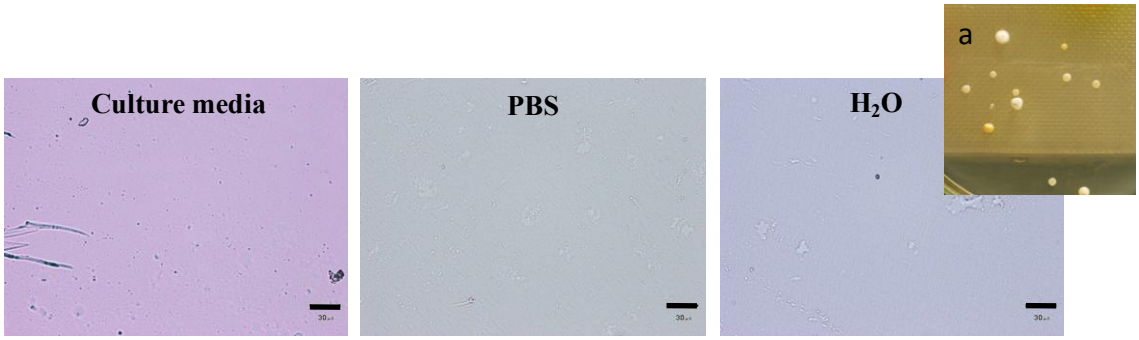

Figure 1.14. Optical microscope images of quatsomes after 24 hours of incubation at 310 K with different media. a) Image of microorganism colonies shown for comparison purposes. Scale bars are 30 μm.

The cytotoxicity of plain quatsomes, which is their quality of being toxic to cells, was also tested. The assays were carried out by the group of Prf. Schwartz in Vall d'Hebron Hospital. Plain quatsomes were tested in two types of cells, HeLa and HMEC-1, using the sulforhodamine B (SRB) assay (Experimental Section 9.2). The SRB assay remains one of the most widely used method for in vitro cytotoxicity screening. The assay relies in the ability of SRB dye to bind to protein components of living cells. As the binding is stoichiometric, the amount of dye extracted from stained cells is directly proporcional to the cell mass. The less the fluorescence is the more toxic the sample since dead cells cannot uptake the SRB dye. In the Figure 1.12, the viability of Hela and HMEC-1 cells after 72 hours incubation versus different concentrations of quatsomes is plotted. For

HMEC-1 cells, the percentage of cell viability was maintained in 100 % until quatsomes reached a concentration of 5 µg of lipid per mL of vesicular suspension. HeLa cells were more sensitive to quatsomes presenting a cell viability percentage near 90 % up to 5µg /mL. After this value, cell viability rapidly decreased reaching cero at 100 µg /mL in both cell types (Figure 1.15).

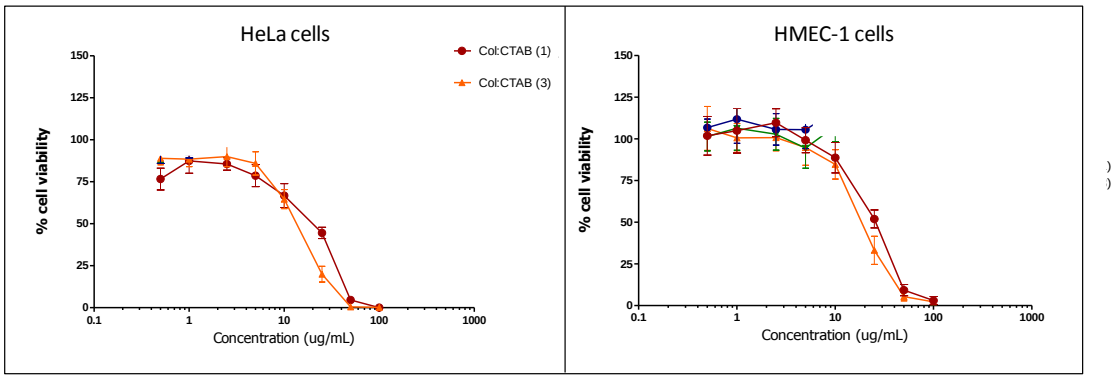

Figure 1.15. Cytotoxicity of quatsomes in Hela (left) and HMEC (right) cell lines. The assay was carried in two replicates

Quatsomes resulted cytotoxic in concentrations higher than 5 µg/mL and therefore not suitable for intravenous administration. As cholesterol is biocompatible, this toxicity can be attributed to the presence of CTAB, which present certain degree of toxicity. Nevertheless this cationic surfactant belongs to the quaternary ammonium surfactant (QUATs) family, which has been widely used in the pharmaceutical and cosmetic fields, especially for topical administration. They are also considered as good antiseptic agents against bacteria and fungi. For these reasons quatsomes can be considered as nanocarriers with great potential for topical delivery.

1.3.3 Preparation of quatsome-bioactive conjugates using DELOS-SUSP.

In order to prove the potential of quatsomes as nanocarriers, different quatsome-bioactive conjugates were prepared by the DELOS-susp procedure. Briefly the method consisted in the loading of a high-pressure autoclave with a solution containing cholesterol in ethanol. The solution was then pressurized with compressed CO_2 at a molar fraction of X_{CO2}= 0.6 until reaching a working pressure of 10 MPa, which produces a volumetric expanded organic solution of cholesterol. Finally, the expanded organic phase was depressurized over an aqueous solution containing CTAB at a

concentration over its critical micellar concentration (CMC), producing during this stage the desired nanovesicles. The molar ratio between the two components in the final formulation was 1 to 1, which have been proven to be the right proportion in order to have a pure vesicular phase. For the preparation of more complex systems containing active molecules, the process was as simple as with plain liposomes but for the addition of these molecules either to the expanded organic phase or to the aqueous medium, depending on their solubility characteristics (Figure 1.16).

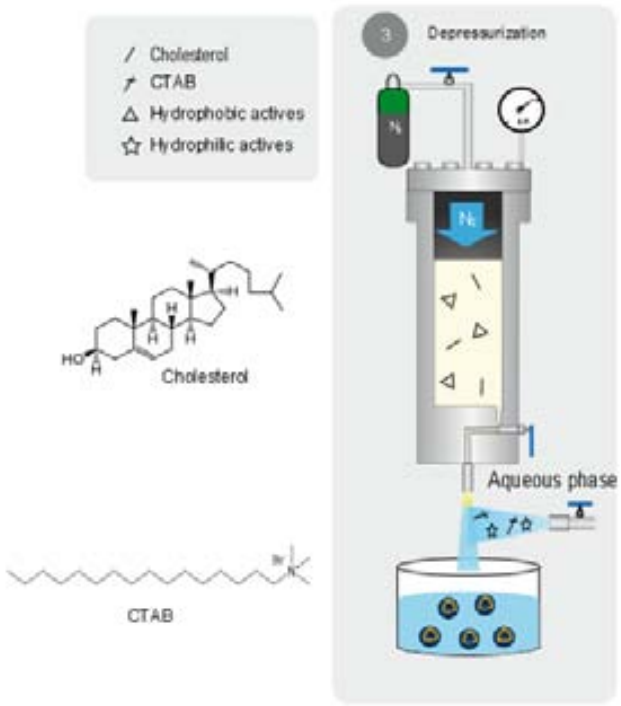

Figure 1.16. Schematic representation of DELOS-SUSP method for the preparation of quatsome-based conjugates together with the molecular structures of CTAB and cholesterol.

In Table 1.1, the composition of the organic and aqueous phases used for the preparation of all quatsome-based conjugates by DELOS-SUSP is given. The physicochemical characteristics of the resulting quatsomes as well as the entrapment efficiency percentages and protein loading achieved for the different formulations are shown in Table 1.2

Table 1.1. Compositions used for the preparation of the different quatsomes-based conjugates by means of the DELOS-SUSP method

Vesicle systems	Organic phase[a]	Aqueous phase[b]	Biom/lipid ratio[c] (µmol/mmol)	Lipidic conc[d]. (mg/mL)
plain quatsomes	cholesterol (68 mM)	CTAB (7.8 mM)	-	5
DiD-quatsomes	cholesterol (68 mM) + DiD (6 µM)	CTAB (7.8 mM)	$4.2*10^{-5}$	5
quatsome_PEG_{1000}	cholesterol (48 mM) + $CHOL\_PEG_{1000}$ (8 mM)	CTAB (7.8 mM) in water	66	5
quatsome_PEG_{2000}	cholesterol (38 mM) + $CHOL\_PEG_{2000}$ (6.3 mM)	CTAB (7.8 mM) in water	58	5
BSA loaded-quatsomes (25 µg/mL)	Cholesterol (68 mM)	CTAB (7.8 mM) + BSA (0.38 µM) in water	0.025	5
BSA loaded-Quatsomes (75 µg/mL)	Cholesterol (68 mM)	CTAB (7.8 mM) + BSA (1.1 µM) in water	0.075	5
BSA loaded-Quatsomes (1 mg/mL)	Cholesterol (68 mM)	CTAB (7.8 mM) + BSA (16 µM) in water	1	5
BSA loaded-Quatsome_PEG_{1000}	Cholesterol (48 mM) + $Cholesterol\_PEG_{1000}$ (8 mM)	CTAB (7.8 mM) + BSA (16 µM) in water	1.2	5

Experiments were performed from CO_2-expanded ethanol at 10 MPa and 308K. [a] Concentration of the membrane components in 2.88 mL of ethanol for Quatsomes is given. [b] A constant aqueous phase volume of 24 mL was used . [c] Ratio between the total amount of the biomolecule and the total amount of lipids present in the formulation. [d] Ratio between the total amount of lipid forming membrane of quatsomes and the volume of the final vesicular suspension.

Table 1.2. Physicochemical characteristics, entrapment efficiency percentages and protein loadings of the different quatsomes-based conjugates prepared by the DELOS-SUSP method

Vesicle systems	Size		Z potential (mV)	EE (%)	Protein loading [c] (μg/mg)
	Mean [a] (nm)	PdI [b]			
plain quatsomes	121 ± 7	0.23 ± 0.01	74 ± 5	-	-
DiD-quatsomes	170 ± 8	0.451± 0.04	73 ± 10	-	-
quatsome_PEG_{1000}	67 ± 6	0.15 ± 0.07	69 ± 8		
quatsome_PEG_{2000}	84 ± 0.5	0.20 ± 0.03	38 ± 1		
BSA loaded-quatsomes (25 μg/mL)	120 ± 0.5	0.38 ± 0.01	76 ± 1	65 ± 4	3
BSA loaded-quatsomes (75 μg/mL)	126 ± 0.3	0.29 ± 0.01	84 ± 2	86 ± 3	12
BSA loaded-quatsomes (1 mg/mL)	149 ± 12	0.26 ± 0.10	75 ± 7	96 ± 1	179
BSA loaded-Quatsome_PEG_{1000}	82 ± 8	0.23 ± 0.01	52 ± 4	84 ± 3	157

[a] Intensity weighted mean hydrodynamic size of the collection of vesicles measured by dynamic light scattering. [b] Polidispersity index showing the width of the particle size distribution. [c] Mass of the integrated protein divided by the total mass of the lipids comprising the membrane

1.3.3.1 Functionalization of quatsomes with fluorescent molecules

Fluorescent dyes were one of the first molecules used to functionalize quatsomes due to their availability, variety, importance and structural simplicity compared to other molecules. The functionalization of quatsomes with different dyes was studied using two approaches: a) the incubation of the plain vesicles with the dye and b) the simultaneous labelling and vesicle formation using the DELOS-SUSP methodology.

a) Functionalization by incubation. The first studies were performed with the sodium salt of fluorescein (FS) by incubation with the quatsomes. When dissolved in aqueous media, the FS molecule dissociates into the anion and the sodium and since the quatsomes have a positively charged membrane, electrostatic interactions were expected to be established between the anion and the membranes (Figure 1.17).

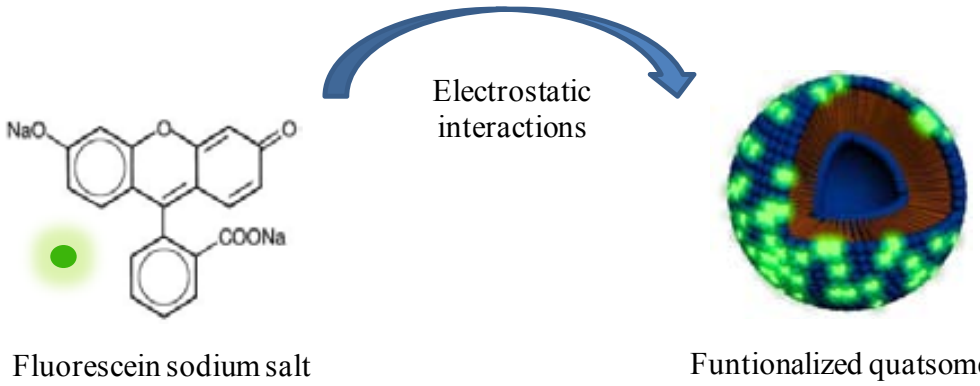

Figure 1.17. Schematic representation of the functionalization of quatsomes by electrostatic interactions between the FS and the quatsomes

The assay was carried out with a small volume of plain quatsomes prepared by DELOS-SUSP, using the conditions described in Table 1.1, by mixing the quatsomes with different amounts of FS in order to study the influence of the molar ratio FS:CTAB in the functionalization (Experimental Section 6.1). The solutions were stirred during 30 minutes and after this period of time the sizes and Z potentials were measured in a dynamic light scattering analyzer and the values obtained plotted versus the used molar ratios of FS:CTAB (Figure 1.18). While the amount of FS was lower than that of CTAB the size of quatsomes remained constant but beyond the molar ratio 1:1 the sizes increased enormously up to 16 and 30 times the initial ones. This increment in size was accompanied by a drop in the Z potential to values in which the vesicles suspensions are considered to be instable.

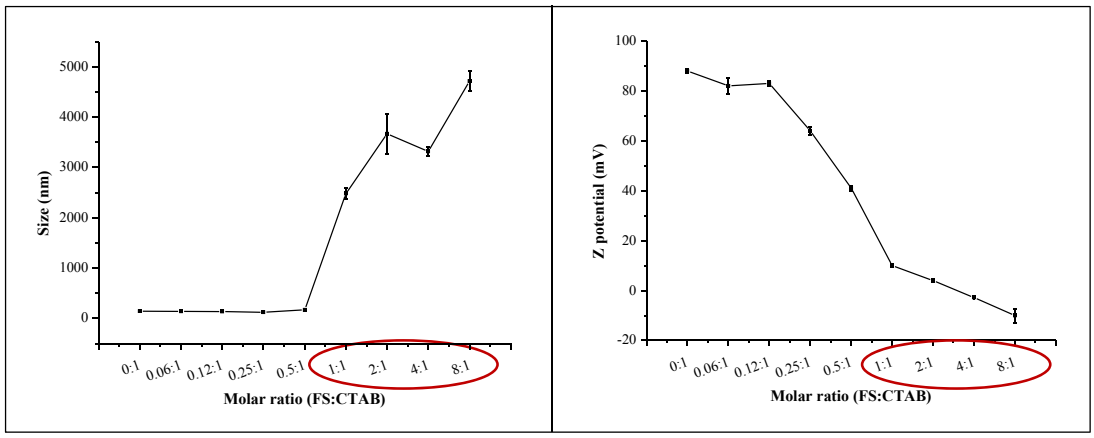

Figure 1.18. Influence of the molar ratio FS:CTAB on of the size (left) and Z potential (right) during the functionalization of quatsomes.

The Z potential values remained higher than 30 until the molar ratio FS:CTAB was below 0.5 while beyond this ratio the Z potential drop below cero suggesting the instability of the system. As a consequence a solid deposition was observed probably corresponding to the presence of cholesterol crystals. Therefore when the concentration of the anion was equal or larger than the CTAB concentration, the supramolecular synthon formed between the CTAB and the cholesterol become unstable and the surfactant molecule prefers to interact electrostatically with the FS. To demonstrate this assumption it was checked if the addition of an anionic surfactant like sodium bis(2-ethylhexyl) sulfosuccinate (AOT), instead of FS salt, produces the same destabilization of quatsomes. Thereby AOT was added to plain quatsomes in a molar concentration four times bigger than CTAB observing the same destabilizing effect in the system. In Figure 1.19, images of quatsomes destabilized by the addition of organic anions are depicted.

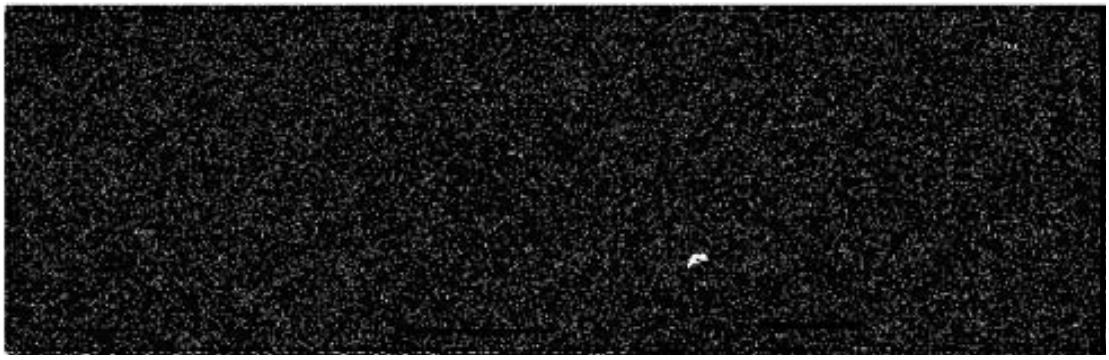

Figure 1.19. Destabilization of quatsomes in the presence of anionic organic molecules. a) Plain quatsomes in aqueous media, b) quatsomes in the presence of fluorescein sodium salt at a molar ratio 4:1 of FS:CTAB c) quatsomes in the presence of AOT salt at a molar ratio 4:1 of AOT:CTAB. Scale bars are 200 nm.

Quatsomes functionalized by fluorescein, obtained using 0.1 molar ratio of FS:CTAB, were characterized by dual-color epifluorescence-total internal reflection fluorescence (EPI-TIRF) microscopy. TIRF-microscopy is a powerful optical technique that allows extremely thin optical sectioning with excellent signal-to-noise ratios. It is often employed to study cellular membrane activities along with phenomena occurring at cellular level, like cellular adhesion, movement, single molecular events or vesicle and protein trafficking. The measurements took place in collaboration with the group of Prof. M. Garcia-Parajo from ICFO.

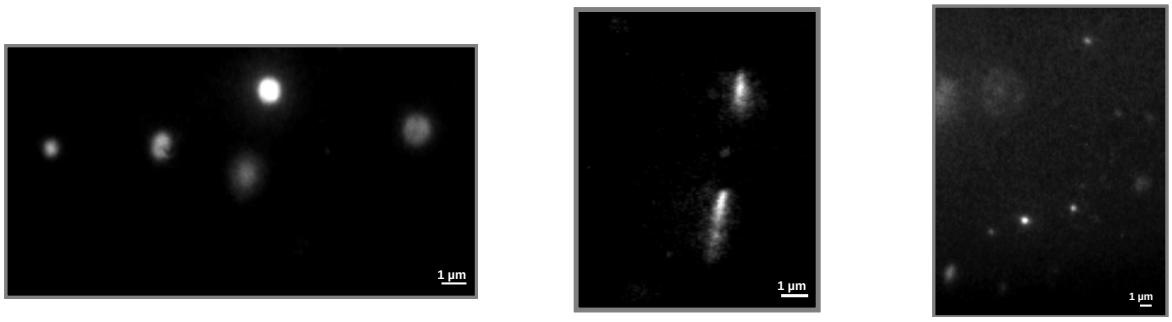

Figure 1.20. EPI-TIRF microscopy images of quatsomes decorated with FS.

The characterization by EPI-TIRF was carried out using a small volume of a suspension of plain quatsomes which were mixed directly with FS during 30 min at room temperature. Dilutions from 1/10 to 1/1000 were performed with the resulting mixture with PBS (pH= 7.4) and HEPES (pH= 7.2) buffers, in order to set the best sample concentration for the TIRF-microscopy images. Figure 1.20 shows three typical images that confirmed the functionalization of the vesicles with fluorescein in the sample with dilution 1/10 in HEPES buffer. The obtaining of good quality images with such samples was very difficult due to the presence of a background of fluorescence that prevented the correct visualization of the labeled vesicles. Since the interactions between FS and CTAB are of electrostatic type, they are strongly influenced by changes on the pH or the ionic strength. Thereby, the use of buffers to make the dilutions provoke the detachment of the anion from the quatsome membranes, creating a fluorescent background that makes difficult the recording of sharp and more defined images.

To avoid this detachment, 1,1'-dioctadecyl-3,3,3',3'-tetramethylindodicarbocyanine perchlorate (DiD), a hydrophobic dye from the families of carbocyanines, was used instead of FS to label the quatsomes. This molecule is widely used for cell membrane labelling since it is inserted into membranes through hydrophobic interactions rather than by electrostatic ones. Therefore it is expected that changes in the buffer will not produce any significant dye detachment (Figure 1.21).

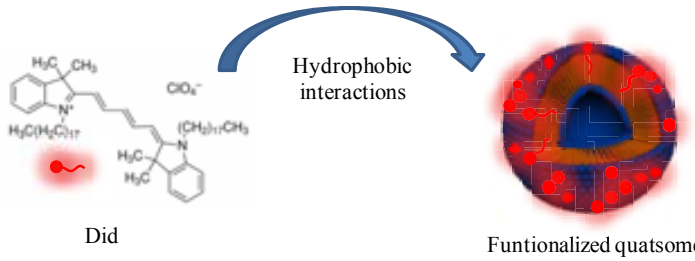

Figure 1.21. Schematic representation of the hydrophobic interaction between DiD and quatsomes. The high hydrophobicity of this dye, which presents a long hydrocarbon chain, favors the easy functionalization of the lipophilic vesicle membranes.

From previous literature data, it was found that the concentrations of DiD dye normally used to label vesicle membranes are between 0.1 mol% and 0.01 mol% of the total membrane composition[48]. Hence we started with DiD concentrations around those values. The first step was to set the optimum DiD/lipid ratio for obtaining good quality EPI-TIRF images. Suspensions of plain quatsomes were mixed with different volumes of a stock solution containing DiD in ethanol (1 mM), to obtain different final concentrations of the dye starting from 15 µM (0.1mol % of total lipid composition). After 30 min of mixing, the free DiD was separated from the sample by gel filtration using a PD SpinTrap G-25 column, designed for a rapid and convenient sample clean-up of proteins/biomolecules. With these columns, small molecules like salts, free labeling agents or other impurities are efficiently separated from the high molecular weight substances of interest. Following the procedure described in the Experimental Section 6.2.1, the columns were equilibrated three times with PBS buffer and then a small volume of sample was added. The separation took place by spin centrifugation. DiD-labeled nanovesicles were 10-fold diluted in a PBS buffer solution and a certain volume of the sample was transferred to a glass coverslip mounted into a microscope chamber. Imaging was performed on a home-built EPI-TIRF setup equipped with a 37ºC heated chamber (Experimental Section 6.2). Following this procedure different concentrations of the dye were tested obtaining the best images in the range from 6nM to 0.006nM. The concentration of 0.6 nM was chosen as the optimum DiD concentration for the labeling of quatsomes (Figure 1.22).

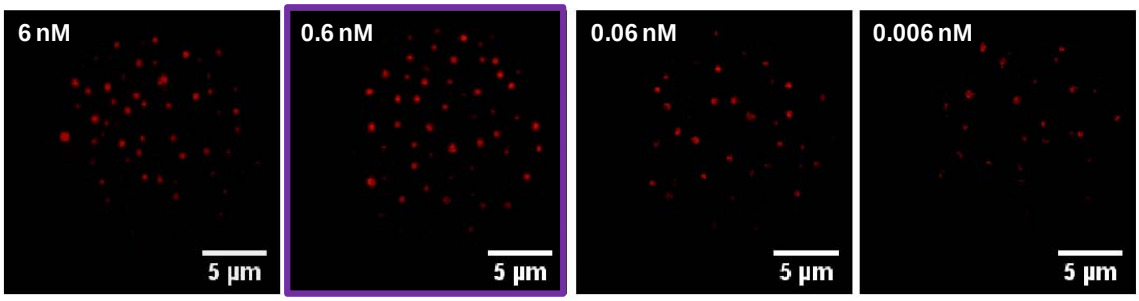

Figure 1.22. Quatsomes labeled with DiD by incubation at different concentrations.

The EPI-TIRF images (Figure 1.23) of labeled quatsomes were compared with standard labeled microspheres of polystyrene with 100 nm in diameter normally used to set the microscope parameters, as well as with a solution of free DiD. Almost no fluorescent signal was detected when the dye was in free solution. Conversely, when the dye was inserted in the quatsomes an image similar to the one obtained for the microspheres was observed, confirming the DiD arrangement on the quatsomes membrane.

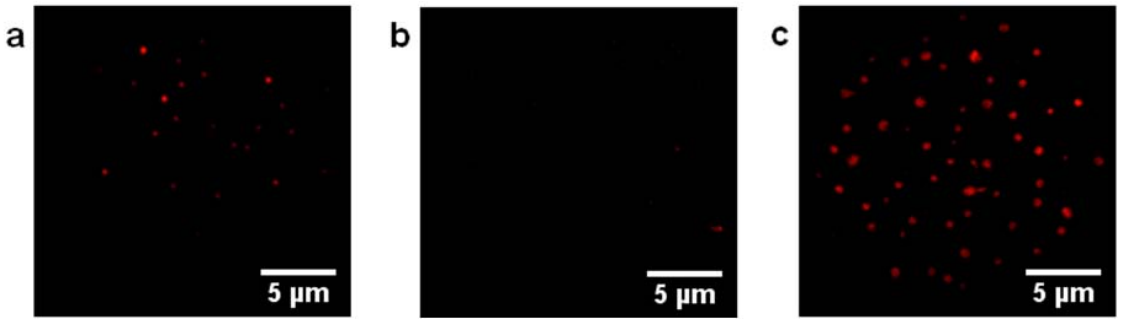

Figure 1.23. Testing the optimized concentration for labeling quatsomes with DiD. (a) Labeled-polystyrene microspheres of 100 nm in diameter. (b) Free DiD dye at a concentration of 0.6 nM; and (c) DiD-labeled quatsomes at a dye concentration of 0.6 nM.

b) Functionalization of quatsomes during their preparation. DiD labeled-quatsomes were also prepared using the DELOS-SUSP process by adding a solution of the dye to the organic phase containing cholesterol. After one hour of equilibration the volumetric expanded organic solution at 333 K was depressurized over an aqueous solution containing CTAB for the formation of labeled vesicles containing DiD (Table 1.1). As observed in Table 1.2 the vesicles obtained with this procedure presented a nanoscopic size and a high and positive Z potential, indicative of a good stability long time. The morphology of quatsomes was unaffected by the incorporation of the DiD and the presence of unilamellar and spherical vesicles was also observed (Figure 1.24). The

images of labeled-quatsomes, taken by EPI-TIRF microscopy, confirmed the dye integration and that the DELOS-SUSP process DiD not affect the dye fluorescence after processing. Therefore the labeling of quatsomes was possible either by the incubation with the dye or by the DELOS-SUSP methodology.

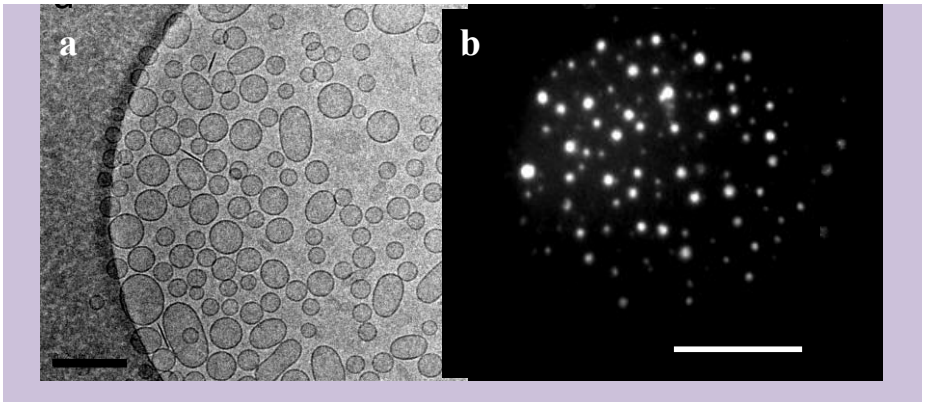

Figure 1.24. Labeling of quatsomes with DiD at 0.6 nM. (a) Cryo-TEM image of labeled-quatsomes prepared using the DELOS-SUSP method. Scale bar is 200 nm (b) The corresponding EPI-TIRF microscopy image of labeled quatsomes. Scale bar is 5 μm.

1.3.3.2 PEGylation of quatsomes

Conventional methodologies, like lipid thin-film hydration or reverse-phase evaporation, are generally employed to prepare PEGylated liposomes. High residence times in blood have been found for PEGylated liposomes with small concentrations (≤ 7 mol %) of PEGs with short chains (1000-4000 Daltons), covalently linked to selected lipid membrane constituents[49,50]. In the present thesis quatsomes grafted with PEG units were directly produced by DELOS-SUSP, adding cholesterol functionalized with PEG, like cholesterol_PEG_{1000} and cholesterol_PEG_{2000}, as part of the vesicle membrane components (Figure 1.12). In all experiments the molar ratio between cholesterol and cholesterol_PEG was 6:1, in order to ensure a content of PEG below 7 mol%. To prepare the quatsome-PEG conjugates, a solution of cholesterol and cholesterol_PEG in ethanol were added to the reactor and pressurized with CO_2. In order to obtain the conjugates, the volumetric expanded organic phase was depressurized over an aqueous solution containing CTAB. The composition of the organic and aqueous phases used for the preparation of the PEGylated vesicular formulations is given in Table 1.1.

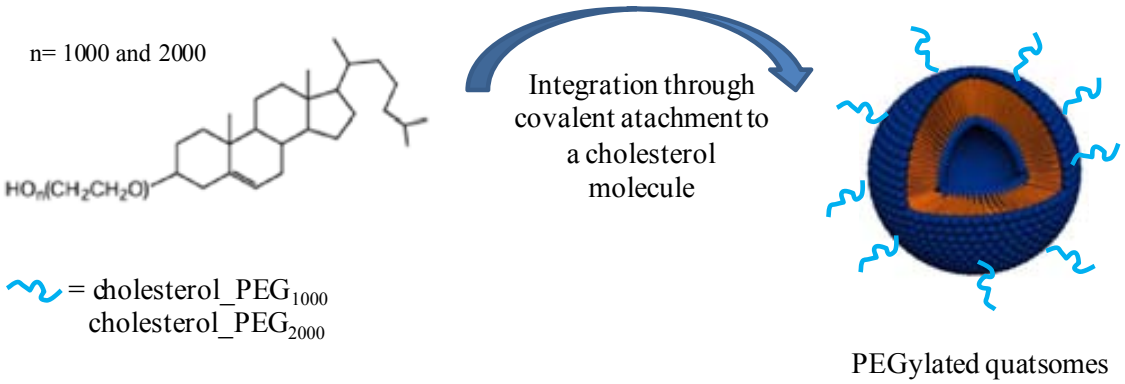

Figure 1.25. Schematic representation of the PEGylation of quatsomes through covalent attachment of a PEG molecule to one of the membrane components, in this case cholesterol.

Their size distribution, polydispersity index and Z potential were determined using a DLS equipment and are reported in Table 1.2. The resulting quatsome-PEG conjugates presented sizes with values below 100 nm, and homogeneous vesicle populations as indicated by their small polydispersity indexes. Besides, their Z potential values were larger than + 30 mV, consistent with their higher stability under storage conditions. Indeed, no significant changes in size and morphology were observed for more than five months, indicating that these vesicular systems are very stable and do not suffer aggregation upon long periods of time (Experimental section 3.4.1). The high stability of quatsome-PEG conjugates is explained by the particular self-assembling of cholesterol and CTAB molecules when forming vesicular structures[33]. The morphology of the samples, studied through the Cryo-TEM images, disclosed homogeneous, spherically-shaped and unilamellar nanovesicles in all cases (Figure 1.26).

It is worth to note that although quatsomes-PEG conjugates cannot be used as vehicles for intravenous delivery of bioactives due to its cytotoxicity, the system served as a model to explore the possibility of preparing PEGylated systems using the DELOS-SUSP method.

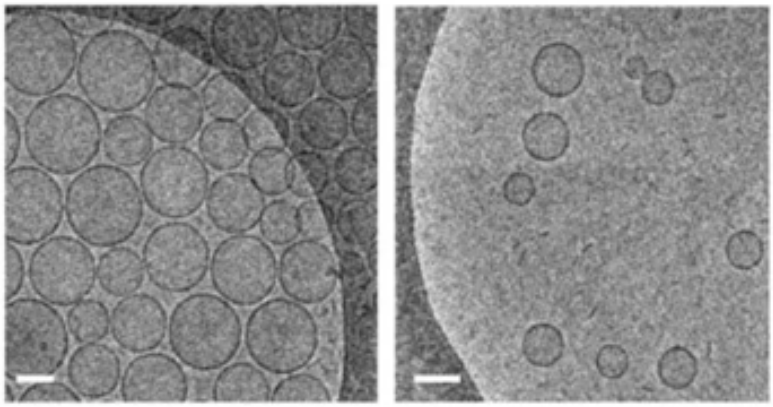

Figure 1.26. Cryo-transmission electron microscopy images of PEGylated quatsomes. Left, PEGgylation with cholesterol_PEG_{1000} and right, with cholesterol_PEG_{2000} (right). Scale bars are 100 nm.

1.3.3.3 Functionalization of quatsomes by incubation with targeting peptides

The functionalization through electrostatic interactions has been extensively used not only for the labeling of liposomes with fluorescent molecules but also to form liposomal complexes with DNA. These complexes are promising as nonviral carriers of DNA vectors for gene therapy[51]. Taken advantage of the homogeneous morphology of the quatsomes obtained by the DELOS-SUSP and their positively charged membrane, we also explored their functionalization by decorating them with the RGD (s-s) targeting peptide. As previously mentioned the capacity of these peptides to bind integrins receptor has made them very popular molecules for the labeling of vesicles. This biomolecule present a cyclic structure that confers more selectivity and stability to the molecule[52]. Due to its isoelectric point (PI=5.3), the presence of negatively charged groups at a working pH of 6 is expected and thus they become attractive for establishing electrostatic interactions with positively charged membranes (Figure 1.27).

For the functionalization, plain quatsomes were prepared by the depressurization of the organic phase containing cholesterol over the aqueous phase containing CTAB. A stable and homogenous system, with sizes around 120 nm, a PdI≤0.3 and a Z potential of 76 mV was obtained (Table 1.3). Subsequently 2 mL of plain vesicles were incubated with RGD (s-s) in a molar ratio 6:1 cholesterol:RGD (s-s) and kept for 1 hour under stirring at 308 K. The physicochemical characteristics of the system functionalized with the peptide are reported in Table 1.3.

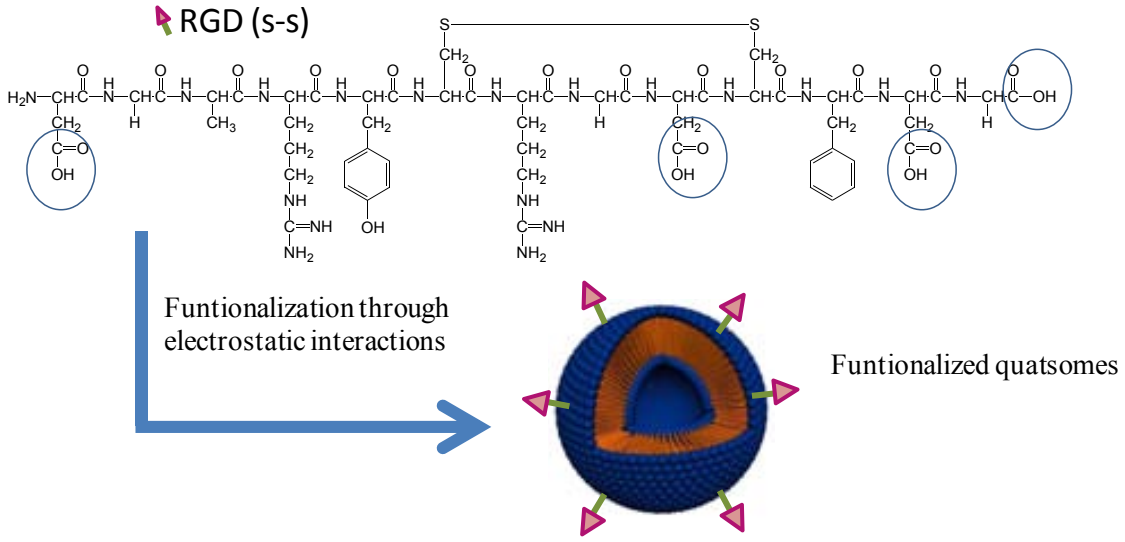

Figure 1.27. Schematic representation of the interaction between RGD (s-s) peptide and quatsomes. At pH=6 the carboxylic groups in the terminal amino acids lose their proton and get negative charge. Above the isoelectric point the peptide presents at least 4 negative charges.

Remarkable is the decrease of the Z potential to the half of the value of plain quatsomes, which indicates the establishment of electrostatic interactions. Presumably the integration of the peptide is promoted by the interaction between the negatively charged RGD (s-s) and the positive polar head of CTAB in the membrane of the vesicles, although hydrophobic interactions can also be present as well. There is a slightly increase in the vesicle size, which might be due to an increase in the hydrodynamic radio of the vesicles produced by the RDG incorporation in the outer part of the membrane. The functionalization was repeated in a different batch and similar data of size and Z potential were obtained.

Table 1.3. Physicochemical characteristics of plain quatsomes and RGD labeled-quatsomes

Vesicle systems	Size		Z potential (mV)
	Mean (nm)[a]	PdI[b]	
Plain Quatsomes (batch 1)	120 ± 2	0.25 ± 0.01	76 ± 1
RGD labeled-Quatsomes	143 ± 3	0.38 ± 0.05	38 ± 4

[a] Intensity weighted mean hydrodynamic size of a collection of vesicles measured by dynamic light scattering. [b] Polidispersity index showing the width of the particle size distribution.

Finally, Cryo-TEM images of the resulting quatsomes (Figure 1.28) showed very homogeneous nanovesicles with no changes in the morphology when the peptide was

added, at the working concentration. Noteworthy is the resulting vesicular organization of the quatsomes functionalized with the targeting peptide, compared to that of plain quatsomes. Indeed, vesicles appear to be interacting through their membranes forming a regular network. This could be produced because the peptides, already integrated in the external part of the membranes, attract neighbouring vesicles through the positive charges present. Therefore it can be conclude that the functionalization of quatsomes by incubation with the targeting peptide RGD (s-s) is possible, obtaining a conjugate with good physicochemical characteristics and homogeneous morphology.

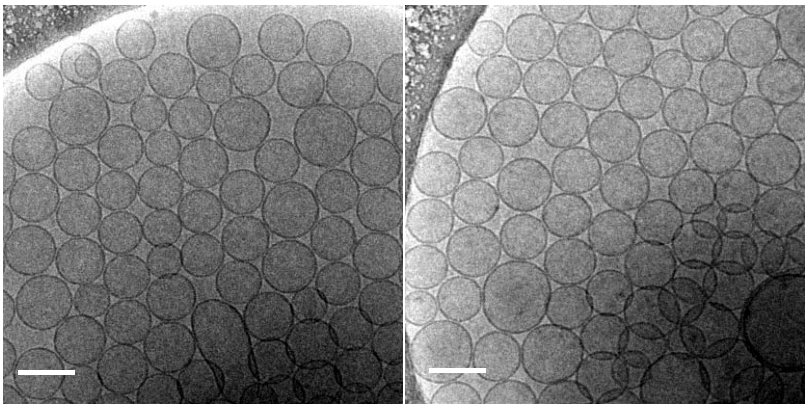

Figure 1.28. Cryo-TEM images of quatsomes functionalized with the RGD (s-s) peptide. Scale bar are 100 nm.

1.3.3.4 Preparation of quatsome-protein conjugates

The encapsulation degree of any drug into vesicles is influenced by several parameters related to the: a) *vesicle composition*, b) the nature of the *drug* and c) the *preparation methodology*[53]. Regarding the *vesicle composition,* besides the selection of the lipids forming the membrane and the presence of charges on it, the type of vesicle plays also an important role. Thus, for hydrophilic drugs, such as proteins or peptides, the encapsulation degree appears to increase in the following order: MLV < SUV < LUV. Nevertheless in the case of hydrophobic drugs, the size and type of liposomes do not seem to play a major role. With respect to the nature of *drugs*, several situations may occur depending on their interaction with the vesicle bilayer. Thus Talsma and Crommelin[54] had divided them into four classes: 1) water soluble, non-bilayer-interacting drugs; 2) hydrophobic, bilayer-interacting drugs that are bound inside the hydrophobic region of the bilayers; 3) drugs in the aqueous domain that can be associated with the bilayer via electrostatic interactions; 4) drugs that are neither water-

soluble, nor bilayer bound nor bilayer associated. The manner in which they become associated with the vesicles will affect the final encapsulation percentage. In the case of therapeutic proteins, after the encapsulation procedure they are expected to reside in the aqueous core, however exposed hydrophobic regions may interact with the lipid membrane. Regarding this general drug classification, proteins could be included into the class 3 although the interactions with the lipid bilayer is not only of an electrostatic nature but also hydrophobic. Such protein lipid interactions generally contribute to retain the bioactivity of the protein[41].

1.3.3.4.1 Preparation of quatsome-BSA conjugates

The goodness of the DELOS-SUSP methodology for encapsulating proteins was evaluated for the first time by the entrapment of the commercially available bovine serum albumine (BSA) protein of 66.5 KDa in quatsomes (Figure 1.29). BSA is the most abundant protein in the blood of mammals and has been extensively used as a model protein in different types of studies such as protein-membrane associations, protein-surfactant interactions and for entrapping into liposomes[55,56]. BSA is a hydrophilic protein with an isoelectric point of 4.7 which therefore presents a negative charge under the physiological conditions. As BSA is a non-expensive commercially available protein, several concentrations of the biomolecule were tested for the entrapment study with quatsomes.

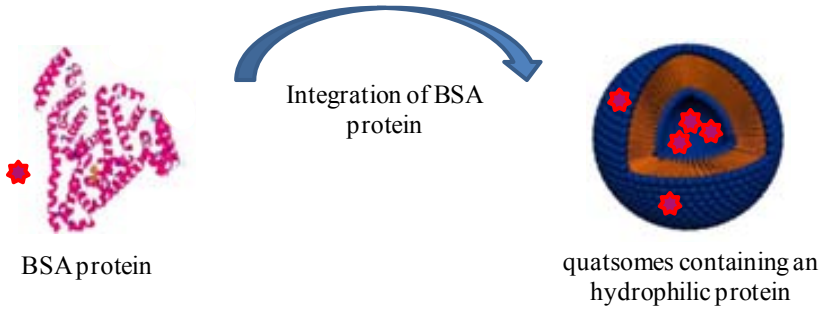

Figure 1.29. Schematic representation of the integration of BSA protein in quatsomes.

To form the conjugates with quatsomes the DELOS-SUSP method schematized in Figure 1.16 was followed. First a solution of cholesterol in ethanol was volumetrically expanded with CO_2 until the working pressure. The protein was added to the aqueous phase containing CTAB and stirred for 10 min. Afterwards the depressurization of the

organic phase over the aqueous solution allowed the formation of BSA-loaded quatsomes containing different concentrations (25 µg/mL, 75 µg/mL and 1 mg/mL) of the protein (Table 1.1). The physicochemical characteristics of the resulting systems are displayed in Table 1.2. Thus, DELOS-SUSP yielded macroscopically stable disperse systems, with nanoscopic sizes ranging from 120 nm to 150 nm. An increase in the size when increasing the initial amount of protein added to the systems was observed. The Z potential values were in all cases positive and very high in agreement with the membrane composition, indicating the great stability of the preparations. Indeed the vesicles were stable for more than five months under the storage conditions (277 K) with no signs of solid deposition (Figure 1.30). For example the particle size distribution of the system loaded with 1 mg/mL did not changed during this time, confirming that the vesicles did not fused or aggregated (Experimental section 3.4.1)

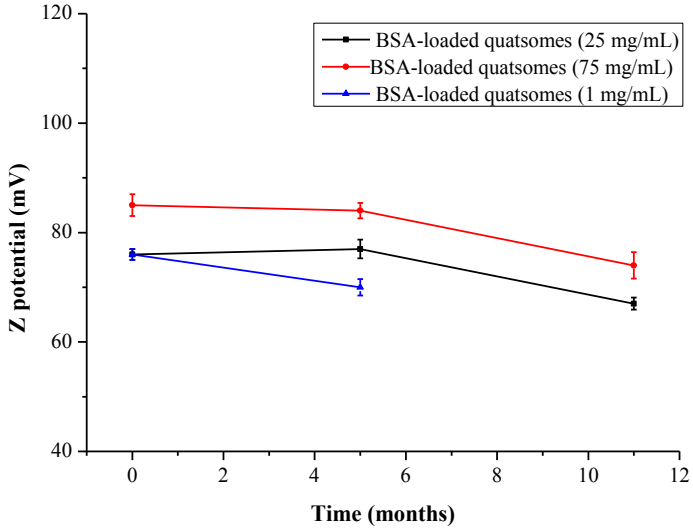

Figure 1.30. Evolution of the Z potential with time of BSA-loaded quatsomes with different initial protein concentrations. The vesicles were kept at 277 K during the stability study.

The Cryo-TEM images (Figure 1.31) showed homogeneous systems with nanoscopic, spherical and unilamellar vesicular structures in all cases.

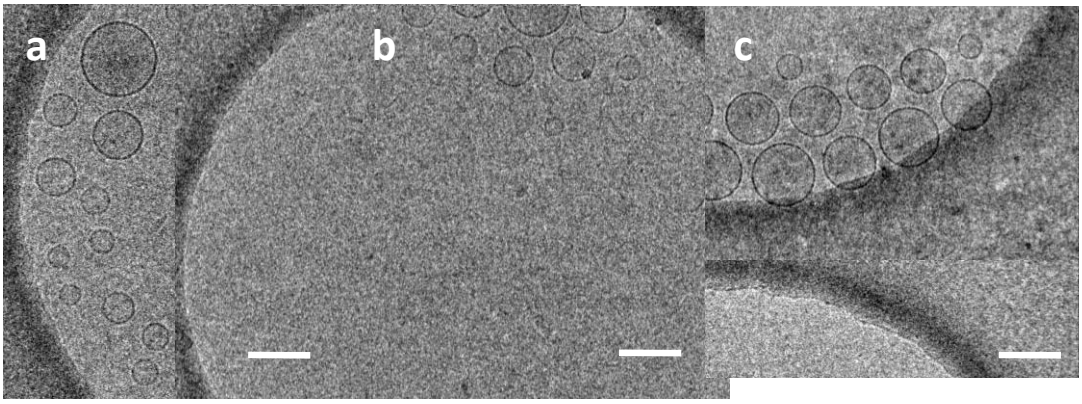

Figure 1.31. Quatsome-BSA conjugates. a) Conjugates with initial BSA concentration of 25 μg/mL b) Conjugates with initial BSA concentration of 75 μg/mL. c) Conjugates with initial BSA concentration of 1 mg/mL. Scale bars are 200 nm.

Determination of the entrapment efficiency was done by separation of BSA-loaded vesicles from the non-incorporated protein using centrifugal filter devices of 100 kDa following the procedure described in Experimental Section 5.1.1. The quantification of BSA content in each fraction was performed using the Micro BCA™ protein assay kit. As the quatsomes themselves interfered with this assay, the determination of the encapsulation efficiency percentage was made using the fractions with the free BSA protein (Experimental Section 4.2.3). The entrapment efficiency and the protein loading were determined using Eqs 1 and 2:

$$Entrapment\ efficiency(\%EE) = \frac{initial\ mass\ of\ active - free\ ative}{initial mass of active} * 100 \qquad \text{(Eq. 1)}$$

$$Protein\ loading\ \left(\frac{w}{w}\right) = \frac{mass of integrated active\ (\text{in } \mu g)}{mass of lipids\ (\text{in mg})} \qquad \text{(Eq. 2)}$$

The percentages of protein entrapment found in the quatsomes resulted very high, considering that BSA is hydrosoluble and that the vesicles are of nanoscopic size (Table 1.2). The higher the initial protein concentration the greater the % EE values, with a 96 % found for the more loaded system. A reasonable explanation for this high degree of encapsulation could be related to the presence of specific protein-membrane interactions. Indeed, BSA has a negative charge under the entrapment conditions, and therefore could form a complex with the cationic quatsomes. This complex together with the entrapment of the protein inside the aqueous core of the vesicles could explain the high encapsulation efficiency. Thus, the use of DELOS-SUSP methodology for encapsulating BSA in quatsomes gave rise to high protein loadings, long stabilities

along time and very homogeneous morphological characteristics meliorating the association efficiencies achieved (20-75 %) for the encapsulation of BSA in liposomal vesicles using conventional methodologies[57].

1.3.3.5 Preparation of multifunctional quatsome-based conjugates

The used of DELOS-SUSP method was extended to the simultaneous PEGylation and protein loading of quatsomes (Figure 1.32). For the preparation of this novel multifunctional system, a CO_2-expanded ethanolic solution containing cholesterol and cholesterol_PEG_{1000} in a molar ratio 6 to 1 was depressurized over an aqueous solution containing CTAB and BSA (Figure 1.16). Details about the composition of the different phases are given in Table 1.1.

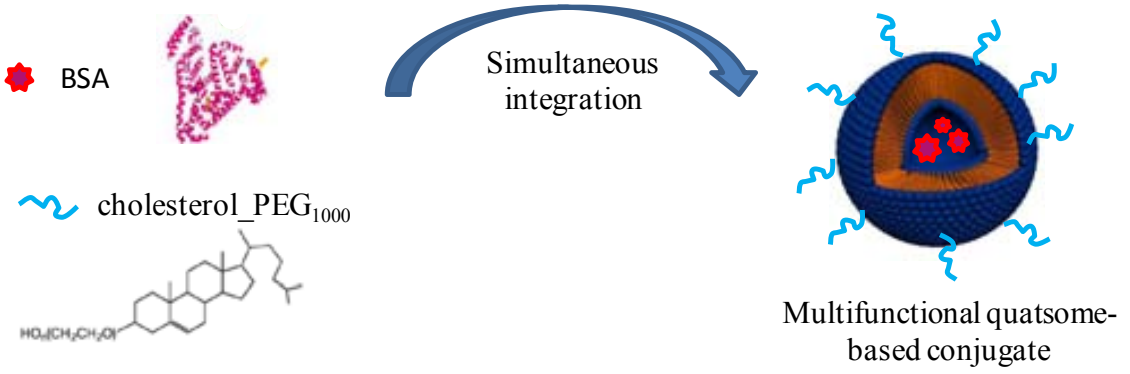

Figure 1.32. Schematic representation of the the simultaneous PEGylation and BSA integration in quatsomes.

The methodology provided multifunctional conjugates with nanoscopic size, homogenous size distribution and high Z potentials. The entrapment efficiency of BSA in the vesicles, determined by the Micro BCA™ protein assay kit, was also high with a value of 84 % (Table 1.2). As observed from the Figure 1.33, the vesicles presented a homogenous morphology similar to those obtained for the quatsomes based-conjugates previously described.

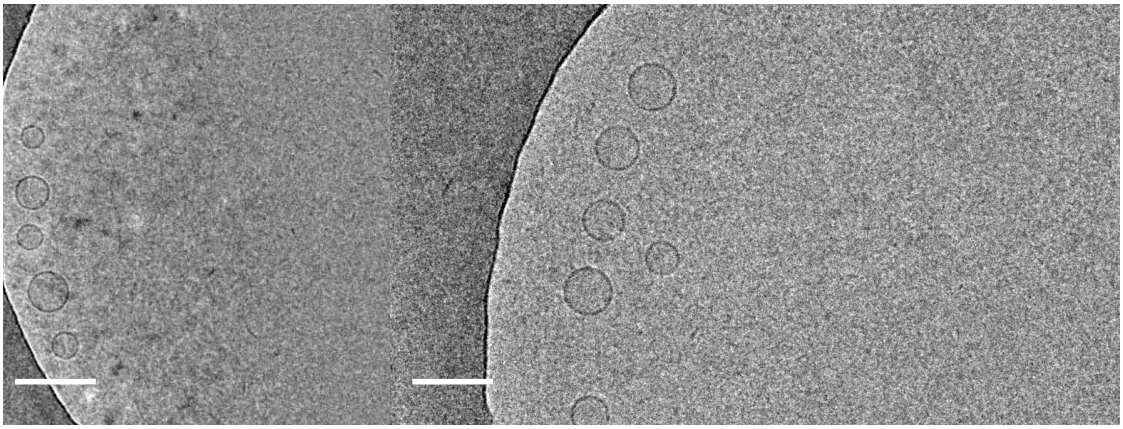

Figure 1.33. Cryo-TEM image of BSA loaded-quatsome_PEG_{1000} conjugates. Scale bar is 100 nm

The stability of the suspension under the storage conditions, evaluated through the evolution in the Z potential, showed that after 5 months the conjugates were still very stable (Figure 1.34). The size of the conjugates also kept constant during this time with no changes in the particle size distribution (Experimental section 3.4.1) and no signs of phase separation in the vesicular suspension.

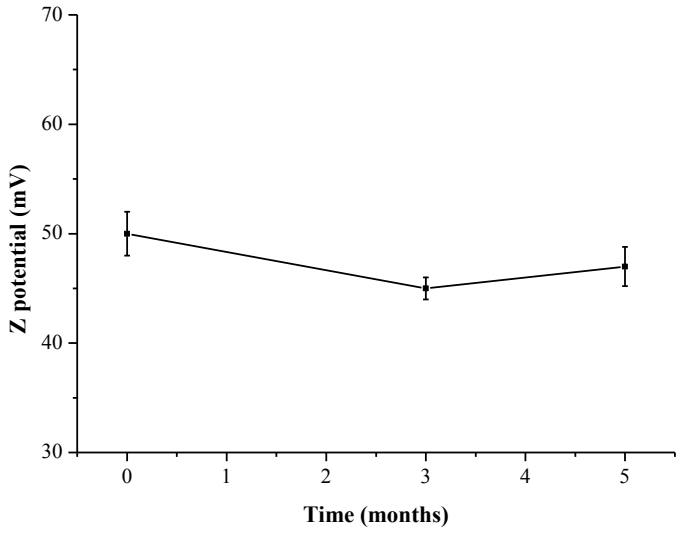

Figure 1.34. Evolution of the Z potential with time for the BSA loaded-quatsome_PEG_{1000} conjugates under storage conditions at 277 K.

These results show that the reported methodology allows for the preparation of multifunctional quatsomes conjugates with a high structural homogeneity in terms of size and lamellarity, high protein loadings and with great stability along time.

1.3.4 Scaling-up production of quatsome-bioactive conjugates using DELOS-SUSP

While the use of vesicles as models of biomembranes is confined to the research laboratory, their successful application in the entrapment and delivery of bioactive agents will depend not only on a demonstration of the superiority of the vesicle carrier for the intended purpose, but also upon technical and economic feasibility of the formulation[58]. Despite all the existing methodologies for vesicle manufacturing at lab-scale, only a very few liposomal products have reached the pharmaceutical market. Among the reasons that prevent a wider use of these systems for human benefit, the low reproducibility, the inefficient drug entrapment and the high cost and difficulty of up-scaling the production, are perhaps the more important ones. An ideal methodology for producing vesicles at industrial scale would be one that allows obtaining vesicle formulations with suitable and batch-to-batch reproducible characteristics, involving a minimum number of steps and equipments, and also meeting the requirements of the pharmaceutical industry and the good manufacturing practices (GMP).

Bench-scale to clinical-scale reproducibility has been checked to evaluate the potentiality of the DELOS-SUSP as a platform for the production of nanovesicle-bioactive conjugates that provides sufficient quantities for clinical studies. The encapsulation of BSA (1 mg/mL) in quatsomes, as a model formulation, was repeated under the same experimental conditions but in a 40-fold larger high pressure reactor (from 7.5 mL to 315 mL) using the same equipment configuration with minor modifications in the automation procedure. For the scale-up experiment the cholesterol (3.8 g) was dissolved in EtOH and introduced in the reactor already warmed at 308 K. After 15 min of thermal equilibration, CO_2 was introduced to achieve the desired working pressure and molar ratio of CO_2 (X_{CO2}= 0.6). After 45 min, the CO_2-expanded solution was depressurized through a one-way automatic valve into a T mixer, to an aqueous solution containing CTAB (3.4 g) and BSA (16 μM), pumped at 900 mL/min. Details of the experimental procedure and the equipment configuration are given in Experimental Section 2.1.2. With this scale-up the batch volume of the resulting vesicle suspension was increased from milliliter up to liter scale, which could allow the production of nanomedicine batches to be used in pre-clinical and even clinical studies. The influence of DELOS-SUSP scale-up on the physicochemical characteristics of the BSA-loaded quatsomes was analyzed in terms of size, morphology and entrapment

efficiency. The results are reported in Table 1.4 together with the results obtained in the small scale reactor for comparison.

Table 1.4. Physicochemical characteristics of the different vesicular formulations obtained by DELOS-SUSP method with different reactors

Vesicle systems	Size		Z potential (mV)	EE (%)	Protein loading[c] (μg/mg)
	Mean [a] (nm)	PdI [b]			
BSA loaded-quatsomes (small scale reactor)	149 ± 12	0.26 ± 0.1	75 ± 7	96 ± 1	179
BSA loaded-quatsomes (large scale reactor)	123 ± 10	0.22 ± 0.01	57 ± 2	99 ± 1	185

[a] Intensity weighted mean hydrodynamic size of the collection of vesicles measured by dynamic light scatering. [b] Polidispersity index showing the width of the particle size distribution. [c] Mass of the integrated protein divided by the total mass of the lipids comprising the membrane

The resulting vesicles showed diameters around 123 nm with narrower particle size distributions, indicating that even a more homogeneous system is obtained at a large scale. The differences in homogeneity are most probably due to the variance of the configuration between the two equipments in the depressurization stage. Thus, in the case of the large reactor, the manual depressurization valve was substituted for an automatic depressurization valve that allows a better operational control and hence a higher vesicle homogeneity and batch-to-batch reproducibility (Experimental Section 2.2). Cryo-TEM images depicted unilamellar and spherical nanovesicles confirming the great degree of homogeneity achieved (Figure 1.35). According to the MicroBCA protein assay, 99 % of BSA was entrapped into the quatsomes prepared with the larger reactor, a value that is similar to that obtained when using the smaller one. Moreover it is important to highlight here that DELOS-SUSP operates under sterile conditions due to the use of compressed CO_2, which is another important issue in the manufacturing of vesicles for human and animal use. The good reproducibility in terms of encapsulation percentages and physicochemical characteristics between batches produced with the two reactors, demonstrate the feasibility of scaling-up the DELOS-SUSP method for the encapsulation of hydrosoluble proteins.

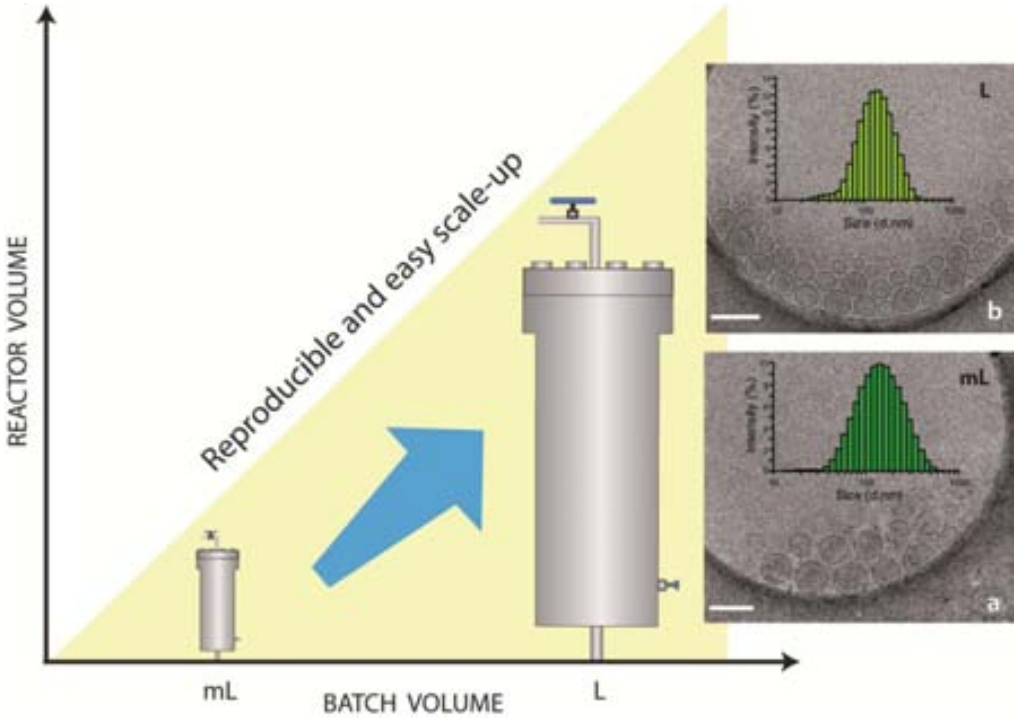

Figure 1.35. Scale-up of DELOS-SUSP method. BSA protein was integrated into quatsomes at a concentration of 16 μM in water using both a small (7.5 mL) and a large (315 mL) high pressure reactors. a) Cryo-TEM image and size distribution of BSA protein loaded quatsomes obtained with the small scale. b) Cryo-TEM image and size distribution of the protein loaded quatsomes obtained with the large scale. Scale bars are 200 nm.

1.4 DELOS-SUSP method for the preparation of liposomes

Although quatsomes are vesicles with outstanding properties its cytotoxicity restricts their use only for dermal delivery purposes. When this PhD Thesis started the DELOS-SUSP methodology was applied only to the preparation of quatsomes. In order to extend DELOS-SUSP to the preparation of other kinds of vesicle systems taking full advantage of the possibilities offered by this process, nanocarriers with different compositions than quatsomes were also undertaken. Phospholipids-based formulations are widely used for drug delivery purposes and for this reason 1,2-dipalmitoyl-*sn*-glycero-3-phosphocholine (DPPC) was selected as a membrane component for the liposome preparation with DELOS-SUSP. DPPC is the major constituent of pulmonary surfactants which controls the dynamic surface tension (DST) and helps maintaining the lung alveoli healthy. It is also one of the most popular phospholipids used for preparing lipid bilayers and model biological membranes[59,60]. Its structure presents a polar head with two hydrophobic tails (Figure 1.36) and unlike cholesterol or CTAB, it forms vesicles by itself in aqueous media. However, vesicles prepared with pure DPPC show a low stability, therefore sometimes they are rigidify by adding cholesterol as a membrane component, which increase enormously the stability of the liposomes[7].

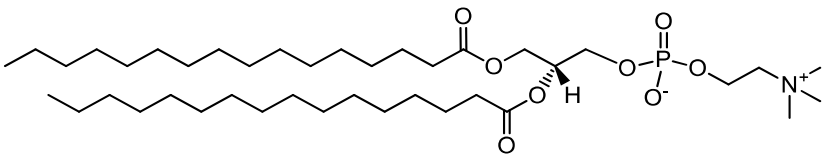

Figure 1.36. Molecular structure of 1,2-dipalmitoyl-*sn*-glycero-3-phosphocholine (DPPC)

DPPC is not water-soluble, presenting a solubility of 30 mg/mL in ethanol. Due to this, in order to produce the liposomes by DELOS-SUSP, both cholesterol and DPPC have to be placed in the organic phase. Therefore the solubility of DPPC in CO_2-expanded ethanol at 10 MPa and 310 K was checked using a variable volume cell. A single phase was formed under such conditions which suggested the suitability of DELOS-SUSP to process this phospholipid (See Experimental section 2.3.1).

The preparation of liposomes was carried out with by adding a solution of ethanol containing both, cholesterol and DPPC into a high pressure reactor (Figure 1.37 a, Table 1.5). Afterwards CO_2 was added in order to form the volumetric expanded organic phase.

The mixture was leave under agitation at 310 K and 10 MPa during one hour in order to attain a complete homogenization and thermal equilibration (Figure 1.37 b). In this case the CO_2 molar fraction was increased up to 0.8 because less amount of organic solvent was used for dissolving the lipids. When the CO_2-expanded solution was depressurized over water, liposomes containing 1.5 mg of total lipids per mL of vesicular suspension were obtained (Figure 1.37 c).

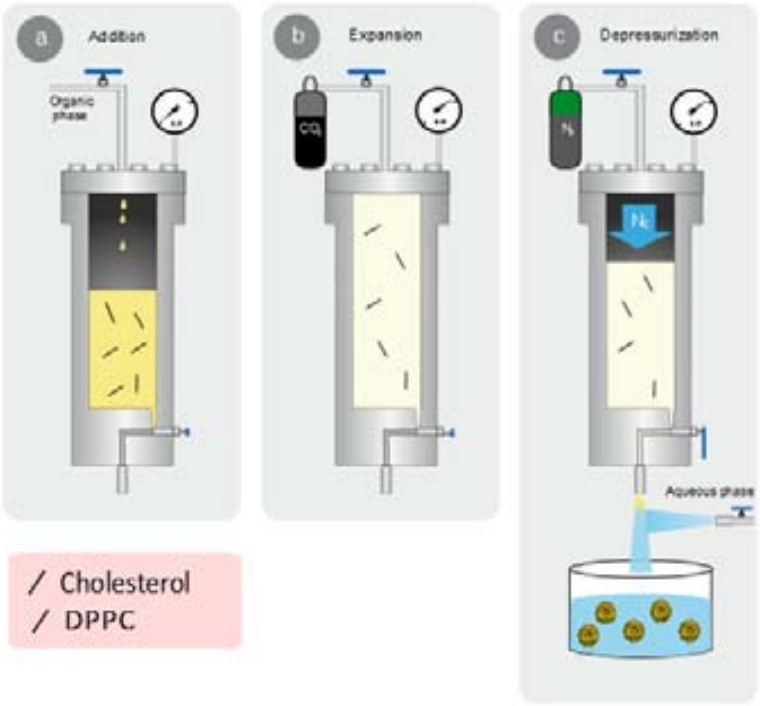

Figure 1.37. Schematic representation of DELOS-SUSP method for the preparation of liposomes composed of cholesterol and DPPC with a 1:1 molar fraction. The procedure includes three stages: a) the loading stage of an organic solution containing cholesterol and DPPC into an autoclave at a working temperature (T_w) and atmospheric pressure; b) the CO_2 addition stage to produce a CO_2-expanded solution, at a given X_{CO2}, working pressure (P_w) and T_w, where the cholesterol and DPPC remain dissolved and c) finally, the depressurization stage of the organic expanded solution over an aqueous solution.

The obtained vesicles were nanoscopic and presented small Z potentials being less stability than the quatsomes (Table 1.6). Indeed signs of some phase separation and solid deposition were observed within the first 15 days after their preparation and storage at 277 K. The morphology of the liposomes, analyzed using Cryo-TEM, was also less homogenous with simultaneous presence of unilamellar and multilamellar vesicles (Figure 1.38).

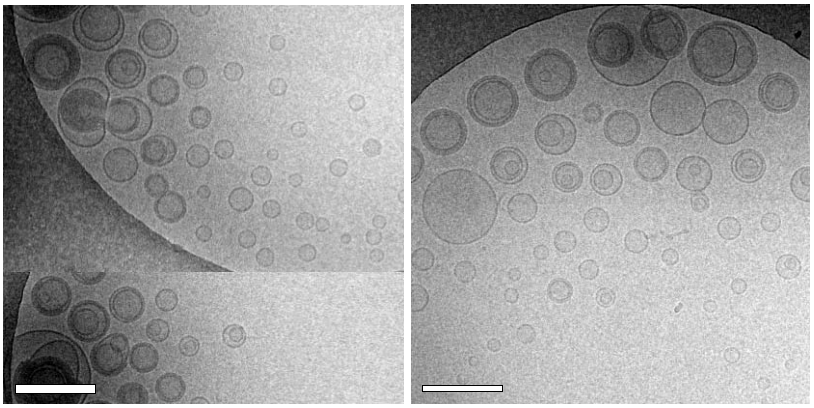

Figure 1.38. Cryo-TEM images of lispomes obtained by DELOS-SUSP

1.4.1 Study of the physicochemical stability of liposomes with temperature

As previously made for quatsomes, the stability of liposomes under different storage temperatures was studied. A sample of liposomes was placed at different temperatures (253, 277, 298 and 310 K) and the physicochemical properties, such as the size and Z potential, were measured after 1, 2, 3, 7 and 15 days. The size was practically constant at all storage temperatures except for 253 K, where an increase in the size from 140 to 190 was observed in two days. As in the case of quatsomes, it is possible that the freezing and thawing processes produced the vesicle aggregation or fusion. The Z potential values decreased during the first three days and then reached a constant value for the assays made at 277, 298 and 310 K. Although there were not big differences for the sizes and Z potentials at the temperatures studied, these properties were slightly better at 277 K. Thus, this temperature was also chosen as optimal for the storage of the liposomes (Figure 1.39)

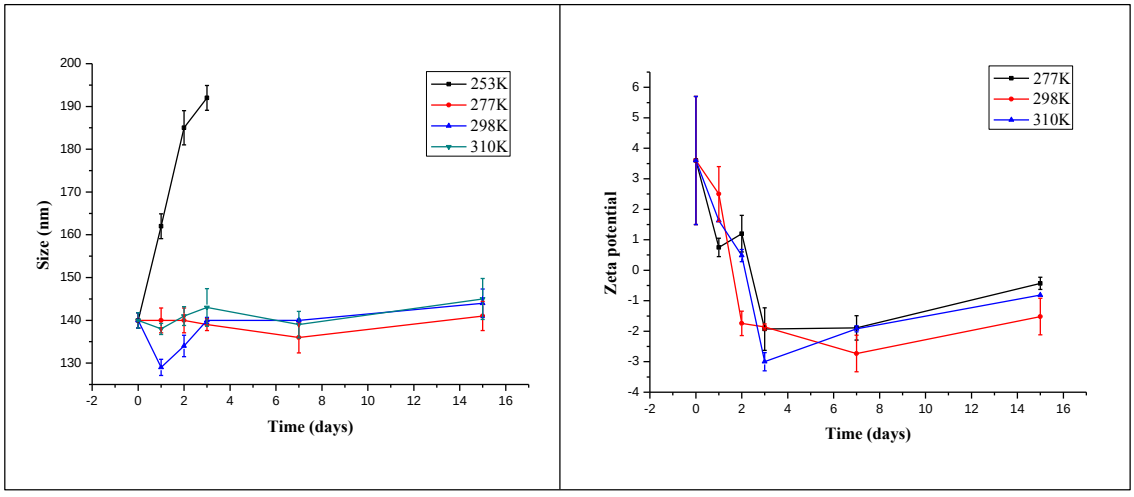

Figure 1.39. Study of the size and Z potential of liposomes with temperature.

1.4.2 Study of the sterility, cytotoxicity and hemocompatibility of liposomes

As made for quatsomes, some basic biological assays were also performed with the liposomes in order to check the suitability of these nanocarriers for being used intravenously. The sterility assay was done in collaboration with the group of Prof. A. Villaverde in the IBB-UAB by measuring their capacity to produce microorganism colonies upon contact with different media. For the assays a vesicle sample (100 µL) were mixed either with water, PBS or culture media in a 6-well plate and incubated overnight at 37^0C (Experimental Section 9.1).

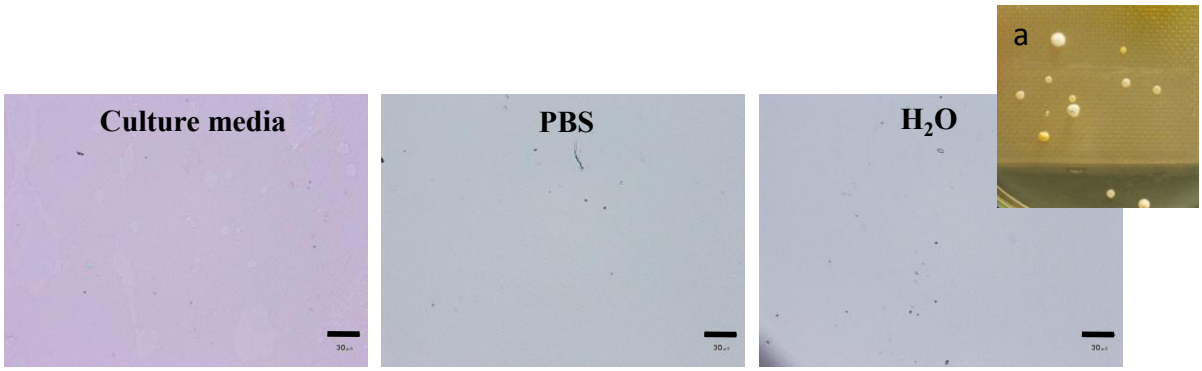

Figure 1.40. Optical microscope images of liposomes after 24 hours of incubation with different media. a) Image of microorganism colonies is shown for comparison purposes. Scale bars are 30 µm.

The presence of colonies in the plate was analyzed visually and using an optical microscope with a coupled camera. No microorganism colonies were observed for any of the three studied media and therefore the liposomes were considered sterile (Figure 1.40). Cytotoxicity assay were carried out by the group of Prof. S. Schwartz from the Vall d'Hebron Hospital. They tested the liposomes in HeLa and HMEC-1 cells using the sulforhodamine B (SRB) assay to reveal their cytotoxicity (Experimental Section 9.2). Figure 1.41 depicts the cytotoxicity graphs of liposomes together with that obtained for quatsomes for comparison. Cell viability of both cell lines was not affected after 72 h incubation with the liposomes at concentrations up to 100 µg/mL, therefore liposomes were considered non-toxic for cells in the concentration range studied.

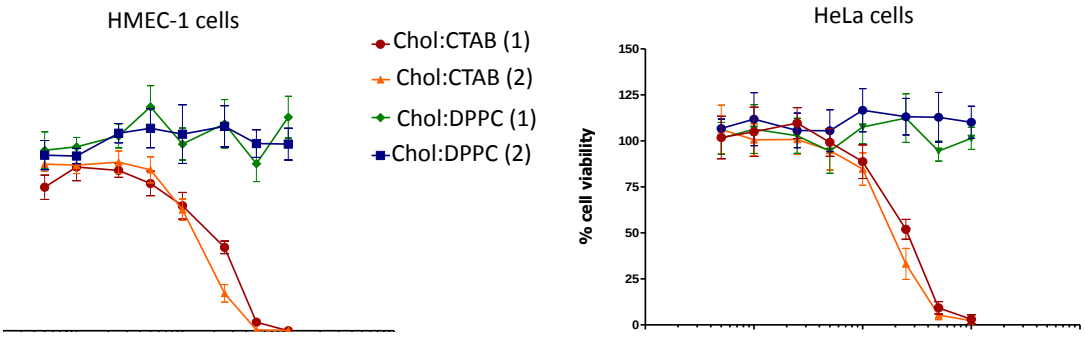

Figure 1.41. Cytotoxicity of liposomes and quatsomes for HeLa and HMEC cell lines. The blue and green lines correspond to two different batches of liposomes.

For the haemocompatibilty assay the liposomes were incubated with red blood cells during 1 hour. After this time there was not release of haemoglobin at any of the concentrations tested, remaining the amount of haemoglobin always below 2% (Figure 1.42).

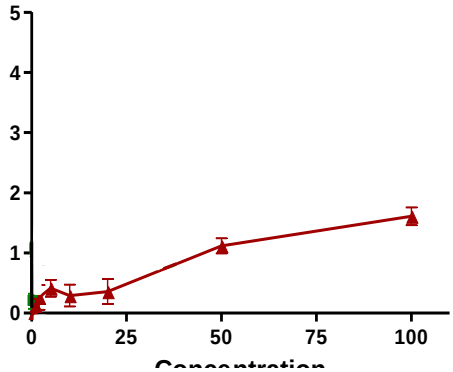

Figure 1.42. Haemocomptibilty of liposomes.

1.4.3 Preparation of liposome-bioactive conjugates using DELOS-SUSP.

Different liposome-bioactive conjugates were prepared with the DELOS-SUSP methodology. For the production of liposome-based conjugates the general procedure was the same as for plain liposomes but the bioactive molecules were added either in the organic or in the aqueous phase, depending on their solubility (Figure 1.43).

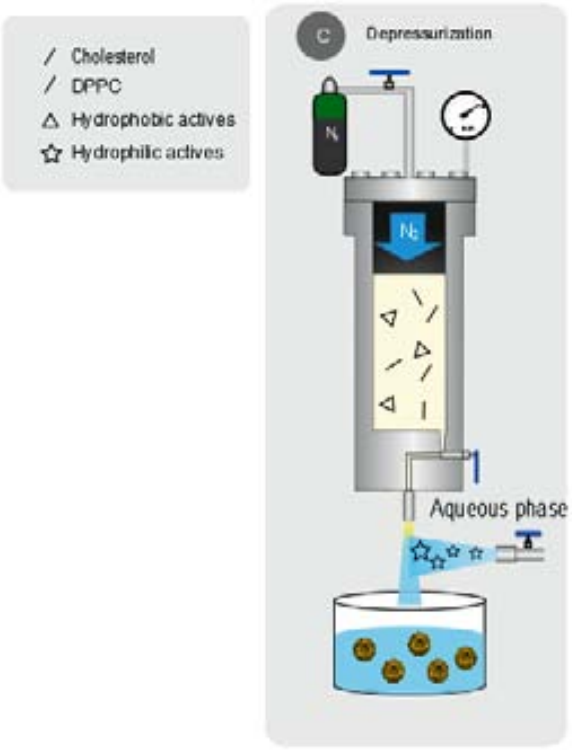

Figure 1.43. Schematic representation of DELOS-SUSP method for the preparation of liposome-based conjugates.

The composition of the organic and aqueous phases used for the preparation of the different vesicular formulations and the physicochemical characteristics of the resulting conjugates prepared are shown in Table 1.5 and Table 1.6, respectively.

Table 1.5. Compositions used for the preparation of the different liposome-based conjugates using the DELOS-SUSP method

Vesicle systems	Organic phase[a]	Aqueous phase[b]	Biom/lipid ratio[c] (μmol/mmol)	Lipidic conc[d]. (mg/mL)
Liposomes	Cholesterol (27 mM) + DPPC (26 mM)	water	-	-
Liposome_PEG_{1000}	Cholesterol (18 mM) + DPPC (27 mM) + $CHOL\_PEG_{1000}$ (3 mM)	water	64	1.4
Liposome_PEG_{2000}	Cholesterol (14mM) + DPPC (27 mM) + $CHOL\_PEG_{2000}$ (2.4 mM)	water	54	1.4
GFP loaded-Liposomes	Cholesterol (26 mM) + DPPC (27 mM)	GFP-H6 (1μM) in TRIS buffer (pH =7.5)	0.4	1.4
Liposome_RGD	Cholesterol (17 mM) + DPPC (27 mM) + $CHOL\_PEG_{200}$–RGD (2.8 mM)	water	59	1.4

Experiments were performed from CO_2-expanded ethanol at 10 MPa and 308 K. [a] Concentration of the membrane components in 1.2 mL of ethanol for liposomes is given. [b]A constant aqueous phase volume of 24 mL was used . [c]Ratio between the total amount of the biomolecule and the total amount of lipids present in the formulation. [d] Ratio between the total amount of lipid forming membrane of quatsomes and the volume of the final vesicular suspension.

Table 1.6. Physicochemical characteristics of the different liposome-based conjugates obtained by the DELOS-SUSP method

Vesicle systems	Size		Z potential (mV)
	Mean (nm)[a]	PdI[b]	
Liposomes	130 ± 9	0.15 ± 0.05	7.0 ± 2.0
Liposome_PEG_{1000}	138 ± 10	0.4 ± 0.10	13.0 ± 2.0
Liposome_PEG_{2000}	135 ± 9	0.47 ± 0.04	8.0 ± 2.0
GFP loaded-Liposomes	228 ± 8	0.42 ± 0.02	-1.2 ± 0.1
Liposome_RGD	144 ± 12	0.25± 0.01	31.0 ± 1.0

[a] Intensity weighted mean hydrodynamic size of the collection of vesicles measured by dynamic light scattering. [b] Polidispersity index.

1.4.3.1 Functionalization of liposomes with fluorescent molecules

Due to the importance of membrane labeling for performing cellular uptake studies, and after the good results obtained for quatsomes, the functionalization of liposomes membrane by incubation with DiD was also performed (Figure 1.44).

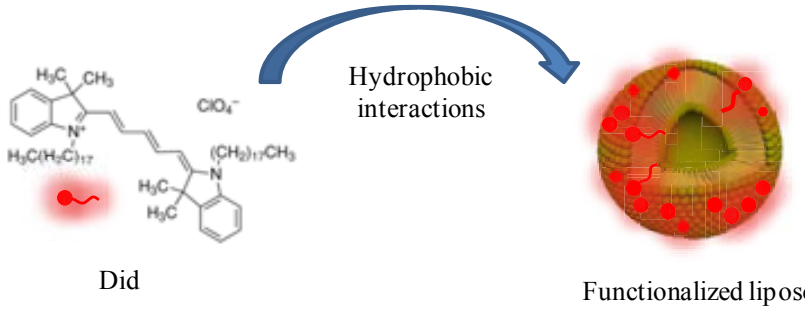

Figure 1.44.. Schematic representation of the functionalization of liposomes with DiD.

For the functionalization of liposomes a small volume of a solution of DiD in ethanol was added to a suspension of liposomes in water (1.4 mg lipids/mL vesicular suspension) in order to have a final concentration of 1 nM. The latter value was selected as the optimum concentration for quatsomes in order to have good EPI-TIRF images. After 30 min of incubation, a small sample was added to a PD S pinTrap G-25 column, previously equilibrated with PBS buffer, with the purpose of eliminate the free dye in the suspension of liposomes by spin centrifugation at 800 × g. The resulting DiD-labeled nanovesicles were then10-fold diluted with PBS buffer and a volume of 200 µl was transferred to a glass coverslip mounted into a microscope chamber and put on the microscope. Imaging was performed on a home-built EPI-TIRF setup equipped with a 37ºC heated chamber (Experimental Section 7.2). Very good TIRF microscopy images were obtained demonstrating the labeling of liposomes by incubation. The morphology of the resulting vesicles was visualized by Cryo-TEM showing that liposomes do not suffer any change after the dye incorporation (Figure 1.45).

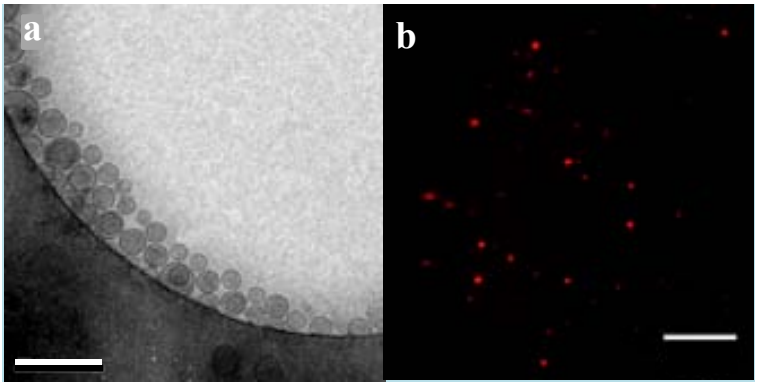

Figure 1.45. Labeling of liposomes with DiD by incubation. a) Cryo-TEM images of labeled liposomes. Scales bar is 200 nm. b) EPI- TIRF microscopy image of labeled liposomes. Scale bar is 5 µm.

1.4.3.2 PEGylation of liposomes

As already mention the most spread strategy to prolong circulation times of vesicles in blood is the functionalization of their membrane with some PEG units. Therefore the PEGylation of the liposomes with PEG units was undertaken using the DELOS-SUSP method, adding either cholesterol_PEG_{1000} or cholesterol_PEG_{2000} as part of the vesicle membrane components (Figure 1.46).

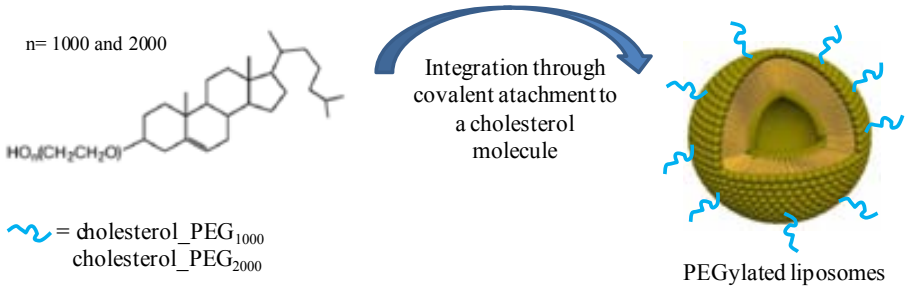

Figure 1.46. Schematic representation of the PEGylation of liposomes through covalent attachment of a PEG molecule to one of the membrane components, in this case the cholesterol.

In all experiments the molar ratio between cholesterol and cholesterol_PEG was 6:1, in order to ensure a molar ratio of PEG below 7%, as explained for the PEGylation of quatsomes. For preparing the liposome-PEG conjugates a solution of cholesterol, cholesterol_PEG and DPPC in ethanol was added to the reactor and pressurized with CO_2. To obtain the conjugates, the volumetric expanded organic phase was depressurized over water. Compositions of the organic and aqueous phases used for the preparation of the PEGylated liposomes are given in Table 1.5. The resulting liposome-PEGs conjugates

were nanoscopic although their sizes and polidispersity were higher than those of quatsome-PEG conjugates (Table 1.6). The Z potentials, with values lower than 30 mV, indicated also a less stability under the storage conditions. Nevertheless, the presence of PEG units increased the stability of the suspensions as compared with plain liposomes (Figure 1.47). While the plain liposomes show a drop in the Z potential as well as some flocculation during the first 15 days, in liposomes-PEGs conjugates the drop is less abrupt and the system remains stable for at least 60 days (Figure 1.47). During this period no vesicle aggregation or fusion was observed as indicated by the particle size distribution measurements (Experimental section 3.4.1).

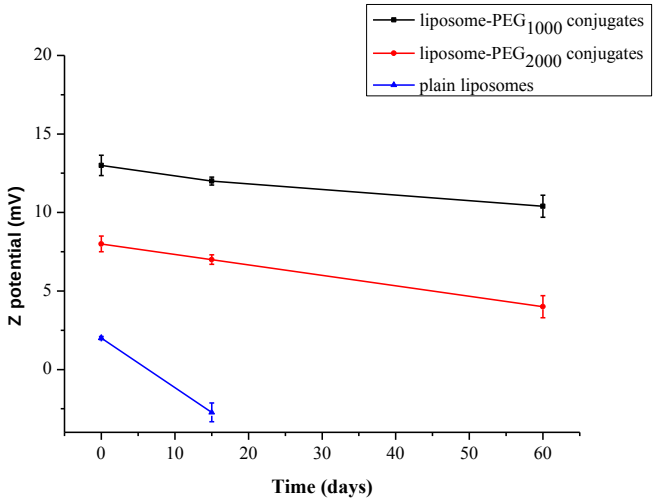

Figure 1.47. Evolution of the Z potential with time. The samples were kept at 4 ^{0}C during the whole study.

The morphology of the samples, determined by the Cryo-TEM images, disclosed spherically shaped and unilamellar vesicles (Figure 1.48).

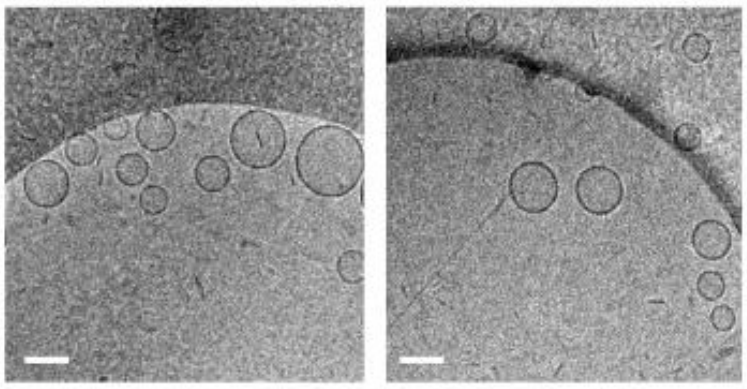

Figure 1.48. Cryo-transmission electron microscopy images of PEGylated liposmes. PEGylated liposomes with cholesterol_PEG_{1000} (left). PEGylated liposomes with cholesterol_PEG_{2000} (right). Scale bars are 100 nm.

Therefore, PEGylated conjugates obtained using DELOS-SUSP have shown very good physicochemical characteristics and homogeneous morphology which make them promising nanocarriers for the delivery of a variety of biomolecules.

1.4.3.3 Preparation of GFP-loaded liposomes

With the entrapment of BSA in quatsomes, it was demonstrated the goodness of DELOS-SUSP to integrate proteins yielding very homogeneous vesicular system, high %EE as well as the feasibility of scaling up such conjugates. The demonstration that the processing conditions used in DELOS-SUSP methodology could be harmless to biomolecule's functionality is also an important issue that needed to be studied before using the conjugates for drug delivery. This was done through the integration of the green florescent protein (GFP). GFP is a widely used protein in biomedicine, whose activity/stability can be easily followed by its intrinsic fluorescence[61,62]. Profiting from this property, GFP was used as a model protein to evaluate the performance of the DELOS-SUSP methodology for encapsulating bioactives molecules ensuring that their biological activity is preserved (Figure 1.49). For this study it was used the GFP-H6 (~27KDa) tagged with six histidine residues, which was produced in the Institut de Biotecnologia i de Biomedicina (UAB) (Experimental Section 5.2).

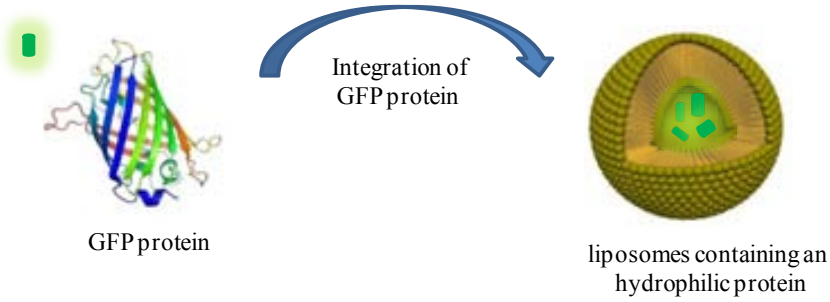

Figure 1.49. Schematic representation of the integration of GFP protein in liposomes.

The preparation of liposome-GFP conjugates was carried out as follows. The reactor was loaded with cholesterol and DPPC in ethanol and pressurized with compressed CO_2. The GFP-H6, kept at -20 ^{0}C, was thawed and dissolved in Tris buffer 25 minutes before performing the depressurization stage. This buffer was used as the aqueous phase because the protein was very stable in this media. The conjugates were formed after depressurize the volumetric expanded organic solution over the aqueous phase (Table 1.5).

The conjugates were prepared twice presenting an average size distribution of 228 ± 8 nm and a low Z potential values (Table 1.6). In spite of such low values the formulations remained macroscopically stable for more than one week, with no changes in the particle size distribution (Experimental Section 3.4.1). Regarding the morphology, Cryo-TEM images revealed the presence of spherical and unilamellar vesicles in both replicates (Figure 1.50).

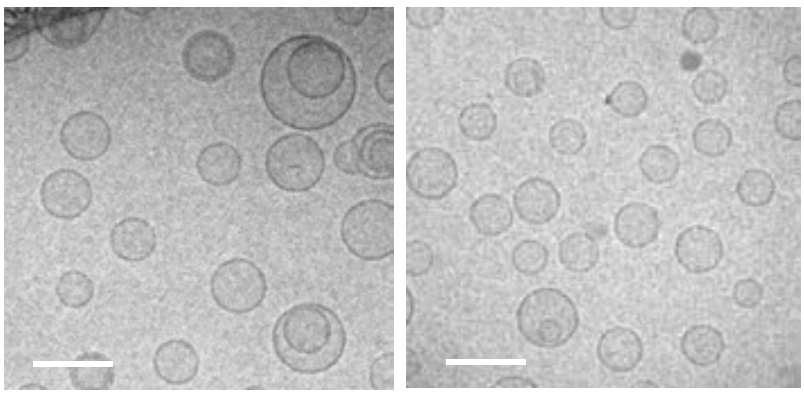

Figure 1.50. Cryo-transmission electron microscopy images of liposomes with integrated GFP protein. Scale bar is 100 nm.

The confirmation of the entrapment of the GFP-H6 protein in the liposomes as well as its fluorescence was assessed using the dual colour total internal reflection fluorescence microscopy in collaboration with the group of Dr. M. Garcia-Parajo from ICFO (Experimental Section 7.2). To performed this experiment DiD was also used as a

membrane marker for labelling the protein-loaded liposomes. To prepare DiD-labelled liposome-GFP conjugates, right after the separation of the free GFP-H6 using centrifugal filter devices, the sample was incubated with DID solution using the same procedure described for the labelling of plain liposomes (Experimental Section 6.2). A small volume of the resulting DiD-labeled liposome-GFP conjugate was deposited on a glass coverslip mounted into a microscope chamber. EPI-TIRF images were collected in two different channels, red and green, to allow the simultaneous monitoring of the signals originated from DiD and GFP, respectively (Figure 1.51). The spatial co-localization of both signals confirmed that the GFP-H6 was successfully incorporated into the liposomes and that its fluorescence was not affected upon processing by DELOS-SUSP

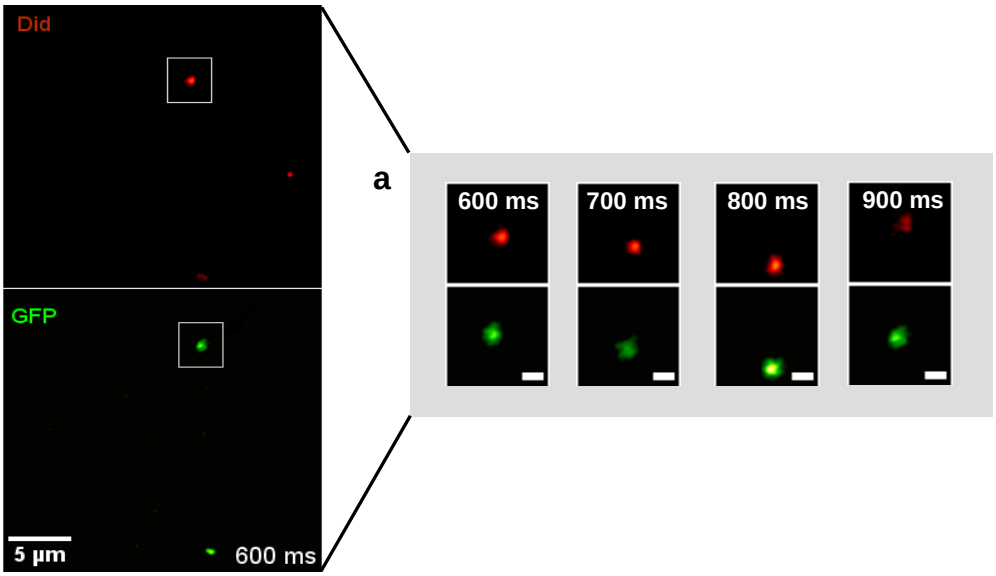

Figure 1.51. Dual color EPI-TIRF microscopy images of liposome-GFP conjugates labeled with DiD. a) Four selected frames from a movie where the movement of the same liposome was followed in two different channels, observing that the two signals remain always in the liposme. Images were taken at 10Hz frame rate.

As discussed before the encapsulation efficiency is an important parameter to be determined for any drug delivery system. So it is crucial to find the right method to separate the non-integrated biomolecules and to quantify the amount of protein in the liposomes. To determine the amount of protein incorporated, the free GFP-H6 was first separated from the system using centrifugal filter devices (100 KDa) and then the loaded vesicles were analyzed by SDS-PAGE and later on by the Western-blot technique (Experimental Sections 4.1.1 and 4.2.2). It is worth to mention that the

quantification could be performed using fluorescence spectrometry by measuring the fluorescence of the different fractions (the loaded vesicles and the diafiltrated waters), with the subsequent extrapolation to a calibration curve to determine the protein content. However the amount of GFP-H6 required to do so, was to large and therefore not available at the moment of the experiments. Hence Western blot technique was used for the quantification. This is a widely accepted analytical technique to detect specific proteins without the need of large amount of biomolecules. It uses gel electrophoresis to separate native proteins by 3-D structure or denatured proteins by the length of the polypeptide. The proteins are then transferred to a membrane (typically of nitrocellulose or PVDF), where they are stained with antibodies specific to the target protein. The protein/lipid loading was calculated using Eq. (2) and the entrapment efficiency (%EE) by the Eq. 3:

$$Entrapment\ efficienty(\%EE) = \frac{massofintagratedactive}{initialmassofactive} * 100 \qquad \text{(Eq. 3)}$$

An entrapment efficiency of 44 ± 7 % of protein encapsulation within the liposomes with a protein/lipid ratio of 8.6 ± 1.4 μg protein/mg total lipid were obtained in the final formulation (Table 1.14). This entrapment efficiency resulted fairly high considering that hydrosoluble proteins generally presents low encapsulations efficiencies, especially in small vesicles with diameters ranging from 50 to 150 nm. Unlike quatsome-BSA conjugate, in this system there is no electrostatic interactions that can contribute to increase the entrapment efficiency. Therefore it is probably the way in which vesicles are produced by the DELOS-SUSP method the key point that promotes the high EE achieved.

1.4.3.4 Functionalization of liposomes with a targeting peptide

Several authors have described the formulation of liposomes where one of the membrane components (ex: phospholipids or cholesterol) are covalently bond to RGD peptides through a PEG linker, for the targeted delivery of therapeutics[11,38,63]. Among the different types of RGD peptides available the cRGDfK was chosen to functionalize the liposomes because it contain a cyclic structure that confers more selectivity and stability to the molecule, and because the presence of a lysine residue makes easier the

further conjugation[64]. In order to use this specific RGD residue, a cholesterol_PEG_{200}_RGD molecule was specially designed and produced by the group of Dr. Miriam Royo (Combinatorial Chemistry Unit, Barcelona Science Park) (Figure 1.52). Although in most of the cases phospholipids molecules are used as the lipid anchor, in this case the cholesterol was selected for the attachment of the RGD peptide. Among the advantages of using cholesterol as a lipid anchor is its higher chemical stability during the storage and the lower cost compared to phospholipid molecules. Besides this sterol is a neutral molecule which can be found as component of most liposomal formulations[50].

In the cholesterol_PEG_{200}_RGD molecule, the cholesterol was first attached to a PEG_{200} unit through an ether bond and the cRGDfK peptide was coupled to this unit through a carbamate bond (Experimental Section 5.1). This cholesterol derivative resulted barely soluble in water or ethanol at room temperature, but soluble in ethanol when heated up.

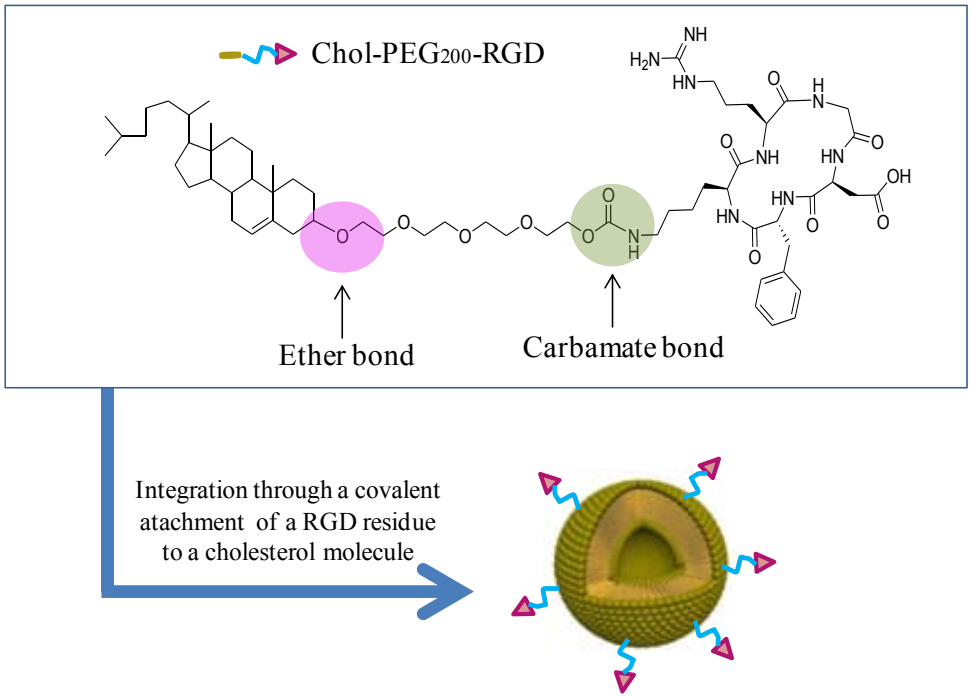

Figure 1.52. Schematic representation of the funtionalization of liposomes with cholesterol-PEG_{200}-RGD molecules. Molecular structure of cholesterol_PEG_{200}_RGD (MW= 1192 g/mol).

For the preparation of liposome-RGD conjugates a mixture of DPPC, cholesterol and cholesterol_PEG_{200}_RGD in a molar ratio of 10:6:1 was dissolved in ethanol and stirred for 90 minutes at 315 K (Table 1.5). The solution was then introduced into the reactor and volumetrically expanded with CO_2. After 1 hour of equilibration, the organic phase

was depressurized over water obtaining a homogeneous vesicle suspension with a narrow particle size distribution (PdI<0.3) centred at 144 nm and with a Z potential of +31 mV (Table 1.6).

To determine the amount of cholesterol_PEG_{200}_RGD incorporated into the membrane, the fraction of non-integrated molecules was separated from the total sample using centrifugal filter devices (30 kDa) (Experimental Section 5.1.1), analyzing the presence of free biomolecules by HPLC. The result of the analysis, performed by the group of Dr. Miriam Royo (Experimental section 4.2.1), showed the absence of free peptide in the mother liquors, resulting in a complete incorporation of the labelled cholesterol within the lipid bilayer. A similar degree of RGD incorporation was achieved by Schiffelers et al. using a multistep methodology[64]. Thus the DELOS-SUSP methodology allows a one-step production of nanoscopic conjugates, with minimum material loss and high yields of the ligand in the final formulation.

Concerning the morphology of the vesicles, Cryo-TEM images surprisingly revealed a much more homogeneous and unilamellar characteristics when cholesterol_PEG_{200}_RGD was inserted into the membrane of liposomes as compared to plain liposomes (Figure 1.54). Other replicas were prepared in order to confirm this unexpected result and liposome-RGD conjugates with similar physicochemical and morphological characteristics were obtained (Figure 1.53)

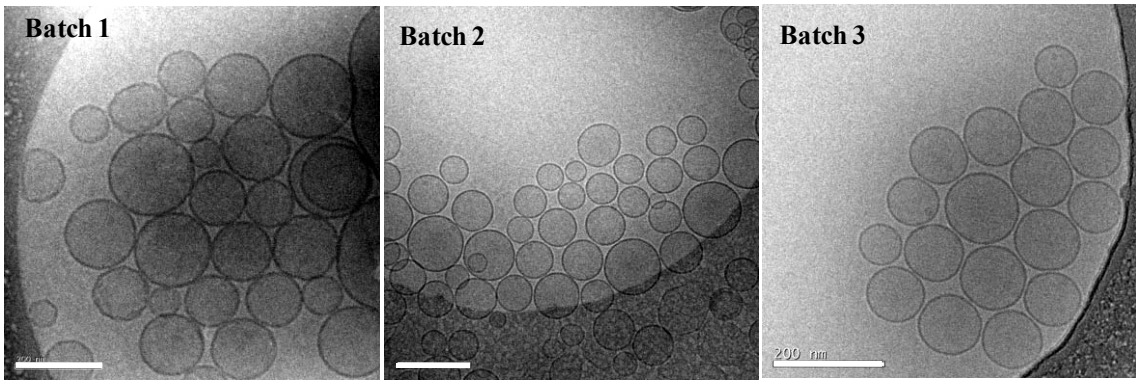

Figure 1.53. Cryo-TEM images of three different batches of liposome-RGD conjugates. Scale bars are 200 nm.

Furthermore, an increase in the Z potential from less than +10 mV up to +30mV was observed when cholesterol_PEG_{200}_RGD was present in the formulation, leading to a higher stability of the dispersion along time. Normally plain liposomes present a low Z potential, and vesicle flocculation is observed since the first week of its preparation.

However the liposome-RGD conjugates remain stable for at least two month, with no signs of vesicle aggregation or flocculation (Experimental section 3.4.1). After this time, some phase separation was observed, in agreement with a drop of the Z potential from around +30 to +7.

To enquire whether these superior properties were related to the use of the DELOS-SUSP method to produce the liposomes or they were exclusively due to the presence of the peptide on the membrane, the liposomes containing cholesterol_PEG_{200}-RGD were prepared, using the conventional lipid thin-film hydration methodology. Solutions of cholesterol, DPPC and cholesterol_PEG_{200}_RGD in chloroform with a molar ratio of 6:10:1 were mixed in a glass vial for a total lipid mass of 1 mg. The solvent was slowly evaporated under N_2 flow to create a thin lipid film and the glass vial was placed under vacuum for 3 hours in order to remove any remaining solvent. The lipid was then hydrated overnight using mQ water, at room temperature. Next, the sample was taken through 10 rounds of freeze/thaw cycles by transferring it between liquid nitrogen and a water bath for finally being extruded through polycarbonate filters with a pore size of 800 nm. More detailed explanation about the preparation of the vesicles with this methodology is included in Experimental Section 2.2. The resulting formulations obtained in the three replica were less homogeneous, highly unstable, multilamellar and with a size distribution centered at 1900 nm (Figure 1.54).

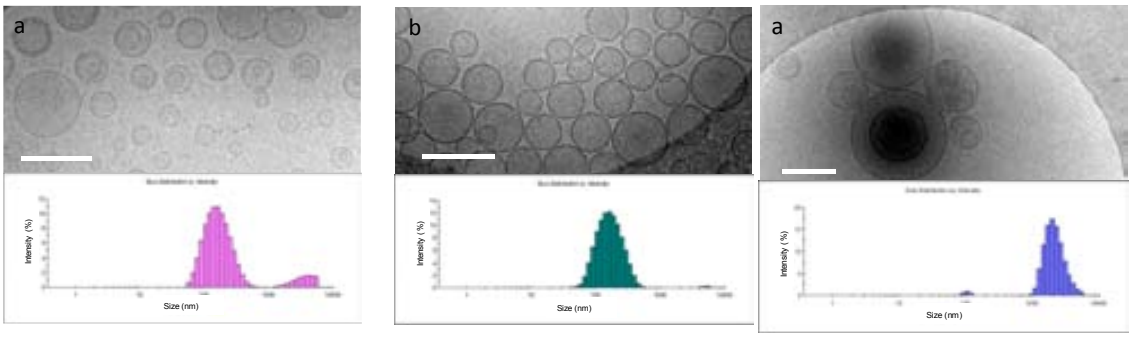

Figure 1.54. Liposome-RGD conjugates and plain liposomes prepared using different methodologies. Plain liposomes prepared using DELOS-SUSP (a), liposome-RGD conjugates prepared using DELOS-SUSP (b) and liposome-RGD conjugates prepared using the lipid thin-film hydration methodology (c).

The higher degree of unilamellarity in the liposome-RGD conjugates was also confirmed with small-angle X-ray scattering (SAXS) measurements (Figure 1.55). The

SAXS data clearly evidenced structural changes of liposomes induced by the preparation route and the functionalization with the RGD peptide. Thus, the SAXS curve of plain liposomes obtained following the lipid thin-film hydration methodology show periodical Bragg peaks (denoted as peaks 1 and 2 in Figure 1.55) indicating that the system is clearly multilamellar. From the q value, we can obtain the repeating distance (d) of these lamellar structures, using the equation $d=2\Pi/q$. In the case of liposomes the repeating distance correspond to the fully hydrated bilayer. Thus, the obtained d value and hence the thickness of a fully hydrated lamella of liposomes prepared by lipid thin-film hydration (red line) is of 6.5 nm. The sharpness of these two peaks is dramatically reduced in the sample prepared by the DELOS-SUSP methodology (black line) indicating that multilamellarity has been significantly decreased without affecting the thickness of the membrane (d= 6.3 nm). The SAXS curve of liposomes-RGD (blue line) corresponds to the profile of mostly unilamellar vesicles with a repeat distance of 7.3 nm. As it was also inferred by the Cryo-TEM images, the introduction of the RGD peptide in the liposome membrane produces a drastic reduction of lamellarity while increasing the bilayer thickness. Details of the SAXS measurements are given in the Experimental Section 3.3.

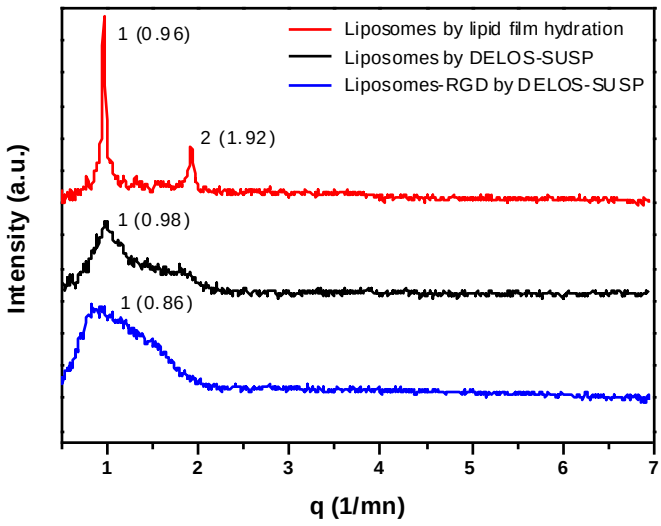

Figure 1.55. SAXS curves showing the influence of the preparation methodology and composition of liposomes in the morphology of vesicles, particularly in their lamellary.

The studies performed up to now demonstrates that both the presence of cholesterol_PEG_{200}_RGD molecule as a membrane component as well as the

preparation methodology are key ingredients for the synthesis of highly homogeneous unilamellar vesicles, with a higher stability along time. On one hand the presence of PEG_{200}_RGD chains in the liposomal membrane seems to be responsible of this, since it is well known that the water solubility and flexibility of the PEG chains prevent liposomes from self-aggregation and fusion processes[65]. On the other hand the DELOS-SUSP method allowed very controlled processing conditions and thus the obtaining of highly organized vesicular structures.

1.4.3.4.1 Influence of the bond between cholesterol and the PEG_{200}_RGD unit in the characteristics of the liposome_RGD conjugates

In most of the cases, the binding between cholesterol and the PEG_RGD unit is through a carbamate or ester bonds[66]. However in our case this union is through an ether bond. In order to study if this small difference could influence the final physico-chemical characteristics and the bioactivity of the conjugates an alternative liposome_RGD vesicles were prepared with a cholesterol(carb)_PEG_{200}_RGD molecule containing a carbamate union between cholesterol and PEG_{200} (Figure 1.56). The molecule was also synthesized by the group of Dr. Miriam Royo. The liposome conjugate with this component was obtained by DELOS-SUSP using same conditions as for the derivative with ether bond, resulting in liposomes named as liposome(carb)_RGD.

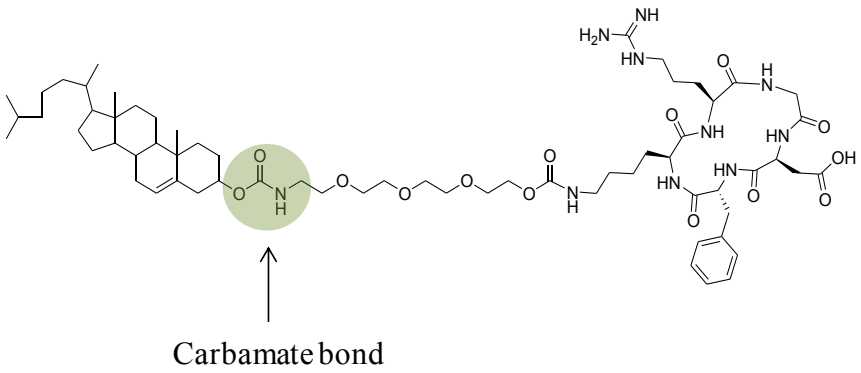

Figure 1.56. Molecular structure of cholesterol(carb)-PEG_{200}-RGD containing a carbamate union between the cholesterol and the PEG unit (MW= 1235 g/mol).

The liposome(carb)_RGD conjugates resulted very similar regarding the macroscopic appearance and the physicochemical characteristics than the liposome_RGD with the ether bond (Table 1.15). Thus, sizes were around 140 nm and the Z potentials were close to +30 mV, indicating a higher stability in time comparing with plain liposomes.

Cryo-TEM images (Figure 1.57) disclosed vesicles with spherical morphology and with a higher unilamellarity that plain liposomes.

Table 1.7. Physicochemical characteristics of liposome-RGD conjugates with ether and carbamate bonds

Vesicle system	Size		Z potential (mV)
	Mean (nm)[a]	PdI[b]	
liposome_RGD	144 ± 12	0.20 ± 0.01	31.0 ± 1.0
liposome(carb)_RGD	136 ± 3	0.35 ± 0.04	28.0 ± 0.3

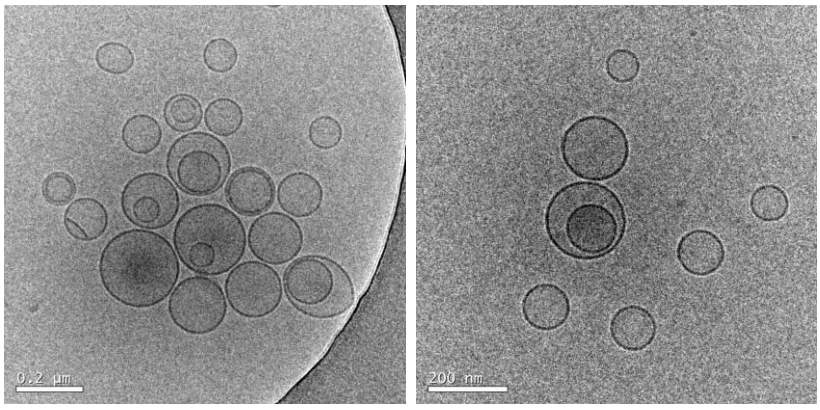

Figure 1.57. Cryo-TEM images of liposome(carb)-RGD conjugates with carbamate bond in its structure. Scale bar are 200 nm.

1.4.3.5 Liposome-RGD conjugates as a novel platform for drug delivery

The suitability of liposome-RGD conjugates for the delivery of APIs was assessed by different in-vitro experiments performed in collaboration with the groups of Dr. M. Garcia-Parajo (ICFO institute) and Dr. Schwartz (Vall d'Hebron Hospital).

1.4.3.5.1 Sterility, cytotoxicity and hemocompatibility

In-vitro sterility, cytotoxicity and hemocompatibility assays were performed with the liposome_RGD conjugates. The sterility test of the conjugates was performed as with quatsomes, showing that the samples were sterile generating less than 100 CFU/mL (Experimental Section 9.1). The cytotoxicity was tested with HeLa and HMEC-1 cells by the SRB method (Experimental Section 9.2). Cell viability of both cell lines was not

affected after 72 h incubation of conjugates at concentrations up to 20 µg of lipid per mL of solution. No differences were observed between plain and RGD-containing liposomes (Figure 1.58), indicating that addition of the RGD moiety was not affecting the cell proliferation and viability.

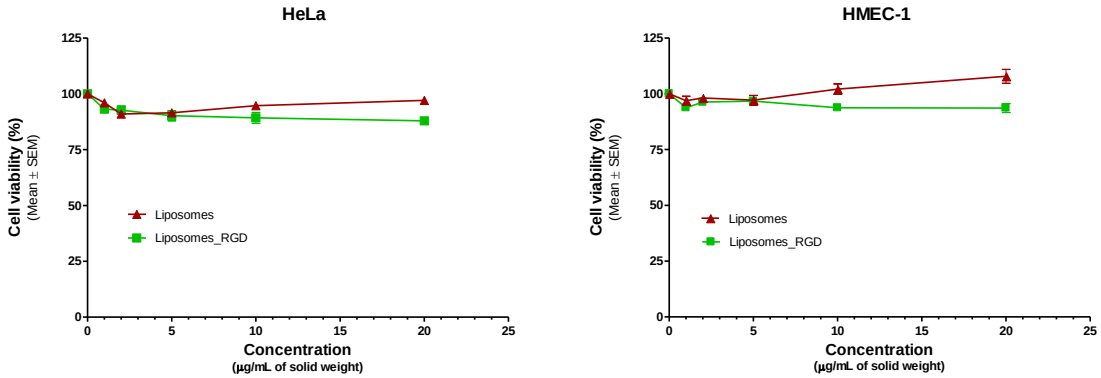

Figure 1.58. Cytotoxicity of liposome-RGD conjugates and plain liposomes.

Hemocompatibility assay was performed by incubating the nanovesicles with red blod cells (Experimental Section 9.3). This incubation did not induced the release of haemoglobin at any of the concentrations tested in the assays, remaining the amount of haemoglobin released after 1 h incubation always below a level of 2% (Figure 1.59).

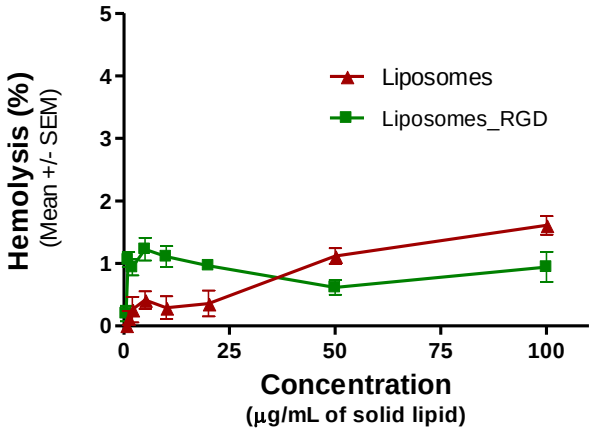

Figure 1.59. Hemocompatibility of liposome-RGD conjugates and plain liposomes.

1.4.3.5.2 Cellular uptake experiments

A special concern with regard to the design of drug delivery systems for lysosomal disorders deals with the design of nanocarriers able to release the drug at the endo-

lysosomal compartments. To investigate the specific lysosomal targeting and to check whether the activity of the integrated biomolecule was maintained after the processing with CO_2-expanded solvents, we examined the internalization capabilities of the liposome-RGD conjugates on endothelial (HMEC-1) cells which express high levels of $\alpha_v\beta_3$ integrins on both their apical and basal membranes, as depicted in Figure 1.60.

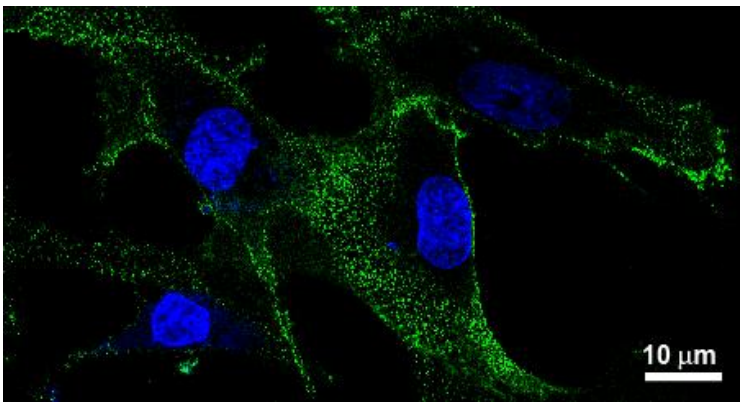

Figure 1.60. Confocal image of HMEC-1 cells labelled with an anti-$\alpha_v\beta_3$ specific antibody (green). Cells nuclei are labelled (blue) with DAPI.

For this experiment the fluorescent the DiD dye was also integrated into liposome-RGD conjugates and plain liposomes, used as blank control, at a concentration of 1 nM following the same procedure described in section 1.5.3.1. HMEC-1 cells were then incubated with DiD-labelled liposomes with and without RGD, for 3 hours at 37ºC in a 5% atmosphere of CO_2, to induce the internalization and were subsequently inspected by laser scanning confocal microscopy (LSCM) following the procedure described in the Experimental Section 7.3. Liposome-RGD conjugates were rapidly uptaken by the cells (Figure 1.61 a) whereas the control plain liposomes were barely internalized (Figure 1.61 b). Importantly, a fraction of liposome-RGD conjugates trafficked to endosomal/lysosomal compartments as judged by co-localization studies with the DiD (red) fluorophore and the lysotracker (green), a fluorescent probe which labels and tracks acidic organelles in live cells. Indeed, three-dimensional reconstructions of z-stacked fluorescence images of live HMEC-1 cells showed a co-localization between DiD-labelled liposome-RGD conjugates and lysotracker after 3 h of incubation at 37ºC (Figure 1.61 c). These data strongly indicate that the RGD peptide on the liposomes membrane enhances their binding and uptake by HMEC-1 cells via $\alpha_v\beta_3$ integrin-mediated endocytosis. The results were further confirmed on a large population of cells

using flow cytometry analysis (Experimental Section 7.4). About 85% of the cells showed enhanced fluorescence when incubated with DiD-labelled liposome-RGD conjugates at 37ºC, whereas this percentage was reduced to 4% for cells incubated with DiD-labelled liposomes (Figure 1.61 d). Furthermore, a decrease in the fraction of positive cells was observed when cells were incubated with DiD-labeled liposome-RGD conjugates at 16ºC, a temperature that reduces the endocytosis (Figure 1.61 d). The mean fluorescence intensity (MFI) values measured for HMEC-1 cells incubated with DiD-labeled liposome-RGD conjugates was 30-fold higher than that of the cells incubated with DiD-labeled plain liposomes (Figure 1.61 e), demonstrating that the presence of the peptide is responsible for the enhanced liposome uptake levels. These studies also confirm that the DELOS-SUSP methodology did not affect the bioactivity of the RGD peptide after its processing with compressed CO_2.

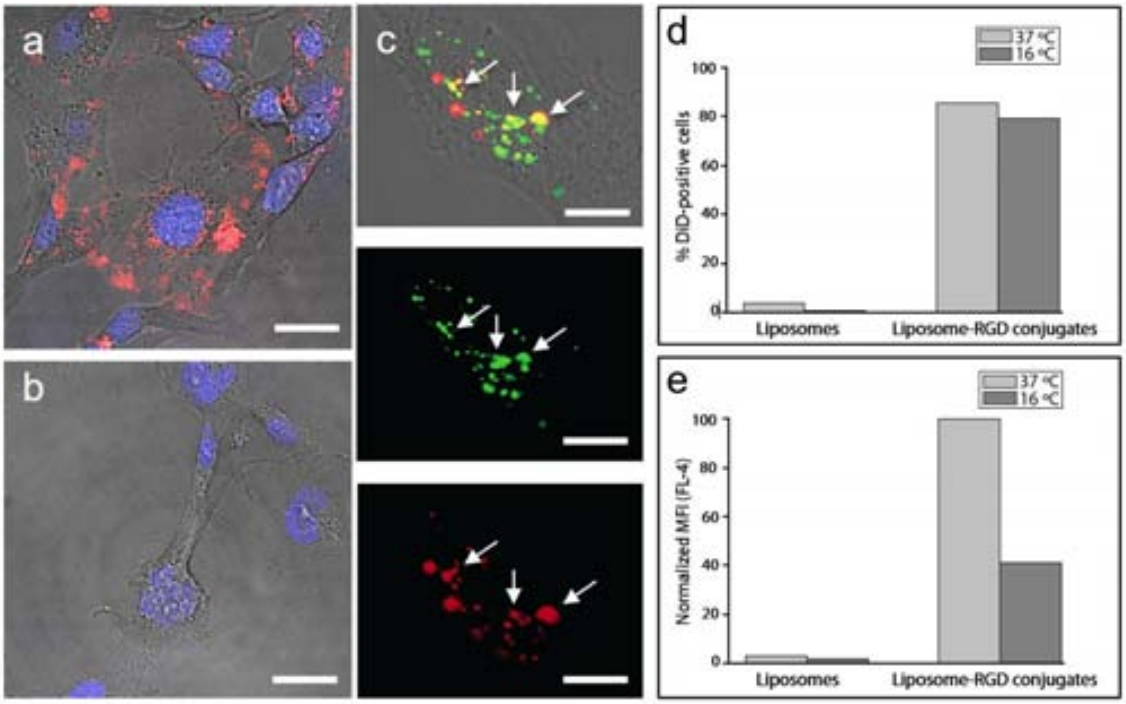

Figure 1.61. Internalization of liposome_RGD conjugates on endothelial cells assessed by fluorescence. Confocal images of HMEC-1 cells incubated with (a) liposomes-RGD (red) at 0.3 mg/mL and (b) plain liposomes at 0.3 mg/mL. Cells nuclei were stained with Hoechst 33342 (blue). (c) Colocalization of liposomes-RGD (red) and the lysotracker (green), as observed by confocal microscopy. The upper image shows the merging of both signals, where the arrows highlight the co-localization of liposomes-RGD with lysosomal compartments. Independent signals are shown in the lower panels. (d) Flow cytometry quantification of the fraction of cells that had bound or internalized plain liposomes and liposome-RGD conjugates as the percentage (%) of DiD-positive cells among the total number of cells counted. (e) Mean fluorescence intensity of DiD in the cells normalized to the maximum fluorescence intensity. Cells were incubated with the liposomes for 3 hours at 16°C or 37°C. All scale bars are 10μm.

1.4.3.5.3 Influence of the bond between cholesterol and PEG_{200}_RGD in the conjugates activities.

The influence of the different bonds in the cholesterol_PEG200_RGD molecules in the in-vitro behaviour of the conjugates was study by cellular uptake experiments. For this purpose both conjugates were labelled with DiD by their incubation with the dye in an ethanolic solution, for a final concentration of 50 nM of DiD in the membrane (Experimental section 6.2). After 30 min of mixing, free DiD was separated from the total sample by centrifugation using PD SpinTrap G-25 columns. A blank sample of plain liposomes was also labelled and included in the study. For the cellular uptake experiment, assessed by laser scanning confocal microscopy (LSCM), HMEC-1 cells were seeded onto Fluorodish culture plates at a density of 2×10^5 cells per plate and allowed to grow for 36-48 hours. 50 µl of DiD-labelled liposomes or DiD-labelled the two liposome-RGD conjugates with union ether or carbamate, were mixed with 200 µl MCDB 131 medium, added into the cells and incubated for 3 h at 37ºC in a humidified atmosphere with 5% CO_2. Subsequently, cells were washed with serum-free MCDB 131 and incubated at 37ºC for 5 min with Lysotracker Green to label the endosomal/lysosomal compartments. Cells were examined under an inverted laser scanning confocal microscope (Experimental Section 7.3). Confocal images of the cellular uptake of plain liposomes and the two liposome-RGD conjugates are shown in the Figure 1.62.

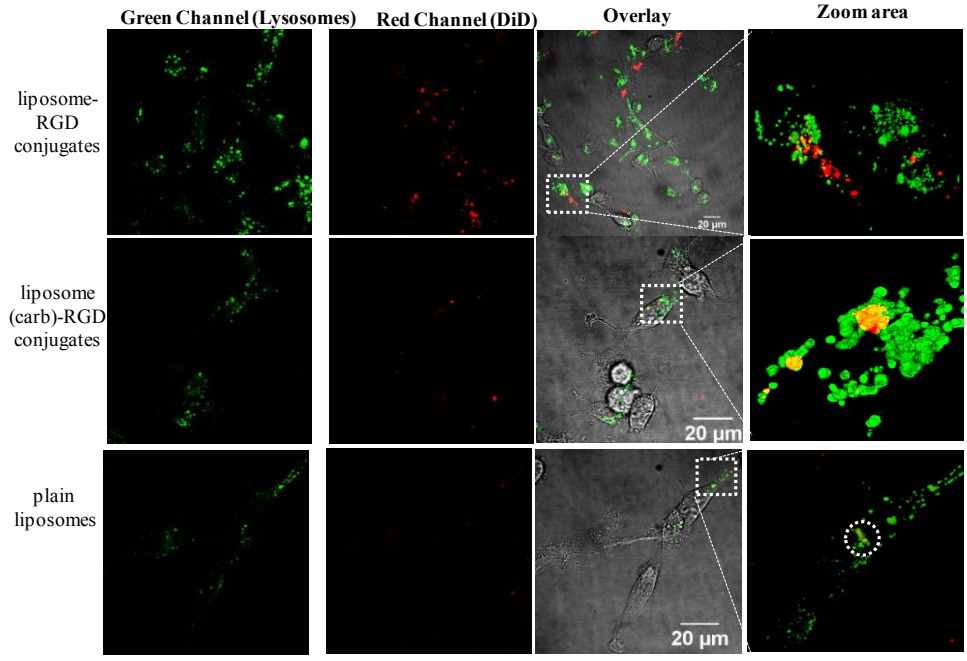

Figure 1.62. Confocal images of the cellular uptake of liposome-RGD conjugate with ether or carbamate bonds, and plain liposomes.

The spots observed in the red channel show the presence of labelled liposomes internalized by the cells. It is clearly observed that for the conjugates with the ether bond this internalization is higher than for the conjugates with the carbamate union. As expected, little internalization was observed for plain liposomes. In the zoomed areas, the co-localization of liposomes-RGD (red) and the lysotracker (green) is observed which again confirm the presence of the conjugates in the lysosome.

This qualitative result was afterwards confirmed by flow cytometry (Experimental section 7.4)**.** Same labelling and incubation protocols than before were followed. The only difference was at the end of the incubation where cells were washed twice with Dulbecco´s phosphate buffered saline (DPBS) solution and detached using trypsin and re-suspended in cell culturing medium before subjecting to fluorescence-activated cell sorting analysis. Data acquisition and analysis was performed using FACS scan (Beckton-Dickinson) and BD FACS Diva software. 10^4 viable cells were evaluated in each experiment. Figure 1.63 shows the fluorescence intensity associated to the cells that have internalized the DID-labelled liposomes. It is shown that this internalisation was significantly higher when using the conjugates with ether bond. The fluorescence intensity for plain liposome was again very small, almost cero confirming the confocal results.

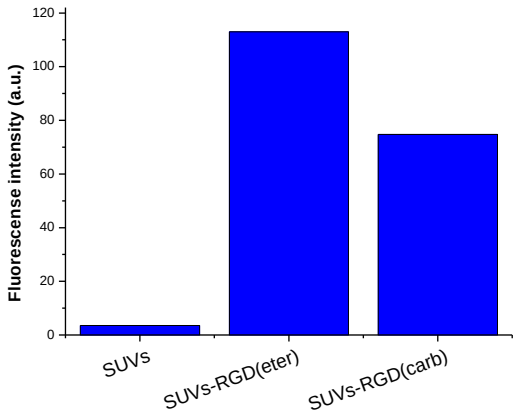

Figure 1.63. Celullar uptake assessed by flow citometry

Surprisingly, the type of bond between the cholesterol and the PEG unit exerted an influence in the in-vitro behaviour of the nanocarriers. The differences found between the two conjugate systems could lay on the differences in flexibility and/or lability of

the two bonds. Carbamate bond is more rigid and more susceptible to hydrolysis than the ether bond. This susceptibility of carbamate union might produce the detaching of PEG_{200}-RGD units from the vesicles so less particle reach the cells after 3 hours of incubation.

In conclusion, the good physico-chemical properties and in-vitro behavior of these new functionalized liposomes can be very advantageous in their production, handling and use for drug delivery purposes.

1.5 Summary and Conclusions

For quatsomes:

- ✓ DELOS-SUSP methodology enables an easy and direct preparation of different quatsome-biomolecule conjugates with nanoscopic sizes, good stability in time and great degrees of unilamelarity.
- ✓ The DELOS-SUSP methodology allows not only the functionalization with protective/targeting units or the integration of hydrophilic proteins with high entrapment efficiency percentages but also the simultaneous incorporation of two biomolecules for the obtaining of multifunctional conjugates.
- ✓ The possibility of scaling-up the method for the encapsulation of hydrosoluble proteins was demonstrated by the good reproducibility in terms of encapsulation percentages and physicochemical characteristics between batches produced with the two reactors of different volumes.
- ✓ Quatsomes prepared by DELOS-SUSP fulfill the structural and physico-chemical requirements to be considered a promising platform for the topical delivery of synthetic or natural APIs.

For liposomes:

- ✓ DELOS-SUSP methodology allows an easy and direct preparation of different liposome-biomolecule conjugates with nanoscopic sizes and great degrees of unilamelarity.
- ✓ The stability along time of the liposome-based conjugates is somewhat smaller than those of quatsomes-based conjugates. Nevertheless this stability can be improved by the addition of stabilizing/targeting units to the formulation.
- ✓ Bioactivity of the integrated biomolecules is unaffected under the processing conditions with CO_2-expanded solvents.
- ✓ Liposomes, and in particular liposome-RGD conjugates, prepared by DELOS-SUSP, fulfill the structural and physico-chemical requirements to be considered a promising platform for the intravenous delivery of synthetic or natural APIs.

1.6 References

1 Allen, T. M. & Cullis, P. R. Drug delivery systems: Entering the mainstream. *Science* **303**, 1818-1822, (2004).

2 Peer, D. *et al.* Nanocarriers as an emerging platform for cancer therapy. *Nature Nanotechnology* **2**, 751-760 (2007).

3 Couvreur, P. & Vauthier, C. Nanotechnology: intelligent design to treat complex disease. *Pharmaceutical research* **23**, 1417-1450, (2006).

4 Farokhzad, O. C. & Langer, R. Impact of Nanotechnology on Drug Delivery. *ACS Nano* **3**, 16-20, (2009).

5 Ganta, S., Devalapally, H., Shahiwala, A. & Amiji, M. A review of stimuli-responsive nanocarriers for drug and gene delivery. *Journal of Controlled Release* **126**, (2008).

6 Torchilin, V. P. Recent advances with liposomes as pharmaceutical carriers. *Nature reviews. Drug discovery* **4**, (2005).

7 Christopher KIRBY, J. C. a. G. G. Effect of the Cholesterol Content of Small Unilamellar Liposomes on their Stability in vivo and in vitro. *Biochem. J.* **186**, 591-598 (1980).

8 Elizondo, E. *et al.* in *Progress in Molecular Biology and Translational Science* Vol. Volume 104 (ed Villaverde Antonio) 1-52 (Academic Press, 2011).

9 Ryan, S. M., Mantovani, G., Wang, X. X., Haddleton, D. M. & Brayden, D. J. Advances in PEGylation of important biotech molecules: delivery aspects. *Expert Opin. Drug Deliv.* **5**, 371-383, (2008).

10 Immordino, M. L., Dosio, F. & Cattel, L. Stealth liposomes: review of the basic science, rationale, and clinical applications, existing and potential. *International journal of nanomedicine* **1**, 297-315 (2006).

11 Cressman, S., Dobson, I., Lee, J. B., Tam, Y. Y. C. & Cullis, P. R. Synthesis of a labeled RGD-lipid, its incorporation into liposomal nanoparticles, and their trafficking in cultured endothelial cells. *Bioconjugate Chemistry* **20**, 1404-1411 (2009).

12 Sawant, R. R. & Torchilin, V. P. Liposomes as 'smart' pharmaceutical nanocarriers. *Soft Matter* **6**, 4026, (2010).

13 Duncan, R. & Gaspar, R. Nanomedicine(s) under the Microscope. *Mol. Pharm.* **8**, 2101-2141, (2011).

14 Malam, Y., Loizidou, M. & Seifalian, A. M. Liposomes and nanoparticles: nanosized vehicles for drug delivery in cancer. *Trends Pharmacol. Sci.* **30**, 592-599, (2009).

15 Petros, R. A. & DeSimone, J. M. Strategies in the design of nanoparticles for therapeutic applications. *Nature reviews. Drug discovery* **9**, 615-627 (2010).

16 Hussain, S., Pluckthun, A., Allen, T. M. & Zangemeister-Wittke, U. Antitumor activity of an epithelial cell adhesion molecule-targeted nanovesicular drug delivery system. *Mol. Cancer Ther.* **6**, 3019-3027, (2007).

17 Colletier, J. P., Chaize, B., Winterhalter, M. & Fournier, D. Protein encapsulation in liposomes: Efficiency depends on interactions between protein and phospholipid bilayer. *BMC Biotechnology* **2** (2002).

18 Glavas-Dodov, M. *et al.* 5-Fluorouracil in topical liposome gels for anticancer treatment - Formulation and evaluation. *Acta Pharmaceutica* **53**, 241-250 (2003).

19 Szoka, F. *et al.* Preparation of unilamellar liposomes of intermediate size (0.1-0.2 μm) by a combination of reverse phase evaporation and extrusion through polycarbonate membranes. *BBA - Biomembranes* **601**, 559-571 (1980).

20 Kubo, T. *et al.* Targeted delivery of anticancer drugs with intravenously administered magnetic liposomes in osteosarcoma-bearing hamsters. *International journal of oncology* **17**, 309-315 (2000).

21 Templeton, N. S. *et al.* Improved DNA: Liposome complexes for increased systemic delivery and gene expression. *Nature Biotechnology* **15**, 647-652 (1997).

22 Yatvin, M. B., Weinstein, J. N., Dennis, W. H. & Blumenthal, R. Design of liposomes for enhanced local release of drugs by hyperthermia. *Science* **202**, 1290-1293 (1978).

23 Mayer, L. D., Hope, M. J. & Cullis, P. R. Vesicles of variable sizes produced by a rapid extrusion procedure. *BBA - Biomembranes* **858**, 161-168 (1986).

24 Olson, F., Hunt, C. A., Szoka, F. C., Vail, W. J. & Papahadjopoulos, D. PREPARATION OF LIPOSOMES OF DEFINED SIZE DISTRIBUTION BY EXTRUSION THROUGH POLYCARBONATE MEMBRANES. *Biochimica Et Biophysica Acta* **557**, 9-23, (1979).

25 Elzainy, A. G., XC ; Simons, FER ; Simons, KJ Hydroxyzine- and cetirizine-loaded liposomes: Effect of duration of thin film hydration, freeze-thawing, and changing buffer pH on encapsulation and stability. *Drug Development and Industrial Pharmacy* **31**, 281-291 (2005).

26 Meure, L. A., Foster, N. R. & Dehghani, F. Conventional and dense gas techniques for the production of liposomes: a review. *AAPS PharmSciTech* **9**, 798-809, (2008).

27 Eaton, M. A. W. Improving the translation in Europe of nanomedicines (a.k.a. drug delivery) from academia to industry. *Journal of controlled release : official journal of the Controlled Release Society* **164**, 370-371, (2012).

28 Beh, C. C., Mammucari, R. & Foster, N. R. Lipids-based drug carrier systems by dense gas technology: A review. *Chemical Engineering Journal* **188**, 1-14, (2012).

29 Nora Ventosa, S. S., and Jaume Veciana. Depressurization of an Expanded Liquid Organic Solution (DELOS): A New Procedure for Obtaining Submicron- or Micron-Sized Crystalline Particles. *Crystal Growth & Design* **1**, 299-303 (2001).

30 Cano-Sarabia, M. *et al.* Preparation of uniform rich cholesterol unilamellar nanovesicles using CO2-expanded solvents. *Langmuir* **24**, 2433-2437 (2008).

31 Marques, E. F. Size and Stability of Catanionic Vesicles: Effects of Formation Path, Sonication, and Aging. *Langmuir* **16**, 4798-4807, (2000).

32 Ahmed, F. & Discher, D. E. Self-porating polymersomes of PEG–PLA and PEG–PCL: hydrolysis-triggered controlled release vesicles. *Journal of Controlled Release* **96**, 37-53, (2004).

33 Lidia Ferrer-Tasies, E. M.-C., Mary Cano-Sarabia, Marcel Aguilella-Arzo, Angelina Angelova, Sylviane Lesieur, Susagna Ricart, Jordi Faraudo, Nora Ventosa, and Jaume Veciana Quatsomes: Vesicles Formed by Self-Assembly of Sterols and Quaternary Ammonium Surfactants. *Langmuir* **29**, 6519-6528 (2013).

34 Elizondo, E. *et al.* Influence of the preparation route on the supramolecular organization of lipids in a vesicular system. *Journal of the American Chemical Society* **134**, 1918-1921, (2012).

35 Elizondo, E. New molecule-based nanostructured drug carriers prepared using compressed fluids. *Thesis, Universidad Autónoma de Barcelona, Spain* (2010).

36 Clement Mugabe, A. O. A. a. A. O. Liposome-mediated gentamicin delivery: development and activity against resistant strains of Pseudomonas aeruginosa isolated from cystic fibrosis patients. *J. Antimicrob. Chemother.* **55**, 269-271 (2005).

37 Zhang, L. *et al.* The use of PEGylated liposomes to prolong the circulation lifetime of salvianolic acid B. *Fitoterapia* **83**, 678-689, doi:10.1016/j.fitote.2012.02.004 (2012).

38 Dubey, P. K., Mishra, V., Jain, S., Mahor, S. & Vyas, S. P. Liposomes modified with cyclic RGD peptide for tumor targeting. *Journal of drug targeting* **12**, 257-264, (2004).

39 Murphy, E. A. *et al.* Nanoparticle-mediated drug delivery to tumor vasculature suppresses metastasis. *Proc Natl Acad Sci U S A* **105**, 9343-9348, (2008).

40 Goddard, P. Therapeutic proteins- a pharmaceutical perspective. *Advanced drug delivery reviews* **6**, 103-131 (1991).

41 Pisal, D. S., Kosloski, M. P. & Balu-Iyer, S. V. Delivery of therapeutic proteins. *Journal of pharmaceutical sciences* **99**, 2557-2575, (2010).

42 Hubbell, J. A. Enhancing drug function. *Science* **300**, 595-596 (2003).

43 Luisa Corvo, M. *et al.* Superoxide dismutase entrapped in long-circulating liposomes: Formulation design and therapeutic activity in rat adjuvant arthritis. *Biochimica et Biophysica Acta - Biomembranes* **1564**, 227-236 (2002).

44 Kisel, M. A. *et al.* Liposomes with phosphatidylethanol as a carrier for oral delivery of insulin: Studies in the rat. *International Journal of Pharmaceutics* **216**, 105-114 (2001).

45 Xu, X., Costa, A. & Burgess, D. J. Protein encapsulation in unilamellar liposomes: high encapsulation efficiency and a novel technique to assess lipid-protein interaction. *Pharmaceutical research* **29**, 1919-1931, (2012).

46 Heurtault, B., Saulnier, P., Pech, B., Proust, J. E. & Benoit, J. P. Physico-chemical stability of colloidal lipid particles. *Biomaterials* **24**, 4283-4300, (2003).

47 Reflection paper on the data requirements for intraveneous liposomal products developed with reference to an innovation liposomal product. *European MedicinesAgency, http://www.ema.europa.eu/ema/index.jsp?curl=pages/regulation/general/general_content_000564.jsp&mid=WC0b01ac05806403e0* (2013).

48 Salvatore Chiantia, J. R., Petra Schwille. Fluorescence correlation spectroscopy in membrane structure elucidation. *Biochimica et Biophysica Acta* **1788**, 225–233 (2009).

49 Moghimi, S. M., Hunter, A. C. & Murray, J. C. Long-circulating and target-specific nanoparticles: Theory to practice. *Pharmacological Reviews* **53**, 283-318 (2001).

50 Zhao, X. B., Muthusamy, N., Byrd, J. C. & Lee, R. J. Cholesterol as a bilayer anchor for PEGylation and targeting ligand in folate-receptor-targeted liposornes. *Journal of pharmaceutical sciences* **96**, 2424-2435, (2007).

51 Radler, J. O., Koltover, I., Salditt, T. & Safinya, C. R. Structure of DNA-cationic liposome complexes: DNA intercalation in multilamellar membranes in distinct interhelical packing regimes. *Science* **275**, 810-814, (1997).

52 Temming, K., Schiffelers, R. M., Molema, G. & Kok, R. J. RGD-based strategies for selective delivery of therapeutics and imaging agents to the tumour

vasculature. *Drug resistance updates : reviews and commentaries in antimicrobial and anticancer chemotherapy* **8**, 381-402, (2005).

53 Kulkarni, S. B., Betageri, G. V. & Singh, M. FACTORS AFFECTING MICROENCAPSULATION OF DRUGS IN LIPOSOMES. *J. Microencapsul.* **12**, 229-246, (1995).

54 Talsma, H. a. C., D.J.A. Liposomes as drug delivery systems. Part 1. **16**, 96-106 (1992).

55 Yokouchi, Y. *et al.* Effect of adsorption of bovine serum albumin on liposomal membrane characteristics. *Colloids and Surfaces B: Biointerfaces* **20**, 95-103 (2001).

56 Dai, C., Wang, B., Zhao, H., Li, B. & Wang, J. Preparation and characterization of liposomes-in-alginate (LIA) for protein delivery system. *Colloids and surfaces. B, Biointerfaces* **47**, 205-210, (2006).

57 Martins, S., Sarmento, B., Ferreira, D. C. & Souto, E. B. Lipid-based colloidal carriers for peptide and protein delivery - Liposomes versus lipid nanoparticles. *International journal of nanomedicine* **2**, 595-607 (2007).

58 Mozafari, M. R. Liposomes: An overview of manufacturing techniques. *Cellular and Molecular Biology Letters* **10**, 711-719 (2005).

59 Lopez-Pinto, J. M., Gonzalez-Rodriguez, M. L. & Rabasco, A. M. Effect of cholesterol and ethanol on dermal delivery from DPPC liposomes. *International Journal of Pharmaceutics* **298**, 1-12, (2005).

60 Cieślik-Boczula, K., Petrus, R. M., Köhler, G., Lis, T. & Koll, A. Interaction of Piperidin Derivative of Mannich Base with DPPC Liposomes. *The Journal of Physical Chemistry B* **117**, 2938-2946, (2013).

61 Chalfie, M., Tu, Y., Euskirchen, G., Ward, W. W. & Prasher, D. C. Green fluorescent protein as a marker for gene expression. *Science* **263**, 802-805 (1994).

62 Nasevicius, A. & Ekker, S. C. Effective targeted gene 'knockdown' in zebrafish. *Nature Genetics* **26**, 216-220 (2000).

63 Fenske, D. B. & Cullis, P. R. Vol. 391 7-40 (2005).

64 Schiffelers, R. M. *et al.* Anti-tumor efficacy of tumor vasculature-targeted liposomal doxorubicin. *Journal of Controlled Release* **91**, 115-122 (2003).

65 Carrion, C., Domingo, J. C. & de Madariaga, M. A. Preparation of long-circulating immunoliposomes using PEG–cholesterol conjugates: effect of the spacer arm between PEG and cholesterol on liposomal characteristics. *Chemistry and Physics of Lipids* **113**, 97-110 (2001).

66 Thompson, B. *et al.* Neutral postgrafted colloidal particles for gene delivery. *Bioconjugate Chemistry* **16**, 608-614 (2005).

Chapter 2: Study of the interaction of hydrophilic protein BSA with CTAB based quatsomes

2.1 Introduction

In the last decades, several new pharmaceutically active proteins have been developed as a consequence of the progress of biotechnological techniques and genetic engineering[1-3]. From a therapeutic perspective, proteins offer the advantage of specific mechanism of action and of been highly potent. Despite these advantages, therapeutic proteins are usually very fragile, present short plasma half-life, poor *in vitro* and *in vivo* stability, immunogenicity and limited ability to cross cell membranes[4-6]. Several strategies have been evaluated in an effort to improve the current limitations of therapeutic proteins in the creation of the so-called ‘‘second generation’’ protein therapeutics. One approach to this would be the entrapment of those biomolecules into a particulate carrier system, such as liposomes, by either their encapsulation within the liposome or by chemical conjugation to the surface groups[7-9]. Liposomes can protect proteins against degradation in vitro and in vivo and offer the opportunity to deliver them directly into cells or even inside individual cellular compartment[10]. The ampiphillic nature of phospholipids, more specifically the presence of an aqueous core and hydrophobic bilayer, make them suitable for use with protein therapeutics displaying a wide variety of biophysical characteristics. Liposomes also allow the intravenous injection of lipophilic drugs with very low water solubility, reducing therefore the toxicity of such drugs[11]. However, chemical and physical stability problems have been described leading to liposome aggregation and drug degradation during storage, compromising therefore the performance of liposome as intravenous drug carriers[6,12]. Moreover there are still problems in order to achieved reproducible particle distribution characteristics and high drug loadings into liposomes, particularly for hydrophilic proteins. Is then still of high interest to find new carriers that protect these therapeutic proteins against premature degradation, increase their stability upon storage and allow high entrapment efficiencies without any bioactivity loss.

2.1.1 Quatsomes as carrier for drug delivery

As already mention in Chapter 1, quatsomes are nanoscopic vesicles composed by quaternary ammonium type surfactants (QUATs) and sterols. An important feature of quatsomes is that none of their individual components spontaneously aggregate into

vesicular structures, since in water the QUATs surfactants are in the form of micelles and/or monomers, depending on their concentration, and insoluble sterol species form crystals. The structural characteristics of these new vesicles have been studied in Nanomol group by experimental techniques and theoretical calculations[13]. As a result of these studies, now is known that in cholesterol:CTAB quatsomes, the cholesterol and CTAB molecules work as a unique bimolecular synthon that can be considered as a single entity. This synthon presents a structure similar to that of phospholipids molecules (e.g DPPC, DOPC, etc), which self-assembles in particularly stable and homogeneous vesicles (Figure 2.1). Theoretical simulations indicates that in the quatsomes, the cholesterol molecules are incorporated in the hydrophobic region of the bilayer (avoiding contact with water) and CTAB molecules arrange into two- layered leaflets with the headgroups in contact with water and the tails in the interior of the bilayer.

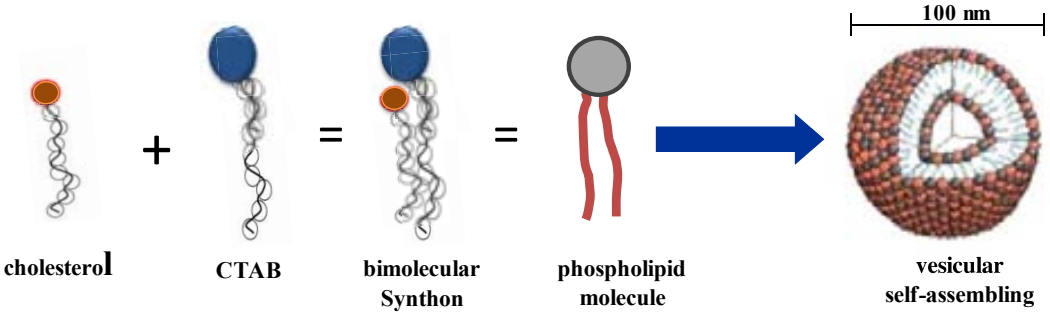

Figure 2.1. Representation of the synthon formed by cholesterol and CTAB and its similarity with a phospholipid molecule

The cholesterol:CTAB quatsomes show an outstanding stability with time, indeed they can be storage for more than 1 year without any change in their physico-chemical properties. Besides this colloidal carriers remain stable with temperature changes and upon dilution, contrary to QUATs micelles which structures are strongly affected with these two parameters[14]. Moreover the homogeneous morphology of quatsomes and their highly ordered membrane supramolecular organization make this system ideal for the precise functionalization of their membranes, which is very important for a robust and efficient drug targeting[15-17]. Another important characteristic of quatsomes is that their membrane components are not expensive and are available at pharmaceutical grade. For instance the surfactants forming the quatsomes membranes are part of the QUACs family, widely used as disinfectants, algaecides, preservatives, detergents and

antistatic[18]. Finally the molecules can be simultaneously integrated in quatsomes, either by covalent attachment to sterol like molecules or by electrostatic interaction with the cationic ammonium head of surfactant units, by hydrophobic interaction with the bilayer or in the inner aqueous lumen. All the described physico-chemical characteristics induced us to explore the suitability of quatsomes as new colloidal drug delivery system.

In Chapter 1, quatsomes-based carriers were presented as suitable platform for the integration of different biomolecules using the DELOS-SUSP methodology. Indeed their membranes were efficiently functionalized with protective/targeting units and hydrophilic proteins like BSA were integrated. Particularly surprising was the high entrapment efficiency percentage achieved for the BSA protein in quatsomes (96 ± 1.3%), taking into account that the hydrophilic biomolecules present lower %EE in liposome structures[19,20]. For instance Dai et *al.* report between 43 and 71 % of BSA encapsulation in multivesicular liposomes composed of phospholipids and cholesterol, prepared using the double emulsification process. The conjugates obtained were in all cases very stable with narrow structural characteristics distributions (size, morphology, lamellarity), making these vesicles very attractive for drug delivery purposes. The unexpected results achieved prompted us to study more deeply the quatsomes as new delivery system of hydrophilic proteins. Thus in this chapter it is thoroughly investigated the interaction of CTAB based quatsomes with BSA, as a model hydrophilic protein. Additionally the impact of protein loading in quatsomes supramolecular structures is addressed.

2.1.2 The bovine serum albumin (BSA) as model protein

Due to its fluorescence properties, low cost and extensive use in different protein-membrane and protein-surfactant interactions, BSA was chosen as the model protein in this study (Figure 2.2). In its native state, it has a molar mass of 66.4 kDa and possesses about 583 amino acids with 17 disulfide bonds and one free cystein group. It has relatively high water solubility because of its large number of ionizable amino acids. BSA can bind many different types of amphiphilic biological molecules, which are believed to play an important role in determining the physiological function[21]. BSA is a transport protein; it possesses numerous sites for ligand binding. Depending on the nature of the ligand, the binding site on BSA varies. The heart-shaped BSA has three

domains; domain I (charge: −10) and domain II (charge: −8) are negatively charged, whereas domain III is neutral at physiological pH [22,23].

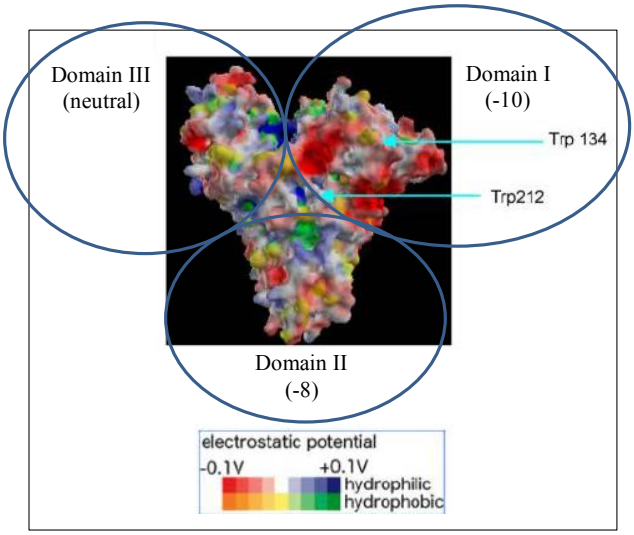

Figure 2.2. Structure of BSA protein at physiological pH. Adapted from 22

Fluorescence emission in BSA is attributed to two tryptophan residues in the protein at positions 134 and 212 (Figure 2.2). Trp212 residue is located in the largest hydrophobic cavity of the protein known as Sudlow's site I, whereas Trp134 is located on the surface of the domain I. The intensity of the fluorescence emission and the maximum wavelength for the BSA is expected to change with the change in the environment of these Trp[24,25]. These changes may be due to variety of physicochemical phenomena like surfactant binding, protein association/dissociation, protein conformational change or combination of all these.

2.2 Study of the interaction of BSA with CTAB micelles

The presence of the quaternary ammonium head in CTAB molecule confers to the membrane of quatsomes a positive charge. In Chapter 1 (section 1.3.3.1) it was shown that this positive charge enables membrane functionalization through electrostatic interactions with different sort of anionic molecules. When the concentration of the anionic charge was equal of larger than that of the cationic charge of CTAB, the quatsome became unstable. These results pointed out the importance of the interaction with the CTAB in the quatsome stability and physicochemical characteristics. Since BSA was positively charge under the entrapment conditions, the large %EE achieved for this protein was also attributed to the interaction with the positively charge membrane. In order to get a better understanding of the role of CTAB in the functionalization and encapsulation processes, the interactions between BSA and pure CTAB in the form of micelles were studied before studying the interactions between this hydrophilic protein and cholesterol:CTAB quatsomes. This interaction was analyzed following two approaches: by studying the influence of BSA in the demicellization process and by adding BSA to a solution of micelles in a wide range of BSA/CTAB molar ratios.

2.2.1 Influence of BSA in the CTAB demicellization process.

CTAB is a cationic surfactant from the families of QUATs. A surfactant (a contraction of the term surface-active agent) is an amphiphilic structure which contains a structural group that has very little attraction for the solvent, known as lyophobic group, together with a group that has strong attraction for the solvent, called the lyophilic group. In aqueous systems, which constitute by far the largest number of surfactant applications, the hydrophobic (lyophobic) group generally includes a long hydrocarbon chain, and less often a halogenated or oxygenated hydrocarbon or siloxane chain. The hydrophilic (lyophilic) group is constituted by an ionic or highly polar group that gives some water solubility to the molecule group[26] (Figure 2.3).

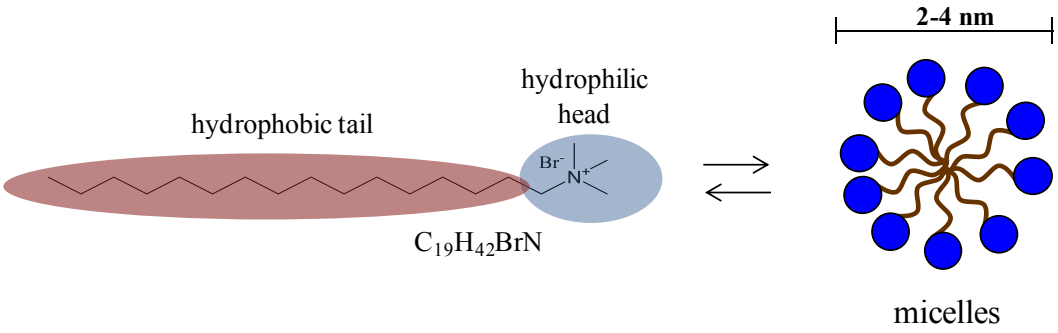

Figure 2.3. Structure of the hexadecyltrimethylammonium bromide surfactant (CTAB) monomers and their supramolecular organization forming micelles.

Above a concentration value known as "critical micelle concentration" (CMC), CTAB self-assemble into micelles. These micellar structures are formed because when the amphiphilic molecules are mixed with water, the hydrophilic regions interact favorably and tend to dissolve in the solvent, whereas the hydrophobic region tends to avoid contact with water (Figure 2.3). The overall phenomenon is termed the hydrophobic effect[27]. The CMC value for a given surfactant in a given medium will depend on temperature, pressure, and on the presence and concentration of other substances that might interact with it (e.g other surfactants, electrolytes, etc)[14]. The CMC of CTAB in water at 298 K is 1 mM[28]. In order to characterize the interaction of BSA with CTAB, it was investigated the influence of this protein in the demicelization process of CTAB at 310 K (physiological temperature). This study was performed by using nano-isothermal titration calorimetry (ITC). ITC is an established and invaluable method for determining the thermodynamic constants, association constant and stoichiometry of molecular interactions in aqueous solutions[29-31]. This technique works by measuring the heat evolved during a reaction or when an interaction takes place, this energy represents the change in enthalpy (ΔH) for the reaction (or interaction). The usual mode of operation is titration, so the stoichiometry and association constant (Ka) can be determined. The system works by comparing thermo coupled sample and reference cells which are enclosed in an adiabatic jacket. Upon titration of a ligand or reactant into the sample cell, heat is either released (exothermic) or absorbed (endothermic), and the heat is measured from the amount of power required to maintain the temperature balance between sample and reference cells[32] (Figure 2.4).

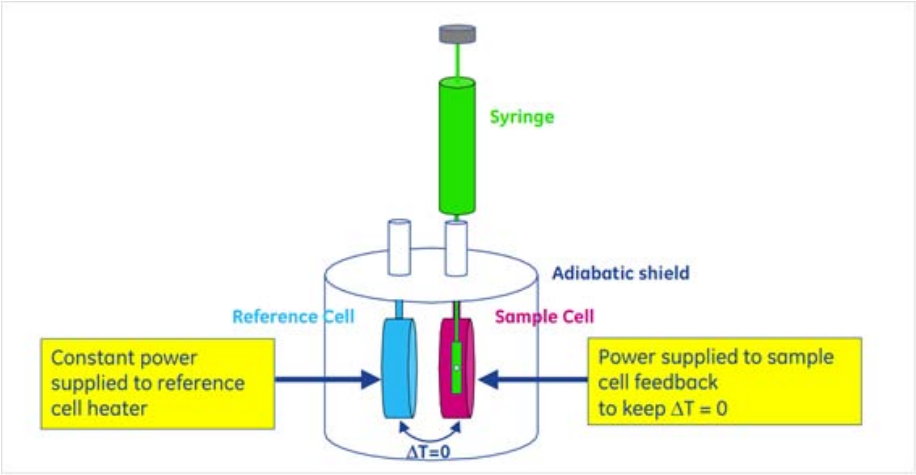

Figure 2.4..Schematic representation of an ITC cell.For the titration the ligand is placed in the syringe and the macromolecule in the sample cell. Both the reference and the sample cells are placed in inside a chamber that works as an adiabatic shield. Adapted from 32.

ITC is a technique capable of measuring the critical micelle concentration (CMC) and the enthalpy of the micellization (ΔHmic) (equal in magnitude but opposite in sign to the heat of demicelization) of a surfactant in a single experiment without the necessity of any probe. Due to this, the CMC of many surfactants as well as ΔHmic have been determined using this calorimetric technique[33]. In Figure 2.5 it is depicted the titration experiment performed in the present thesis in order to measure the CMC of CTAB. Following the protocol described in Experimental section 10.1 a syringe containing CTAB at 10 mM was progressively added in water contained in the sample cell, in order to obtain the demicellization curve and the CMC value (Figure 2.5). The concentration of micellar solution in the syringe was chosen in such a way that, during the titration, the CMC was reached in the sample cell. After each injection the heat evolved was measured, and a sigmoidal curve was obtained by plotting this heat versus the CTAB amount added to the cell upon each injection (Figure 2.5, left).

This curve can be divided into three concentration regions according with the events that are occurring in the cell. On the first few injections the dissociation of micelles into monomers and the dilution of these monomers are the events contributing to the enthalpy changes (Region I). When more micellar solution is added to the cell the CMC is eventually achieved (Region II). If more micellar solution is added beyond the CMC concentration, the micelles no longer dissociate and contribution to the enthalpy is due to the micellar solution dilution. At this particular case the process was endothermic at 310 K.

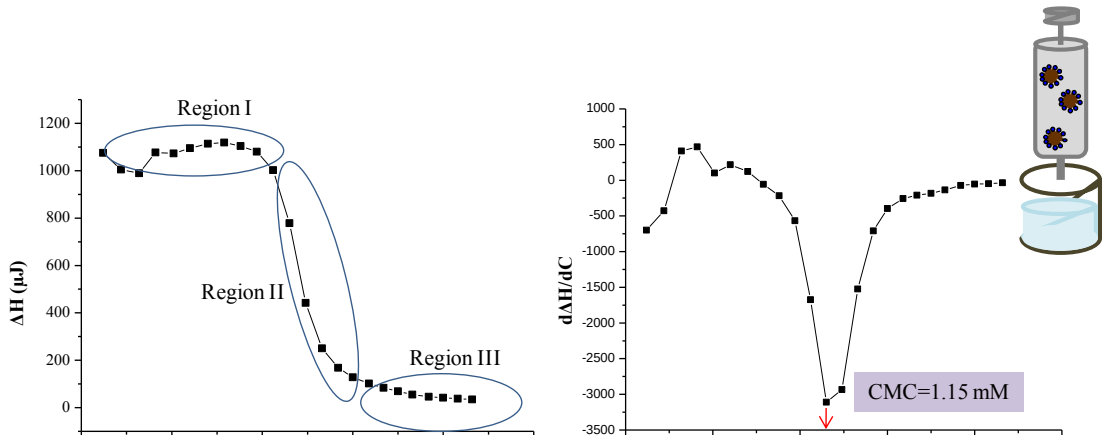

Figure 2.5. Curve of demicellization for the CTAB (left). Determination of CMC by calculating the first derivative of the reaction heat respect to the total CTAB concentration (right).

The CMC was easily determined calculating the first derivative of the demicellization curve respect to the total CTAB concentration in the sample cell (Figure 2.5, right). As expected the CMC value at 310 K (1.15mM) was higher than the one at 298 K (1 mM) since the increase in temperature cause an increase in the solubility of CTAB monomers[34]. The ΔHmic (-2.7 kJ/mol) was also calculated as explain in detail in Experimental section 10.1.1.

In order to study the CTAB demicellization process in the presence of BSA, a solution of this protein placed in the sample cell was titrated with CTAB at 10 mM and the curve obtained was compared to that in the absence of the protein. Three different concentrations were tested. The first one, 0.015 mM, was the same concentration protein used in the preparation of BSA-quatsomes colloidal formulation reported in Chaper 1, and the other two concentrations correspond to the doble (0.030 mM) and the triple (0.045 mM) of this value. The sample cell was always under agitation at 300 rpm and the temperature was settled at 310 K. The result of enthalpy changes versus the surfactant concentration of the three different titration experiments are depicted in Figure 2.6.

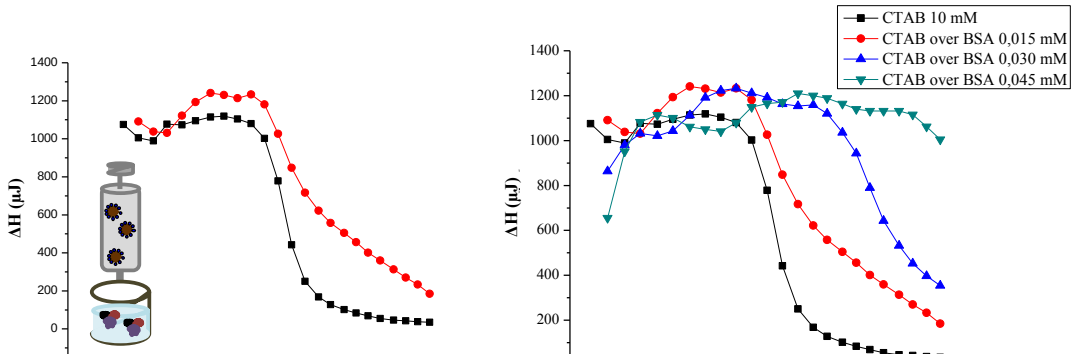

Figure 2.6. Demicellization curve of CTAB over an aqueous solution of BSA at 0.015 mM together with the demicelization curve of CTAB (10 mM) in pure water (left). Dependence of demicellization process on the protein concentration (right)

The presence of protein in the reaction cell caused an appreciable change in the CTAB demicellization curve, which was more significant with the increase in the protein concentration (Figure 2.6, right). It is well described in the literature that the binding isotherms of cationic surfactants with proteins show four characteristic regions[24]:

I. The initial region, at very low surfactant concentration, is associated with the binding of surfactant monomers to the specific high-energy sites of the proteins and the interactions are expected to be electrostatic in nature.

II. The second region in which more surfactants bound to the BSA not only through electrostatic but also through hydrophobics interactions.

III. The third region corresponds to a massive increase in binding caused by cooperative interactions of surfactants with already bound surfactant molecules. The unfolding of proteins is believed to start in this region.

IV. The fourth region is reached beyond the saturation point of the protein. In this region the surfactant molecules will not bind to the protein anymore and normal micelles start to form.

For the three BSA concentrations tested, it is observed that the protein is all the time interacting with the CTAB. This is more clearly depicted in Figure 2.6 (left) were the demicelization curve of CTAB in the presence of 0.015 mM of BSA is represented. The fact that BSA interacts with CTAB means that the higher the protein concentration in

the sample cell, the latter the CMC will be reached. In Figure 2.7 (left) the first derivative of the demicelization curve respect to the total CTAB concentration for the isotherm binding curve between CTAB and BSA 0.015 mM is depicted. The CMC value obtained is higher than the value for pure CTAB at 310 K. The CMC (1.24 mM) is reached at CTAB/BSA molar ratio of 83, which means that below this molar ratio no micelles will be found and all CTAB monomers will be somehow interacting with the protein (Figure 2.7, right).

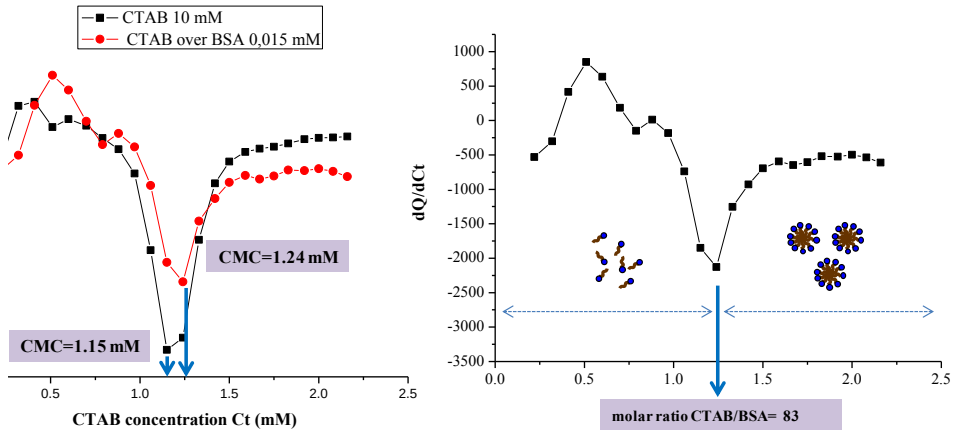

Figure 2.7. Determination of the CMC of CTAB 10 mM over a solution of BSA at 0.015 mM (left) and the regions were the presence of micelles or monomers can be expected (right). The determination of CMC for a solution of CTAB 10 mM over water is included for comparison.

2.2.1.1 Turbidity evolution during CTAB demicelization in the presence of BSA

Following the procedure described in Experimental section 10.2, it was measured the change in turbidity of an aqueous solution of BSA upon the addition of CTAB (10 mM). For doing this, the optical density was measured in a UV-VIS Spectrometer at a wavelength in which the samples do not absorbed the light. Turbidity experiments were performed for the same three protein concentrations used in the ITC experiments. Solutions of BSA were placed in a glass vial and heat up until 310 K. Aliquots of CTAB solution were injected at intervals of 300 s into the glass vial. BSA solutions were stirred throughout the experiment using a magnetic stirrer. At the end of each injection period, the turbidity of the solution was measured at 600 nm.

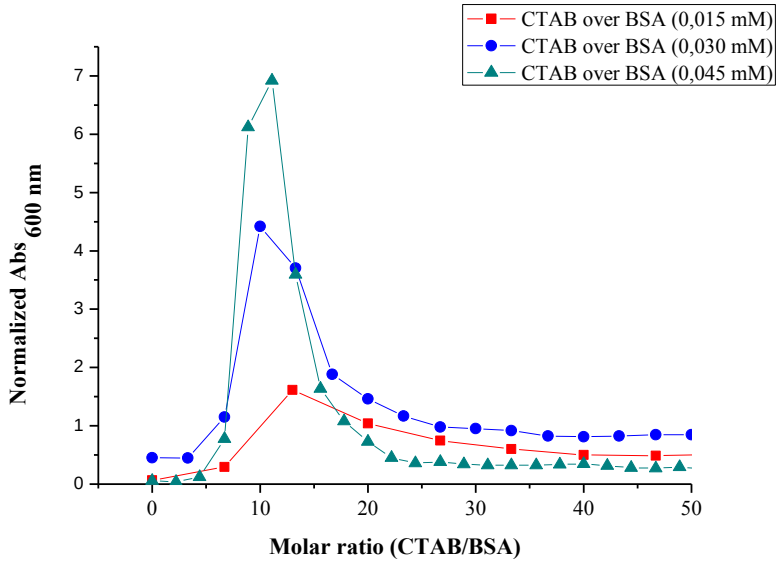

Figure 2.8. Turbidity measurements of BSA aqueous solutions in the presence of CTAB at different CTAB/BSA molar ratios.

The turbidity values were normalized with respect to the protein concentration in the reaction cell to avoid changes due to protein dilution during the experiment[35]. From the first addition of CTAB to the BSA solution until the molar ratio CTAB/BSA= 20, a change in turbidity was observed for the three protein concentrations (Figure 2.8) with maximums at molar ratios CTAB/BSA around 10. As previously observed from the demicelization curves, the CTAB is interacting with the BSA in the range of molar ratios studied so at this specific molar ratio value there should be a change in the characteristics of the complex formed which induce to aggregation phenomena. In order to find out the cause of this maximum in turbidity, the interaction between the surfactant and the protein in a range of molar ratio CTAB/BSA between 0 and 30, was studied.

2.2.1.2 Physico-chemical characterization of BSA aggregates in the presence of CTAB monomers.

2.2.1.2.3 ITC measurements

ITC calorimetric experiments were used to study the interaction between BSA and CTAB monomers. In these experiments CTAB was placed in the sample cell at a concentration below its CMC (0.4 mM) in order to guarantee the presence of the monomers and to avoid the interference of demicelization process in the measurements.

The BSA protein dissolved in water was placed in the syringe (1 mM). A nano-isothermal titration calorimeter was used to measure the enthalpies of interaction at 310 K (Experimental section 10.1). Control experiments were performed by injecting BSA into water under the same working conditions. The resulting heat change was subtracted from the titration data for each experiment. Figure 2.9 showed the final heat release curve and the corresponding isotherm (or binding curve) of one of the 3 replica. The curves (Figure 2.9) show that the non-covalent interactions between BSA and CTAB are of an exothermic nature.

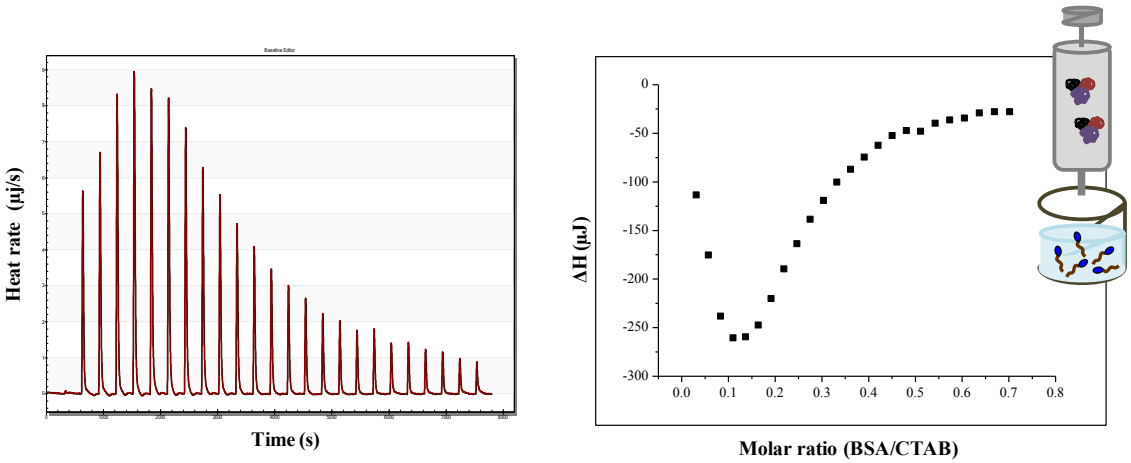

Figure 2.9. Exothermic heat released curve (left graph) and binding curve describing the interactions between BSA and CTAB monomers.

The negative value of enthalpy is directly related to weak Van der Waals interactions and/or electrostatic interactions during the protein-monomer interaction[36]. At working pH=6 and in the absence of surfactant, BSA molecules are negatively charged because the protein is above its isoelectric point. Consequently, electrostatic interaction between this molecule and the CTAB monomers are expected. During the first 4 points of each curve, although the net value of energy is exothermic, some endothermic contributions can be observed. This contributions become less important with each injection and finally disappear at molar ratio BSA/CTAB around 0.1 (CTAB/BSA= 10), where the higher turbidity values was found in the turbidity measurements previously performed

It is not possible from ITC measurements alone to understand the interactions between BSA and CTAB, therefore turbidity, florescence and DLS measurements, were performed on the same system. Charge, size and aggregation upon interaction of BSA with CTAB were characterized by turbidity, DLS and fluorescence measurements.

2.2.1.2.1 Turbidity and DLS measurements

Turbidity, size and z potential measurements were carried out under conditions designed to mimic those used in the ITC experiments. In order to do so a solution of CTAB was placed in a glass vial and heat up until 310 K. Aliquots of BSA solution were injected into a glass vial initially containing the CTAB monomers. BSA solutions were stirred throughout the experiment using a magnetic stirrer. At the end of each injection period, the turbidity was measured by optical density at 600 nm and the size and Z potential were measure using a DLS equipment (Experimental section 10.2 and 10.4).

Figure 2.10 shows the results obtained from the turbidity, size and z potential measurements for a range of molar ratios BSA/CTAB between 0.02 and 0.6 (this corresponds to CTAB/BSA molar ratio from 2 to 40). In the turbidity curve it is observed that since the first addition of BSA up to a molar ratio BSA/CTAB equal to 0.2 (CTAB/BSA= 5), a change in the turbidity is observed. It was convenient, for a better understanding, to divide the turbidity curve into three regions depending on the molar ratio BSA/CTAB. Molar ratios lower than 0.1 belong to the region I; molar ratios between 0.1 and 0.2 belong to the region II and ratios higher that 0.2 belong region III.

In region I, where the higher CTAB molecules per BSA protein are present, the increase in solution turbidity is an indication of the formation of aggregates that are large enough to scatter light. When the protein is added to the CTAB solution the positively charged monomers bind to negatively charged COO^- groups and hydrophobic groups on the protein surface, thus reducing the net negative charge on the protein and probably changing its conformation. Indeed the Z potential of the BSA-CTAB complexes in this zone goes from a positive value to cero. An increment in the size from 5.6 to 9 nm is also observed, probably due to the increment in the size of the aggregates formed.

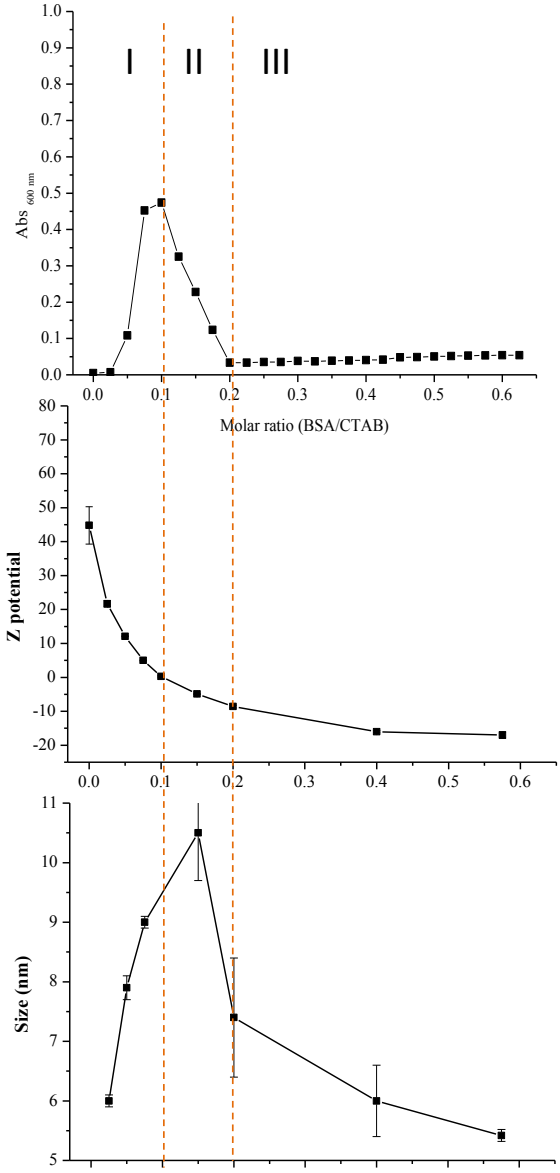

Figure 2.10. Turbidity measurements and evolution of Z potential and size with the molar ratio BSA/CTAB.

In the maximum turbidity, at the interface of region I and II (molar ratio CTAB/BSA= 10), the electrical charge on the protein-CTAB complex is neutralize, as observed form the Z potential value. This lack of charge provokes the protein aggregation which is in agreement with a point of maximum turbidity and maximum size. In region II, more protein is added so the ratio BSA/CTAB increases and the net charge become increasingly negative in the protein as seen from the Z potential, opposing the aggregation process. The size also begins decreasing in this region as a result of the aggregates dilution. In region III the negative charge in the protein–surfactant

complexes would be sufficiently large to complete dissociate the aggregates. Therefore the Z potential reach a value of -17, the size reach it initial value and the solution become transparent again with turbidity values close to cero. These turbidity, size and Z potential variations must be accompanied by structural changes in BSA; this is why fluorescent measurements were also carried out.

Fluorescent spectroscopy was used in order to detect structural changes in the BSA protein upon interaction with CTAB. These structural changes might cause changes in the position and orientation of the Trp residues altering their exposure to solvent and as a consequence their fluorescence. Using same conditions as in ITC, turbidity and DLS experiments, fluorescence of aqueous solutions of BSA in the presence of CTAB were measure at different BSA/CTAB ratios (Figure 2.11). Intrinsic tryptophan fluorescences were obtained at excitation wavelength of 295 nm and the emission spectras were recorder from 300 nm to 450 nm (Experimental section 10.3). For comparison purposes, fluorescence was also measured on BSA solutions, free of CTAB, at the same protein concentrations.

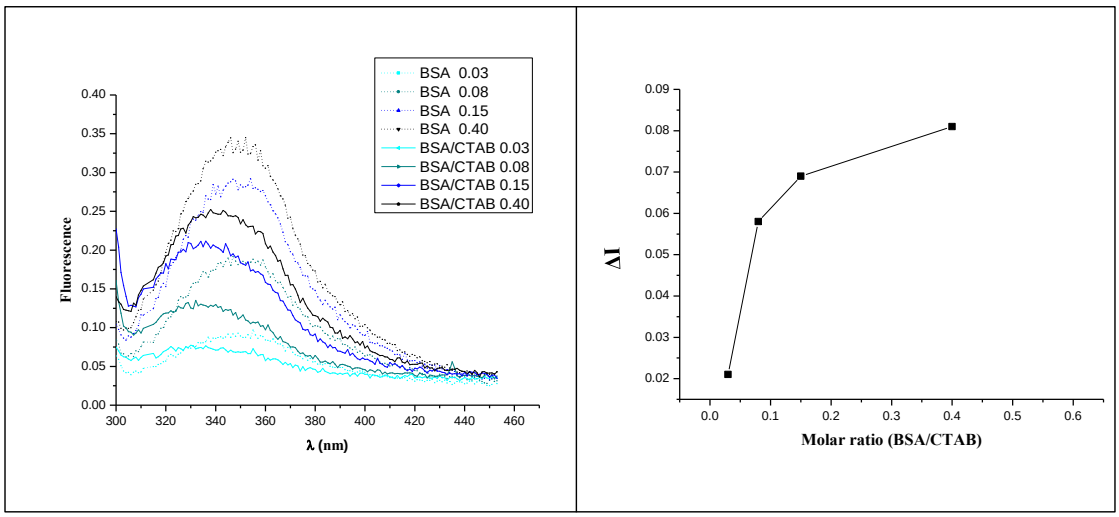

Figure 2.11. Fluorescent measurements at different BSA/CTAB molar ratios (left) compared to the fluorescence of BSA in water. Differences in the fluorescence intensities at λ_{max} (ΔI) between the curves of BSA in water and BSA in the presence of CTAB, at the different BSA/CTAB molar ratios (right).

As observed in Figure 2.11 (left) there is a shift of the maximum wavelength toward shorter wavelength together with a decrease in the fluorescent intensity for all molar ratios, compared to the corresponding BSA curves in water. This shift might indicate that the Trps groups present in BSA have been transferred to a more hydrophobic environment composed of the bound surfactants. For proteins with tryptophan groups,

both, changes in fluorescence intensity and shifts in wavelength, might also indicate protein conformational changes[25]. The changes in fluorescence are more clearly represented in Figure 2.11(right).

In figure Figure 2.12 the shift in the maximum wavelength of BSA solutions in the presence of CTAB versus the molar ratio BSA/CTAB is also plotted. It should be taken into account that the maximum wavelength of BSA in water is at 350 nm. The maximum shift is observed in the region I, which is coincident with a higher number of CTAB molecules bound to BSA and the more hydrophobic environment of the Trp. As the number of bound monomers decrease toward the end of the titration, the shift is also smaller.

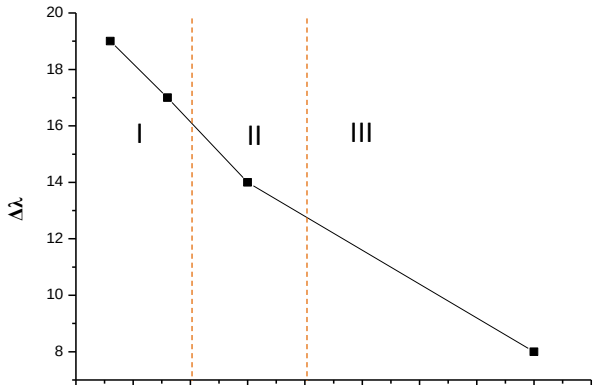

Figure 2.12. Change in the maximum wavelength with the molar ratio. $\Delta\lambda$ is the difference between the λ_{max} of BSA in water (350 nm) and BSA in the presence of CTAB at different BSA/CTAB molar ratios

The fact that Trp are in a hydrophobic environment during the whole titration means that the biding sites are in the vicinity of Trp. In Figure 2.2 is observed that Trp 134 and Tryp 212 are located in the Domain I, which have a high density of hydrophilic zones and negative charges. Therefore the main interactions between CTAB and BSA in this range of molar ratios should be produce in this domain. As Trp212 lies in a hydrophobic cavity, the binding must occur in close vicinity of Trp134.

2.2.1.2.3 Interpretation at molecular level of aggregation phenomena in BSA solutions in the presence of CTAB.

The characterization of molecule association and aggregation phenomena occurring in aqueous mixtures of BSA and CTAB in a range of molar ratios CTAB/BSA between 2 and 40, at CTAB concentration below CMC, was obtained by combining different techniques. In order to explained what occurs during the whole titration the three regions defined earlier are going to be used.

At the beginning of the titration (region I) the maximum number of CTAB monomers bound to BSA molecule (between 40 and 10) occupying all the strong binding sites and forming a complex. The origin of this interaction is believed to be electrostatic attraction between the cationic surfactant head group and anionic protein groups, in combination with hydrophobic attraction between the non-polar surfactant tail group and nearby hydrophobic patches on the protein surface[25]. As such binding occurs, the electronic character of the protein changes, as confirmed by the change in z potential in this region from positive values down to cero (Figure 2.13). The energy involved in the complex formed between CTAB and BSA is exothermic while the conformational changes that can occur in the protein due to the binding of the monomers are of an endothermic nature. Another contribution to the endothermic energy is the one coming from the interaction of the hydrophobic tails of the surfactant molecules with the hydrophobic patches in the protein. This could explain the endothermic contributions at the beginning of the heat release curve.

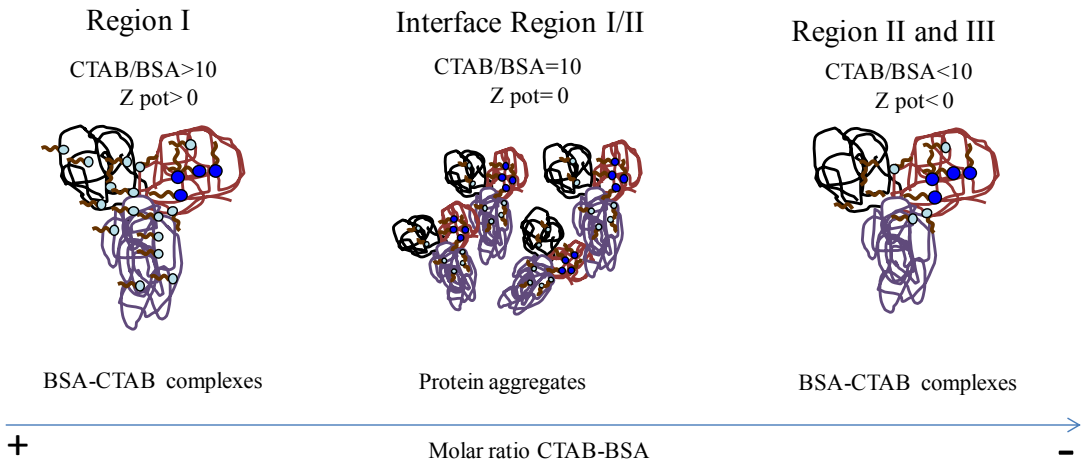

Figure 2.13.. Schematic representation of the BSA-CTAB complexes depending on the molar ratio BSA/CTAB. The dark blue spheres represent the high affinity interactions of the monomers of CTAB with the protein.

In the interface between regions I and II, the charge neutralization of the BSA occurs, resulting in the formation of protein aggregates (Figure 2.13). This is why at this point the bigger value of turbidity and size are found and the Z potential value is cero, confirming the charge neutralization. In region II the concentration of BSA increase so the number of monomers interacting with the protein decrease. In fact at this point the complex becomes more and more negative, preventing the aggregation of the protein (Figure 2.13). In this region the electrostatic contributions become more important than the hydrophobic ones coming from the non-polar surfactant tail group interacting with nearby hydrophobic patches on the protein. At the region III few monomers are bound to the protein, which is negatively charge. The aggregates completely disappear and the turbidity goes to almost cero again. As observed from the florescent measurements the highly affinity interaction of the CTAB monomers with the protein occurs in the domain I in BSA protein.

2.2.2 Study of the interactions of BSA with CTAB micelles

After studying the interaction of BSA with CTAB monomers, and the influence of the protein in the demicellization of this surfactant , the interactions between the BSA and the micelles were study. Turbidity and DLS measurements were carried out to characterized transformations at supramolecular and nanoscopic level, in a micelar solution of CTAB (10 mM) titrated with increasing amounts of BSA (Experimental section 10.2 and 10.4). In Figure 2.14 are represented the optical density, size distribution and Z potential of a micellar solution at different BSA/CTAB molar ratios.

It is observed that the turbidity values are very low during the whole titration indicating that the formation of big aggregates does not take place. Nevertheless below the molar ratio BSA/CTAB 0.010 (molar ratio CTAB/BSA=100) there is a slightly increase in the turbidity. From the studies of the influence of BSA in the demicellization process was obtained that at molar ratios CTAB/BSA below 83 there are not micelles in the solution and the monomers present are all interacting with BSA forming protein-monomer complexes. Therefore the slightly increase in turbidity should be due to the formation of these protein-BSA complexes.

The Z potential decreases from point to point during the all experiment which prove that electrostatic interaction are occurring during the BSA-micelles interaction. The size increases from the micelles size (4 nm) until 11 nm and then decrease down to 4 nm

again. In the region of maximun size the turbidity values are near cero and the z potential are still high and positives thus the increment in size is probably associated to protein conformational changes and not to the formation of the BSA-CTAB aggregates.

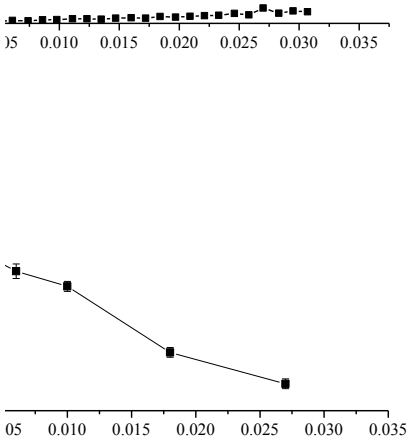

Figure 2.14. Turbidity, size and Z potential measurements of aqueous solutions of BSA and CTAB at different BSA/CTAB molar ratios.

2.2.2.1 BSA fluorescence variation induced by the presence of CTAB micelles

Taken advantage of the presence of Trp groups, fluorescence experiments were conducted under the conditions used for the previous measurements. Six points of the

entire titration curve were studied corresponding to the BSA/CTAB molar ratios: 0.004, 0.006, 0.011, 0.018, 0.027 (molar ratios CTAB/BSA: 250-37). Intrinsic tryptophan fluorescence of BSA-micelles solutions at the different molar ratios chosen were obtained at excitation wavelength of 295 nm and the excitation spectra were recorder from 300 nm to 450 nm.

As observed in Figure 2.15 for all solutions of BSA in the presence of CTAB micelles there was a shift to shorter wavelength and a decrease in the maximum fluorescent intensity, in relation to the observed for BSA in pure water. This result indicates that the Trp group is transferred to a more hydrophobic environment after the addition of BSA to the CTAB micelles. The changes in fluorescence intensity could also indicate certain protein conformational changes. The differences between the maximum wavelength intensity of BSA in water and BSA interacting with CTAB micelles are represented in order to see these differences more clearly (Figure 2.15).

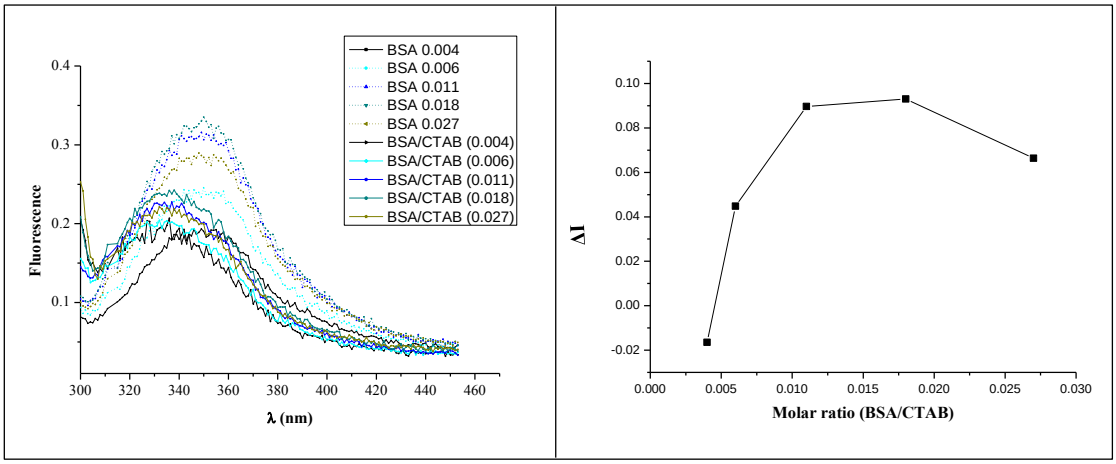

Figure 2.15. Fluorescent measurements at different molar ratios BSA/CTAB (left). Differences in the fluorescence intensities at λ_{max} (ΔI) between the curves of BSA in water and BSA in the presence of CTAB, at different BSA/CTAB molar ratios (right).

There was not variation in the maximum wavelength intensity with the molar ratio, indicating that the Trp kept the same hydrophobic environment along the entire experiment (Figure 2.16).

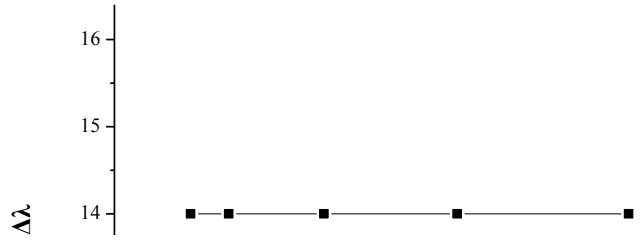

Figure 2.16. Change in the maximum BSA wavelength with the molar ratio. Δλ is the difference between the λ_{max} of BSA in water (350 nm) and BSA in the presence of CTAB at different BSA/CTAB molar ratios

2.2.2.3 Calorimetric study of BSA interaction with micelles

Finally in order to know the nature of the interactions involved in the BSA-micelles interaction, ITC experiments were performed. Following the procedure described in Experimental section 10.1, consecutives injections of the protein (0.86 mM) were added into the calorimetric cell filled with CTAB solution above its CMC (7 mM) at 310 K. The protein and the micelles were both prepared in water. Control experiments of BSA dilution were subtracted from the measure heats and the experiment was performed by triplicated (Figure 2.17).

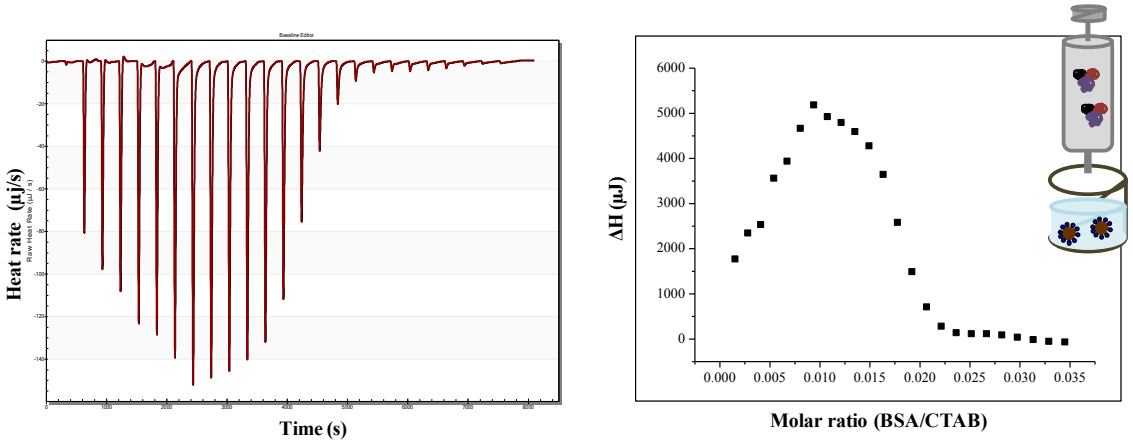

Figure 2.17. Exothermic heat released curve (left graph) and binding curve (right) of CTAB micelles titrated with BSA protein.

The heat release curve (Figure 2.17, left), shows that the injection of the protein into vesicles gives large endothermic heats of binding, which decreases in magnitude with subsequent injections, showing saturation behavior. Although the net process is endothermic, exothermic contribution are observed in the first 6 injections of the titration. From Ross and Subramanian correlation between the process and the values of enthalpy we can say that the net interactions are hydrophobic in nature[36].

2.2.2.3 Origin of the interactions between BSA and CTAB in the form of micelles.

The characterization of the interactions between BSA protein and CTAB micelles was obtained in the range of molar rations BSA/CTAB from.008 to 0.03 (corresponding to CTAB/BSA molar ratios from 125 to 33), using different techniques.

As shown in the demicellization studies, at CTAB/BSA ratios higher than 83 (BSA/CTAB= 0.012), the presence of micelles can be expected in the solution. Therefore in this specific case and above this molar ratio there should be micelles in the solution interacting somehow with the BSA. From the heat release curve obtained using ITC, it is observed that the net interaction in this region is endothermic although some exothermic contributions are observed. It is reported that in this range of CTAB/BSA molar ratios the surfactant can binds to the BSA forming micelle-like aggregates[24,35,37]. The formation of micelle-like aggregates should be an exothermic process, opposite of demicelization, and the aggregates may be formed due to the hydrophobic interaction between the surfactants with already bound surfactant molecules. The formation of the micelle-like aggregates can produce conformational changes in the protein (endothermic process), which is an agreement with the size increment observed in this part of the titation. The exothermic contributions observed at the beginning of the heat release curve can be explained by the formation of the micelle-like structures (Figure 2.18). This kind of aggregates have been described in literature on the basis of the "pearl-necklace" model, where surfactant micelles (pearls) decorate an unfolded protein chain (necklace)[38,39]. Among several proposed models of the protein–surfactant complexes, the necklace model is the most accepted for understanding the interaction of these two components in their complex formation. These structures have been identified in numerous protein−surfactant complexes, using techniques such as SANS, SAXS, and Cryo-TEM[40-42].

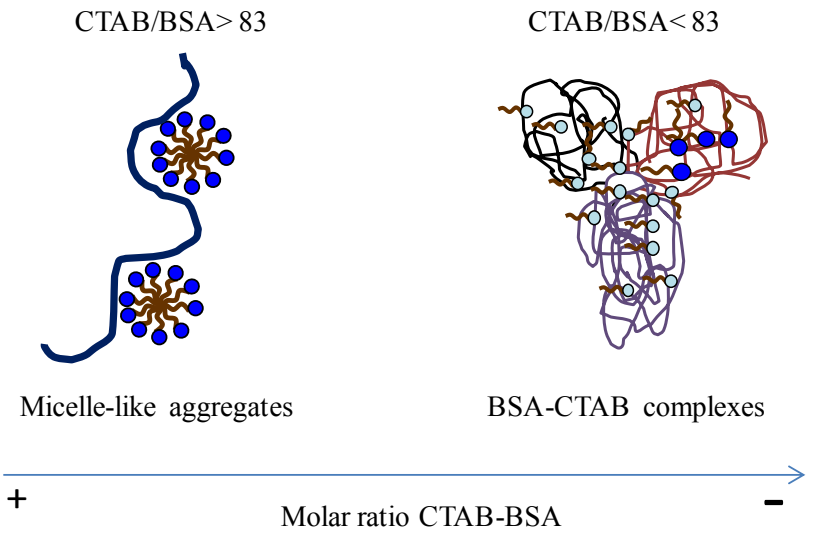

Figure 2.18. Schematic representation of micelle-like aggregates with the micelles bound to the polypeptide chain of the protein as pearls in a necklace. The due to the great amount of CTAB bounded in the region I, the size of the unfolded protein is around 9 nm.

At BSA/CTAB above 0.012 (CTAB/BSA< 83), the formation of the BSA-surfactant complexes begins (**¡Error! No se encuentra el origen de la referencia.**). The monomers bound to BSA producing conformational changes in the protein but in much less extent, as observed from the decrease in the size of the protein in this region. The turbidity slightly increases due to the presence of BSA-monomer complexes, although the values are still low because the charge of the complexes is high and positive, which avoid aggregation. The formation of these complexes also produces changes in the fluorescence of the Trp groups present in the BSA, which indicates that the Domain I of the protein is involved in the interaction. The overall process is endothermic, due to the conformational changes that occur in the protein and the hydrophobic interactions of the surfactant tails with the hydrophobic patches in BSA. Nevertheless there are also exothermic contributions related with the electrostatic interactions between the polar head of the surfactants and the protein.

It can be concluded that BSA interact with the CTAB micelles forming protein-surfactant complexes or micelle-like aggregates, depending on the molar ratio BSA/CTAB.

2.3 Study of the interaction of BSA with CTAB/cholesterol quatsomes

After characterizing the interaction between BSA and CTAB forming micelles, the study was carried out in quatsomes. It is good to point out that, compared to micelles, quatsomes are much bigger in size (around 100 nm), they are much more stable with temperature and upon dilutions and they are formed not only by CTAB but also by cholesterol.

2.3.1 Turbidity measurements

As in previous studies with CTAB monomer and micelles, turbidity measurements were carried out performing the titration of the quatsomes with a solution of BSA. The range of molar ratio BSA/CTAB studied, between 0.0031 and 0.076 (CTAB/BSA between 322 and 13). For this experiment aliquots of BSA solution were injected at intervals of 300 s into a glass vial containing the CTAB self-assemble in quatsomes at 310 K. The solution was measured at 600 nm at the end of each injection period (Experimental section 10.2). Figure 2.19 shows an interesting curve where an increment in turbidity is observed since the first injection indicating the formation of some kind of complexes between the protein and the vesicles, big enough to scattered light. Two main regions can be identified: region I, below the molar ratio BSA/CTAB= 0.02 (CTAB/BSA= 50) and region II, above this molar ratio. In the region I there is a constant and moderated increase in turbidity but in region II a drastic jump from around 0.6 up to 2.2 is observed. Then the turbidity values reach a plateau and in the last injections a small decrease in the turbidity is observed but still the values remains very high. The high turbidity values in this region indicate the formation of aggregates much bigger than those formed at the beginning of the titration.

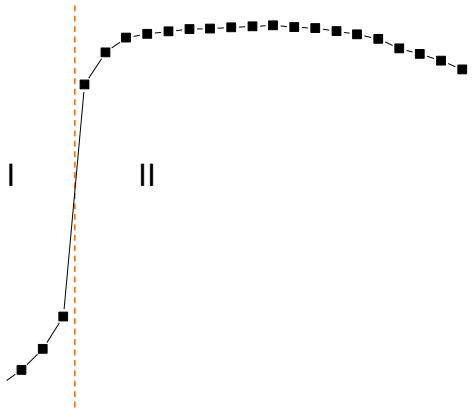

Figure 2.19. Turbidity measurements of BSA-Quatsomes complexes

3.4.3 Size and Z potential of BSA-Quatsomes complexes

Physico-chemical parameters of the protein-quatsomes complexes were measure to bring more clarity to the previous turbidity studies. The size and Z potential were measured using same experimental conditions than in the turbidity experiment (Experimental section 10.4). Briefly, aliquots of BSA solution were injected into a glass vial containing the solution of quatsomes at 310 K and at the end of each injection period, the size and Z potential were measured using dynamic light scattering equipment. During the measurement the temperature was also maintain at 310 K inside the equipment.

Figure 2.20 shows the graphs obtained which were divided into the two regions previously established. In region I, where the lower turbidity is present, the size increases from 85 to 109 nm and the Z potential decreases from 82 to 19. This suggests that the protein could be interacting with the membrane and that these interactions are probably of electrostatic nature. Indeed, Hyun Jung et al. obtain cationic charged liposomes coated with BSA, by incubating with the protein once the liposomes are formed[43]. The mean particle diameter of their functionalized liposomes increases from 100 nm to 120nm, and the Z potential also decreased.

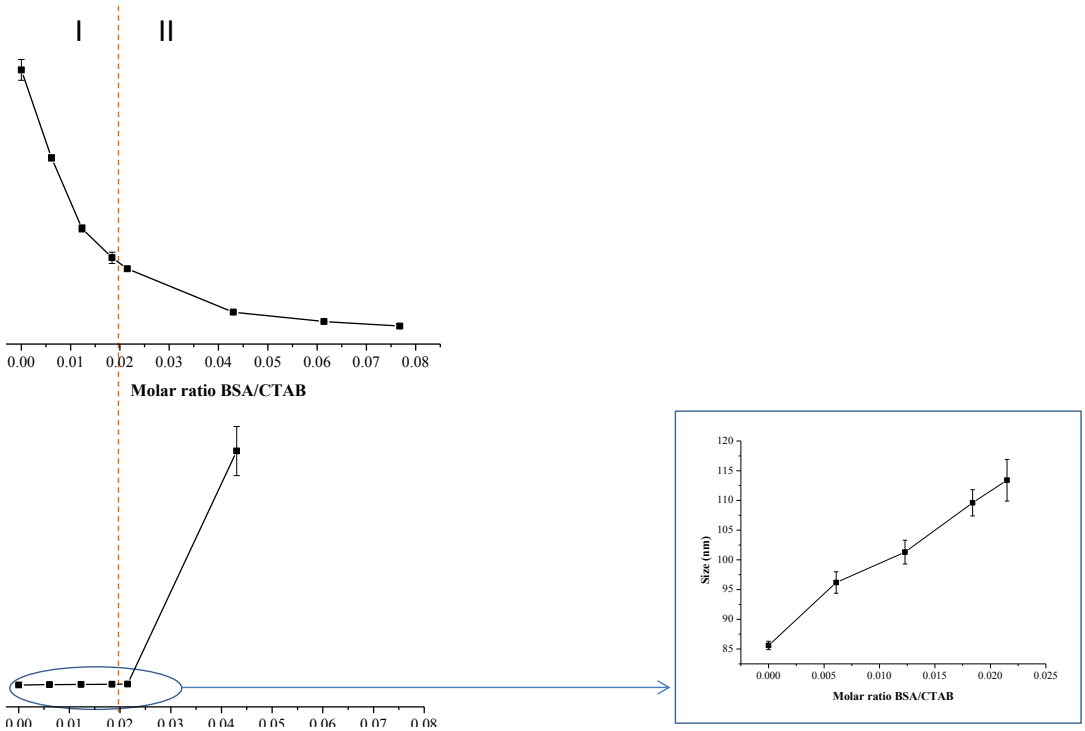

Figure 2.20. Evolution of the size and the Z potential with the molar ratio BSA/CTAB. A zoom of the size versus molar ratio in the region I is also represented.

In the region II the size of the BSA-quatsome complexes increases up to micrometric values and the Z potential decreases down to negative values. As shown in chapter 1, quatsomes are instable in the presence of organic anionic anions when their negative charge exceed the CTAB positive charge in the membrane. The fact that Z potential are below zero in this region, indicates that the negative charges are higher than the positive CTAB charges in the last points of the titration; hence quatsomes membrane rupture might occur. In order to check whether the aggregates were form due to the quatsomes rupture, Cryo-TEM microscopy technique was used.

3.4.4 Morphological characterization

Cryo-TEM microscopic provides visual information at a nanometric scale. As quatsomes are very homogenous regarding size and lamellarity, any morphologic change occurred in their structure due to the interactions with the protein should be observed. In order to perform these experiment aliquots of BSA were added the vesicles

placed in a glass vial and heat up until 310 K. Samples at different molar ratios BSA/CTAB (0.01, 0.02, 0.04 and 0.07) were withdrawn from the glass vial in situ and were analyzed by Cryo-TEM (Experimental section 3.2). The images obtained depict the presence of a layer around vesicle membranes at a molar ratio BSA/CTAB=0.012 (CTAB/BSA= 83) (Figure 2.21), which is in the region I. The thickness of this layer, measured using a program provided by the manufacturer of the Cryo-TEM microscope, was 4.8 ± 0.8 nm. With these images it was confirmed that in the region I the BSA interacts with the quatsome forming a coating layer around the membrane.

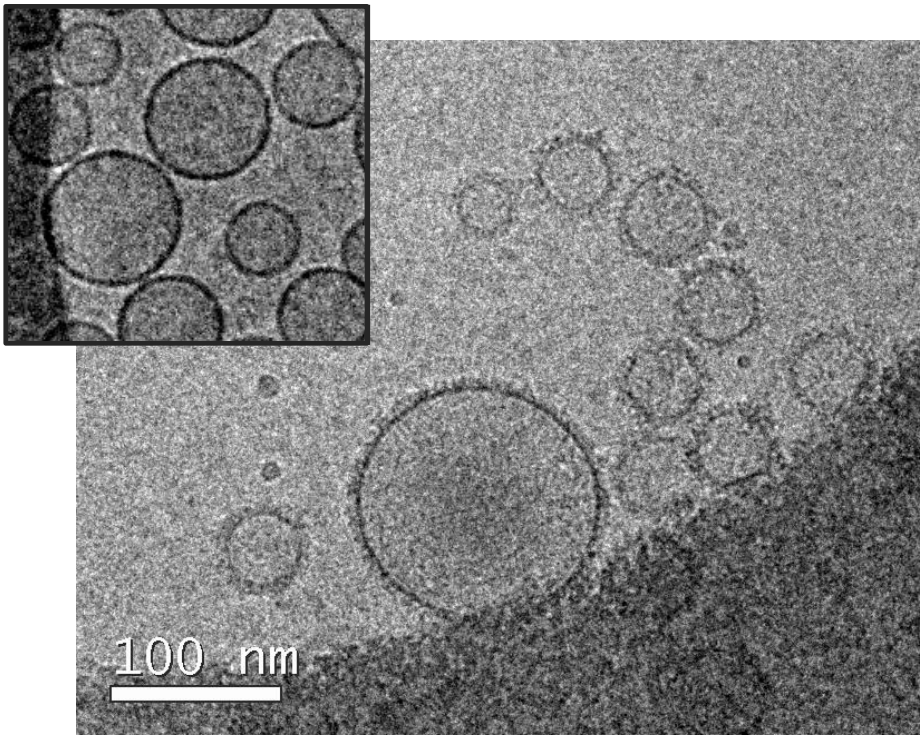

Figure 2.21. Presence of a BSA layer in the quatsome membrane at a molar ratio BSA/CTAB=0.01. An image of plain quatsomes is provided for comparison.

At molar ratio BSA/CTAB= 0.02 (CTAB/BSA=50) aggregates of several vesicles as well as bigger vesicles entrapping other vesicles appears (Figure 2.22). The aggregates at this molar ratio could be form because the BSA attached to the membrane of a vesicle can attracts CTAB groups from other vesicles forming multi-vesicular complexes where the BSA acts as glue. As the quatsomes morphology is very homogeneous regarding size and lamellarity, the presence of big vesicles entrapping smaller vesicles can only be explained by the membrane rupture and fusion into bigger vesicles. At molar ratio BSA/CTAB= 0.04 corresponding to a Z potential near cero the vesicles rupture become

massive due to the neutralization of the positive CTAB charge in the system. The Cryo-TEM image depicts big aggregates composed of coated vesicles, and probably pieces of membranes and free molecules of BSA, CTAB and cholesterol crystals.

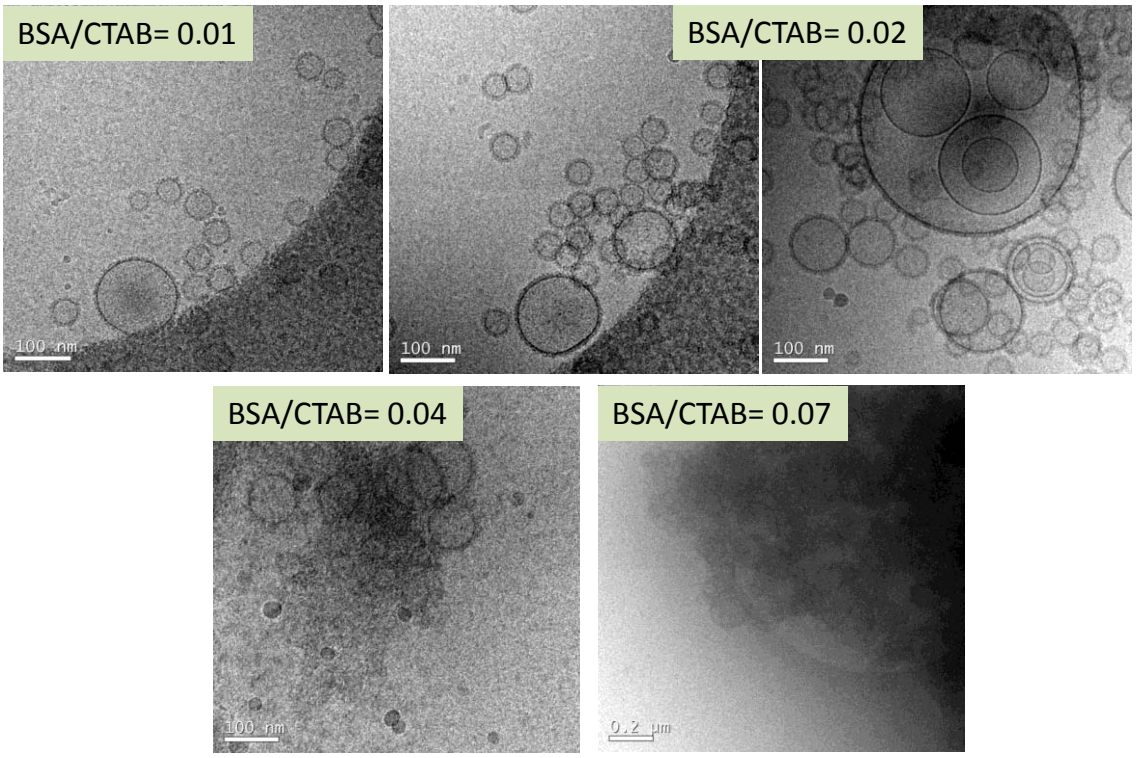

Figure 2.22. Cryo-TEM images of the morphology at different CTAB/BSA molar ratios during the interaction between BSA and Quatsomes. Scale bars are 100 nm in all case except for the molar ratio BSA/CTAB where the scale bar is 200 nm.

Finally at the end of the titration no individual vesicles were observed, instead big aggregates with a size around 5 µm were formed. Indeed the deposition of a white solid was clearly notice in the solution. Infrared spectroscopy was used for the qualitative study of this solid. IR expectrum of the white precipitate were recorded together with the spectra for pure cholesterol, CTAB, water and ethanol, for comparison (Experimental Section 5). As observed in Figure A4 in the Anexxes there are two bands in the precipitate spectrum that are characteristics of pure cholesterol. When the precipitate spectrum was compared with the one corresponding to CTAB (Figure A5), there were not coincident peaks which means that the white precipitate is mainly formed by cholesterol crystals and that the CTAB remains dissolved in the aqueous media.

3.4.5 Fluorescent measurements

Taken advantage of the presence of Trp in the BSA structure, a fluorescent experiment was performed under the conditions used for the previous experiments (Experimental section 10.3). Intrinsic tryptophan fluorescence of BSA-quatsome solutions at the different molar ratios BSA/CTAB (0.006, 0.02, 0.04), were obtained at excitation wavelength of 295 nm. The excitation spectra were recorder from 300 nm to 450 nm.

It is observed that there is a shift to shorter wavelength and a decrease in the maximum intensity for all molar ratios which means that the Trp is transferred to a more hydrophobic environment (Figure 2.23, left). This is also an indication that the domain I, negatively charge and where the Trp groups are located, is involved in the interactions with the liposome membrane.

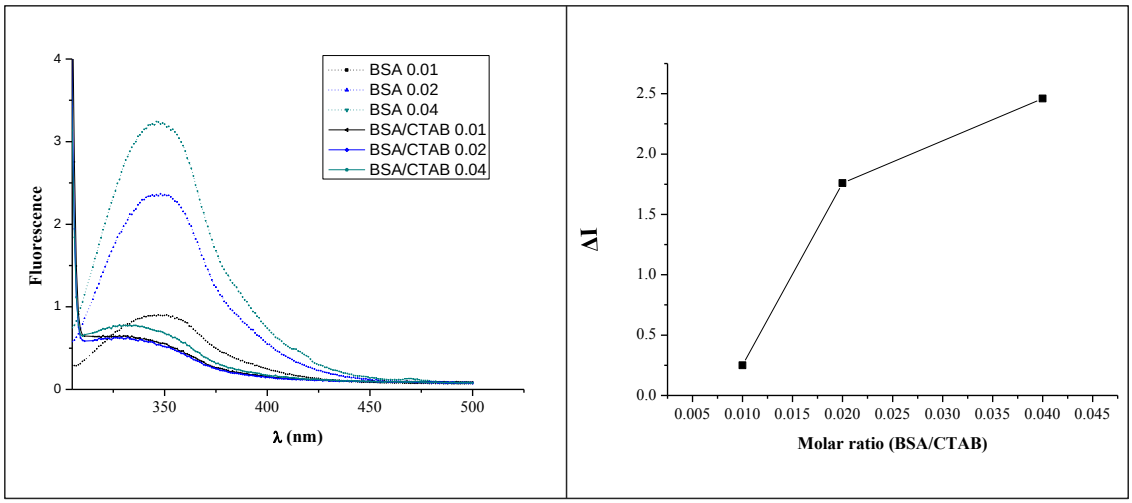

Figure 2.23. Fluorescent measurements at different molar ratios BSA/CTAB (left). Differences in the fluorescence intensities at λ_{max} (ΔI) between the curves of BSA in water and BSA interacting with quatsomes at different BSA/CTAB molar ratios (right).

The differences between the maximum wavelength of BSA-quatsome complexes and BSA in water are represented in Figure 2.23 (right). The differences are bigger than for the BSA-monomers and BSA-micelles interactions which mean that the protein conformational changes could be bigger in this case. The formation of the BSA-quatsome complexes involving more than one vesicle are likely contributing to this high unfolding and thus to the endothermic enthalpy. When the maximum wavelength of the fluorescence spectra of BSA protein interacting with the quatsomes, were potted against the molar ratio BSA/CTAB no variation was observed, therefore the hydrophobic environment of the Trp did not change along the titration (Figure 2.24).

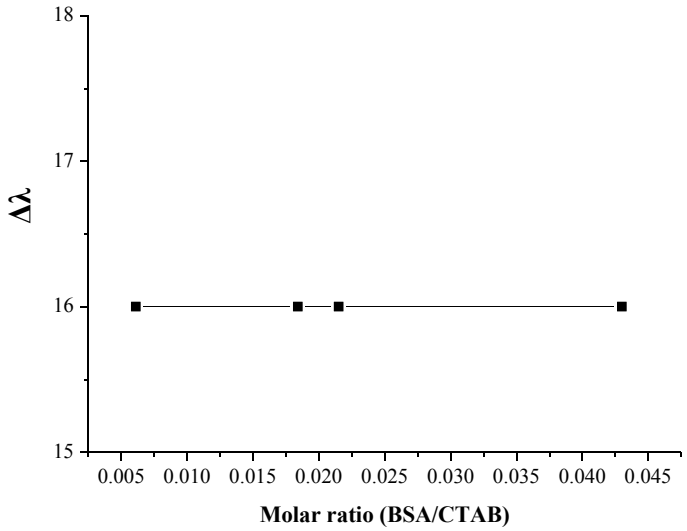

Figure 2.24. Change in the maximum wavelength with the molar ratio BSA/CTAB.

2.3.4 ITC experiments

The interaction between the protein and the quatsomes was finally investigated by ITC at 310 K. Consecutives injections of the protein were added into the calorimetric cell filled with the quatsomes (Experimental section 10.1). Control experiments of BSA dilution were substracted from the measure heats. The experiment was performed by triplicated.

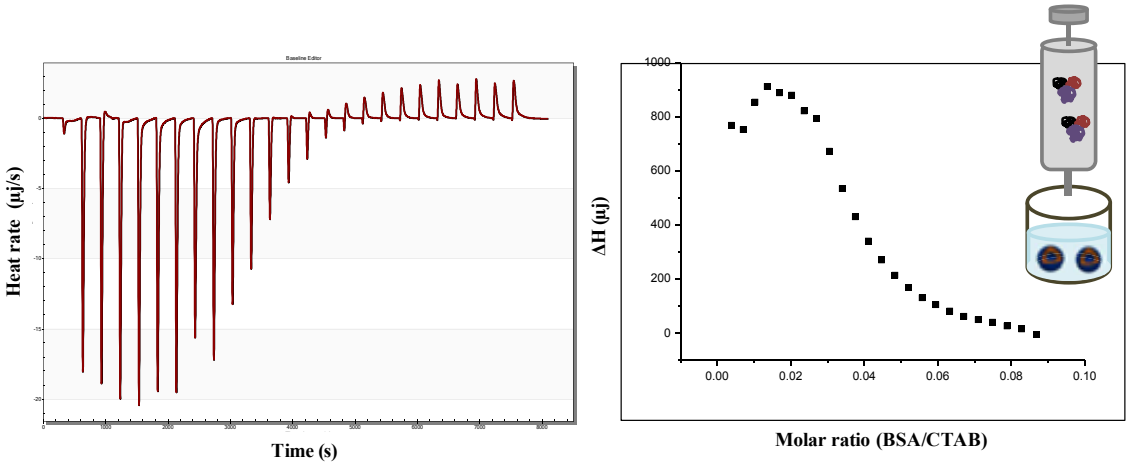

Figure 2.25. Endotermic heat released curve (left graph) and binding curve (right) of quatsomes titrated with BSA protein.

The heat release and the bindig curves (Figure 2.25), show that the injections of the protein into vesicles give endothermic heats of binding, which decreases in magnitude with subsequent injections. This endothermic enthalpy indicates that hydrophobic interactions play a predominant role in the association between BSA and the vesicle membranes[36]. It can also be observed that some exothermic contributions are present during the first injections and in the last part of the row data curve. Although electrostatic interactions were expected due to the negative charge of the protein and the positive membrane of quatsomes, instead the protein-vesicle binding resulted more of a hydrophobic nature. Endothermic binding of proteins and peptides to lipid membranes has been reported in other studies[23,44]. In the particular case of BSA, some studies suggest that the absorption of this protein on liposomes is more related with hydrophobic interactions. Thus is reported the absorption of BSA on uncharged DPPC and negatively charged DPPC/DPPG liposomes, but not on positively charge DPPC/SA liposomes[23].

2.3.5 Origin of BSA-quatsomes interactions

For most protein, a combination of two complementary forces electrostatic and hydrophobic plays an important role in their interaction with lipid membranes[45]. In the case of BSA it is known that this protein may deeply absorb into bilayer due to hydrophobic dehydration forces acting at a very close protein–membrane approach[36,46]. This is corroborated from the positive values of enthalpy obtained from the ITC data. In the region I BSA is coating the vesicle membrane, so a little increment in the size and decrease in the Z potential is observed. The interaction could be produce by electrostatic interaction in the first place and by short range hydrophobic forces when the protein is close enough to the membrane. Once the protein is close enough, the BSA may penetrate partially into the core of the lipid bilayer probably using its neutral domain III. This is why, although the net enthalpy contribution is endothermic, some exothermic contributions related to this electrostatic interaction are present at the beginning of the heat released curve in the ITC experiments. This is also in agreement with the non-polar environment found for the Trp groups during the entire titration. Such interactions can produce conformational changes in the protein which may lead to the exposure of previously inaccessible hydrophobic portions of the molecule. In Figure 2.26 a scheme showing the possible orientation of BSA protein when it interacts with quatsomes is proposed. Possibly the protein interacts electrostatically with membrane through the

domains I (-10) allowing the domain III(0) penetrates in the lipid bilayer through hydrophobic interactions. The domain II (-8) could remain more exposed to the solvent.

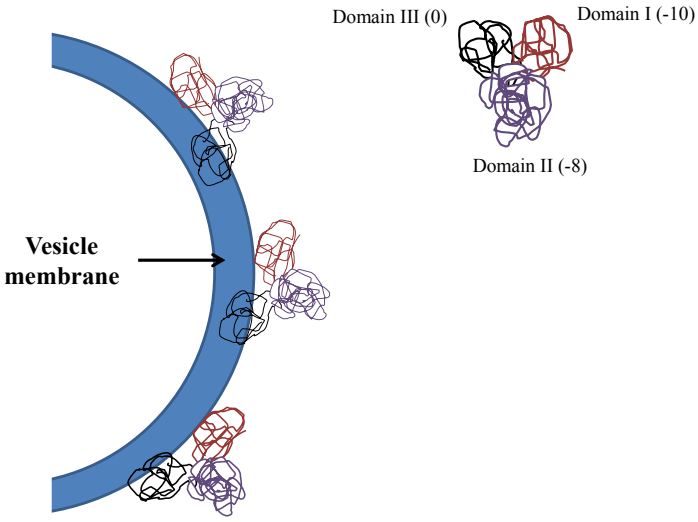

Figure 2.26. Scheme representing the possible orientation of the BSA protein when interacts with the membrane of the quatsomes.

It is known that when nanoparticles are exposed to biological fluids, they become coated with proteins and other biomolecules to form a "protein corona". Human serum albumin is among the proteins that can make up this corona forming a monolayer around the particles of 3.3 nm approximately. The HSA is folded into three domains structure with an overall heart-shape conformation that can be approximately an equilateral triangular prism, with sides of ~ 8 nm and a height of ~3nm. Measures of fluorescence correlation spectroscopy have suggested that HSA molecule cover the surface with their larger triangular faces[47] (Figure 2.27).

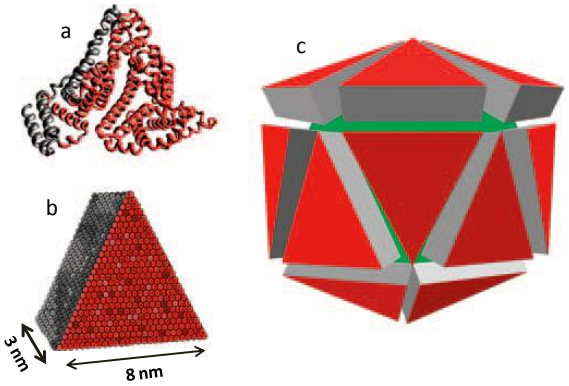

Figure 2.27. Structure of HAS and the protein corona. Representation of HAS polypeptide chain (a), which can be approximated by an equilateral triangular prism (b). At concentrations of HAS typically found in serum, the surface of the nanoparticles (eg, polymer-coated FePt) is covered by a monolayer of the protein. Adapted from (Wolfgang Nature)

The equilateral triangular prism model shape has been also confirmed for BSA, using triangular sides of 8.4 nm and a thickness of 3.15 nm. The fact that the thickness measure around the quatsomes was 4,8 nm suggests that the protein is probably not interacting using its larger triangular phases. This could confirm the possible orientation propose for the protein in Figure 2.26 with the domains I (-10) and III (0) interacting with the membrane, and the domain II (-8) more exposed to the solvent.

At the interface between the region I and II (molar ratio BSA/CTAB= 0.02) the formation of BSA-quatsome complexes involving several vesicles coexist with BSA-coated vesicles. The domain II (-8), more exposed to the solvent, might be responsible for the vesicle-vesicle interaction acting as glue during complexes formation. In this region membrane rupture is produce and bigger vesicles enclosing smaller vesicles are formed. The big size of the complexes and multivesicular vesicles formed lead to an increase in the turbidity signal that was maintained until the end of the titration. In the region II the negative charge of BSA overcomes the net positive charge of CTAB, destabilizing the CTAB/cholesterol shynton and producing the rupture of quatsomes. In this region, complexes between BSA and the free CTAB monomers could be formed, which would explained the small exothermic peaks that appear in the last part of the titration.

It could be conclude from this part that the amount of protein added to the system strongly influences the physicochemical characteristics and morphology of the vesicles. The system experiences an important restructuring and phase transformation in the presence of high amounts of this negatively charge protein.

3.6 Summary

- ✓ BSA protein interacts with pure CTAB forming different kind of complexes depending on the molar ratio BSA/CTAB and on the concentration of CTAB.

- ✓ When BSA protein interact with CTAB in form of micelles, at BSA/CTAB molar ratios higher than 0.012 (CTAB/BSA< 83) the formation of BSA-CTAB complexes is produce. The formation of these complexes involved both electrostatic interactions (in greater extent) and hydrophobic interactions. At BSA/CTAB molar ratios lower than 0.012 (CTAB/BSA> 83) micelles interact with BSA forming micelles like aggregates.

- ✓ The BSA protein interacts with quatsomes membranes forming a layer of 4.8 nm approximately at molar ratio BSA/CTAB smaller than 0.02. BSA interacts with quatsomes through electrostatic interaction in the first place and by short range hydrophobic forces when the protein is close enough to the membrane.

- ✓ The BSA protein added to the quatsomes at molar ratios BSA/CTAB higher than 0.02 produces changes in the morphology and the physicochemical characteristics of quatsomes. Therefore is highly recommended to perform some interaction studies between the negatively charge proteins and in general any protein, and the quatsomes if encapsulation or functionalization experiments are going to be carried out.

- ✓ The strong influence of proteins such as BSA, very similar to HSA (the more abundant protein in the blood), in the stability and morphology of the quatsomes indicates that this carrier might not be suitable for intravenous drug delivery. Instead they could have promising application in topic delivery.

3.7 References

1 Talmadge, J. E. The pharmaceutics and delivery of therapeutic polypeptides and proteins. *Advanced drug delivery reviews* **10**, 247-299 (1993).

2 Nayak, A. K. Advances in therapeutic protein production and delivery. *International Journal of Pharmacy and Pharmaceutical Sciences* **2**, 1-5 (2010).

3 Eui, N. L. *et al.* Stabilizing peptide fusion for solving the stability and solubility problems of therapeutic proteins. *Pharmaceutical research* **22**, 1735-1746 (2005).

4 Colletier, J. P., Chaize, B., Winterhalter, M. & Fournier, D. Protein encapsulation in liposomes: Efficiency depends on interactions between protein and phospholipid bilayer. *BMC Biotechnology* **2** (2002).

5 Brinks, V., Jiskoot, W. & Schellekens, H. Immunogenicity of therapeutic proteins: The use of animal models. *Pharmaceutical research* **28**, 2379-2385 (2011).

6 Martins, S., Sarmento, B., Ferreira, D. C. & Souto, E. B. Lipid-based colloidal carriers for peptide and protein delivery - Liposomes versus lipid nanoparticles. *International journal of nanomedicine* **2**, 595-607 (2007).

7 Pisal, D. S., Kosloski, M. P. & Balu-Iyer, S. V. Delivery of therapeutic proteins. *Journal of pharmaceutical sciences* **99**, 2557-2575, doi: 10.1002/jps.22054 (2010).

8 Hwang, S. Y. *et al.* Effects of operating parameters on the efficiency of liposomal encapsulation of enzymes. *Colloids and Surfaces B: Biointerfaces* **94**, 296-303 (2012).

9 Yatuv, R., Robinson, M., Dayan, I. & Baru, M. Enhancement of the efficacy of therapeutic proteins by formulation with PEGylated liposomes; A case of FVIII, FVIIa and G-CSF. *Expert Opin. Drug Deliv.* **7**, 187-201 (2010).

10 Torchilin, V. P. Recent advances with liposomes as pharmaceutical carriers. *Nature Rev. Drug Discov.* **4**, 145-160 (2005).

11 Janknegt, R., De Marie, S., Bakker-Woudenberg, I. A. J. M. & Crommelin, D. J. A. Liposomal and lipid formulations of amphotericin B. Clinical pharmacokinetics. *Clinical Pharmacokinetics* **23**, 279-291 (1992).

12 Couvreur, P., Dubernet, C. & Puisieux, F. Controlled drug delivery with nanoparticles: Current possibilities and future trends. *European Journal of Pharmaceutics and Biopharmaceutics* **41**, 2-13 (1995).

13 Lidia Ferrer-Tasies, E. M. -C., Mary Cano-Sarabia, Marcel Aguilella-Arzo, Angelina Angelova, Sylviane Lesieur, Susagna Ricart, Jordi Faraudo, Nora Ventosa, and Jaume Veciana Quatsomes: Vesicles Formed by Self-Assembly of Sterols and Quaternary Ammonium Surfactants. *Langmuir* **29**, 6519-6528 (2013).

14 Krister Holmberg, B. J., Bengt Kronberg and Bjorn Lindman. Surfactants and polymers in aqueous solution. *Copyright © 2002 John Wiley & Sons, Ltd.*, 2003.

15 Azarmi, S., Roa, W. H. & Löbenberg, R. Targeted delivery of nanoparticles for the treatment of lung diseases. *Advanced drug delivery reviews* **60**, 863-875, (2008).

16 Kubo, T. *et al.* Targeted delivery of anticancer drugs with intravenously administered magnetic liposomes in osteosarcoma-bearing hamsters. *International journal of oncology* **17**, 309-315 (2000).

17 Sawant, R. R. & Torchilin, V. P. Liposomes as 'smart' pharmaceutical nanocarriers. *Soft Matter* **6**, 4026, doi:10.1039/b923535n (2010).

18 Søren T. Larsen, H. V. a. G. D. N. Airway Effects of Inhaled Quaternary Ammonium Compounds in Mice. *Basic & Clinical Pharmacology & Toxicology* **110**, 537-543 (2012).

19 Chang, W. K. *et al.* The comparison of protein-entrapped liposomes and lipoparticles: preparation, characterization, and efficacy of cellular uptake. *International journal of nanomedicine* **6**, 2403-2417 (2011).

20 Luisa Corvo, M. *et al.* Superoxide dismutase entrapped in long-circulating liposomes: Formulation design and therapeutic activity in rat adjuvant arthritis. *Biochimica et Biophysica Acta - Biomembranes* **1564**, 227-236 (2002).

21 Li, Y., Wang, X. & Wang, Y. Comparative Studies on Interactions of Bovine Serum Albumin with Cationic Gemini and Single-Chain Surfactants. *The Journal of Physical Chemistry B* **110**, 8499-8505, doi:10.1021/jp060532n (2006).

22 Chakraborti, S. *et al.* Interaction of Polyethyleneimine-Functionalized ZnO Nanoparticles with Bovine Serum Albumin. *Langmuir* **28**, 11142-11152, doi:10.1021/la3007603 (2012).

23 Yokouchi, Y. *et al.* Effect of adsorption of bovine serum albumin on liposomal membrane characteristics. *Colloids and Surfaces B: Biointerfaces* **20**, 95-103, (2001).

24 Yajuan Li, X. W., and Yilin Wang. Comparative Studies on Interactions of Bovine Serum Albumin with Cationic Gemini and Single-Chain Surfactants. *J. Phys. Chem. B* **110**, 8499-8505 (2006).

25 Deep, S. & Ahluwalia, J. C. Interaction of bovine serum albumin with anionic surfactants. *Physical Chemistry Chemical Physics* **3**, 4583-4591 (2001).

26 New, D. M. Surfaces, Interfaces, and Colloids: Principles and Applications, Second Edition. *John Wiley & Sons, Inc.* (1999).

27 Myers, D. Surfaces, Interfaces, and Colloids: Principles and Applications, Second Edition. *Copyright 1999 John Wiley & Sons, Inc.* (1999).

28 Blandamer, M. J., Cullis, P. M., Soldi, L. G., Rao, K. C. & Subha, M. C. S. Effects of added dotab on the cmc and enthalpy of micelle formation at 298.2 K for CTAB(aq). *Journal of Thermal Analysis* **46**, 1583-1588 (1996).

29 Collins, R. J. F. a. B. M. Survey of the year 2009: applications of isothermal titration calorimetry. *J. Mol. Recognit.* **24**, 1–16 (2011).

30 Kawthar Bouchemala, F. A., Armand Koffi, Madeleine Djabourov and Gilles Ponchel. What can isothermal titration microcalorimetry experiments tell us about the self-organization of surfactants into micelles? *J. Mol. Recognit.* **23**, 335–342 (2010).

31 Bouchemal, K. New challenges for pharmaceutical formulations and drug delivery systems characterization using isothermal titration calorimetry. *Drug Discov. Today* **13**, 960-972, (2008).

32 ITC., I. t. MicroCal manual. (2010).

33 Katja Beyer, D. L., Alfred Blume. The demicellization of alkyltrimethylammonium bromides in 0.1M sodium chloride solution studied by isothermal titration calorimetry. *Colloids and Surfaces B: Biointerfaces* **49**, 31–39 (2006).

34 Katja Beyer, D. L., Alfred Blume. The demicellization of alkyltrimethylammonium bromides in 0.1M sodium chloride solution studied by isothermal titration calorimetry. *Colloids and Surfaces B: Biointerfaces*

49, 31-39 (2006).

35 Kelley, D. & McClements, D. J. Interactions of bovine serum albumin with ionic surfactants in aqueous solutions. *Food Hydrocolloids* **17**, 73-85 (2003).
36 Ross, P. D. & Subramanian, S. Thermodynamics of protein association reactions: forces contributing to stability. *Biochemistry* **20**, 3096-3102 (1981).
37 Gull, N. *et al.* Spectroscopic studies on the interaction of cationic surfactants with bovine serum albumin. *Colloids and Surfaces B: Biointerfaces* **69**, 122-128 (2009).
38 Franklin, J. M., Surampudi, L. N., Ashbaugh, H. S. & Pozzo, D. C. Numerical validation of IFT in the analysis of protein-surfactant complexes with SAXS and SANS. *Langmuir* **28**, 12593-12600 (2012).
39 Montserrat Samsó, J.-R. D., Steen Hansen, Gareth. R Jones. Evidence for sodium dodecyl sulphate/protein complexes adopting a necklace structure. *Eur. J. Biochem* **232**, 818-824 (1995).
40 Gull, N., Chodankar, S., Aswal, V. K. & Kabir Ud, D. Small angle neutron scattering studies on the interaction of cationic surfactants with bovine serum albumin. *Pramana - Journal of Physics* **71**, 1027-1031 (2008).
41 Ibel, K. *et al.* Protein-decorated micelle structure of sodium-dodecyl-sulfate-protein complexes as determined by neutron scattering. *European Journal of Biochemistry* **190**, 311-318 (1990).
42 Chodankar, S., Aswal, V. K., Kohlbrecher, J., Vavrin, R. & Wagh, A. G. Surfactant-induced protein unfolding as studied by small-angle neutron scattering and dynamic light scattering. *Journal of Physics Condensed Matter* **19** (2007).
43 Jung, S. H. *et al.* Increased stability in plasma and enhanced cellular uptake of thermally denatured albumin-coated liposomes. *Colloids and Surfaces B: Biointerfaces* **76**, 434-440 (2010).
44 Anbazhagan, V., Sankhala, R. S., Singh, B. P. & Swamy, M. J. Isothermal titration calorimetric studies on the interaction of the major bovine seminal plasma protein, PDC-109 with phospholipid membranes. *PLoS ONE* **6** (2011).
45 Yu-LiLo, Y.-E. R. Protein location in liposomes, A drug carrier: A prediction by Differencial Scanning Calorimetry. *Journal of Pharmaceutical Sicences* (1995).
46 Dimitrova, M. N., Matsumura, H., Terezova, N. & Neytchev, V. Binding of globular proteins to lipid membranes studied by isothermal titration calorimetry and fluorescence. *Colloids and Surfaces B: Biointerfaces* **24**, 53-61 (2002).
47 Röcker, C., Pötzl, M., Zhang, F., Parak, W. J. & Nienhaus, G. U. A quantitative fluorescence study of protein monolayer formation on colloidal nanoparticles. *Nature Nanotechnology* **4**, 577-580 (2009).

Chapter 3: Nanovesicle-GLAconjugates prepared by DELOS-SUSP as nanomedicine candidate for the treatment of Fabry disease.

3.1 Introduction

In Chapter 1 it has been shown the suitability of DELOS-SUSP for the production of nanovesicle-bioactive conjugates with outstanding morphological and physicochemical characteristics. Importantly, the activity of the integrated biomolecules was not affected after the processing and the methodology was scalable allowing the obtaining of nanoconjugates with good physicochemical and morphological characteristics. Using this one-step methodology, liposome and quatsome-based platforms with great potentiality as drug delivery nanocarriers, were developed. In this chapter we explore for the first time the possibility of using these delivery platforms and DELOS-SUSP methodology for the preparation of a new nanomedicine candidate for the treatment of the Fabry's disease.

3.2 GLA loaded- liposome_RGD conjugates for the treatment of Fabry disease

3.2.1 Fabry's disease

Fabry's disease is a lysosomal storage disorder, caused by a gene mutation of the X-chromosome resulting in an alpha-galactosidase (GLA) enzyme deficiency. This lack of enzyme provokes the accumulation of naturally produce glycosphingolipids, mainly globotriaosylceramide (Gb3), at the lysosomes of some cells. The Gb3 progressive accumulation into a variety cell types, including vascular endothelial cells (the main affected cells), renal cell types, cardio-myocytes and neurons, lead to multi-systemic clinical symptoms[1,2]. The lysosomal enzyme α-galactosidase (GLA) is a homodimeric glycoprotein formed by two identical molecules, each one composed of two domains, one active and other non-active (Figure 3.1).

This disease affects both males and females with an estimated incidence of 1 per 117 000 live births[2], so it is included in the group of "rare diseases", also called "orphan diseases". First signs of the illness usually appear during the childhood but due to the non-specific symptoms, a correct diagnosis sometimes is delayed and with it, a treatment in earlier stages of the disease. Patiens with the Fabry's disease can present severe kidney disfunctions[3], cardiac issues[4,5], neurological involvement[6], among others affections.

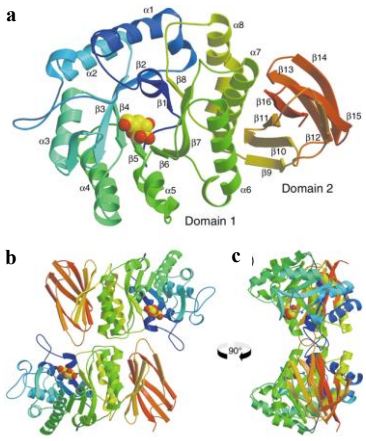

Figure 3.1. Structure of GLA . (a) The GLA monomer composed by domain 1, containing the active site and domain 2. (b) and (c) are two views of GLA dimer.

The current treatment, available since 2001, is the enzyme replacement therapy (ERT) in which two recombinant protein replacement drugs are used: agalsidase alfa (Replagal® from Shire Human Genetic Therapies, Dublin, Ireland) and agalsidase beta (Fabrazyme® from Genzyme Corporation, Cambridge, MA) both approved for intravenous administration at different doses[7-9]. Although both enzymes contain a recombinant human GLA enzyme and exhibit identical biochemical composition, their production processes are different. The ERT has demonstrated positive short-term effects on different organs, reducing the progression of the disease and improving the quality of life of patients[10,11]. However this approach presents some disadvantages related to its limited efficacy in patients with an advance stage of the disease, due to the partially removal of the enzyme from the circulation by the liver and the spleen and also the high cost of the treatment[2,12]. For this reason new treatment strategies are nowadays under investigation. For instance, there are some emerging therapies based on small molecular drugs, such as gene therapy[13], substrate reduction[14,15], residual enzyme activation[16] and chemical chaperones therapy[17-19]. Of these, only the chemical chaperones therapy has recently arise as a potential real therapeutic alternative for the Fabry's disease. These molecules can bind to mutant enzyme proteins and assist in their correct folding maturation and trafficking to their functional site, such as the lysosomes. Other approach under development is the use of drug delivery systems for the targeted delivery of the GLA enzyme in order to enhance the efficacy of the ERT and reduce its cost. Polymeric particles coated with an antibody to ICAM-1, a protein expressed on the gastrointestinal epithelium and other tissues, and loaded with GLA have shown an

increase enzyme delivery to organs in the body and vascular endothelial cells as well as a high Gb3 degradation[20]. Along the same direction, Giannotti et al. recently reported the formation of stable polyelectrolyte complexes (PECs) between trimethyl chitosan (TMC) and the GLA protein, and their traffic to lysosomal compartments of human endothelial cells[21].

In this context came out the NanoFabry project, a consortium of Catalan research teams founded by the "Fundació La Marató de TV3", with the objective of ameliorate the current ERT's of Fabry's disieases. Taking into consideration the good results obtained with DELOS-SUSP in the preparation of different nanoconjugates, in the present Thesis and in the framework of NanoFabry project, our goal was the preparation of functionalized vesicle-GLA nanoconjugates capable of a specific deliver of the GLA enzyme to endothelial cells.

For this purpose a His-tagged human α-Galactosidase A enzyme produced by the Instituto de Biotecnologia y Biomedicina (IBB-UAB) was used. The particularity of this GLA enzyme is the presence of a 6_histidine tag in its structure (100 KDa) that allows the enzyme purification in a single step[22]. More over for the production of this sample a transient gene expression of recombinant human a-galactosidase A was developed (Experimental Section 5.3). With this protocol they were able to produce up to several milligrams per liter of highly pure active enzyme in a time as short as a few days. It should be noted that the treatment of Fabry's patients is for life and it is necessary to use doses of several milligrams per patient every 2 weeks. Therefore, successful alternatives to obtain GLA for therapeutic uses could alleviate the cost of such highly expensive treatment. Besides, the availability of large quantities of recombinant human GLA by a simple, fast procedure is necessary for the development and evaluation of alternatives treatments like the one undertaken in this Thesis.

3.2.2 Selecting a suitable nanocarrier for the encapsulation of GLA

The physicochemical and structural characteristics of a nanocarrier exert a direct influence in the pharmacological properties and the behavior of a nanocarrier-bioactive conjugate[23]. Therefore the selection of the suitable nanocarrier for each application is of a great importance. For the treatment of Fabry's disease GLA should be administrated intravenously and hence besides good physicochemical characteristics like a proper size lower than 200 nm, homogeneous morphology and stability, the nanocarrier should be sterile, no cytotoxic and non-hemolytic. Another important aspect is that the nanocarrier

should be able to reach the lysosomes, were the accumulation of Gb3 takes place. In Chapter 1 different vesicle-based platforms such as plain liposomes, liposome_PEG and liposomes_RGD were successfully prepared and characterized. Although all these platforms meet the requirements to be administrated intravenously, only the liposomes functionalized with the RGD targeting moiety, were in principle able to reach the lysosomes. Besides, RGD can recognize integrins, that are over-expressed in cells affected with the Fabry's disease which could allow a more specific and effective targeting. Therefore liposome_RGD conjugates were selected as optimal nanocarriers for the encapsulation of the enzyme.

It is described that the higher the lipid concentration, the greater the loading capabilities of a liposome[24]. Accordingly and in order to enhance the capabilities of the vesicles to incorporate more amounts of protein, plain liposome_RGD conjugates three times more concentrated in lipid mass were synthesized. For doing this, a volumetrically expanded organic phase containing DPPC, cholesterol and cholesterol-PEG_{200}-RGD in a molar ratio 10:6:1 was depressurized in a small volume of mQ water (Table 3.1). Note that DELOS-SUSP process was carried out maintaining the same composition in the organic phase but adding less water to the aqueous phase. With this small change the actual concentration of the lipids forming the liposomes increased from 1.4 to 5 mg/mL, as well as the ethanol percentage from rises 4.7 to 16.7 %. The resulting liposome-RGD conjugates presented bigger sizes (199 nm) and smaller Z potential (+13) than those described in Chapter 1, made with a lipid concentration of 1.4 mg/mL (Table 3.1). Nevertheless the cryo-TEM images of liposomes with a higher lipid concentration and with a 36 % molar in cholesterol content, depicted spherical and unilamellar characteristics (Figure 3.2).

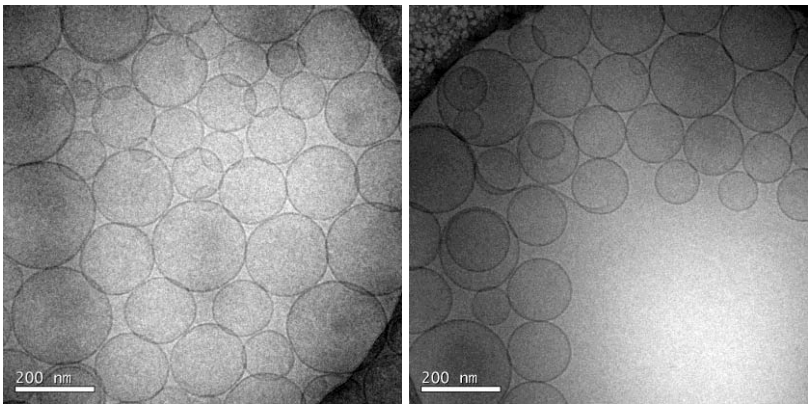

Figure 3.2. Morphology of the liposome-RGD conjugates whit a lipid concentration of 5 mg/mL.

The stability of the system under storage conditions was also assayed. First signs of flocculation were observed after 6 days of preparation, a phenomenon that was coincident with a drop in the Z potential from +13 to +6 (Figure 3.3). Therefore the stability of the liposomes was lower than for those reported in Chapter 1, which stay stable for at least 60 days.

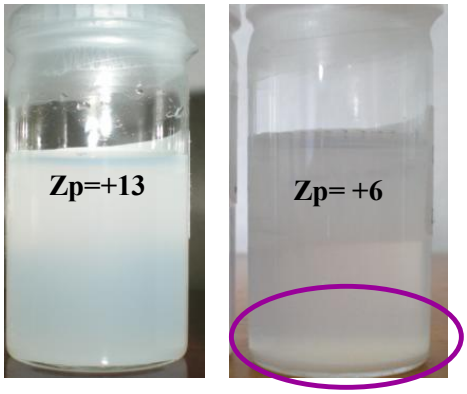

Figure 3.3. Macroscopic appearances of liposome_RGD nanoconjugates with a lipid concentration of 5 mg/mL as prepared (left) and 6 days later (right).

The stability, cytotoxicity and hemocompatibility of the liposome-RGD conjugate with the higher lipid concentrations were tested by the group of Dr.Simó Schwartz Jr. (Vall d'Hebron Hospital) for comparison with the liposomes prepared with a lower lipid concentration. The cytotoxicity and hemocompatibility assays were performed using HMEC and HeLa cells, following the protocols described in the Experimental Section 9.2 and 9.3. The liposome_RGD conjugates with a lipid concentration of 5 mg/mL resulted non-toxic and non-hemolytic. Their stability in different media was also tested by incubating the conjugates with PBS buffer, saline serum and culture media at room temperature. After one day of incubation the presence of aggregates was detected only in the vesicles with higher lipidic concentration, indicating some instability of the fomulation (Figure 3.4).

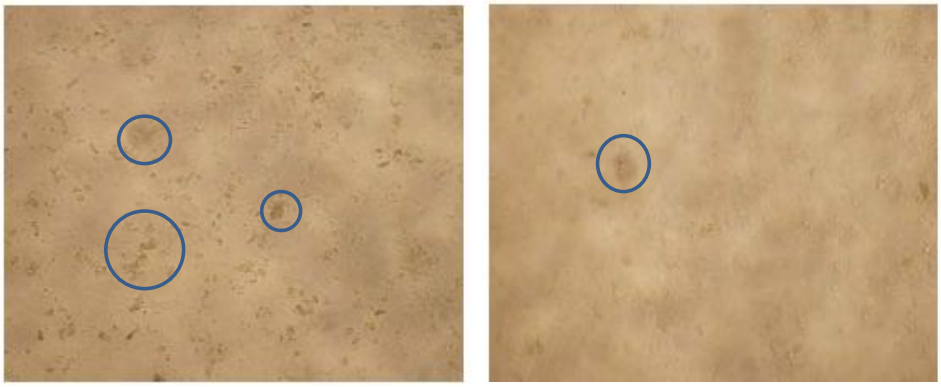

Figure 3.4. Appearance of the precipitates found when liposome_RGD conjugates (5 mg/mL) where incubated with culture media. The blue circles are pointing the precipitates.

Vesicles aggregation and precipitate formation are undesirable phenomena for a nanocarrier to be used in intravenous drug delivery since they could produce embolia. Therefore, even if the loading capacity is lower, the nanocarriers with a lipid concentration of 1.5 mg/mL, that show a higher stability in the different media, was selected for the encapsulation experiments of GLA enzyme.

Liposome-RGD conjugates with different percentage of cholesterol content were also prepared since it is well known that the presence of cholesterol confers rigidity to the membrane of liposomes[25]. Specifically, liposomes with 3 to 23 % mol content of cholesterol were prepared using DELOS-SUSP along with the previously obtained liposomes containing 36 % mol. Liposomes containing only DPPC were also prepare for comparison purposes. The compositions of the organic phase used for the preparation of these nanocarriers are shown in Table 3.1. The depressurization step took place always in mQ water. When analyzing the physicochemical characteristics of the new carriers obtained, it was observed that the higher the cholesterol concentration the smaller the size of the liposomes and the higher the Z potentials (Table 3.1).

Table 3.1. Compositions used for the preparation different liposome-RGD carriers by DELOS-SUSP method and their physicochemical characteristics.

Vesicle systems (% mol cholesterol)[a]	Organic phase	Aqueous phase	Lipidic concentration (mg/mL)[b]	Size	Z pot.
Liposomes (0%)	DPPC (41 mM)	water	1.4	873±22	19±13
Liposome_RGD (3 %)	DPPC (27 mM) + CHOL_PEG_{200}–RGD (2.8 mM)	water	1.1	530±82	25±1
Liposome_RGD (23 %)	Cholesterol (8.6mM) + DPPC (27 mM) + CHOL_PEG_{200}–RGD (2.8 mM)	water	1.3	228±4	33.0±0.4
Liposome_RGD (36 %)[c]	Cholesterol (17 mM) + DPPC (27 mM) + CHOL_PEG_{200}–RGD (2.8 mM)	water	1.4	144±11	31±2
Liposome_RGD (36 %)	Cholesterol (17 mM) + DPPC (27 mM) + CHOL_PEG_{200}–RGD (2.8 mM)	water[d]	5	199±3	12.5±0.4

Experiments were performed from CO_2-expanded ethanol at 10 MPa, 308K and X_{CO2}= 0.85. [a]Percentage of cholesterol in moles with respect of total amount of lipid moles. [b]Ratio between the total amount of lipids forming the membrane and the volume of the final vesicular suspension. [c]Percentage of cholesterol in moles normally used in liposome_RGD conjugates (see Chapter 1). [d]The volume of the aqueous phase in this case was 6 mL.

The cryo-TEM images showed that when the cholesterol content was small or when this sterol was not included in the formulation, the vesicles were bigger in size and inhomogeneous. The presence of high cholesterol percentage was essential in order to achieve small vesicles with homogeneous morphology (Figure 3.5).

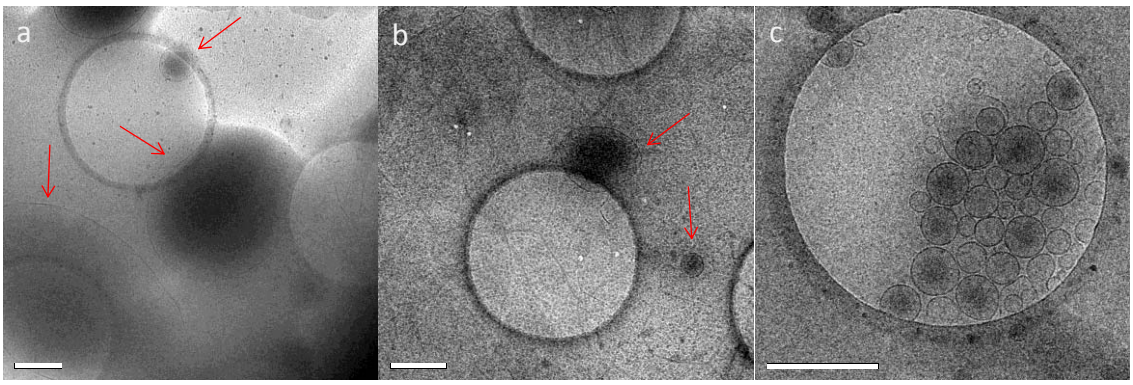

Figure 3.5. Cryo-TEM images of Liposome-RGD conjugates with different percentages of cholesterol. a) 0%, b) 3 %, c) 23 %. The red arrows are pointing liposomes. Scale bars are 500 nm

3.2.3 Influence of DELOS-SUSP in the GLA bioactivity

Before starting the encapsulation experiments of GLA in liposome_RGD carriers, the influence of the preparation methodology on the biological activity of this enzyme was studied. The biological activity is an important parameter usually correlated with the function of enzymes, proteins and peptides. A practical way to express this parameter is the specific activity, which is the enzyme activity per milligram of total protein and is usually constant for a pure enzyme. The enzyme activity is a measure of the quantity of active enzyme present in the studied sample and is dependent on conditions, which should be specified. This activity is determined *in vitro* and is equal to the moles of substrate, which is the molecule upon which an enzyme acts, converted per unit of time. Due to the importance of this parameter, the stability of active GLAduring the DELOS-SUSP processing was studied through specific enzymatic activity measurements. In order to do so, the process was performed without the presence of lipids (Figure 3.6). Thus, the organic phase formed by a small volume of ethanol was volumetrically expanded with CO_2 and afterwards depressurized over the aqueous phase containing the enzyme at a concentration of 2.9 μg/mL. A reference sample of GLAin water (2.9 μg/mL) and a blank of ethanol expanded with CO_2 in water were also prepared.

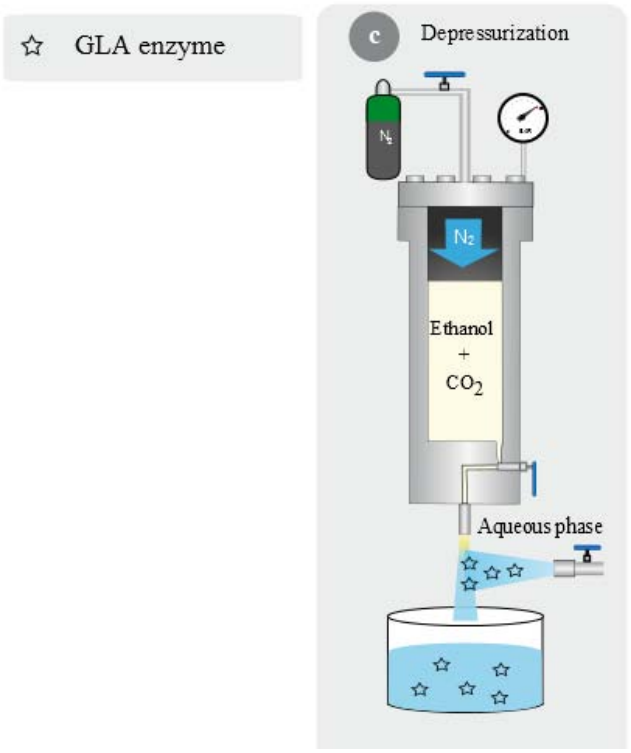

Figure 3.6. Schematic representation of DELOS-SUSP process performed in presence of the enzyme but without the presence of lipids.

Following a fluorescent protocol described in Experimental Section 7.2.1, the enzymatic activity was measured for duplicated in each sample (Table 3.2).

Table 3.2. Influence of DELOS-SUSP process in the enzymatic activity of α–GLA

Sample	Time (h)	Fluorescence	Enzymatic activity[a] (ng 4-MU /mL)
Blank (EtOH/Water)	1	3.50 ± 0.01	2.1 ± 0.01
α–GAL/ H_2O (No DELOS-SUSP)	1	796 ± 40	364 ± 18
α–GAL/ H_2O (AfterDELOS-SUSP)	1	841 ± 21	385 ± 9

[a] The measuring unit of the enzymatic activity is refer to the ng of substrate, which is in this case 4-metilumbeliferona (4-MU), per milliliter of the solution containing the enzyme.

No significant differences were encountered in the enzymatic activity of GLA before and after the processing with the DELOS-SUSP, which indicated that this compressed fluid based-process was suitable for preparing GLA loaded-liposome_RGD conjugates.

3.2.4 Preparation of GLA loaded-liposome_RGD conjugates using DELOS-SUSP.

As showed in Chapter 1, liposome-RGD nanocarriers constitute excellent candidates for the specific delivery of active molecules to endothelial cells. Therefore encapsulation experiments of GLA enzyme in the carriers were performed using DELOS-SUSP method. This enzyme presents a high molecular weight of 100 KDa, is water soluble and is preserved in acetic buffer (pH=5.7) at -20 ^{0}C until its use. The enzyme working concentration for the encapsulation experiments was selected based on the minimum GLA concentration necessary to perform further in-vitro activity assays and on the characteristics of the α-GAL. Taking into account this data, the selected GLA concentration for starting the entrapment experiments was 1.5 μg/mL. For the nanonjugates preparation, an ethanolic solution containing DPPC, cholesterol and cholesterol_PEG_{200} in a molar ratio 6:10:1 was added to the reactor and pressurized with CO_2 (Experimental Section 2.1.1). 20 minutes before the depressurization, the enzyme kept all the time at -20 ^{0} C, was taken out from the freezer and leaved at room temperature until defrost. Once defrost, a volume of this solution was dissolved in 24 mL of mQ water. Finally the liposomal formulation was formed by depressurizing the CO_2-expanded solution of lipids over the aqueous solution containing the GLA (Figure 3.7). The final nominal enzyme concentration in the vesicular suspension was 1.5 μg/mL.

Using the previously described procedure, other GLA loaded liposome_RGD conjugates were prepared varying the vesicular media, the amount of enzyme to be entrapped and the nanocarriers compositions. In Table 3.3 the compositions of the organic and the aqueous phases used for the preparation of all conjugates are described. Plain liposome_RGD nanocarriers were also synthesis for comparison with the loaded liposomes.

Table 3.3. Compositions used for the preparation of different GLA loaded liposome_RGD conjugates by DELOS-SUSP method

Vesicular systems (code)	Organic phase	Aqueous phase	GLA/lipid ratio[a] (nmol/mmol)	Lipidic. conc.[b] (mg/mL)
GLA loaded liposome_RGD (1)	Cholesterol (17 mM) + DPPC (27 mM) + $CHOL\_PEG_{200}$–RGD (2.8 mM)	GLA in water (15.7 nM)[c]	6	1.4
GLA loaded liposome_RGD (2)	Cholesterol (17 mM) + DPPC (27 mM) + $CHOL\_PEG_{200}$–RGD (2.8 mM)	GLA in acetic buffer (78.7 nM)[c]	33	1.4
GLA loaded liposome_RGD (3)	Cholesterol (17 mM) + DPPC (27 mM) + $CHOL\_PEG_{200}$–RGD (2.8 mM)	GLA in water (78.7 nM)[c]	33	1.4
GLA loaded liposome_RGD (4)	Cholesterol (8.6 mM) + DPPC (27 mM) + $CHOL\_PEG_{200}$–RGD (2.8 mM)	GLA in water (89.2nM)[d]	46	1.3
GLA loaded liposome_RGD (5)	Cholesterol (17mM) + DPPC (27 mM) + $CHOL\_PEG_{200}$–RGD (2.8 mM)	GLA in water (89.2nM)[d]	38	1.4
liposome-RGD	Cholesterol (17 mM) + DPPC (27 mM) + $CHOL\_PEG_{200}$–RGD (2.8 mM)	water	-	1.4

Entrapment experiments were performed from CO_2-expanded ethanol at 10 MPa, 308K and X_{CO2}= 0.85. [a]Ratio between the moles of initial enzyme and the total moles of lipids forming the liposome membrane. [b]Ratio between the total amount of lipid forming membrane and the volume of the final vesicular suspension. [c]Characteristics of the used GLAbatch 120308 with an enzymatic activity of 2518 μmol/h.mg and an enzyme concentration of 0.32 mg/mL.[d]Characteristics of the used GLAbatch 120531with an enzymatic activity=2151 μmol/h.mg and an enzyme concentration of 0.25 mg/mL.

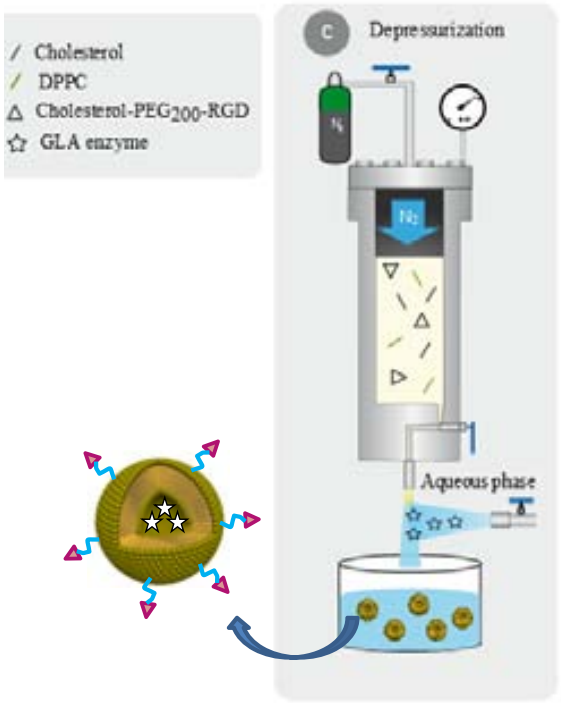

Figure 3.7. Schematic representation of DELOS-SUSP depressurization stage to prepare GLA loaded liposome_RGD conjugates. In this stage the volumetric expanded organic phase containing the lipid forming the membrane, are depressurized over the aqueous solution containing the enzyme to produce the conjugates. The overall process lasted 2 hours approximately.

3.3.4.1 Characterization of the GLA loaded liposome_RGD conjugates

The physicochemical characteristics of the conjugates were measured using a dynamic light scattering analyser (Table 3.4). All prepared systems presented nanoscopic sizes and a Z potentials smaller than that for the plain liposome_RGD carrier. The bigger sizes and polidispersity indexes were found for the conjugates prepared in the acetic buffer (Table 3.4 entry # 2) and for those prepared with less amount of cholesterol in the membrane (Table 3.4 entry # 4) indicating that the conjugates with the best physico-chemical characteristics were the ones prepared in water and containing 36% mol of cholesterol. Cryo-TEM images showed that the suspensions were mainly formed by unilamellar nanoscopic spherical vesicles (Figure 3.8).

Table 3.4. Physicochemical characteristics, entrapment efficiency and loading of GLA loaded liposome_RGD conjugates. The physic-chemical characteristics of the conjugates after the separation of the non-integrated enzyme are given between brackets.

Vesicle systems (code)	Size		Z potential (mV)	EE (%)	Enzyme loading [c] (μg/mg)	Enzyme conc.[d] (μg/mL)
	Mean [a] (nm)	PdI [b]				
GLA loaded liposome_RGD (1)	150±1 (203±8)	0.29±0.02 (0.38±0.03)	12±1 (8±2)	25±5	0.3	1.5 (0.4)
GLA loaded liposome_RGD (2)	210±3 (334±13)	0.52±0.01 (0.74±0.04)	4.10±0.43 (6± 1)	22	1.2	7.5 (1.6)
GLA loaded liposome_RGD (3)	159±12 (230 ± 12)	0.32±0.01 (0.42±0.03)	5.3±0.4 (-46 ± 1)	32±5	1.7	7.5 (2.4)
GLA loaded liposome_RGD (4)	470±23 (1016±49)	0.70±0.1 (0.43±0.10)	16.2±0.3 (12.5 ± 0.1)	36	2.4	8.5 (3)
GLA loaded liposome_RGD (5)	202±10 (321±22)	0.40±0.01 (0.78±0.20)	21±3 (13±7)	30±1	1.8	8.5 (2.5)
Liposome-RGD/water (blank)	151 ± 4	0.30 ± 0 .01	29 ± 1	-	-	

[a] Intensity weighted mean hydrodynamic size of the collection of vesicles measured by dynamic light scatering. [b] Polidispersity index showing the width of the particle size distribution. [c] Mass of the integrated protein divided by the total mass of the lipids comprising the membrane.[d] Mass of the total amount of protein present divided by the volume of the vesicular suspension.

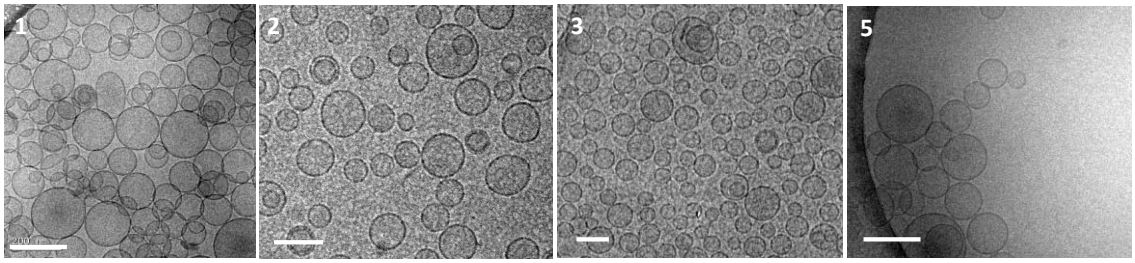

Figure 3.8. Cryo-TEM image depicting the morphology of GLA loaded liposome_RGD conjugates. The number on the image corresponds to the same code assigned to each liposomal system on the Table 3.4. Scale bars are 200 nm

The enzyme loading in the nanovesicles were measured after separating the free enzyme from the total vesicle suspension. The first attempts for separating the free enzyme were made by centrifugation with centricons and by Size Exclusion Chromatography (SEC) but these processes were not appropriated. On the contrary a centrifugation process allowed making the separation of the enzyme. The procedure consisted in placing 1.5 mL of the sample in an eppendorf tube and centrifuging consecutively at 277 K and at different speeds (6000, 9000 and 12000 rpm), during 1 h (Experimental

Section 4.1.2). After the supernatant withdrawn, the resulting pellet was re-suspended until the same initial volume of 1.5 mL was attained (Figure 3.9).

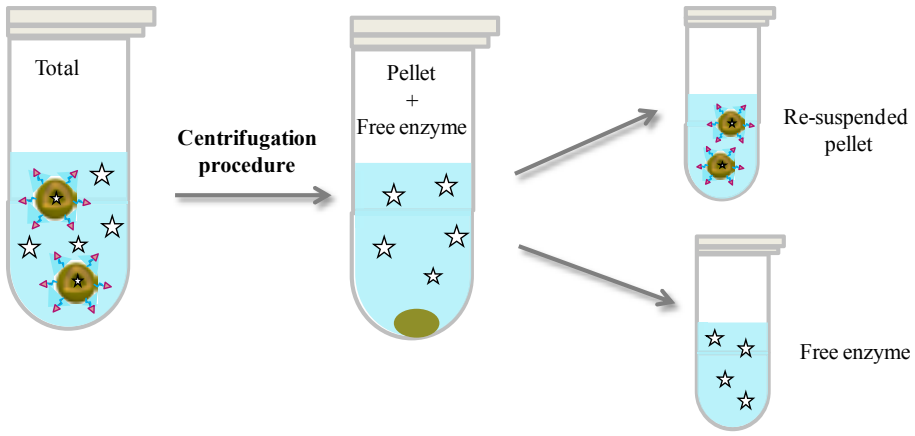

Figure 3.9. Scheme of the centrifugation procedure performed in order to separate the free enzyme from the loaded conjugates.

The amount of incorporated enzyme into the liposomes was quantified by the group of Prof. Villaverde (IBB). For this quantification, the total sample, the re-suspended pellet, the supernatant liquid and a blank of liposome_RGD conjugates were analyzed and quantified by SDS-PAGE and later on by Western-blot (Experimental Section 4.2.4). The entrapment efficiency and the active loading were calculated using Eq. 1 and 2:

$$Entrapmentefficienty(\%EE) = \frac{mass\ of\ integrated\ active}{initialmassofactive} * 100 \qquad \text{(Eq. 1)}$$

$$Protein\ loading\left(\frac{w}{w}\right) = \frac{massofintegratedactive}{massoflipids} \qquad \text{(Eq. 2)}$$

The final result of this quantification and the enzyme loading for the conjugates is shown is Table 3.4. It is observed that all entrapment efficiencies are above the 25% which is considered as high values taken into account that the hydrosoluble enzyme is encapsulated in SUVs. For the conjugates n° 1, 3 and 5, prepared with the same membrane composition and dispersant media, the higher the initial enzyme concentration the better the %EE and the enzyme loading. In the case of the conjugates n° 2 and 3, prepared with the same membrane composition and initial enzyme/lipid ratio, but in different media, although the liposomes obtained were spherical and

unilamellar, smaller sizes and better loading were achieved for the conjugates prepared in water.

After the centrifugation process the physico-chemical characteristics and the morphology were also measured for the loaded conjugates (re-suspended pellets) free of the non-integrated enzyme (Table 3.4). It can be observed that there is an increase in the size of all loaded conjugates indicating the formation of bigger vesicles. The polidispersity index was also bigger after the centrifugation which means that the re-suspended systems are also less homogenous. Cryo-TEM images depicted bigger liposomes and the presence of multilamellar structures. Although the centrifugation methodology was able to separate the free enzyme, the resulting loaded systems presented a less homogenous vesicular system regarding size and lamellarity (Figure 3.10).

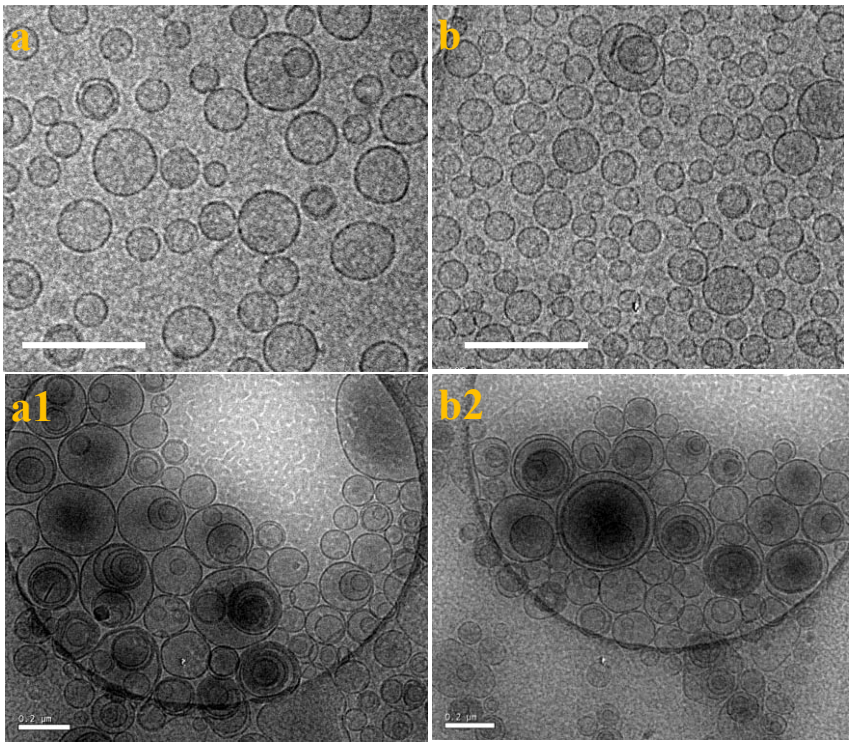

Figure 3.10. Cryo-TEM images of (a) GLA loaded liposome-RGD conjugates in acetic buffer and (b) in water. (a1) GLA loaded liposome-RGD conjugates in acetic buffer after the centrifugation procedure. (a2) GLA loaded liposome-RGD conjugates in water after the centrifugation procedure. Scale bars are 200 nm

3.2.5 Cytotoxicity and hemocompatibility assays

Sterility, cytotoxicity and hemocompatibility assays of the GLA loaded liposome_RGD conjugates were carried out by the group of Prof. Simó Schwartz Jr. (Vall d'Hebron

Hospital). The cytotoxicity of these conjugates was tested with HeLa and HMEC-1 cells by the SRB method. The resulting values were compared with those obtained for liposome-RGD conjugates and plain liposomes (Figure 3.11). For the three samples the cell viability of both cell lines was not affected after 72 h incubation with the vesicles, at lipid concentrations lower than 100 µg/mL. No significant differences were observed between plain or RGD containing liposomes with respect to those containing α-GAL, indicating that addition of the enzyme did not affect cell proliferation and viability. Therefore the studied liposomes were non-toxic at lipid concentration lower than 100 µg/mL.

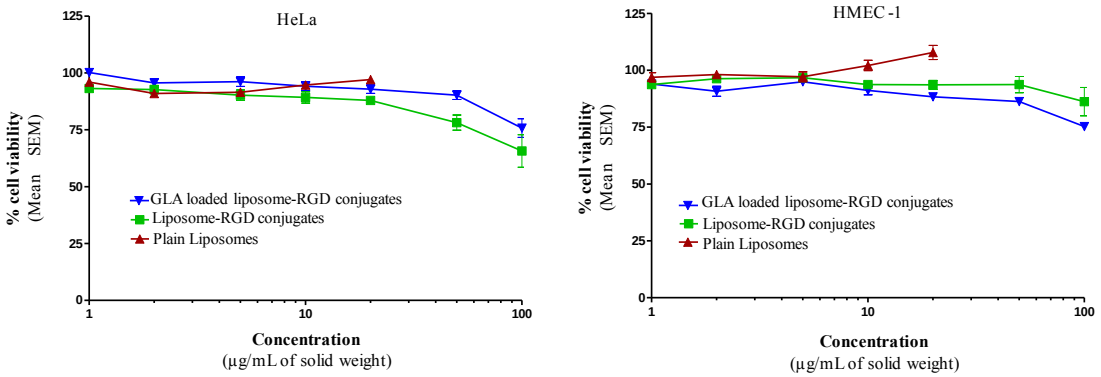

Figure 3.11. Citotoxicity of plain liposomes, liposome-RGD conjugates and GLA loaded liposome-RGD (sample 1) conjugates in HeLa and HMEC-1 cells.

When performed the hemocompatibility assays, the haemolisys percentages for the three studied liposomal systems were always under 2% meaning that the they were not hemolytic (Figure 3.12) and thus suitable to be administrated intravenously.

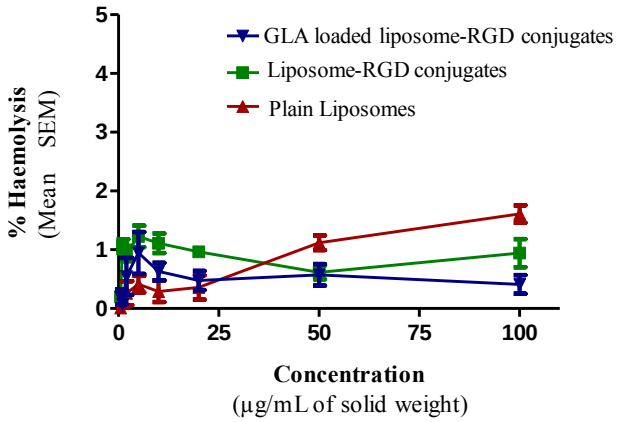

Figure 3.12. Haemolisys of plain liposomes, liposome_RGD conjugates and GLA loaded liposome_RGD conjugates carried out on blood cell fractions of three mice.

3.2.6 Stability of the GLA loaded liposome_RGD conjugates

An important requisite for the effective use of liposomes as drug carriers is their stability. The stability is influenced not only by the structural characteristics of the carriers but also by the biological environment with which liposomes come into contact[25]. Therefore this complex property must be studied under different conditions and with distinct techniques.

3.2.6.1 Stability under the storage conditions

The stability of the conjugates was firstly evaluated under the storage conditions at 277K by following changes in their size with time. Among the different conjugates prepared, two of them were chosen for this study: the GLA loaded liposome_RGD conjugate n^{o} 1**,** containing the lower concentration of enzyme (1.5 µg/mL) and the conjugate n^{o} 5 containing the higher concentration of GLA (8.5 µg/mL). As observed in Figure 3.13 there was not significant changes in the average size of both conjugates, which after 60 days remain stable.

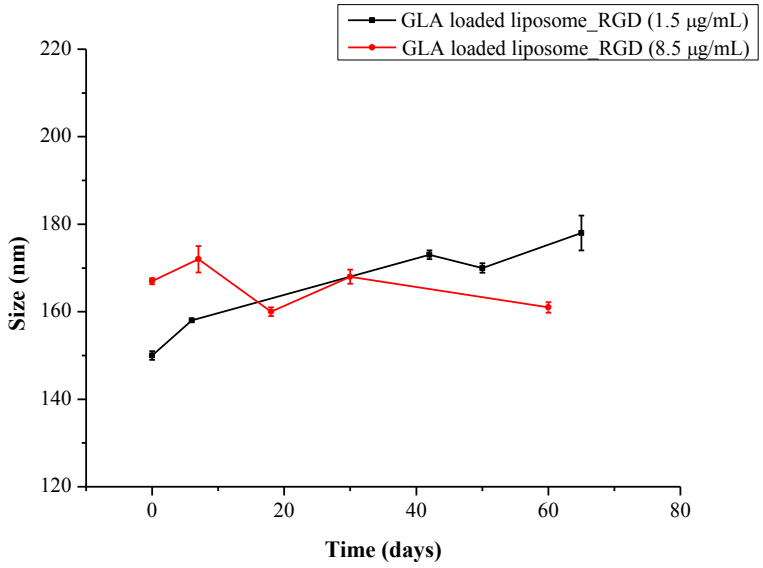

Figure 3.13. Evolution of the size of GLA loaded liposome_RGD conjugates under the storage conditions.

Another way to evaluate a vesicle-based conjugate stability is through the extent to which the carrier retains its drug contents. In order to check the retention of the GLA in the liposomes, 16 mL of the conjugate n^{o} 5 initially containing 8.5 µg/mL of enzyme were passed through the diafiltration equipment in order to separate the non-integrated enzyme. The resulting pool of loaded vesicles was storage at 277 K and every week during one month 4 mL from this pool was passed through the diafiltration equipment. The remaining loaded vesicles were storaged for further quantification by Western-blot technique. Figure 3.14 depicts the percentage of enzyme remaining in the liposomes with respect to the initial amount of entrapped enzyme. This percentage decreases down to 81 % after two weeks, remaining at this level after three further weeks. This means that at the beginning part of the GLA is released from the formulation, but then an equilibrium is established between the free enzyme and the loaded vesicles. As an average the conjugate retains around the 84 % of the initial encapsulated enzyme when it is storage at 277 K during 21 days.

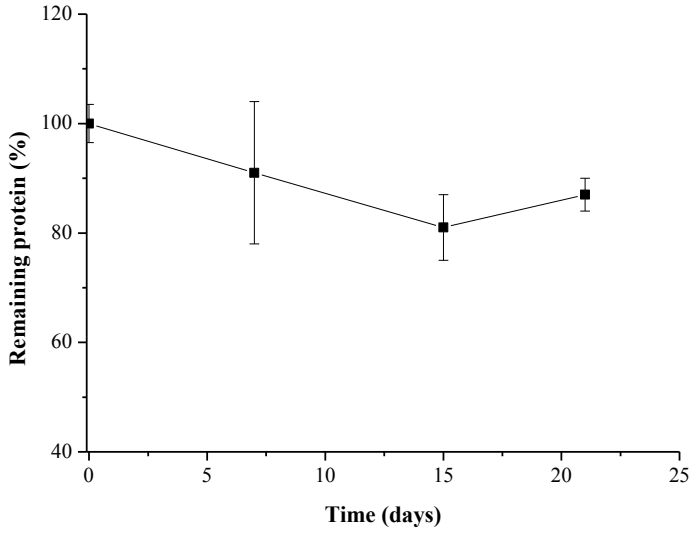

Figure 3.14. Study of the GLA release from liposome-RGD conjugates with time

The enzyme release profile of GLA was also evaluated under the storage conditions. For this, 8 mL of a pool of loaded vesicles, with the same characteristics of the one previously described, was storaged at 277 K. Every week and during one month, the entire pool was passed through the diafiltration equipment to separate the GLA released during this time. From the remaining loaded vesicles 500 µL were storaged for further quantification by Western-blot technique. In Figure 3.15 (left) is observed that the

amount of entrapped GLA decreases with time and after 21 days 37 % of the initial encapsulated enzyme still remain in the formulation. The release percentage in each week with respect to the former one was always constant and around the 30 % (Figure 3.15, right).

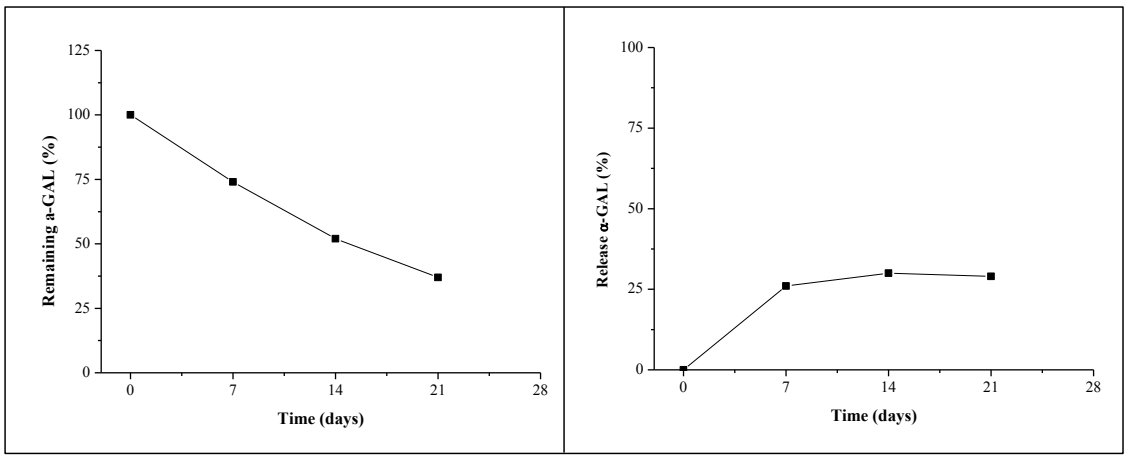

Figure 3.15. GLA percentage release with time given by the amount of enzyme still remaining in the formulation (left panel) and the percentage release in one week with respect with the previous one (right).

3.2.6.2 Stability in different media

The stability of the GLA conjugates was also evaluated in more complex media by measuring the change in the mean particle size with time. For this evaluation a small volume of the GLA loaded conjugates 5 containing 8.5 µg/mL of enzyme were mixed with 1600 µL of water, PBS and cellular growth media (GM). The growth media was composed of basal medium (elemental medium with essential amino acids and salts) with a 10% of fetal bovine serum. The samples were incubated for 48 hours at 310 K in a humidified atmosphere with 5% CO_2. The particle size of the conjugates was analyzed at different incubation times (0, 4, 19 and 40 h) using a dynamic light scattering equipment and the results are shown in Figure 3.16. A blank of plain liposome_RGD conjugates was included in the study for comparison.

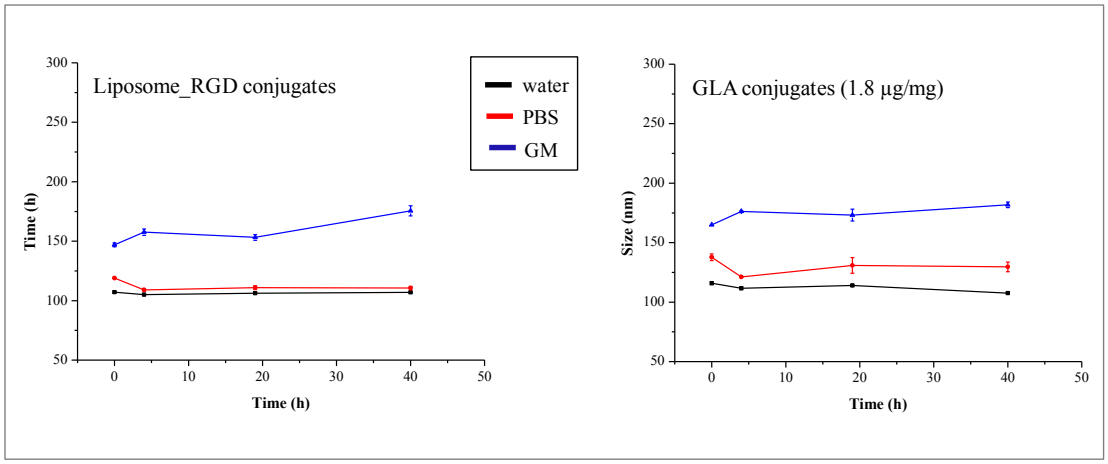

Figure 3.16. Stability of α-GLA liposome_RGD conjugates with different in loadings in water, PBS and GM.

Although the size of the conjugate incubated in PBS increased around 15 nm with respect to the same conjugate incubated in water, there was no evidence of vesicle aggregation or fusion and the conjugate remained stable for 40 hours. In the growth media the loaded liposomes and the blank, increased their size since the beginning but then remain quite stable during the next 40 hours. It is described that when nanoparticles enter in contact with a biological fluid for example blood, plasma or interstitial fluid, they get coated with proteins forming the so-called protein corona, As a consequence the hydrodynamic radio of the nanoparticle increase. The growth media contains proteins so the initial increase in the size can be attributed to the interaction of the proteins with the vesicle membrane. In general both, the conjugate and the blank remain quite stable in all media during the time of the experiments.

3.2.7 Enzymatic activity of GLA loaded liposome_RGD conjugates

3.2.7.1 *In vitro* specific enzymatic activity

The specific activity was measured in all liposomal fractions (total, re-suspended pellet and supernatant waters) of all conjugates using the fluorescent methodology explained in Experimental Section 9.4.1. A blank sample of plain liposome-RGD conjugates was also included in the study. Before the depressurization step, 1 mL of GLA was separated from each aqueous phase as a reference, to compare with the encapsulated enzyme. Surprisingly there was an increase in the activity of the enzyme contained in the different fractions when it was associated to the nanovesicles if compared with the GLA in water (Table 3.5). Theoretically the total fraction and the fractions of GLA in water should have similar amount of enzyme and thus similar specific enzymatic

activities. However the specific activity in the total fractions (T) exceeds the values obtained for the free enzyme which suggesting that this fact is related with the association enzyme-nanovesicle. This activity enhancement was also observed in the fractions of re-suspended pellets (**P**) and supernatants liquids (**S**). As expected no activity was detected for the blank of liposome-RGD conjugates.

Table 3.5. Specific enzymatic activities in μmol/h.mg determined for the different fractions of GLA loaded liposome_RGD conjugates.

Vesicle samples (code #)	Total (**T**)	Re-suspended pellet (**P**)	Supernatant (**S**)	α-GAL/water
GLA loaded liposome_RGD (# 2)	1349±14	1570±9	713±32	312±25
GLA loaded liposome_RGD (# 3)	1175±90	1337±500	725±58	291±99
GLA loaded liposome_RGD (# 4)	2001±172	1934±70	731±42	109±35
α- GAL loaded liposome_RGD (# 5)	1497 ± 61	1764 ± 21	722 ± 164	95 ± 19
liposome_RGD (blank)	0	0	0	0

At first glance, the rise in enzymatic activity observed in the supernatant fractions was contradictory with the idea of relating the increment of activity with the enzyme-vesicle association, since in the supernatant we supposed to find only the free enzyme. However cryo-TEM images and DLS measurements of the supernatant liquids show the presence of nanovesicles and DLS measurements with a size distribution centered in 106 ± 0.5 nm (Figure 3.17). The presence of vesicles in this fraction can explain the increment in activity encountered. This experiment also proved that the centrifugation methodology not only affected the nanostructuration of the loaded system but also the adequate separation of the non-integrated GLA.

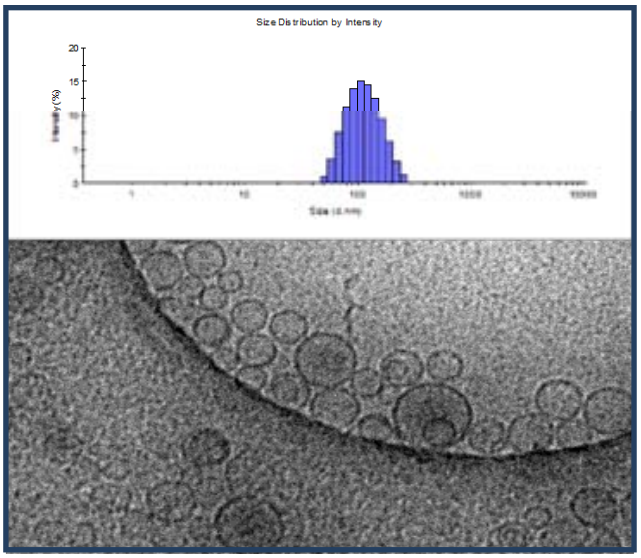

Figure 3.17. Cryo-TEM image and particle size distribution of the vesicles present in the supernatant fraction after centrifugation.

The increment in specific activity has already been reported for this enzyme supported on specific particles by J.LCorchero et. al[26]. They described that the specific activity of immobilized GLA in solid magnetic particles was higher than that of the free, soluble version of α-GLA. They related this fact to the covalent anchoring of the enzyme in a "site-specific" oriented manner or alternatively to cooperative effects produced by the processing. In this case, the enzyme immobilization takes place through a covalent union to the surface of particles. An explanation for the specific activity increment in our case could also be the inmobilization of GLA, in a "site-specific" and oriented manner, on the lipid bilayer of the vesicles. The difference from what is reported is that this immobilization is not through covalent binding, but to other kind of interactions between the enzyme and the lipid membrane components. Indeed the GLA used in this study presents an isoelectric point of 5.7; so the enzyme is negatively charge under the entrapment conditions (pH~ 6). Liposome-RGD conjugates have a positive charge membrane (See Table 2.5) and hence the inmobilization could be produced at least in part, by electrostatic interactions between the enzyme and the liposome membrane. On the other hand the immobilization could be also promoted by the DELOS-SUSP process itself through the entrapment of the enzyme within the lipidic bilayer. It is worth to note that in conventional process, like thin-film hydration, the protein is added in the hydration step, when the lipid membrane has been already formed. In contrast, in the DELOS-SUSP, the vesicle formation and biomolecule entrapment take place

simultaneously, so probably part of the enzyme is trapped in the membrane during the encapsulation process.

3.2.7.1.1 Stability of the specific activity of GLA under the entrapment conditions

The maintenance of the specific activity with time, which gives an idea of the stability of the enzyme under the entrapment conditions, was studied (Figure 3.18). This parameter was followed in the different fractions where GLA was present (total, re-suspended pellets and GLA in water), during 4 weeks. Neither the activity of the GLA in water nor the activity of the enzyme associated to the vesicles was affected after one month. Although no differences in stability were found between the free and the encapsulated enzyme along time, the higher specific activity present in the fractions were the GLA was associated to vesicles, with respect to the free enzyme remained during the 4 weeks. The specific activity was measured again after 14 weeks in the fractions were the enzyme was associated to the liposomes (total and loaded vesicles) and around 70 % of the initial activity was still remaining in the formulation.

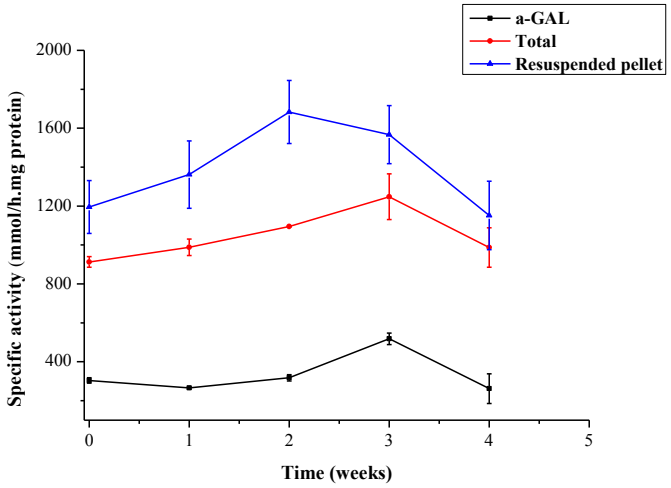

Figure 3.18. Evolution of the specific enzymatic activity of the GLA loaded liposome_RGD conjugates with time.

3.2.7.2 Enzymatic activity in cells

The enzymatic activity assay in cells of the prepared nanoconjugates was performed by the group of Porf. Schwartz (Vall d'Hebron Hospital). With this assay the capacity of the conjugates to degrade Gb3 molecules, whose accumulation is the cause of Fabry disease, is tested in-vitro. The fractions of re-suspended pellets from the nanoconjugates n^{o} 2 and n^{o} 3, were co-incubated during 48 hours with NBD-Gb3 molecules in a cell

line unable to produce Gb3; specifically in endothelial MAEC cells obtained from GAL KO mice. (Experimental Section 9.4.2). NBD is a dye residue that when is covalently attached to the Gb3 molecules shows a higher fluorescence in comparison with when it is free. This property allows using NBD-Gb3 for quantify the activity of enzymes degrading Gb3. Thus, if NBD-Gb3 is degraded after the co-incubation with the conjugates, less fluorescence values will be found in the cells, as measured by fluorescence flow citometry. Therefore, the less the fluorescence, the less active the conjugate will be considered (Figure 3.19).

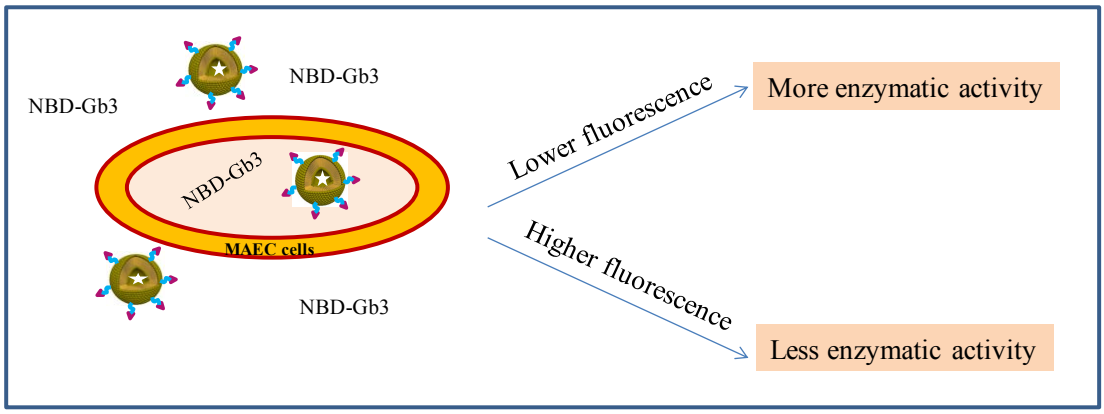

Figure 3.19. Schematic representation of the enzymatic activity assay performed with MAEC cells.

Despite the increment in the specific enzymatic activity found when the conjugate was incubated with a fluorescent substrate, non Gb3 inhibition was detected for the fractions tested in cells (Figure 3.20). However, the commercial enzyme currently used in ETR (Replagal®) and the GLA in water, showed activity in the range of concentration tested.

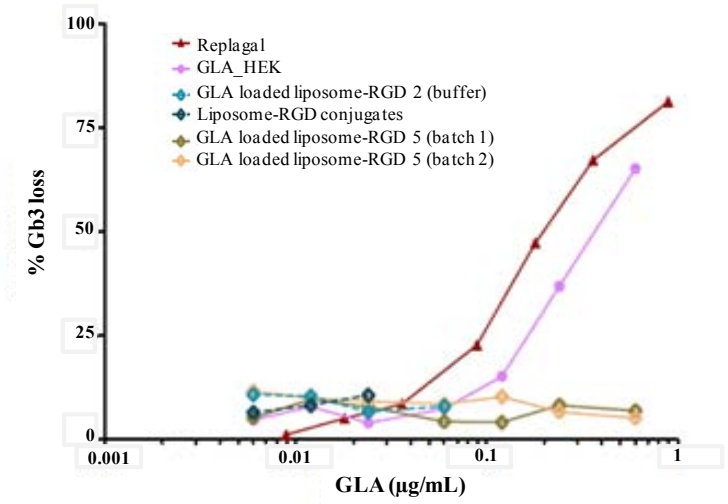

Figure 3.20. Effect of nanoconjugates in the NBD-GB3 loss in primary culture of endothelial mouse cells.

The inactivity of the re-suspended pellet tested was attributed to the inability of the vesicles to release the enzyme, produced either by the loss of the homogeneous and unilamellar morphology and/or by the high rigidity of the membrane due to the presence of high cholesterol content (36 % mol). It has been already shown in cryo-TEM images (Figure 3.10) that the morphology of the re-suspended pellet consists of a mixture of multilamellar and unilamellar vesicles, with different sizes. This inhomogenous morphology can prevent a faster and efficient enzyme release affecting the good performance of the nanoconjugate.

In order to find out whether the cholesterol percentage and/or the differences in nanostructuration were influencing the enzyme release, the efficacy to degrade Gb3 was tested in all fractions from the nanoconjugates n^{o} 4 and n^{o} 5, which presents different amounts of cholesterol in the membrane. In Figure 3.21 the relative efficacy of the fractions for all batches is represented with respect to that of Replagal®. The volume of each sample used in this assays was chosen in order to have a final enzyme concentration of 1.5 µg/mL.

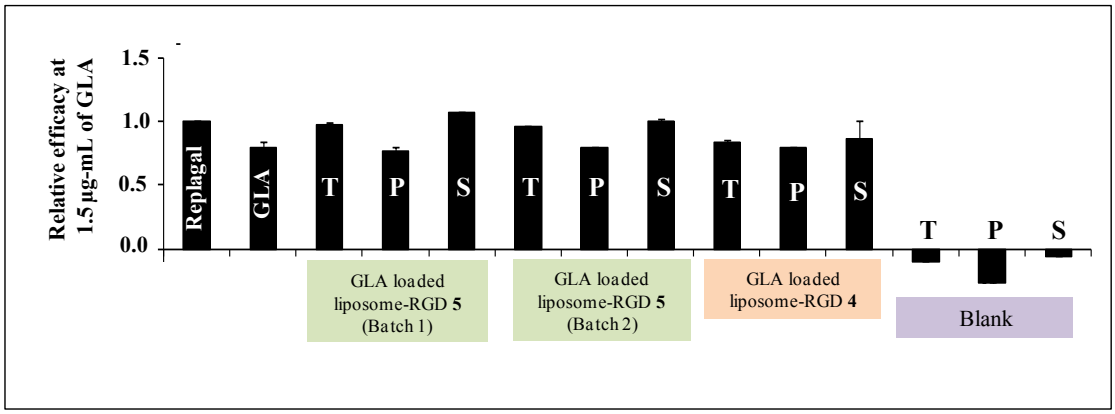

Figure 3.21. Relative efficacy of GLAloaded conjugates with respect to Replagal® in the Gb3 loss in MAEC-KO cells. For each nanoconjugate and the blank the total (T), re-suspended pellet (P) and supernatant (S) are represented.

All the fractions tested were able to degrade Gb3 showing an efficacy comparable to that of commercial Replagal®. The total sample (T) and supernatant waters (S) of the batches containing 36% of cholesterol, were more active than pure GLA in water and comparable to Replagal. The order of relative efficacy for these fractions was: supernatant> total> re-suspended pellet. The explanation for this behavior could layout on the size and nanostructuration of each fraction. It is reported that nanoparticle-

mediated cellular response is size-dependent and the internalization processes have the most efficient cellular uptake when particles have a size within the 25-50 nm[27]. A good response in this in-vitro Gb3 inhibition assay depends on how much the nanoconjugate is internalized and on the amount of GLA released. The re-suspended pellet fraction presents multilamellar vesicles and a bimodal size distribution. Accordingly we can assume that the inhomogeneity in size and morphology makes difficult both the cellular uptake and the enzyme release (Figure 3.22).

In the total sample and the supernatant there are vesicles and free enzyme, the systems are more homogeneous than the one forming the pellets and the vesicles are unilamellar. Although in the supernatant the amount of enzyme is lower, it is appreciated an efficacy slightly better. The different behavior could be related with the size. In the total sample a wider size distribution is encountered, with sizes ranging from 30 to 800 nm, with the maximum population around 200 nm. The vesicles comprising the supernatant present a narrower particle size distribution centered in 135 nm which make this fraction the most effective in the %Gb3 loss assays (Figure 3.22). This experiment showed that the size and the vesicle structuration exert a significant influence in the conjugate behavior.

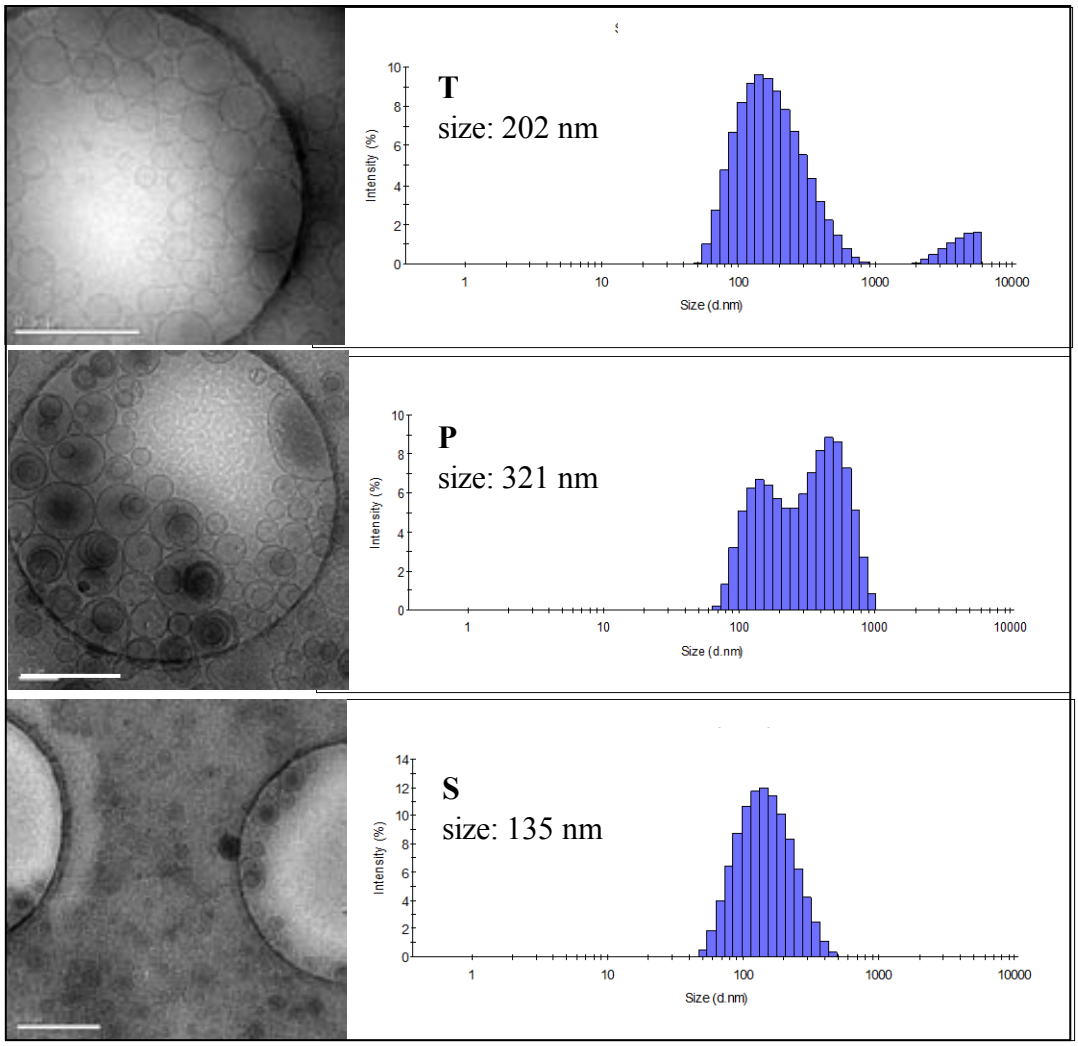

Figure 3.22. Morphology and particle size distributions (by intensity) of the vesicles in the different fractions, for GLA loaded liposome_RGD (1.4 mg/mL) conjugates. Scale bars are 500 nm

Regarding the percentage of cholesterol in the membrane, no significant differences were observed in the efficacy of the nanoconjugates prepared with the two cholesterol contents. Due to this result it was decided to continue working with the liposomes containg a 36 % mol of cholesterol that additionally presented the better physico-chemical characteristics.

Finally the efficacy of the different fractions of GLA loaded liposome_RGD conjugates (n^{o} 5) to degrade Gb3 was studied for different concentration of the encapsulated enzyme and compared with that obtained for the GLA in water and for the Replagal® at similar concentrations (Figure 3.23). In general, a reduction in NBD-Gb3 deposits from the cell was observed in the range of concentrations tested.

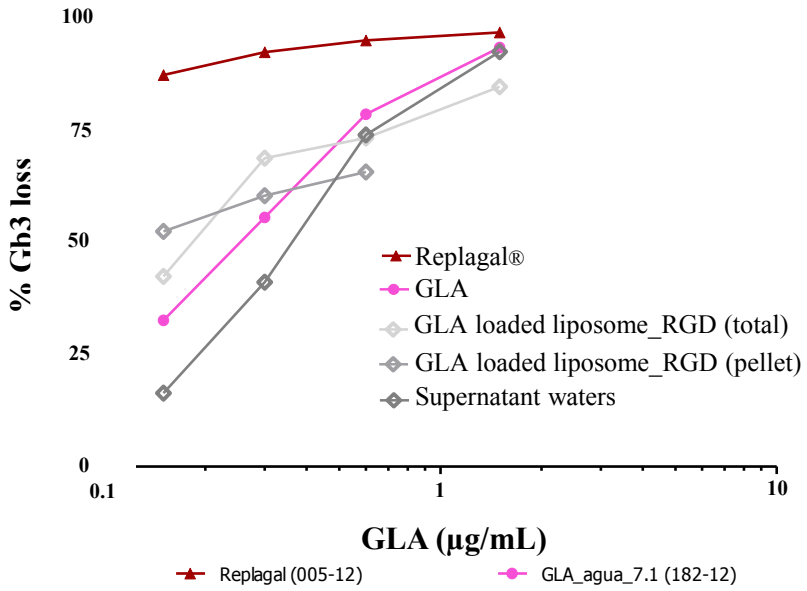

Figure 3.23. Effect of GLA loaded liposome_RGD nanoconjugates in the Gb3 inhibition in mouse endothelial cells. The curves of Replagal and GLA are added for comparison.

The efficacy of the GLA conjugates to produce Gb3 reduction resulted similar to the one obtained for the commercial Replagal and the free GLA, at high enzyme concentrations (1.5 µg/mL) as was already shown in Figure 3.21. However, at lower concentrations, the efficacy of GLA conjugates was comparable to free GLA but not to that of Replagal®, which presented a higher Gb3 reduction efficiency. With the commercial enzyme fewer doses were required to inhibit same amount of Gb3. Nevertheless to make a fair comparison a Replagal® entrapment experiment should be performed since the efficacy curve of free GLA in water is already different from Replagal's curve.

From the above reported results it can be summarized that the GLA conjugates comprising 36 % of cholesterol in the membrane were able to degraded Gb3 but their efficacy was dependent on the size and structuration of the vesicles. It was also proven the necessity of a new separation methodology because the centrifugation procedure affected the vesicle size and structuration and therefore the efficiency of the conjugates in the in-vitro cell assays.

3.2.8 Use of a diafiltration procedure to separate the free enzyme

In order improve the free GLA separation step from the loaded liposomes, a diafiltration methodology, through the KrossFlo® Research IIi TFF System (KR2i), was evaluated.

This equipment allows performing automatic diafiltration/ultrafiltration processes using different columns, depending on the size of the protein. The columns are supposed to retain the loaded vesicles diafiltrating the free enzyme through the membrane pores. The advantage of using the KR2i equipment is that one can separate the non-encapsulate biomolecule, concentrate the sample and change the dispersant medium simultaneously if desired (Experimental Section 5.1.3).

Conjugates of GLA loaded liposome-RGD were synthesed by DELOS-SUSP with an enzyme content of 8.5 μg/mL and lipid concentration of 1.5 mg/mL. A sample of GLA (batch #120531) with an specific activity of 2151 μmol/h.mg and a concentration of 0.25 mg/mL was used for this purpose. The non-incorporated enzyme was separated using a 300 kDa column and a six cycle protocol. 8 ml of the total sample were passed through the diafiltration equipment to get 8 mL of loaded vesicles and 48 mL of diafiltrated waters with the free GLA. The physico-chemical characteristics and the morphology were checked in the fraction of loaded vesicles and no significant changes were observed (Figure 3.24). The liposomes presented small, spherical and unilamellar characteristics similar to those of the total sample. After the diafiltration, the amount of ethanol, determined by HPLC, was reduced down to 200 ppm in the final suspension. This reduction in the ethanol percentage changes the dispersant medium, causing a change in the Z potential from 18 to -33. The enzyme quantification, performed by Western-blot, showed a higher %EE of 39 %. As the process was more efficient separating the free enzyme from the loaded vesicles, the entrapment efficiency (39 %) and protein/ lipid loading (2.32 μg/mg) also increased. A comparison of the characteristics of centrifugation and diafiltration methodologies is given in Experimental Section 4.1.4.

Once confirmed that the diafiltration process did not substantially change the structural characteristics of the vesicles, the specific enzymatic activity was measured (Experimental Section 9.4.1). Table 3.6 showed the values obtained for the total sample; the diafiltered loaded vesicles, the diafiltrated waters, as well as the specific activity for the GLA in water for comparison purposes. It is clearly noted that in both the total and the diafiltered loaded vesicles, the enzyme has more activity than in water, which is consistent with the results previously obtained. The diafiltrated waters did not presented any activity.

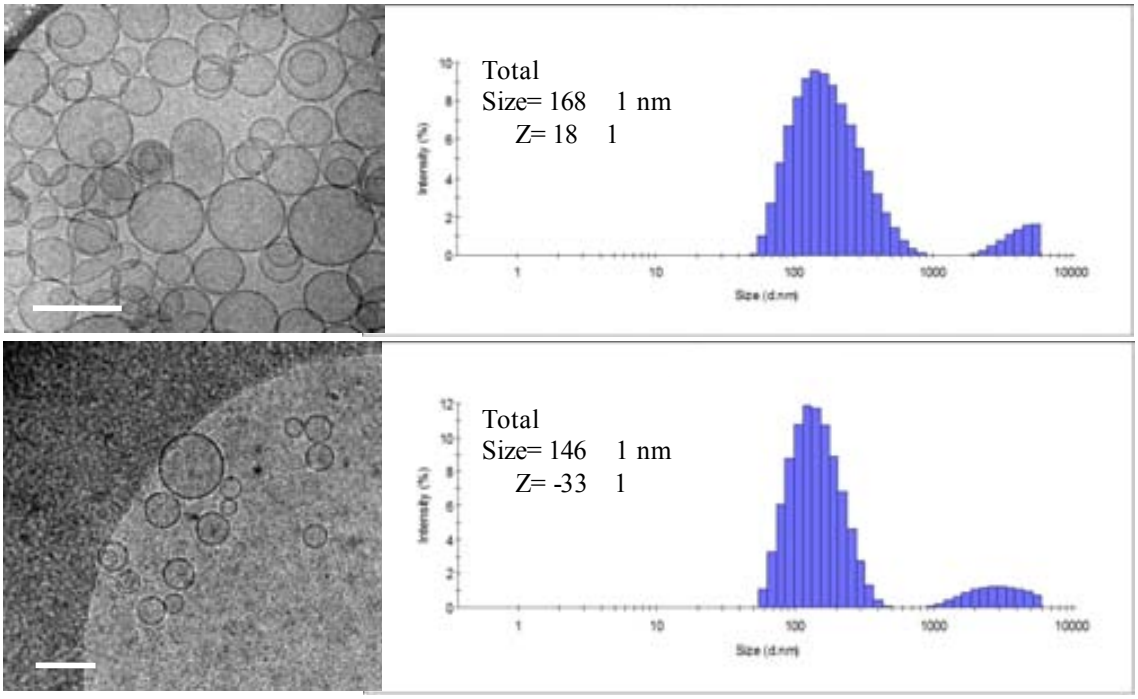

Figure 3.24. Cryo-TEM images and particle size distributions of GLAloaded liposome_RGD conjugate before (above) and after (below) the separation of the free enzyme. Scale bar are 100 nm.

Table 3.6. Specific enzymatic activities (in µmol/h.mg) determined for the different fractions of GLA loaded liposome_RGD conjugates.

Vesicle sample (µg enzyme/mL vesicular suspension)	Total	Loaded vesicles	Diafiltrated waters	α-GAL/water
GLA loaded liposome_RGD (8.5 µg/mL)	913±27	924±89	n.d	304±14

As a conclusion we can say that the diafiltration process allowed an efficient separation of the non-incorporated enzyme from the loaded system, which shown good physicochemical and structural characteristics and a high loading.

3.2.8.1 Stability in the specific activity of GLA under the entrapment conditions

The specific activity was followed in the different fractions where GLA was present (e.g total, diafiltrated loaded vesicles and GLA in water) during 4 weeks. Neither the activity of the GLA in water nor the activity of the enzyme associated to the vesicles was affected after one month. The specific activity was measure again after 14 weeks in the

fractions were the enzyme was associated to the liposomes (total and loaded vesicles) and around 70 % of the initial activity was still remaining in the formulation.

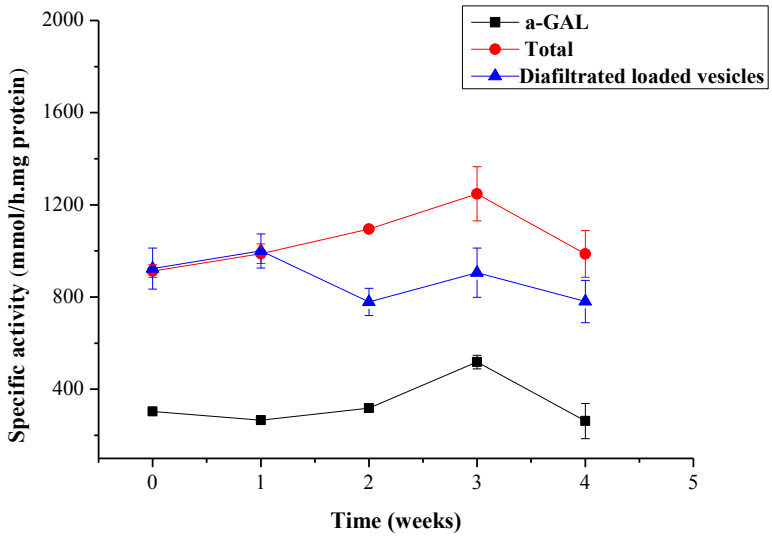

Figure 3.25. Evolution of the specific enzymatic activity of the GLA loaded liposome_RGD conjugates with time.

2.2.9 Location of the enzyme in the vesicles

As already mentioned, the increase in specific activity of GLA integrated in the vesicle has been associated to the enzyme immobilization at the vesicle membrane. In order to experimentally confirm this point an inmunomicoscopy technique was used. Inmunomicoscopy is a staining technique used in electron microscopy in which colloidal gold particles are attached to antibodies which bind to a specific protein. Gold is used due to its high electron density which increases the electron scattering to give high contrast dark spots. For this study the loaded conjugates (2.3 µg/mL) free from the non-incorporated GLA, prepared in Section 2.2.8, were used. Following the protocol described in the Experimental Sections 8 and 8.1, the sample was placed in a grid and incubated with a first antibody that binds to the enzyme. After a washing step, the sample was incubated with a second anti-rabit antibody which binds to the first antibody and contains the gold nanoparticles of 10 nm. Blanks were also prepared in order to discard unspecific unions and false positives. As the binding antigen-antibody is so specific, if the active site of the protein is located at the outer part of the membrane, black spots corresponding to the gold nanoparticles will be observed. In Figure 3.26, the TEM images depicted the liposomes with some small black spots, confirming the

presence of GLA at the lipid bilayer of the liposomes. In accordance with this localization, the high specific activities encountered for GLA can be associated to the immobilization of the enzyme at the membrane.

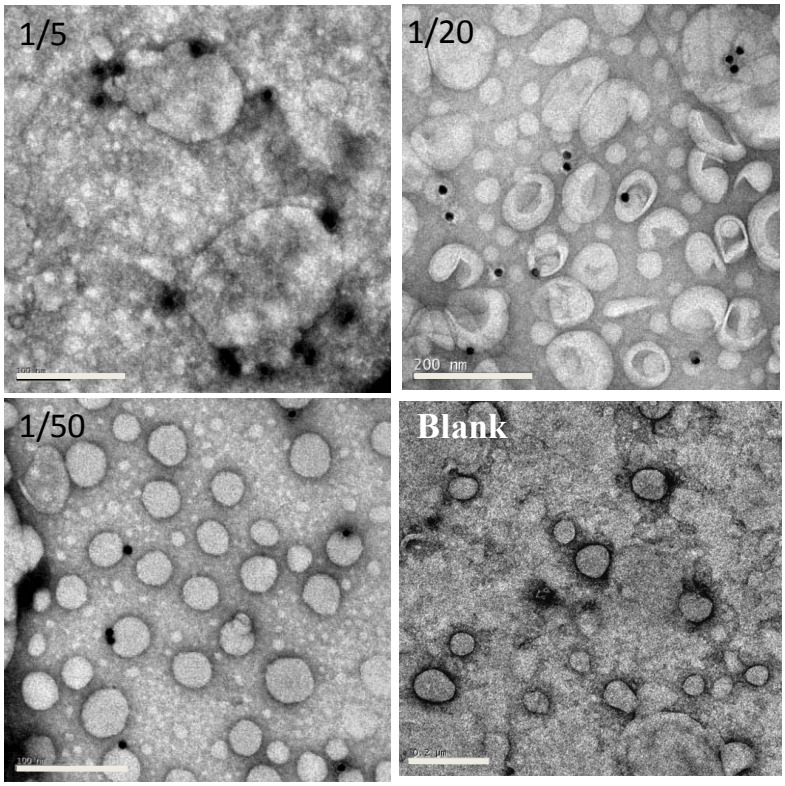

Figure 3.26. Inmunomicroscopy images of α-GLA loaded liposomes_RGD conjugates using gold nanoparticles of 10 nm. Scale bars are 200 nm.

3.2.10 Influence of the enzyme loading in the nanoconjugates characteristics

Until now GLA loaded liposome_RGD conjugates containing 8.5 μg/mL as initial enzyme concentration, with nanoscopic size, unilamellar membranes and able to degrade Gb3 molecules, have been prepared using DELOS-SUSP. In order to synthesize nanoconjugates with a higher enzyme loading, we also investigated the possibility of increasing GLA concentration while keeping constant the amount of lipids in the formulation. Moreover, due to the good results obtained for the GLA conjugates we also performed the entrapment of the commercially available Replagal® in liposome-RGD nanocarriers. Unlike α-GAL, Replagal® does not present the histidine tail, which makes their structures somewhat different.

Batches containing an initial GLA concentration of 20 μg/mL and 42.5 μg/mL, and Replagal® at 20 μg/mL, were prepared using the phase compositions enclosed in Table

3.7 and the procedure described in Experimental Section 2.1.1. For all conjugates the organic phase was the same with the only difference in the amount and type of enzyme added to the aqueous solution before depressurization. Samples were prepared several times and a blank was also included in the set of experiments as a control.

Table 3.7. Compositions used for the preparation GLA loaded-liposomes_RGD and Replagal loaded-liposomes_RGD using DELOS-SUSP method

Vesicle system (# code)	Organic phase	Aqueous phase	Biom/lipid Ratio[a] (nmol/mmol)	Lipidic. conc[b] (mg/mL)
GLA loaded liposome_RGD (# 7)	Cholesterol (17 mM) + DPPC (27 mM) + CHOL_PEG_{200}–RGD (2.8 mM)	GLA in water (200 nM)[c]	88.8	1.4
GLA loaded liposome_RGD (# 8)	Cholesterol (17 mM) + DPPC (27 mM) + CHOL_PEG_{200}–RGD (2.8 mM)	GLA in water (425 nM)[c]	188.6	1.4
Replagal loaded liposome_RGD (# 9)	Cholesterol (17 mM) + DPPC (27 mM) + CHOL_PEG_{200}–RGD (2.8 mM)	GLA in water (200 nM)[d]	88.8	1.4
Liposome_RGD (blank)	Cholesterol (17 mM) + DPPC (27 mM) + CHOL_PEG_{200}–RGD (2.8 mM)	water	-	1.4

Entrapment experiments were performed from CO_2-expanded ethanol at 10 MPa, 308K and X_{CO2}= 0.85.
[a] Ratio between the moles of initial enzyme and the total moles of lipids forming the liposome membrane. [b] Ratio between the total amount of lipid forming membrane and the volume of the final vesicular suspension. [c] Characteristics of the used GLA batch 130213 with an enzymatic activity of 889 μmol/h.mg and an enzyme concentration of 0.34 mg/mL. [d] The Replagal batch with a concentration of 1 mg/mL was provided by the Vall d'Hebron Hospital.

The physicochemical characteristics of the new liposomal preparations together with the characteristics of the previous batch prepared at 8.5 μg/mL are shown in Table 3.8. When comparing the results, one can see that the higher the initial enzyme concentration the bigger the particle size. The polidispersity presented the same behavior which indicates that there is a tendency toward less homogeneous system when increasing the initial enzyme concentration. The stability under the storage conditions also decrease with the amount of enzyme which is observed from the decrease in the Z potential. Although the entrapment efficiency percentage was similar in all cases, the protein loading was higher for the liposomes with the higher initial concentration of protein.

The size, %EE and enzyme loading values for the Replagal® conjugates were similar to those obtained for α–GLA loaded liposome_RGD conjugates prepared at the same enzyme concentration, which is an indication of the reproducibility and robustness of the DELOS-SUSP methodology (Table 3.8). The Z potential was smaller possibly due to the different media in which the enzyme is initially dissolved. In the case of α-GLA, this media was acetic buffer whereas in the case of Replagal® the media was a mixture of sodium phosphate monobasic, monohydrate, polysorbate 20, sodium chloride, sodium hydroxide and water; a media commonly used for therapy with injections.

Table 3.8. Physicochemical characteristics, entrapment efficiency and loading of GLA loaded liposome_RGD and Replagal loaded liposome_RGD conjugates . The physic-chemical characteristics of the conjugates after the separation of the non-integrated enzyme are given between brackets.

Vesicle systems (# code)	Size		Z potential (mV)	EE (%)	Enzyme loading[c] (µg/mL)	Enzyme conc.[d] (µg/mL)
	Mean(nm)[a]	PdI[b]				
GLA loaded liposome_RGD (# 6)	168±1 (146±1)	0.33±0.01 (0.29±0.03)	18±1 (-33±1)	39±10	2.3	8.5 (3.3)
GLA loaded liposome_RGD (# 7)	216±8 (195±1)	0.40±0.01 (0.40±0.01)	14±1 (-24±2)	37±9	5.8	20 (7.4)
GLA loaded liposome_RGD (# 8)	226±3 (215± 56)	0.45±0.04 (0.33±0.02)	9.8±0.4 (-32 ± 1)	38±8	11.3	40.5 (15.4)
Replagal loaded liposome_RGD (# 9)	199±3 (174± 56)	0.47±0.04 (0.38±0.01)	5.2±0.5 (-1.9 ± 0.4)	35±17	4.9	20 (7)
Liposome-RGD/water (blank)	160 ± 1	0.38±0.02	30 ± 2	-	-	-

[a]Intensity weighted mean hydrodynamic size of the ensemble collection of vesicles measured by dynamic light scatering. [b]Polidispersity index showing the width of the particle size distribution. [c]Mass of the integrated protein divided by the total mass of the lipids comprising the membrane.[d]Mass of the total amount of protein present divided by the volume of the vesicular suspension.

After the diafiltration process to separate the free enzyme, the liposomal systems presented lower particle sizes and polidispersity indexes. The Z potentials move from values that indicate a moderate stability toward values where the vesicle suspensions are considered stable. These results might respond to the fact that Z-potential depend on the dispersant medium and after the diafiltration all the ethanol and not integrated protein is eliminated thus all the formulations have similar dispersant media.

Finally, Cryo-TEM was used to analyze the effect of increasing the GLA concentration in the nanoconjugate morphology. Figure 3.27 shows that the amount of initial enzyme influences the final morphology of the conjugates.

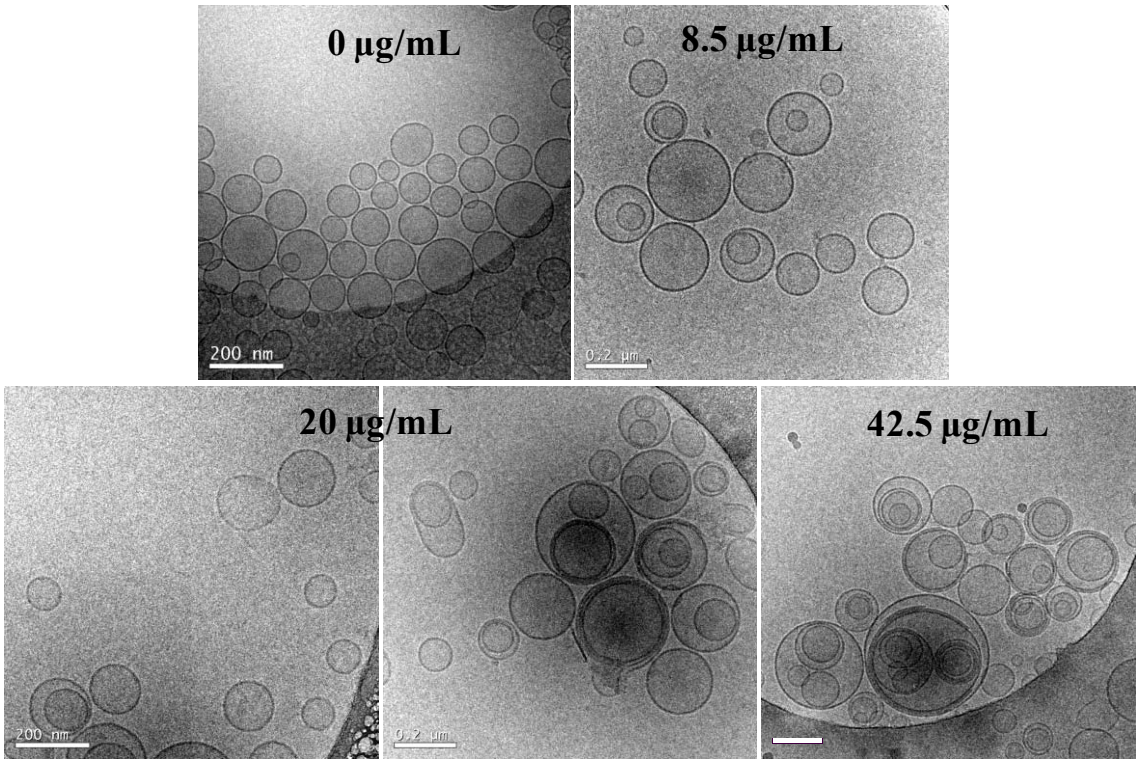

Figure 3.27. Cryo-TEM pictures showing the morphology of the nanoconjugates with different GLA concentrations. Scale bars are 200 nm.

When there is no protein integrated, homogenous vesicles with unilamellar membranes and spherical shapes are observed. This morphology is maintained at the lower GLA concentration (8.5 µg/mL). However at 20 µg/mL the homogeneity decreases and zones of a large homogeneity are found together with zones with multilamellar vesicles with different sizes. When the enzyme concentration is 42.5 µg/mL, the number of multilamellar vesicles increases as well as the inhomogeneity in size, which probes that the enzyme concentration has a strong impact in the morphology of the conjugates. Indeed it is described that biomolecules may induce phase transformations, free energy releases, restructuring and dissolution at the nanomaterial surfaces[28].

Cryo-TEM images of Replagal® loaded liposome_RGD depicted a morphology in which a mix of unilamellar and some multilamellar vesicles is observed (Figure 3.28).

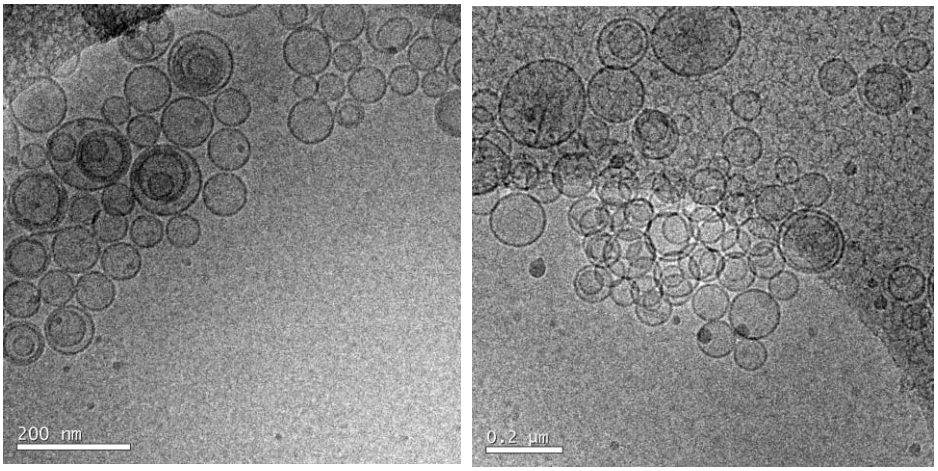

Figure 3.28. Cryo-TEM images of Replagal loaded liposome_RGD conjugates prepared using DELOS-SUSP.

3.2.10.1 *In vitro* specific activity

The specific activity for the different conjugates was measure by the group of Prof. A. Villaverde (IBB) (Experimental Section 9.4.1). Table 3.9 show the specific activity of the total sample, the loaded conjugate and the GLA or Replagal® in water, withdrawn from the aqueous phase before the depressurization stage for comparison purposes. In all cases the specific activity increases when the enzyme was conjugated to the vesicles.

Table 3.9. Specific enzymatic activities (in µmol/h.mg) determined for GLA loaded liposome_RGD conjugates.

Vesicle systems (# code)	Total	Loaded vesicles	GLA/water
GLA loaded liposome_RGD (# 6)	913±27	924±89	304±14
GLA loaded liposome_RGD (# 7)	846 ± 270	1253 ± 65	400 ± 49
GLA loaded liposome_RGD (# 8)	879 ± 140	705 ± 88	548 ± 200
Replagal loaded liposome_RGD (# 9)	3250±680	1586±282	1070±350

The ratio between the specific activities in the loaded fractions and in the free GLA is represented in Figure 3.29. It is observed that an increment of the specific activity is three times for the conjugates loaded with 2.3 µg/mg (# 6) and 5.8 µg/mg (# 7) and 1.3

times for the conjugate loaded with 11.3 µg/mg (# 8). The higher activity increment found for the less loaded liposomes can be explained by the easier release and more accessibility of the enzyme in the activity assays due to a more homogeneous morphology regarding size and lamellarity. The conjugates loaded with 11.3 µg/mL of GLA are mostly composed of multilamellar vesicles which influence negatively in the in-vitro behavior of the system.

On the other hand the increment in activity has been related until now with the immobilization of the enzyme due to interaction with the membrane probably promoted by electrostatic interactions and DELOS-SUSP method. The amount of protein that can be accommodated around or within the membrane has a saturation limit thus at some point this amount will not increases with the enzyme loading.

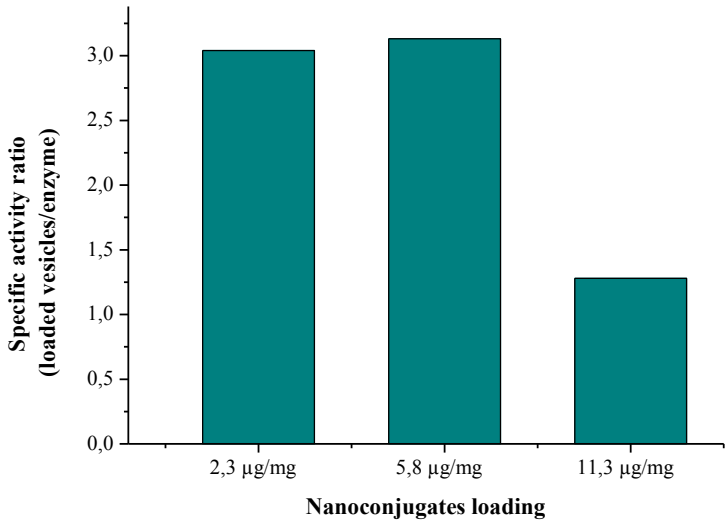

Figure 3.29. Ratio between the **s**pecific activity of the loaded conjugates and the GLA in water for different enzyme protein loadings

After analyzing the physic-chemical parameters, the loading, morphology and specific activity assays for the different conjugates, it can be concluded that the best performance is obtained for the conjugates loaded with 2.3 µg/mg and 5.8 µg/mg of α-GAL. Importantly, the amount of protein incorporated to the system has a strong impact in the physico-chemical characteristics and morphology of the vesicles.

3.2.10.2 Cellular internalization studies

In Chapter 1 it was proven that RGD peptides anchored on the liposome membranes not only modify its nanostructure but also enhance their binding and uptake by HMEC-1

cells, via $\alpha_v\beta_3$ integrins-mediated endocytosis. It was also demonstrated that a fraction of liposome-RGD conjugates trafficked to endosomal/lysosomal compartments. As the concentration of the enzyme in the carrier can influence not only the physico-chemical characteristics of the vesicles but also their internalization capabilities, the internalization of two α-GLA conjugates with different enzyme loading was studied using endothelial cells. First the conjugates loaded with 2.3 and 5.8 μg/mg of enzyme were labelled with Did by incubating them with an ethanolic solution of Did for attaining a final concentration of 50 nM of the dye in the membrane (Experimental Section 6.2). A blank of liposome-RGD conjugates was also labelled and included in the study for comparison. Cellular uptake experiments were assessed by laser scanning confocal microscopy (LSCM). HMEC-1 cells were incubated with a small volume of Did-labelled conjugates for 3 h at 37ºC in a humidified atmosphere with 5% CO_2. Afterwards cells were examined under an inverted Leica SP5 laser scanning confocal spectral microscope (Experimental Section 7.3). Confocal images of the cellular uptake of the conjugates are shown in the Figure 3.30.

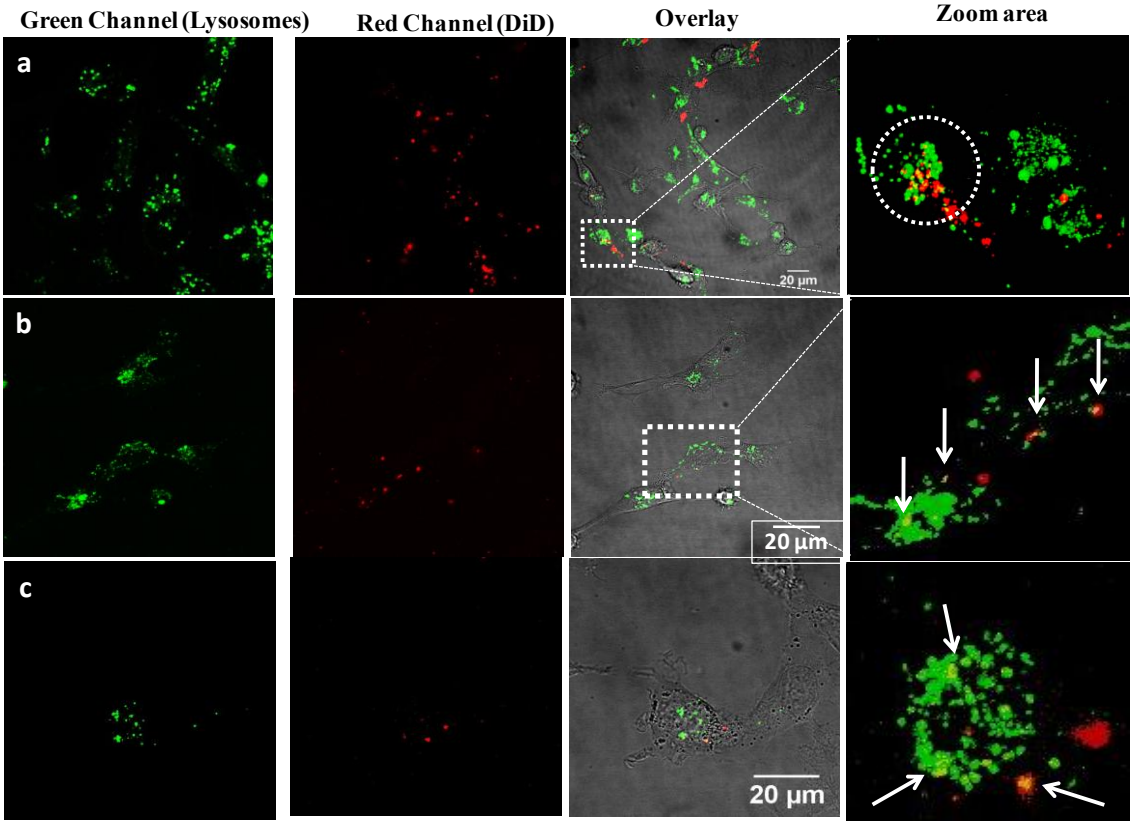

Figure 3.30. Confocal images of the cellular uptake of GLA loaded liposomes-RGD and liposome-RGD conjugates. (a) Liposome-RGD conjugates, (b) GLA loaded lipsosome_RGD conjugates 2.3 μg/mL, (c) GLA loaded lipsosome_RGD conjugates 5.8 μ/mL.

From the confocal images is observed that both GLA conjugates are internalized but in a less extend than the non-loaded vesicles. The co-localization images of the conjugates (red) with the lysotracker (green) indicate that part of the conjugates is in the lysosome. This is a remarkable result since it is one of the prerequisites for a nanocarrier to be used in the treatment of Fabry disease. The confocal results were afterwards confirmed by flow cytometry. For such experiments the same labelling and incubation protocols than before were followed. The only difference was at the end of the incubation step where cells were washed twice with Dulbecco´s phosphate buffered saline (DPBS) solution and detached using trypsin and re-suspended in a cell culturing medium before subjecting to fluorescence-activated cell sorting analysis. Data acquisition and analysis was performed using FACS scan (Beckton-Dickinson) and BD FACS Diva software. 10^4 viable cells were evaluated in each experiment. Figure 3.31 shows the fluorescence intensity associated to the cells that have internalized the DID-labelled conjugates. It is shown that the internalisation is higher for the liposome-RGD conjugates than for the liposomes containing α-GAL. Among the loaded conjugates, the one with the lower loading presented more internalization in the cells. This is probably related with the smaller size and higher homogeneity of the system which allow a faster and greater cellular uptake. Anyway the experiment was performed during 3 h, to check if the RGD also promoted a faster internalization in these complex systems. Probably to have a better idea of the internalization behaviour for this conjugates, further experiments including longer incubation times will be needed.

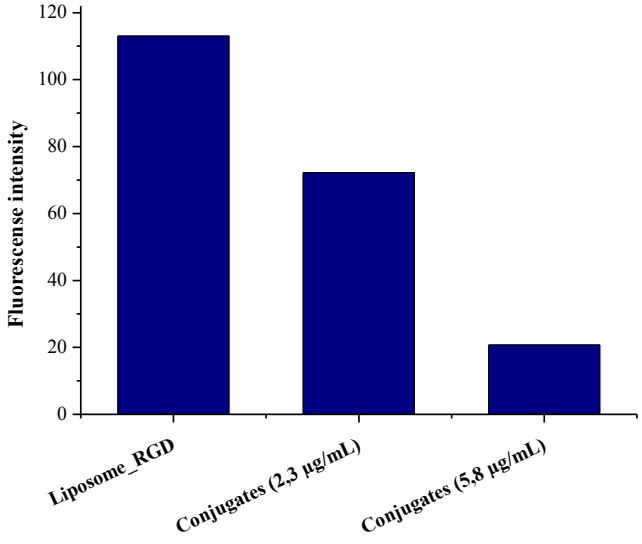

Figure 3.31. Cellular uptake of Liposome-RGD-GLA conjugates assessed by flow cytometry.

3.2.10.3 Enzymatic activity in cells for the GLA loaded liposome_RGD and Replagal® loaded liposome_RGD conjugates.

The activity of the conjugates was tested in Vall d'Hebron Hospital by measuring the capacity of the vesicle systems to eliminate Gb3 upon incubation with cells (Experimental Section 9.4.2). Figure 3.32 shows that with respect to free Replagal® the total conjugate have a superior efficacy while the loaded vesicles presented a similar behavior.

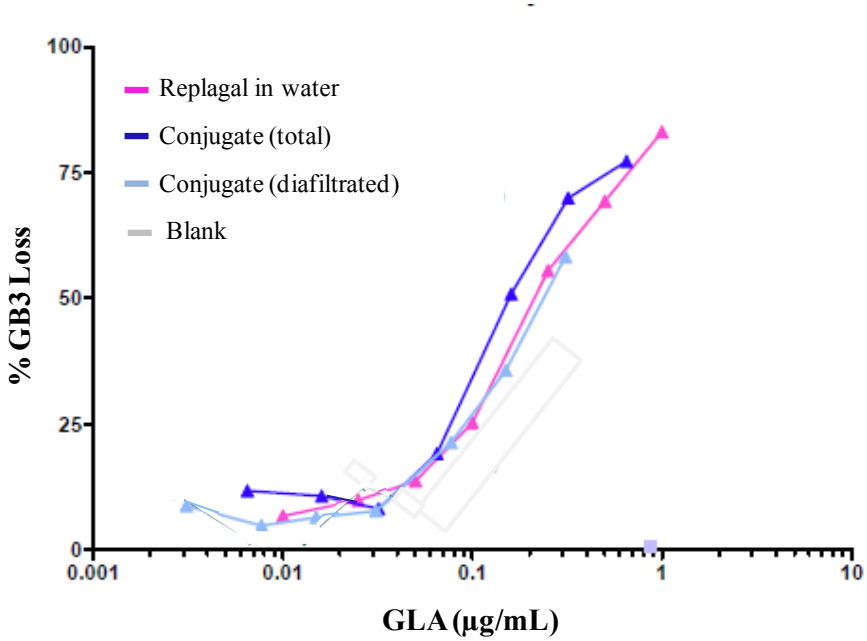

Figure 3.32.. Effect of Replagal loaded liposome_RGD conjugates in the inhibition of Gb3 in mouse endothelial cells. The curve of Replagal is added for comparison.

Figure 3.33 shows the effect in the Gb3 loss for the total formulation, the loaded conjugate and the GLA in water. Both the total formulation and the conjugate sample produced the Gb3 elimination more efficiently than the free form of the enzyme. This is in agreement with the fact in this formulations the specific activity of the enzyme is potentiated. As observed from the Gb3 elimination curves, at concentration higher than 0.1 µg/mL both the total and the loaded conjugates behave more efficiently and for instance at 0.2 µg/mL, the loaded conjugate is able to degraded more than 50 % of the initial Gb3 while the free enzyme only degrades around a 10 %. The results demonstrate that this multifunctional conjugate, produce by DELOS-SUSP method, can improve the efficacy of the free enzyme in the *in vitro* cell assays.

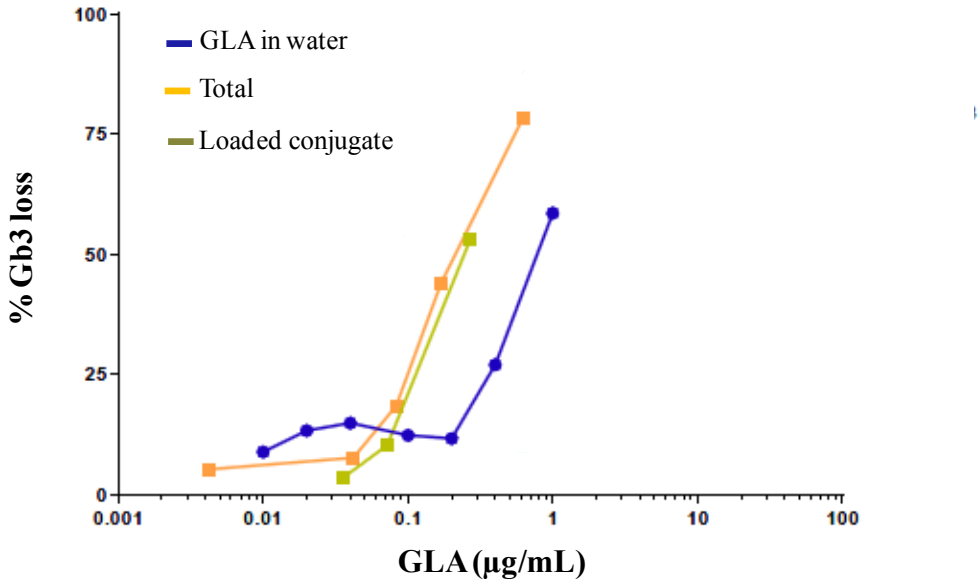

Figure 3.33. Effect of GLA conjugates (5.8 µg/mL) in the Gb3 loss in MAEK KO cells.

The good results obtained for the GLA conjugates and Replagal® conjugates encourage the performance of in-vivo pharmacokinetic studies in animal models that will be undertaken soon.

3.3 Summary

- ✓ Multifunctional conjugates composed by liposomes functionalized with RGD peptides and with encapsulated GLA enzyme, were successfully prepared using the DELOS-SUSP methodology.

- ✓ The methodology yield nanometric conjugates with particle size between 150-220 nm, which are stables for more than two months, and show high homogeneity and unilamellarity.

- ✓ The encapsulation efficiency of the GLA within the SUVs was 38 % and the formulations turned to be non cytotoxic, non haemolytic and sterile.

- ✓ Enzymatic activity assays performed with the GLA conjugates showed a significant increase in the activity when GAL was conjugated to the liposomes in comparison with the values obtained for free GAL in water.

- ✓ *In vitro* activity studies using MAEK KO cells show that the GLA conjugates were able to reduce the Gb3 deposits from the cells. The efficacy of the conjugates to produce a Gb3 reduction is better than that obtained with the free α-GAL.

- ✓ The separation methodology and the enzyme concentration in the conjugates strongly influence the physico-chemical characteristics and morphology of the vesicles.

- ✓ The encapsulation of the commercial Replagal® in liposome-RGD vesicles yields a formulation with good physicochemical characteristics and with an *in vitro* performance superior to that of the free Replagal®.

- ✓ GLA loaded liposome-RGD and Replagal® loaded liposome-RGD conjugates constitute two formulations with excellent perspectives to be used in the enzyme replace therapy of the Fabry disease.

3.4 References

1 Roland M. Schaefer, A. T.-S. a. M. J. H. Enzyme Replacement Therapy for Fabry Disease: A Systematic Review of Available Evidence. *Drugs* **69**, 2179-2205 (2009).

2 Pisani, A. *et al.* Enzyme replacement therapy in patients with Fabry disease: State of the art and review of the literature. *Mol. Genet. Metab.* **107**, 267-275 (2012).

3 West, M. *et al.* Agalsidase alfa and kidney dysfunction in Fabry disease. *Journal of the American Society of Nephrology* **20**, 1132-1139 (2009).

4 Viana-Baptista, M. Stroke and Fabry disease. *J. Neurol.* **259**, 1019-1028 (2012).

5 Fernandez, J., Sigurdsson, G. & Farivar, R. S. Cardiac surgery in patients with Fabry's disease: Review of literature. *J. Card. Surg.* **27**, 478-480 (2012).

6 Bersano A, L. S., Valcarenghi C, Bresolin N, Micieli G, Baron P. Neurological features of Fabry disease: clinical, pathophysiological aspects and therapy. *Acta Neurol Scand* **126**, 77-79 (2012).

7 Eng, C. M. *et al.* Safety and efficacy of recombinant human alpha-galactosidase a replacement therapy in Fabry's disease. *N. Engl. J. Med.* **345**, 9-16 (2001).

8 Lee, K. *et al.* A biochemical and pharmacological comparison of enzyme replacement therapies for the glycolipid storage disorder Fabry disease. *Glycobiology* **13**, 305-313 (2003).

9 European Medicines Agency, F. s. o. p. c. *Available at: http://www.emea.europa.eu/humandocs/Humans/EPAR/fabrazyme/fabrazyme.htm* (2009).

10 Siatskas, C. & Medin, J. A. Gene therapy for Fabry disease. *Journal of Inherited Metabolic Disease* **24**, 25-41 (2001).

11 Fernando C Fervenza, R. T., David G Warnock. Safety and effi cacy of enzyme replacement therapy in the nephropathy of Fabry disease. *Biologics: Targets & Therapy* **2**, 823–843 (2008).

12 Cheng, S. H. & Smith, A. E. Gene therapy progress and prospects: gene therapy of lysosomal storage disorders. *Gene Ther.* **10**, 1275-1281 (2003).

13 M.S. Sands, B. L. D. Gene therapy for lysosomal storage diseases. *Mol.Ther.* **13**, 839–849 (2006).

14 R.A. Dwek, T. D. B., F.M. Platt, N. Zitzmann. Targeting glycosylation as a therapeutic approach. *Nat. Rev. Drug Discov.* **1**, 65–75 (2002).

15 T. Cox, R. L., C. Hollak, et al., Novel oral treatment of Gaucher's disease, with N-butyldeoxynojirimycin (OGT 918) to decrease substrate biosynthesis & 1481–1485, L. Novel oral treatment of Gaucher's disease with N-butyldeoxynojirimycin (OGT 918) to decrease substrate biosynthesis. *Lancet* **355**, 1481–1485 (2000).

16 M.E. Gelsthorpe, N. B., E. Millard, et al. & . Niemann-Pick type C1 I1061T mutant encodes a functional protein that is selected for endoplasmic reticulumassociated degradation due to protein misfolding. *J. Biol. Chem* **283**, 8229–8236 (2008).

17 C. Porto, M. C., F. Fontana, et al. The pharmacological chaperone N-butyldeoxynojirimycin enhances enzyme replacement therapy in Pompe disease fibroblasts. *Mol. Ther.* **17**, 964–971 (2009).

18 J.Q. Fan, S. I. Active-site-specific chaperone therapy for Fabry disease. Yin and Yang of enzyme inhibitors. *Febs Journal* **274**, 4962–4971 (2007).

19 Fan, J.-Q. & Ishii, S. Active-site-specific chaperone therapy for Fabry disease. *Febs Journal* **274**, 4962-4971 (2007).

20 Hsu, J. *et al.* Enhanced endothelial delivery and biochemical effects of α-galactosidase by ICAM-1-targeted nanocarriers for Fabry disease. *Journal of Controlled Release* **149**, 323-331, (2011).

21 Giannotti, M. I., Esteban, O., Oliva, M., Garcia-Parajo, M. F. & Sanz, F. pH-Responsive Polysaccharide-Based Polyelectrolyte Complexes As Nanocarriers for Lysosomal Delivery of Therapeutic Proteins. *Biomacromolecules* **12**, 2524-2533, (2011).

22 JoséLuis Corchero, R. M., Julia Lorenzo, Victor Rodrı´guez-Sureda,Carmen Domínguez, Esther Vázquez, Neus Ferrer-Miralles and Antonio Villaverde. Integrated Approach to Produce a Recombinant, His-Tagged Human a-Galactosidase A in Mammalian Cells. *Biotechnol. Prog.* **Vol. 00** (2011).

23 Reflection paper on the data requirements for intraveneous liposomal products developed with reference to an innovation liposomal product. *European MedicinesAgency,* *http://www.ema.europa.eu/ema/index.jsp?curl=pages/regulation/general/general_content_000564.jsp&mid=WC0b01ac05806403e0* (2013).

24 Colletier, J. P., Chaize, B., Winterhalter, M. & Fournier, D. Protein encapsulation in liposomes: Efficiency depends on interactions between protein and phospholipid bilayer. *BMC Biotechnology* **2** (2002).

25 Christopher KIRBY, J. C. a. G. G. Effect of the Cholesterol Content of Small Unilamellar Liposomes on their Stability in vivo and in vitro. *Biochem. J.* **186**, 591-598 (1980).

26 Corchero, J. L. *et al.* Enzymatic characterization of highly stable human alpha-galactosidase A displayed on magnetic particles. *Biochemical Engineering Journal* **67**, 20-27 (2012).

27 Jiang, W., Kim, B. Y. S., Rutka, J. T. & Chan, W. C. W. Nanoparticle-mediated cellular response is size-dependent. *Nature Nanotechnology* **3**, 145-150 (2008).

28 Nel, A. E. *et al.* Understanding biophysicochemical interactions at the nano-bio interface. *Nature Materials* **8**, 543-557 (2009).

Chapter 4. Nanovesicle-EGF conjugates prepared by DELOS-SUSP as nanomedicine candidate for the treatment of complex wounds

4.1 Introdution

4.1.1 Complex wounds

A wound can be described as a defect or a break in the skin, resulting from a physical or thermal damage or as a result of the presence of an underlying medical or physiological condition[1,2]. Based on the nature of the healing process, wounds can be classified as acute or chronic wounds. Acute wounds are usually tissue injuries that heal completely, within the expected time frame of 8–12 weeks[3]. Chronic wounds on the other hand arise from tissue injuries that heal slowly and that have not healed beyond 12 weeks and often reoccur[4]. Such wounds fail to heal due to repeated tissue insults or underlying physiological conditions, such as diabetes and malignancies, persistent infections, poor primary treatment and other patient related factors[5].

Ferreira et al. have described wounds, both acute and chronic, that are difficult to heal as 'complex wounds' with unique characteristics[6]. One or more of the following conditions must be present for a wound to be categorized as a "complex" type:

a) Extensive loss of the integument which comprises skin, hair, and associated glands.

b) Infection is frequently present as a complication in chronic wounds and in itself may be the cause of the problem that resulted in tissue loss, as happens in aggressive infections like Fournier's gangrene.

c) Compromised viability of superficial tissues like clear necrosis, or signs of circulation impairment either localized or more extensive, usually in the limbs, leading to extensive loss of substance.

d) Association with systemic pathologies that impair a normal healing causing wounds to fail to heal with simple care and requiring special attention.

Among the major groups of complex wounds we can find the diabetic wounds, pressure sores, chronic venous ulcers, post-infection soft-tissue gangrenes, and ulcers resulting from vasculitis. Due to the complexity of these wounds they should be treated by multidisciplinary teams in specialized hospital centers. Complex wounds defy cure using conventional and simple "dressings" therapy, and in most cases surgical treatments are unavoidable. This is why new technologies that improve the conventional treatments should be introduced.

4.1.2 Epidermal growth factor (EGF)

Epidermal growth factor or EGF is a small polypeptide with a molecular weight of 6200 Da and a structure consisting of simple chain with 53 amino acid residues (Table 4.1). Since its discovery by Cohen in 1962, all aspects of EGF biology have attracted intense research interest due to the potential applications in various facets of human health care[7]. EGF is one of the products designed to correct several aspects of wound biochemistry and cell biology associated with impaired wound healing[8]. EGF exerts a potent mitogenic activity through binding to a specific cell membrane receptor promoting the epidermal regeneration and the corneal epithelialization by a number of actions[9,10]. Such actions include enhancing epithelial cell proliferation and migration to the wound, stimulating the production of proteins such as fibronectin, and increasing the number of fibroblasts in the wound[11]. Although this polypeptide has shown much promise in the treatment of gastrointestinal illness, ulcerative colitis, etc, probably its wider applications is found in the healing of wounds and ulcers of different tissues in the human body[12-14].

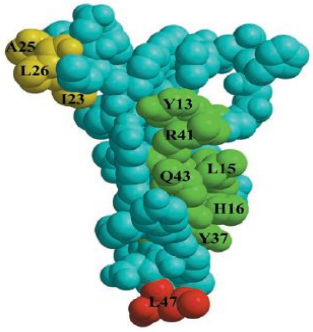

Figure 4.1. Schematic representation of the tertiary structure of rhEGF.

Over the last years, some institutions of the Havana Western Scientific Pole in Cuba have been developing and marketing novel therapeutic products using the recombinant human EGF (rhEGF), known as Heberprot-P® and Cimavax EGF®. Particularly Heberprot-P, developed by the Center of Genetic Engineer and Biotechnology (CIGB), is a novel and unique therapeutical drug prescribed for diabetic foot ulcer (DFU), which is based on the recombinant human growth factor and which is delivered by intralesional infiltration directly into the wound sites. DFU is a major complication of diabetes mellitus, which concerns 15% of the 200 million patients with diabetes worldwide and precedes more than 60 % of all lower leg amputations[15-17]. Major increase in mortality among diabetic patients, observed over the past 20 years, is

considered to be due to the development of macro and micro vascular complications, including a failure of the wound healing process[18]. The treatment with Heberprot-P accelerates the healing of deep and complex DFU, reduces the risk of amputations, decreases the healing time and thus future complications, such as gangrene or infections, contributing significantly to improve the quality of life in patients. It is known that chronic wounds, such as diabetic foot ulcers, present a proteolytic environment that can affect the bioavailability of the drugs used during the treatment. Consequently the encapsulation of drugs within nanocarriers can increase the effectiveness of their action. Vesicles can provide such protection together with an effective delivery of the active molecules in the site of action. Indeed the encapsulation of EGF in liposomes of different compositions has been reported for different medical applications[19-21]. Topical delivery of drugs from liposomal formulations has produced a considerable interest since they can enhance the percutaneous delivery aiding the transport of hydrophilic and lipophilic compounds[22-25]. However, it is generally agreed that classic liposomal carriers for transdermal drug delivery present a poor penetration into the skin, and rather remain confined to the upper layer of the stratum corneum[26,27]. Only specially designed vesicles, such as ethosomes which contains ethanol in relatively high concentrations (20-30 %), have been able to allow transdermal delivery[27-29]. Their good performance is related to the presence of a high content of ethanol in the formulation, which is known as an efficient permeation enhancer. Other studies indicate that the cholesterol content might be of crucial importance for the effective delivery of liposome-entrapped substances into the skin[26].

Quatsomes formed by cholesterol and CTAB constitute an attractive alternative to conventional liposomes for the topical delivery of EGF. This type of vesicles presents some advantages over conventional liposomes like being extremely homogeneous and much more stable (more 1 year) under normal storage conditions. Moreover the presence of a high ethanol percentage in the dispersant media (10 %) and their high cholesterol content (50%) makes quatsomes promising for attaining good skin penetrability and an effective delivery of the cargo. Additionally CTAB is part of the family of quaternary ammonium surfactants (QUATs) which are known acting as antiseptics and disinfectants and are widely used in pharmaceutical formulations[30,31].

In this Chapter, and in the frame of a collaborative project with the CIGB Institute, the possibility of preparing new topical formulations based on rhEGF loaded quatsomes, using the DELOS-SUSP method, is explored. The main goal of this project was the

obtaining of nanoconjugaes with good pharmacological properties and therapeutic activities, in order to improve the treatment for patients with complex wounds, particularly with diabetic foot ulcers. The protein used in the experiments presented in this chapter was prepared and provided by CIGB.

4.2 Preliminary interaction studies between quatsomes and the rhEGF protein

Despite the homogeneous morphology and great stability of quatsomes, it has been proven that after certain concentration of negatively charged molecules integrated on them, changes in the morphology and instability of their structures are produced. rhEGF is a small protein with an isoelectric point of 4.5 which is stable at pH between 5 and 7. Therefore at the working conditions the protein is negatively charged. Due to these results it was considered important to study the interaction between quatsomes and the negatively charged rhEGF resulting from incubation experiments. To this end plain quatsomes were prepared by the depressurization of expanded organic solution containing cholesterol (68 mM) over 24 mL of an aqueous solution containing the CTAB (7.8 mM). The vesicles were characterized and then kept at 277 K until use. For the incubation experiments different volumes of an rhEGF solution (1.4 mM) were added to plain quatsomes in order to have 3 mL of a final solution containing protein concentrations between 25 and 200 µg/mL and protein/CTAB ratios between 0.6 and 5.0 mmol/mol (Figure 4.2). The solutions were stirred for 15 min at room temperature and kept at 277 K until characterization. The range of concentrations of rhEGF was selected based on the normal doses that are used in the treatments of diabetic foot care with the Heberprot-P®.

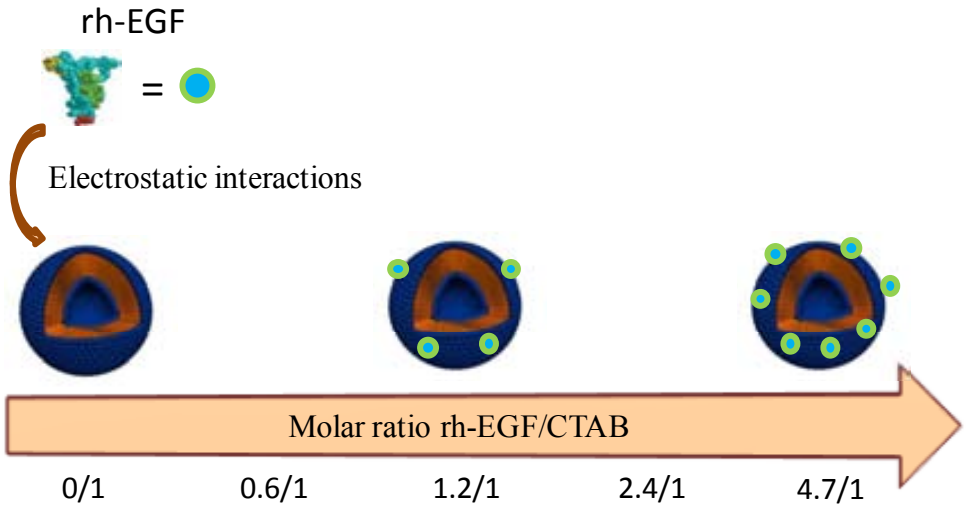

Figure 4.2. Different protein/CTAB ratios tested in the incubation studies

The size, polidispersity index and Z potential of the resulting solutions were determined using dynamic light scattering equipment (Table 4.1). First observation was a decrease

in the Z potential of the vesicles when increasing the protein/CTAB ratio which indicates that the protein interacts electrostatically with the membrane of quatsomes. This interaction is in agreement with the negative charge of the protein at the pH (~ 6) of the used solutions. At concentrations of rhEGF larger than 25 μg/mL the size of the quatsomes increased, probably due to the incorporation of the protein on the membrane. However at a protein concentration of 200 μg/mL the size of quatsomes increase in more than 100 nm, indicating that important structural changes occur in the vesicles. As shown in Chapter 2, quatsomes rupture occur after certain ratio BSA/CTAB when the net positively charge of the vesicles due to CTAB, is overpassed. This rupture produces a decrease in the Z potential toward values lower than cero and an increase in the size from nm to μm. At this protein concentration (200 μg/mL), the z potential is still high and positive and the size is in the nm range. Therefore it can be assumed that although the membrane of quatsomes is somehow perturbed by the presence of the protein, a rupture of the vesicles seems not to be produced.

In order to confirm this assumption, Cryo-TEM images were performed to quatsomes functionalized with rhEGF in a molar ratio rhEGH/CTAB 4.7:1 mmol/mol (Table 4.3). It is clearly observed the presence of some vesicles aggregates. This phenomenon was also observed in Chapter 2 for the BSA protein which was also negatively charged under the experiment conditions. A plausible explanation for this aggregation could be the fact that part of the protein already interacting with the membrane of quatsomes, attract other vesicles, forming this multi-vesicular complexes were the protein acts as glue. It is then confirmed that although the membrane of the protein is perturbed, no vesicle rupture is observed.

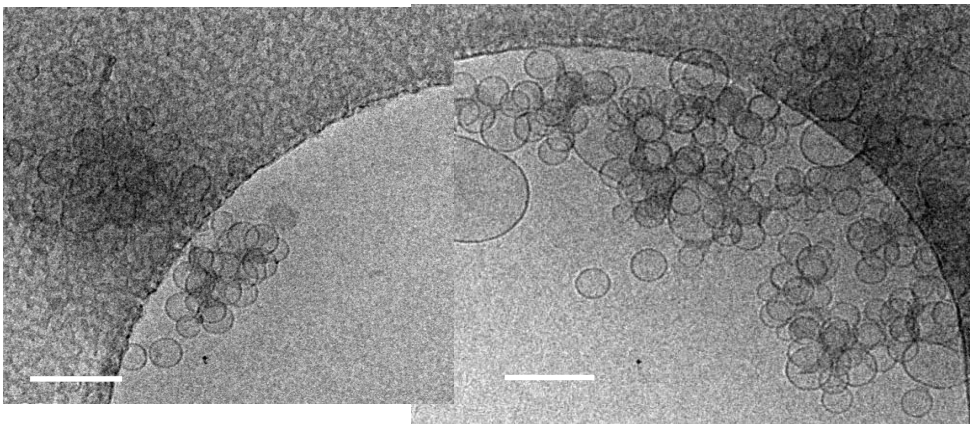

Figure 4.3. Cryo-TEM images of quatsomes functionalized with rh-EGF at a molar ratio rhEGF/CTAB of 4.7:1 mmol/mol. Scale bars are 200 nm

Table 4.1. Physicochemical characteristics of quatsomes and liposomes after their functionalization with rhEGF

	rhEGF (μg/mL)	Molar ratio (mmol/mol)	Size (nm)	Pdl	Z potential
Quatsomes		*EGF/CTAB*			
	0	0/1	121±1	0.2±0.01	70±1
	25	0.6/1	129±2	0.29±0.03	52±2
	50	1.2/1	135±1	0.34±0.02	55±1
	100	2.4/1	153±4	0.50±0.01	54±2
	200	4.7/1	235±2	0.66±0.02	42±1
Liposomes		*EGF/DPPC*			
	0	0/1	119±2	0.15±0.01	3.2±0.3
	25	3.1/1	126±1	0.18±0.01	6.4±2
	50	6.3/1	125±1	0.15±0.03	4.5±0.7
	100	12.5/1	131±3	0.13±0.06	7.2±1
	200	25/1	132±2	0.16±0.03	7.4±2.1
EGF/water	200	-	3±1	0.47±0.01	-17±4

In order to compare the results obtained for quatsomes with a classic liposomal formulation, the integration study was repeated using liposomes comprising cholesterol and DPPC. Plain liposomes were prepared using DELOS-SUSP by depressurizing an expanded solution containing cholesterol (26 mM) and DPPC (27 mM) over water. Then distinct volumes of a rhEGF solution (1.4 mM) were added to these plain liposomes in order to have 3 mL of a final solution with different protein concentrations (25-200 μg/mL) and protein/phospholipids ratios (3.1-25 mmol/mol). Even though this liposomes do not present any charge on their surface, hydrophobic interaction can occur between the hydrophobic patches in the surface of the protein, and the membrane. The effect of adding different amounts of protein was studied by measuring the physicochemical parameters of the resulting liposomes. As seen in Table 4.1, the size increased slightly for all the concentrations of rhEGF tested but in less extent than for quatsomes. This slight size increase could be an indication of the existence of some protein-membrane interaction. No significant changes were observed for the Z potential when the concentration of the protein was increased, in accordance with the absence of charge in the liposomes.

In order to complement the previous results, the interactions between the protein and the two types of vesicles were also studied by measuring the change in the fluorescence of the two tryptophan (Trp) groups present in the rhEGF structure. As already mentioned in Chapter 2, for proteins containing Trp groups, both a shift to a shorter wavelength

and changes in fluorescence intensity, are observed upon decreasing the polarity of the protein environment. The emission fluorescence spectra of a solution of rhEGF in water and the functionalized vesicles with the same initial amount of protein were recorded after exciting at 295 nm. For quatsomes (molar ratio of EGF/CTAB= 1.8 mmol/mol and concentrations rhEGF= 75 µg/mL), a shift in the maximum wavelength toward the blue (351.5 nm) and an increase in the intensity is observed with respect to the initial solution in water (356 nm) (Figure 4.4). This result indicates a change in the polarity media surrounding the Trp groups, suggesting that the rhEGF is interacting with the membrane quatsomes. For the liposomes (molar ratio of EGF/DPPC= 9.4 mmol/mol and concentration of rhEGF= 75 µg/mL) the shift in the wavelength was not observed. This result suggests that the Trp groups of the protein do not interact with the membrane of liposomes under the experimental conditions tested or that the interaction is produced through a part of the protein structure far from the Trp groups (Figure 4.4).

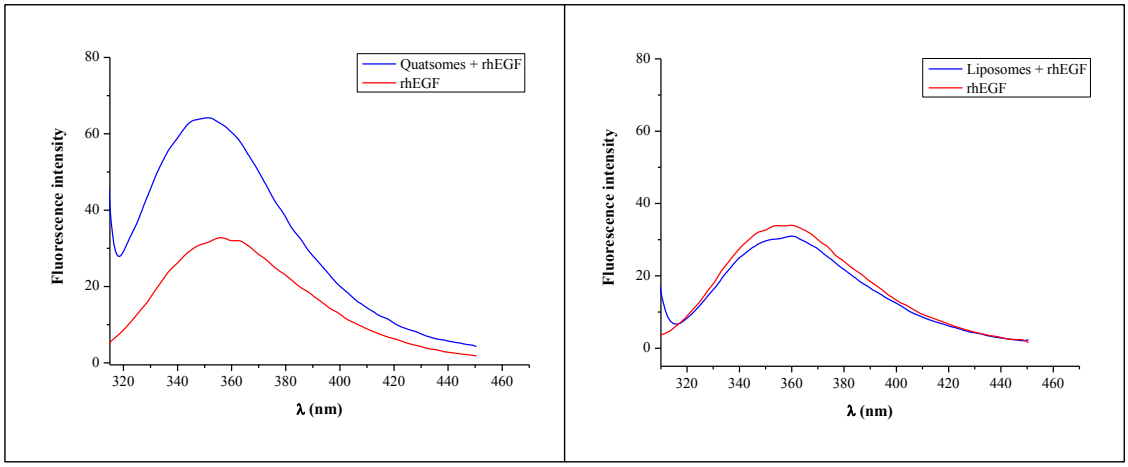

Figure 4.4. Emission fluorescence spectra of rhEGF in water and after incubation with plain vesicles. Quatsomes (left) and liposomes (right).

From this study one can conclude that the rhEGF protein interacts electrostatically with quatsomes forming a conjugate that is stable from the molar ratio EGF/CTAB 0.6 to 2.4 mmol/mol. After this molar ratio, and particularly at 4.7 mmol/mol, some structural changes are observed.

4.3 Preparation and characterization of rhEGF loaded quatsomes.

After studying the interaction between the rhEGF protein and quatsomes in order to establish the range of EGF/CTAB molar ratios in which the quatsomes structure is not perturbed by the protein, entrapment experiments were performed. As schematically

depicted in Figure 4.5 , rhEGF loaded quatsomes and rhEGF loaded liposomes were prepared by DELOS-SUSP methodology . For the preparation of rhEGF loaded quatsomes at different protein/CTAB molar ratios (0.6-4.7 mmol/mol) a solution of ethanol containing cholesterol (68 mM) was loaded into the reactor (7.5 mL) and pressurized with compressed CO_2 (X_w= 0.6). After one hour, the depressurization of the volumetric expanded organic phase was performed over 24 mL of an aqueous solution containing CTAB (7.8 mM) and the protein at the desired concentration. Protein loaded liposomes at different rhEGF/DPPC molar ratios (3.1-25 mmol/mol) were also prepared for comparison purposes. To form the conjugates, the volumetric expanded organic solution containing cholesterol (26 mM) and DPPC (27 mM) was depressurized over water containing the protein (Figure 4.5 , right). Information about the compositions used for the preparation of the loaded-vesicles and more details of the process is given in Table 4.2 and Experimental Section 2.1.1 respectively.

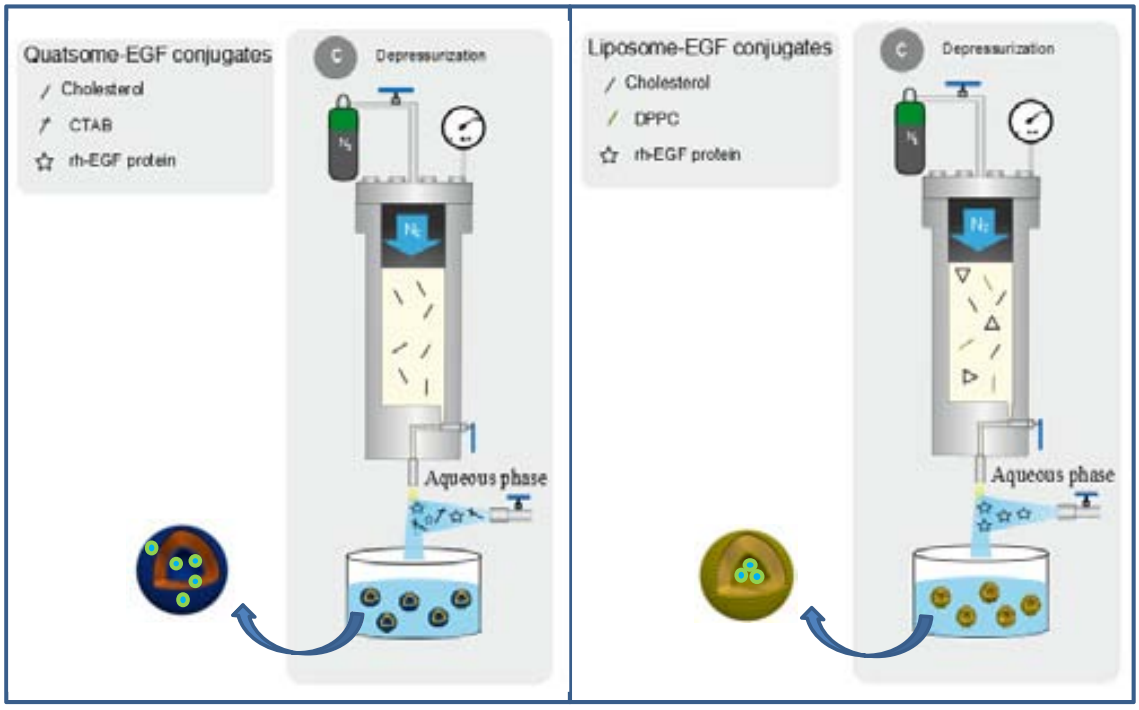

Figure 4.5. Schematic representation of DELOS-SUSP process used to prepare rhEGF loaded quatsomes (left panel) and liposomes (right panel).

Table 4.2. Compositions used for the preparation rhEGF loaded quatsomes and liposomes by DELOS-SUSP method

Vesicle systems (rhEGF concentration in μg/mL)	Organic phase	Aqueous phase [a]	EGF/lipid ratio [b] (mmol/mol)	Lipidic conc.[c] (mg/mL)
rhEGF loaded-quatsomes			EGF/CTAB	
(25)	Cholesterol (68 mM)	CTAB 7.8 mM + rhEGF mM	0.6	5
(75)	Cholesterol (68 mM)	CTAB 7.8 mM + rhEGF mM	1.8	5
(125)	Cholesterol (68 mM)	CTAB 7.8 mM + rhEGF mM	2.9	5
(200)	Cholesterol (68 mM)	CTAB 7.8 mM + rhEGF mM	4.7	5
rhEGF loaded-liposomes			EGF/DPPC	
(75)	Cholesterol (26 mM) + DPPC (27 mM)	rhEGF mM	9.4	1.4
(125)	Cholesterol (26 mM) + DPPC (27 mM)	rhEGF mM	15.6	1.4
(200)	Cholesterol (26 mM) + DPPC (27 mM)	rhEGF mM	25	1.4

Entrapment experiments were performed from CO_2-expanded ethanol at 10 MPa and 308K and X_{CO2}= 0.6 (for quatsomes) and X_{CO2}= 0.85 (for liposomes). [a] The aqueous phase was always prepared from 24 mL of mQ water. [b] Ratio between the moles of initial enzyme and the total moles of lipids forming the liposome membrane.[c] Ratio between the total amount of lipid forming the membrane and the volume of the final vesicular suspension.

All nanoconjugates were prepared by triplicate and kept at 277 K until their characterization. Table 4.3 shows the physicochemical characteristics obtained for all the conjugates just after their preparation. The size of the rhEGF loaded quatsomes increase with increasing the amount of protein used in the preparation whereas no differences in Z potentials were observed when the protein concentration was in the range of 25 to 125 μg/mL. The Z potential values were very high in accordance with the great stability of these conjugates, which remain stable for more than 5 months under storage conditions. Nevertheless the system prepared with a protein concentration of 200 μg/mL showed a very low Z potential and accordingly it was macroscopically stable once prepared but after 7 days a clear phase separation with a solid deposition

was observed (Figure 4.6). This instability was also observed during the functionalization studies at the same protein concentration and rhEGF/CTAB molar ratio (4.7 mmol/mol), which confirms the importance of biomolecule-quatsome interaction studies before any entrapment or functionalization experiment.

Table 4.3. Physicochemical characteristics of rhEGF loaded quastome and liposome conjugates obtained by DELOS-SUSP method

Vesicle systems (rhEGF concentration in µg/mL)	EGF/lipid ratio (mmol/mol)	Size		Z potential (mV)
		Mean[a] (nm)	PdI[b]	
rhEGF loaded quatsomes	EGF/CTAB			
(0)	0/1	121 ± 7	0.23 ± 0.01	74 ± 5
(25)	0.6/1	98± 4	0.3 ± 0.01	73 ± 5
(75)	1.8/1	131 ± 9	0.34±0.02	77 ± 3
(125)	2.9/1	146 ± 14	0.45±0.01	78 ± 4
(200)	4.7/1	184 ± 4	0.44±0.03	0.9 ± 0.1
rhEGF loaded liposomes	EGF/DPPC			
(0)	0/1	123 ± 6	0.20±0.004	3 ± 0.6
(75)	9.4/1	183 ± 7	0.31 ± 0.01	3.15 ± 1
(125)	15.6/1	233 ± 10	0.39±0.01	5 ± 2
(200)	25/1	209 ± 20	0.40±0.02	-1.12 ± 0.45

[a]Intensity weighted mean hydrodynamic size of the collection of vesicles measured by dynamic light scattering. [b]Polidispersity index showing to the width of the particle size distribution.

For the rhEGF loaded liposomes, an increment in size with increasing the protein amount was also observed. The Z potential values of such conjugates were very low, in the range of poor stability for the suspensions. Indeed the liposomes were macroscopically stable once prepared but just after 7 days of storage at 277 K a partial phase separation was observed in all cases (Figure 4.6). This solid deposition was higher for conjugates prepared with larger protein/lipid ratios and it disappeared by shaking the samples.

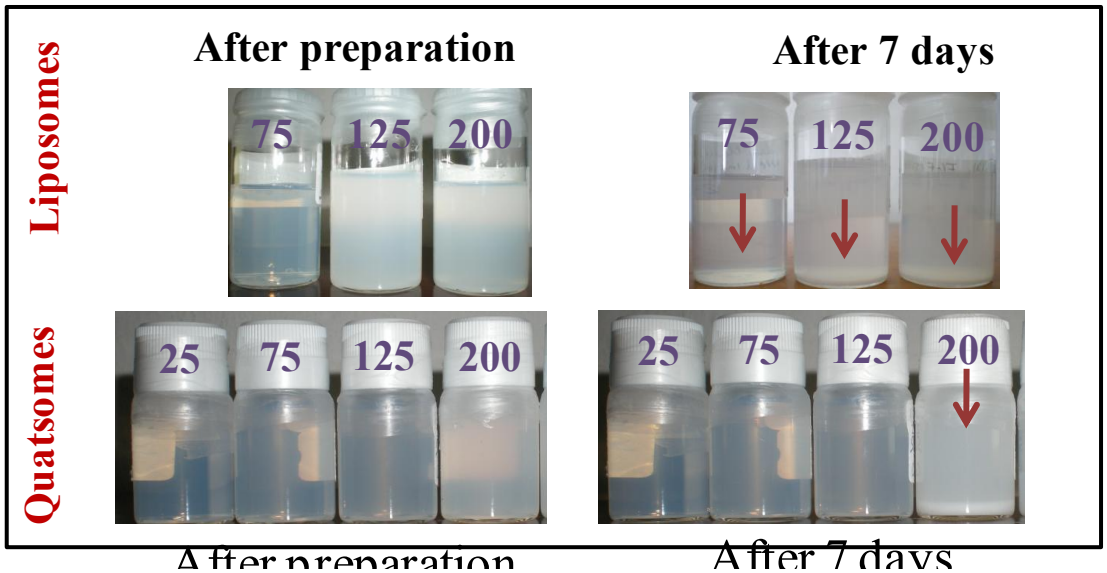

Figure 4.6. Macroscopic appearance of rhEGF loaded quatsomes and rhEGF loaded liposomes prepared with at different concentrations of rhEGF (25-200 µg/mL) as prepared and 7 days later.

Cryo-TEM images of the rhEGF loaded quatsomes prepared with protein concentrations of 25, 75 and 125 µg/mL were taken. The formulation at 200 µg/mL was not included due to its instability. Figure 4.7 depicts the presence of spherical and unilamellar vesicles for all rhEGF loaded quatsomes. The increase in the size with the rhEGF loading was also observed in the images (Figure 4.7, top panel). Interestingly, at 125 µg/mL, although the vesicles keep their homogeneous morphology the presence of stick-like structures (or pieces of membranes) inside the quatsomes can be observed. Currently, theoretical and calorimetric studies are being carried out in order to understand this morphological change. The rhEGF loaded liposomes present a less homogeneous morphology with a mixture of unilamellar and multilamellar vesicles (Figure 4.7, bottom panel). The increase in the size with the rhEGF protein loading is also observed.

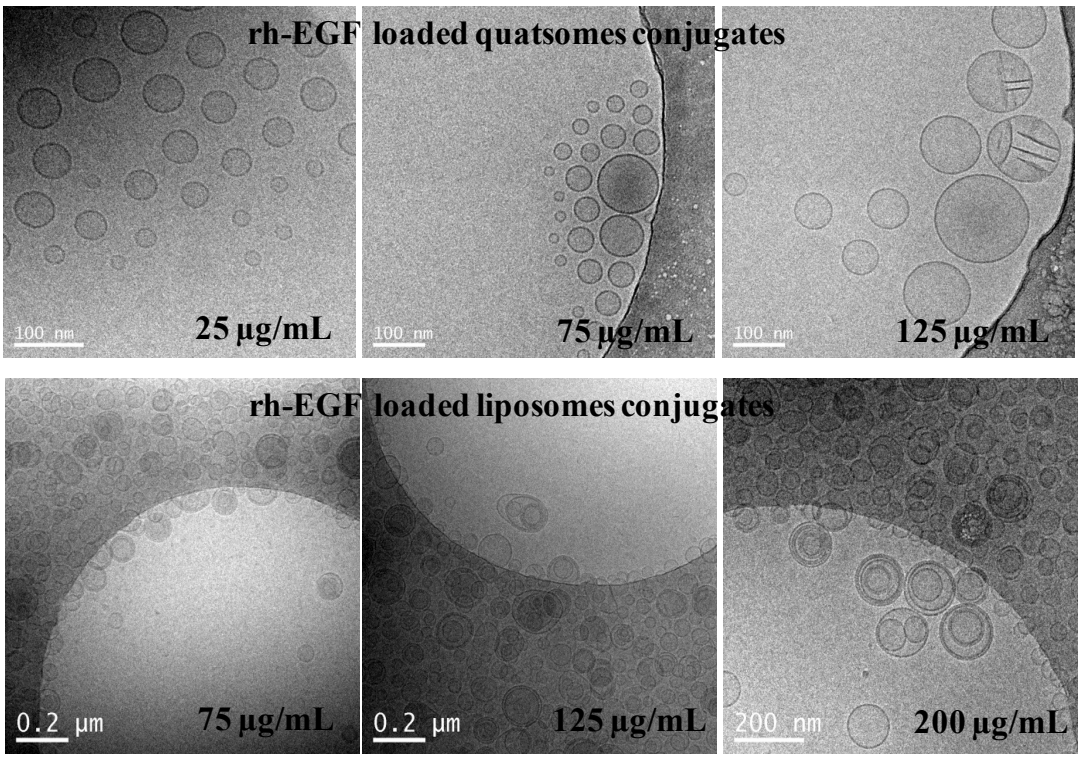

Figure 4.7. Cryo-TEM images of rhEGF loaded quatsomes and rhEGF loaded liposomes prepared by DELOS-SUSP methodology. Scale bar for quatsomes are 100 nm and for liposomes 200 nm.

Once both sets of conjugates were characterized, the entrapment efficiency percentages and the protein loadings were determined. As proven for α-GAL loaded liposome-RGD conjugates, it is very important to use an appropriated methodology to separate the non-integrated active from the loaded conjugates and also an adequate quantification methodology of the integrated active. Different procedures were tested in order to separate the free protein from the loaded conjugates. First a centrifugation procedure was used for both rhEGF loaded liposomes and rhEGF loaded quatsomes. For this a volume of 500 mL was placed in an eppendorf tube and centrifuged for 1 hour at 20 000 rpm and 4 ^{0}C. A pellet was formed for liposomes but not for quatsomes probably due to the higher stability of such the vesicles. Centrifugal filter devices of 30 KDa were then tested in order to separate the free rhEGF from the loaded vesicles following the procedure described in Experimental Section 4.1.1. After the separation processes a solution of Triton X-100 10 % (Tx-100) was added to 500 µL of loaded quatsomes and loaded liposomes, to have a final concentration of the surfactant in the solution equal to 1%. The solutions were stirred during 1 hour. It has been reported that non-ionic surfactants, like Tx-100, can break down the liposome membranes releasing the

entrapped rhEGF for further quantification. This quantification was performed by means of an enzyme-linked immunosorbent assay (ELISA) developed at the Liquid and Lyophilized Laboratory of CIGB (Experimental Section 4.2.5). This assay is based on the unique ability of an antibody to bind with a high specificity to one or a very limited group of molecules (antigens). Immunoassays can be carried out for either member of an antigen/antibody pair and it has been used as a diagnostic tool in medicine and plant pathology, as well as for quality-control tests in various industries. Briefly, for the quantification, a first antibody is added to a 96 well plate, then the sample with the protein that specifically binds to this antibody and finally a third conjugation antibody that recognize our protein, forming a kind of molecular sandwich (Figure 4.8). Subsequently a substrate, that forms a colored complex with the conjugation antibody, is added and the absorbance is read at 492 nm. A calibration curve is included in each plate and the concentration of the protein is proportional to the intensity of color in each well. For all batches the total sample, the loaded vesicles after the rupture with Tx-100 and the waters with the free protein were measured. Using the Eqs. 1 and 2, the entrapment efficiency and the protein loading were determined (Table 4.4).

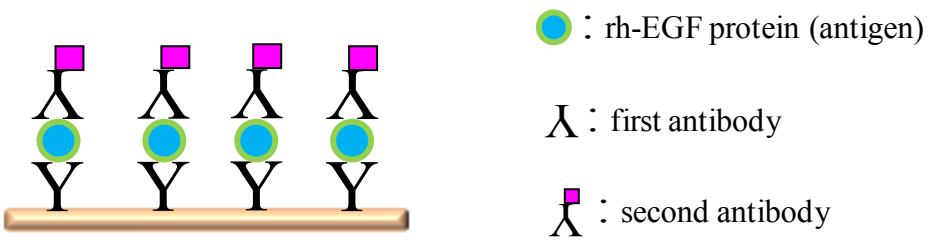

Figure 4.8. Schematic representation of a sandwich type ELISA immunoassay

Very low encapsulation percentages (between 1 and 9 %) were found for the rhEGF loaded liposomes. As rhEGF is water soluble and the vesicles are nanoscopic, the volume that is entrapped inside the vesicles is small contributing to small entrapment efficiencies. Besides it is described that a factor that can enhance the entrapment is the interaction between the biomolecules and the liposome lipid bilayer that seems to be not present in this case[32]. When determined the amount of rhEGF in the quatsomes using ELISA, the values obtained for the fraction of loaded vesicles and the total sample were higher than the theoretically one expected. Probably this overestimation was produced

because the Tx-100 surfactant was not able to break down the quatsomes, producing the cloudy appearance of vesicles an interference in the spectrophotometric measurements. For this reason the entrapment efficiency was determined from the fraction of diafiltrated waters containing the free protein and using the following equation:

$$Entrapment\ efficienty\ (\%EE) = \frac{initial\ mass\ of\ active - free\ ative}{initialmassofactive} * 100 \qquad \text{(Eq 3)}$$

It was found that for rhEGF loaded quatsomes almost all the protein was integrated in the vesicles for all the molar ratios protein/CTAB tested. The entrapment efficiency and the protein loading increase with the amount of the initial protein used. Indeed the maximum value was reached at 125 µg/mL of rhEGF (Table 4.4). In this case the interaction between the membrane of quatsomes and the rhEGH protein strongly favors the high entrapment efficiency achieved.

Table 4.4. .Entrapment efficiencies and loadings of the different rhEGF loaded quatsomes and liposomes prepared by DELOS-SUSP.

Vesicle systems (rhEGF concentration in µg/mL)	EGF/lipid ratio (mmol/mol)	EE (%)	Protein loading (µg/mg)
rhEGF loaded quatsomes	rhEGF/CTAB		
(25)	0.6/1	98.0±1.3	4.6
(75)	1.8/1	99.0±1.0	13.8
(125)	2.9/1	99.3±0.5	23
rhEGF loaded liposomes	rhEGF/DPPC		
(75)	9.4/1	1±0.2	0.5
(125)	15.6/1	2.7±0.3	2.4
(200)	25/1	8.7±0.6	12

As proven for the GLA loaded liposomes, it is important that the separation methodology does not affect the characteristics of the vesicles, due to the presumably impact of their size and morphology in the *in vitro* and *in vivo* behaviors. Cryo-TEM images of the loaded vesicles collected from the filter device of the sample reservoir after the separation procedure were taken for analysing possible morphological changes

after the diafiltration of conjugates. As observed in Figure 4.9 the vesicles continued to be nanoscopic and unilamellar, proving that the diafiltration process did not modify their morphology.

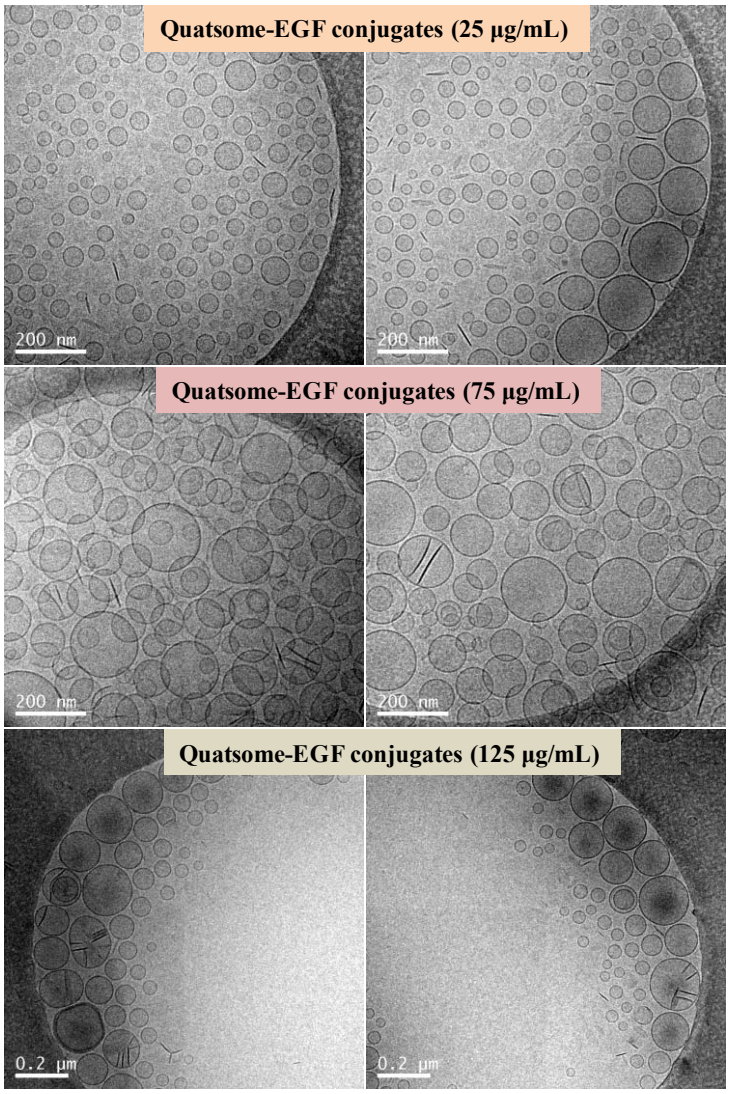

Figure 4.9. Cryo-TEM images of rhEGF loaded quatsomes after the separation of the non-integrated protein using centricons.

When the Trp fluorescence emission spectra for the encapsulated rhEGF (75 µg/mL) was measured and compared with the one in water, a shift in the wavelength towards a shorter wavelength was appreciated for the rhEGF integrated in quatsomes as well as an increase in the fluorescence intensity (Figure 4.10). Being a hydrosoluble protein, one can expect a rhEGF entrapment in the inner aqueous core of liposomes but this shift in the wavelength clearly indicates that a hydrophobic environment is surrounding the

protein which again confirms that at least part of the rhEGF is interacting with the membranes of quatsomes.

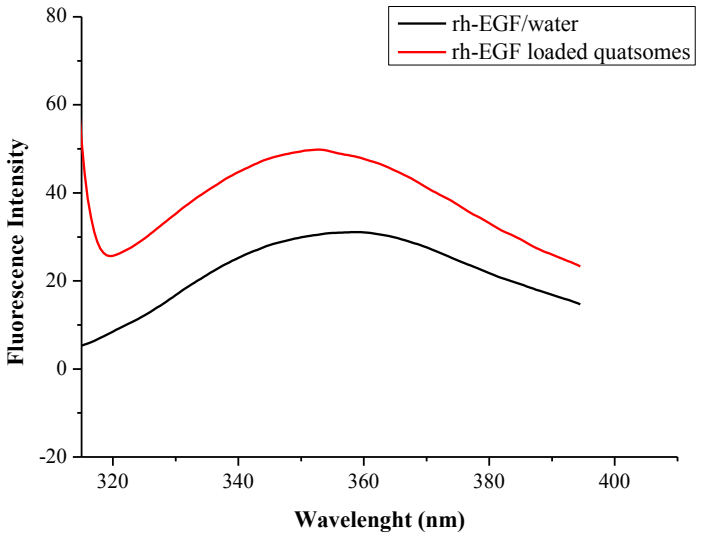

Figure 4.10.. Emission fluorescence spectra of rhEGF integrated in quatsomes and in water.

The differences in the entrapment efficiencies for the two types of nanocarriers, quatsomes and liposomes, were confirmed by mean of electrophoresis experiments, which were performed at the CIGB laboratories (Experimental Section 9.5) Polyacrylamide gel electrophoresis (PAGE) technique is usually employed to performed protein separation according to the molecular weight allowing the detection of aggregates, fragments of degradation or the presence of sample contaminants. In this case the electrophoresis was performed in native conditions, which means that the gels and the buffers used in the assay were prepared without sodium dodecyl sulfate (SDS) surfactant. The SDS is an anionic surfactant and its addition to the vesicles produces the breaking of their membranes and the release of the protein. In the Figure 4.11 the PAGE experiments are depicted for rhEGF loaded quatsomes and liposomes, both prepared with a protein concentration of 125 µg/mL, with increasing amounts of SDS. Free rhEGF in water at the same concentration is also included in each gel for comparison. In the case of quatsomes, when SDS is not present in the sample (0%), non-free protein is detected. However the more surfactant is added to the vesicles (from 0.05%-1%), the more protein is released and detected. On the contrary in the liposome-EGF system, as

the %EE is very low and there is a lot of free protein, rhEGF is detected even when the SDS is not added. This experiment confirmed that most of the protein present in the system is associated to the quatsomes.

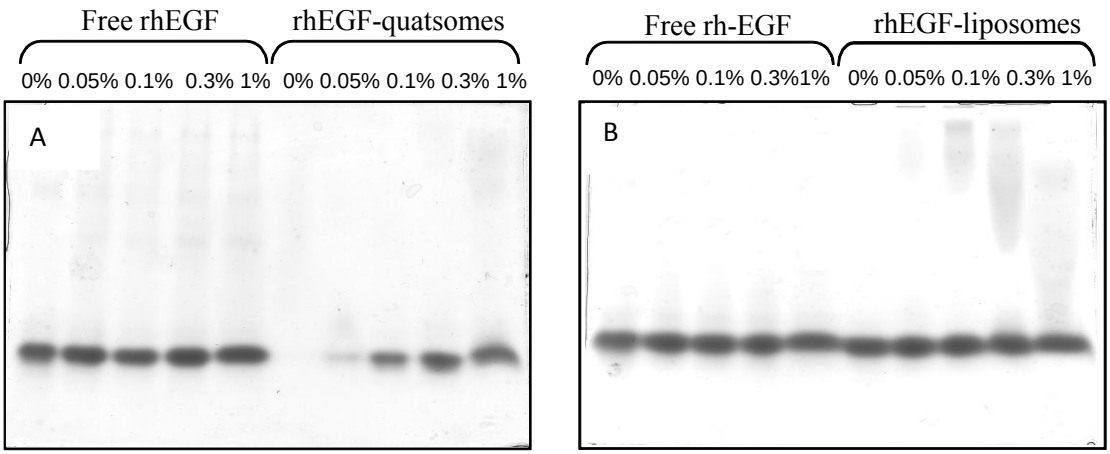

Figure 4.11. Polyacrylamide gel electrophoresis esperiments under native conditions

Compared to liposomes, th rhEGF loaded quatsomes presented better physicochemical characteristics, longer stability under storage conditions, more homogenous morphology and higher entrapment efficiency making this formulation a better candidate for the ultimate topical applications.

One of the most important requisite for the effective use of nanocarriers in drug delivery applications is their stability under storage conditions. The stability of the system once the protein was integrated was evaluated by the capacity of quatsomes to retain the loaded protein. For this experiment the entrapment efficiency and the protein loading were determined in different batches of rhEGF loaded quatsomes at 14, 29 and 32 months after their preparation by DELOS-SUSP. Separation of free protein was carried out by centrifugation with centricons and the quantification of the protein was performed by the ELISA assay.

Table 4.5. rhEGF loss and protein loading of different rhEGF loaded quatsomes storaged at 277 K

Batch (rhEGF concentration in μg/mL)	Storage time (months)	rhEGF loss (%)	Protein loading (μg/mg)
rhEGF-quatsome-1 (25 μg/mL)	14	4	4.5
rhEGF-quatsome-2 (25 μg/mL)	14	0	4.7
rhEGF-quatsome-3 (25 μg/mL)	14	7	4.3
rhEGF-quatsome-1 (25 μg/mL)	29	27	3.4
rhEGF-quatsome-2 (25 μg/mL)	29	24	3.5
rhEGF-quatsome-1 (75 μg/mL)	29	35	9.1
rhEGF-quatsome-2 (75 μg/mL)	32	29	9.9

The formulations at 25 μg/mL remain very stable after 14 months, retaining almost all the protein that was initially encapsulated. After 29 months, the amount of protein entrapped in the conjugates was around one third of the initial which is also a very high value considering the elapsed time. This reduction in the loading and in the amount of integrated protein after 2 years was also observed for batches containing 75 μg/mL of rhEGF protein. The high protein retention, promoted by the strong electrostatic interactions between the protein and the quatsome membrane, indicates that the formulations remain stable for long periods of time under normal storage conditions.

Finally for using a drug delivery system as nanomedicine it is essential a complete reproducibility of their physicochemical characteristics, morphology and loading among the different batches produced in distinct experiments. Robustness and reproducibility of DELOS-SUSP methodology was evaluated by measuring the size, polidispersity, Z potential, and entrapment efficiency values of batches prepared in different dates but under similar experimental conditions. The physicochemical characteristics of the rhEGF loaded quatsomes prepared with two different protein/CTAB molar ratios, 0.6 and 1.8 mmol/mol, are shown in Table 4.6 and 4.7.

Table 4.6. Physicochemical characteristics and entrapment efficiency of rhEGF loaded quatsomes for a protein/CTAB molar ratio equal to 0.6 mmol/mol.

Batch date	Size (nm)	PdI	Z-Potencial	EE (%)
26/10/2010	103,3	0,363	69,5	98,1
29/10/2010	96,7	0,376	79,7	97,3
10/02/2011	101,4	0,311	77	97,2
18/11/2011	92,8	0,351	76	96,6
10/02/2012	113,6	0,281	75,9	95,8
10/02/2012	111,3	0,335	70,1	98,6
Average	103 ± 8	0.34 ± 0.03	75 ± 4	97 ± 1

Table 4.7. Physicochemical characteristics and entrapment efficiency of rhEGF loaded quatsomes for a protein/CTAB molar ratio equal to 1.8 mmol/mol.

Batch Date	Size (nm)	PdI	Z-Potencial	EE (%)
29/10/10	141,7	0,419	80,4	99,4
24/02/11	139,5	0,278	74	98,1
28/02/11	142,2	0,275	72,9	99,7
29/06/11	139.0	0,353	77	99,1
30/06/11	140,9	0,357	77,5	98,6
12/07/11	141,4	0,319	76,0	99,5
Average	140 ± 1	0.33 ± 0.05	76 ± 3	99 ± 1

From the obtained average data, one can see that the standard deviation of the size and Z potential values is small. Indeed the variation coefficient (CV= standard deviation/average), which gives an idea of the data dispersion, was very small in all cases (0.7-7 %) indicating a great degree of reproducibility of DELOS-SUSP for the preparation of rhEGF loaded quatsomes.

4.4 Bioactivity studies of rhEGF loaded quatsomes

It is very important that the process used to prepare a vesicle-based conjugate does not affect the protein bioactivity with the consequent loss of its function in the site of action. The values of bioactivity for the rhEGF loaded quatsomes were determined by the ability of the samples to induce a cell proliferation with 3T3 A31 mouse cells. Details of the determinations, which were performed at the Biological Assay

Department of CIGB institute, are given in Experimental Section 9.4.3. In order to compare different vesicle loadings and free rhEGF, the specific activity of the samples were calculated using the Eq. 4, where UI means international unit.

$$EGF\ specific\ activity\ \left(\frac{UI}{mg}\right) = \frac{EGF\ biological\ activity\ (UI/mL)}{EGF\ concentration\ (mg/mL)} \qquad \text{Eq. 4}$$

A blank sample of plain quatsomes was included as a control in these assays and non-cytotoxic effect or cell proliferation increment was observed. The results obtained were very surprising (Figure 4.12). Indeed the bioactivity was not only preserved after the processing but increased at least twice when the protein was associated to the vesicles compared to the activity measured for the free biomolecule in water. The increment reached was higher for the preparation containing 25 µg/mL of protein.

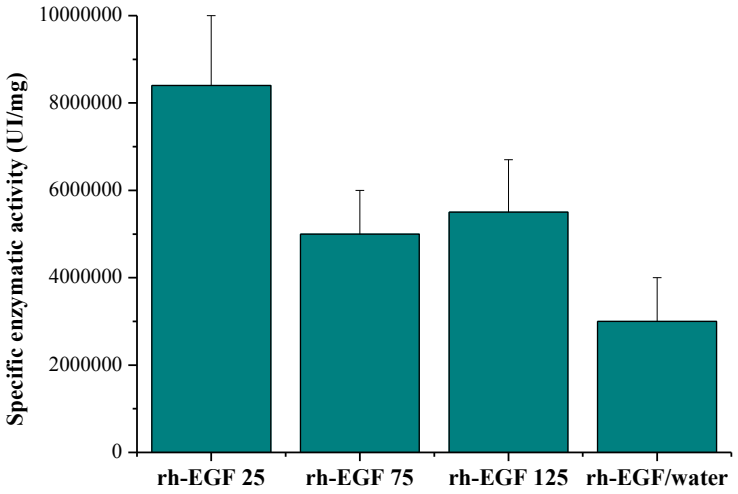

Figure 4.12. Specific activity for rhEGF loaded quatsomes.

As discussed for the α-GAL conjugates in Chapter 3, this increment could be related with the immobilization of the protein in a "site-specific" and oriented manner with the consequent exposure of the actives sites of the protein toward the surrounding media. As many other experiments performed along this Chapter, the bioactivity assays strongly suggests that part of the protein might be interacting with the membrane producing its immobilization.

In order to demonstrate experimentally the localization of rh-EGF protein in the membrane of quatsomes, inmunomicroscopy images were taken in the Microscopy

Department at the CIGB institute. Details of the sample preparation protocol are given in the Experimental Section 8 and 8.2. Inmunomicroscopy images for the rhEGF loaded quatsomes prepared by DELOS-SUSP and containing 25 µg/mL, 75 µg/mL and 125 µg/mL of protein, are depicted in Figure 4.13. In order to ensure that all black dots observed were due to the presence of a protein and not to an unspecific binding of the antibodies to the vesicles, the sample protocol was also performed in a blank sample of plain quatsomes and analyzed with the same transmission microscopy.

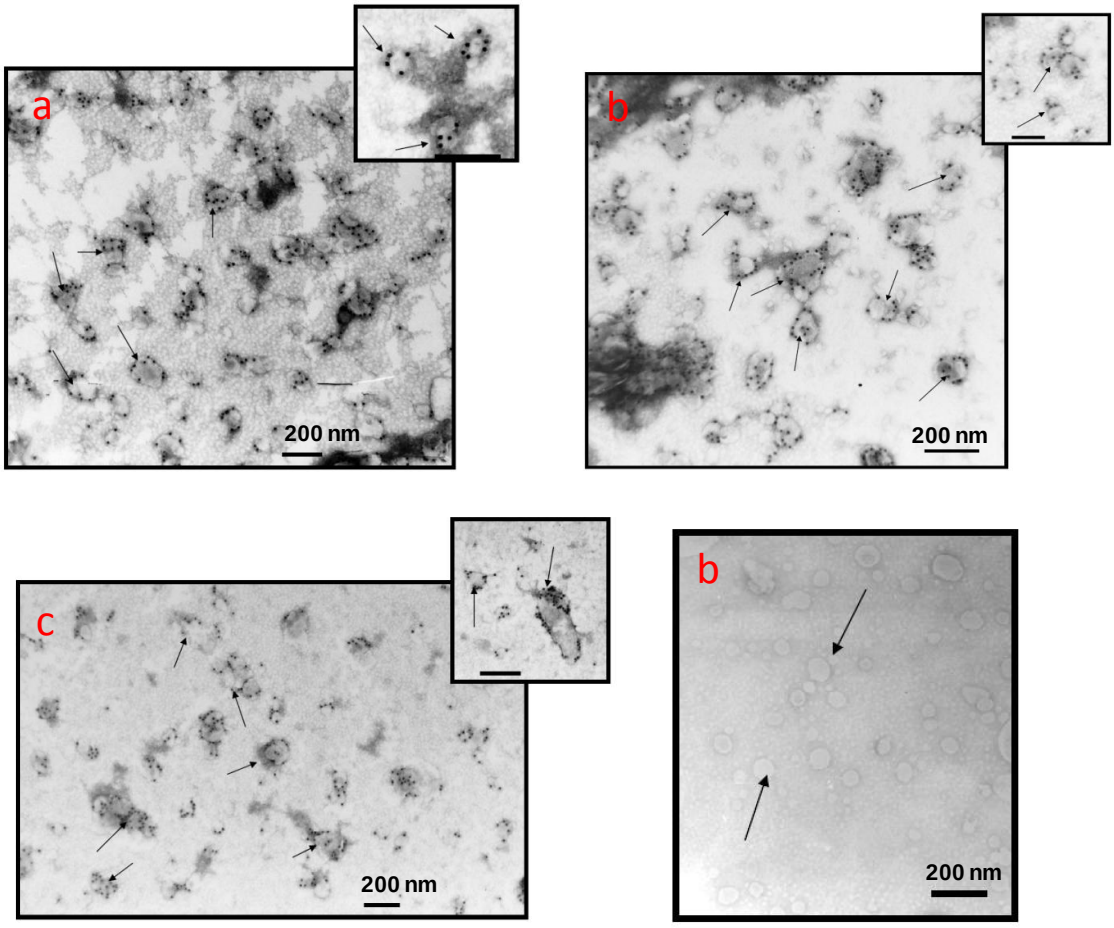

Figure 4.13. Inmunomicroscopy images of the rhEGF entrapped in the quatsomes. a) rhEGF-quatsomes conjugates at 25 µg/mL, b) rhEGF-quatsomes conjugates at 75 µg/mL, c) rhEGF-quatsomes conjugates at 125 µg/mL, d) plain quatsomes.

It is easily noted the presence of black dots in the vesicles membrane of the samples that contain the conjugates and not in the blank sample with plain quatsomes, confirming the localization of rhEGF in the lipidic part of the vesicles. At 125 µg/mL a higher density of the small black dots was observed, which is coincident with the highest concentration of the protein in this formulation. It can also be noted that in general there are more

protein molecules attached to the membrane than in the case of α-GAL. Here again not only the strong electrostatic interactions between the protein and the membrane, but also the employed DELOS-SUSP process might play an important role in this respect.

A simple experiment was performed in order to prove the latter assumption. The pH of the rhEGF loaded quatsomes containing 25 μg/mL of the protein and a loading of 4.6 μg/mg, was lowered from around 6 to 3, using an acetic/acetate buffer. At this pH the protein is positively charged (PI= 4.7) so if the high presence of the protein in the conjugate is only due to the electrostatic interaction, the %EE and the protein loading should decrease to very low values. After the pH was set to 3, the free protein was separated from the total sample using centricons and the amount of protein remaining in the vesicles was determined using ELISA assay. The entrapment efficiency obtained (50 ± 10%) and the loading (2.3 μg/mg) indicated that a great part of the interactions are of an electrostatic nature. The fact the protein loading was still high confirmed that part of the protein could be located within the membrane. As in the case of BSA, rhEGF is mixed with CTAB micelles in the aqueous phase previous to the depressurization step in the DELOS-SUSP process. Therefore, some kind of complex between rhEGF and CTAB might be formed, promoting the location of the protein within the membrane. This hypothesis should be checked by conducting studies of rhEGF-CTAB interactions, similar to those made with BSA and CTAB in Chapter 2.

Summing up the high entrapment efficiency and protein loading achieved for quatsomes in the range of protein concentration between 25 and 125 μg/mL could be explained due to the contributions of three effects: protein-membrane electrostatic interactions, encapsulation of the protein in the aqueous core of the vesicles and the entrapment of the protein within the membrane due to DELOS-SUSP process.

4.5 *In vitro* assays

All the *in vitro* assays were performed by members of the different specialized laboratories in CIGB.

4.5.1 Resistance to proteases

It is known that chronic wounds, such as diabetic foot ulcers, present a proteolytic environment that can affect the bioavailability of the protein-based drugs used during a treatment[33]. The resistance of rhEGF conjugates to protease experiments had the aim of evaluating the protective properties of quatsomes, through the capacity of preserving the

rhEGF stability and bioactivity in the presence of proteases. Proteases are enzymes that bring about the breakdown of proteins into peptides or amino acids by hydrolysis. In this study trypsin was selected as a protease model. The enzymatic reactions were prepared in Tris buffer at pH= 8.5 with a trypsin concentration of 0.5 µg/mL and using nanoconjugate concentrations of 25, 75 and 125 µg/mL. A reaction with a free rhEGF sample was also run for comparison purposes. The different samples were incubated during 4, 8, 16 o 24 hours at 37 ^{0}C. In order to quantify the amount of remaining rhEGF, the samples were treated for further quantification using HPLC with a reverse C18 phase column. Details of the entire assay are described in Experimental Section 9.6. The percentage of the remaining protein in each sample after the incubation with trypsin was calculated from the Eq. 5:

$$Remaining\ EGF\ (\%) = \frac{EGF\ conc.after\ incubation\ with\ tripsine}{EGF\ initial\ concentration} * 100 \qquad \text{Eq. 5}$$

The results showed that in general all rhEGF loaded quatsomes presented an increased stability against tripsin when compared with the free protein (Figure 4.14). During the first 4 hours the amount of protein decreases in all cases but for the quatsome formulations the decrease was smaller. Between 4 and 16 hours of incubation, meanwhile the amount of protein remains practically constant in the nanoconjugates, in the free EGF fraction there was a decrease of 30 %. Finally after 24 hours there was 53%, 41 % and 35% of remaining protein in the rh-EGF loaded quatsomes at concentrations of 25, 75 and 125 µg/mL respectively, and a decrease down to 8 % was observed in the free protein sample. As the final purpose is the use of the nanoconjugates as a topical formulation, this result can be translated to a better bioavailability and more effective action in the affected areas, if the rhEGF is integrated in the quatsomes.

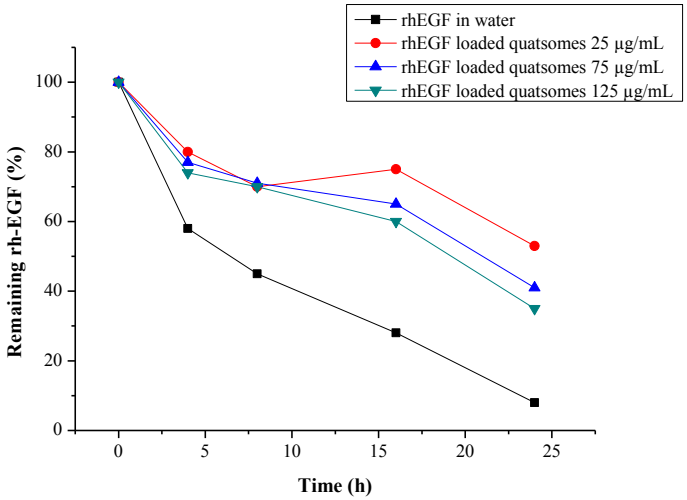

Figure 4.14. Remaining rhEGF after the incubation of samples with trypsin.

4.5.2 Antimicrobial activity

The antimicrobial action of a substance or formulation is given by their capacity to destroy the pathogenic microorganisms such as bacteria, molds, yeasts and viruses in the living environment, which cause severe infections in human beings. The rhEGF loaded quatsomes were tested *in vitro* in order to evaluate their antimicrobial and fungicidal activity. Their effectiveness of the different suspentions were assayed against two Gram positive bacteria (*Bacillus subtilis*, *Staphylococcus aureus*), two Gram negative (*E. coli, Proteus mirabilis*) and two fungus (*Candida albicans, Aspergillus niger*), using the using the technique of wells in nutrient agar plates (Experimental Section 9.7). This method consists in growing a known quantity of bacteria on agar plates in the presence of thin wafers containing the antibiotics. If the bacteria are susceptible to a particular antibiotic, a clear area also called zone of inhibition, surrounds the wafer where the bacteria are not capable of growing (Figure 4.15).

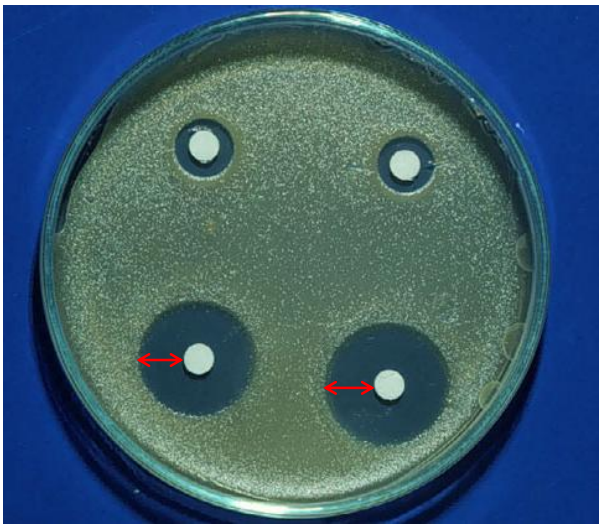

Figure 4.15. Agar plate with bacteria and in the presence of four wafers containing the antibiotics. The red arrows are signaling two different zones of inhibition.

After the bacteria and fungus grown, the plain quatsomes, the nanoconjugate at a concentration of 25 μg/mL, ciprofloxacin and fluconazole (100 μg/mL), were added to the plates. Ciprofloxacin and fluconazole (100 μg/ml) are antibiotics that were used as positive controls for bacteria and fungi, respectively. Assay plates were incubated at 310 K for 24 hours for bacteria, and at 301 K, during 72 hours for fungi, depending on the incubation time required for visible growth.

Table 4.8. Antimicrobial and fungicidal activity of rhEGF loaded quatsomes and plain quatsomes against bacteria and fungus.

Sample	Antimicrobial activity (inhibition zone in mm)				Fungicidal activity (inhibition zone in m)	
	B. subtilis	*S. aureus*	*E. coli*	*P. mirabilis*	*A. niger*	*C. albicans*
Plain quatsomes	22	18	R*	10	16	16
rhEGF loaded quatsomes	12	6	R	4	6	6
Ciprofloxacina	22	20	18	18	-	-
Fluconazol	-	-	-	-	21	22

*R means resistant

The different suspensions present an antimicrobial effect against Gram positive bacteria and fungi although microorganisms were more sensitive to plain quatsomes (Table 4.8).

Against certain microorganisms, plain quatsomes showed antibacterial and fungicidal activity comparable to ciprofloxacin and fluconazole, respectively.

The *in vitro* assays showed the great potential of the preparations based on quatsomes and rhEGF to be applied as topical formulation. After the better resistant of the integrated rhEGF to proteases environment and the presence of microbial activity, we decided to go one step further and test the nanoconjugates in *in vivo* assays using animal models

4.6 *In vivo* assays

All the *in vivo* assays were performed by members of the different specialized laboratories in CIGB.

4.6.1 Pharmacodynamic effect of rhEGF loaded quatsomes in animal models

Pharmacokinetics (PK) and pharmacodynamics (PD), play an essential role in the understanding of drug action and therapy. Pharmacodynamics is the study of the biochemical and physiological effects of certain drug at a given concentration on the body while pharmacokinetics describes the time courses of a drug concentration in body fluids resulting from the administration of a certain dose of the drug. The rationale for PK/PD- modeling is to link pharmacokinetics and pharmacodynamics in order to establish and evaluate dose-concentration-response relationships and subsequently describe and predict the effect-time courses resulting from a drug dose. The expanded use of PK/PD-modeling is assumed to be highly beneficial for drug development as well as applied pharmacotherapy and will most likely improve the current state of applied therapeutics[34]. To evaluate the pharmacological efficacy of the formulation an experimental model of chronic ulcer of total thickness was developed on the back of rats (Experimental Section). Sprague Dawley rats of 250-270 grams were used for such experiments, which were randomly allocated to constitute 3 experimental groups with 10 animals each. After inducing two symmetric chronic ulcers in each rat, the different treatments under study were applied as described below:

Experimental group # 1: Treated with a saline solution

Experimental group # 2: Treated with a suspension of plain quatsomes

Experimental group # 3: Treated with a suspension of rhEGF loaded quatsomes at a concentration of 25 µg /ml

The formulation containing 25 µg /ml was chosen due its higher specific activity compared with the preparations containing the protein in higher concentrations like 75 µg /ml and 125 µg /ml. The formulations were applied topically after cleaning the wounds by nebulization, twice a day and during 14 days. The animals were submitted to autopsy for sample collection and analysis. The obtained averaged data, summarized on Table 4.9, were obtained from two independent measurements.

Table 4.9. Pharmacodynamic effect of different formulations in a rat model of chronic ulcer.

Group	Inflammatory infiltrate (1 to 5 degrees)	Fibro-angiogenic answer (1 to 5 points)	Epithelial migration (µm)	Edge Contraction (%)
1 (Saline solution)	4.6 ±1.0	2.9±0.7	$3.0\pm1.1x10^3$	24±5
2 (Plain quatsomes)	3.8 ±1.00	2.6±0.9	$3.0\pm1.6x10^3$	22±5
3 (rhEGF loaded quatsomes)	1.18 ±0.04	4.2±0.2	$6.3\pm0.3x10^3$	89±6

It was found that the rhEGF loaded quatsomes significantly stimulated the overall healing process, as compared to the treatment with plain quatsomes and with a saline solution. It was noticeable the anti-inflamatory wound effect observed for the group # 3. This was related with the highest fibro-angiogenic response value and the higher wound edge contraction of 89 % obtained. Angiogenesis literally means the creation of new blood vessels in the treated areas. When a new tissue is formed, it is vital that it has enough blood supply for its growth and sustenance. Some of the situations where angiogenesis is important and necessary include those for wounds repairing. A great epithelial migration effect was also promoted by the rhEGF loaded quatsomes, as revealed by a stratified epidermis observed under the microscope.

4.7 Summary

- ✓ rhEGF loaded quatsome conjugates with nanometric sizes, between 100-150 nm, very stables along time and with a great degree of unilamellarity, with high entrapment efficiencies (~99 %) and protein loadings between 4.6 and 23 μg/mg were successfully prepared using DELOS-SUSP.

- ✓ These conjugates resulted very stable regarding the release of the entrapped rhEGF protein keeping the same protein/lipid loadings for more than one year.

- ✓ The specific enzymatic activity of the rhEGF entrapped in the quatsomes was at least two times higher than that for the free protein.

- ✓ The high entrapment efficiencies achieved in the rhEGF conjugates could be explained by the contribution of three phenomena: a) the protein-membrane electrostatic interactions, b) the encapsulation of the protein in the aqueous lumen of the vesicles and c) the entrapment of the protein within the membrane due to the characteristics of the DELOS-SUSP process.

- ✓ The protein integrated in the quatsomes presented an antimicrobial activity and showed 8 times more resistance to degradation by proteases compared with free rhEGF.

- ✓ The pharmacological efficacy of the developed rhEGF loaded quatsome conjugates was successfully evaluated *in vivo*, with an experimental animal model showing a considerable effect in the treatment of induced bilateral ulcers.

- ✓ The rh-EGF loaded quatsomes were used for the compassionate treatment of 12 patients showing outstanding results in the cicatrization of the complex wounds treated.

- ✓ The rhEGF loaded quatsomes can be considered as a future potential nanomedicine for the topical treatment of diabetic foot ulcer and in general for complex wounds.

4.8 References

1 Boateng, J. S., Matthews, K. H., Stevens, H. N. E. & Eccleston, G. M. Wound healing dressings and drug delivery systems: A review. *Journal of pharmaceutical sciences* **97**, 2892-2923 (2008).

2 Lazarus, G. S. *et al.* Definitions and guidelines for assessment of wounds and evaluation of healing. *Archives of Dermatology* **130**, 489-493 (1994).

3 Di Mascio, L. Classification and management of acute wounds and open fractures. *Surgery* **29**, 76-79 (2011).

4 Harding KG, M. H., Patel GK. . . Science, medicine and the future: Healing chronic wounds. *Br Med J* **324**, 160–163(2002).

5 Moore, K., McCallion, R., Searle, R. J., Stacey, M. C. & Harding, K. G. Prediction and monitoring the therapeutic response of chronic dermal wounds. *Int. Wound J.* **3**, 89-96 (2006).

6 Ferreira, M. C., Tuma Jr, P., Carvalho, V. F. & Kamamoto, F. Complex wounds. *Clinics* **61**, 571-578 (2006).

7 Cohen, S. Isolation of a Mouse Submaxillary Gland Protein Accelerating Incisor Eruption and Eyelid Opening in the New-born Animal. *J. Biol. Chem* **237,**, 1555-1562 (1962).

8 Game, F. *et al.* A systematic review of interventions to enhance the healing of chronic ulcers of the foot in diabetes. *Diabetes Metab. Res. Rev.* **28**, 119–141 (2012).

9 Bazley, L. & Gullick, W. The epidermal growth factor receptor family. *Endocr. Relat. Cancer* **12**, S17–S27 (2005).

10 Ten Dijke, P. & Iwata, K. K. Growth factors for wound healing. *Bio/Technology* **7**, 793-798 (1989).

11 Berlanga, J. *et al.* Epidermal growth factor intralesional infiltrations can prevent amputation in patients with advanced diabetic foot wounds. *Int. Wound J.* **3**, 232-239 (2006).

12 Babül, A., Gönül, B., Dinçer, S., Erdoğan, D. & Özoğul, C. The effect of EGF application in gel form on histamine content of experimentally induced wound in mice. *Amino Acids* **27**, 321-326 (2004).

13 Choi, J. S., Leong, K. W. & Yoo, H. S. In vivo wound healing of diabetic ulcers using electrospun nanofibers immobilized with human epidermal growth factor (EGF). *Biomaterials* **29**, 587-596 (2008).

14 Shirakata, Y. *et al.* Heparin-binding EGF-like growth factor accelerates keratinocyte migration and skin wound healing. *Journal of Cell Science* **118**, 2363-2370 (2005).

15 Vuorisalo, S. *et al.* Treatment of diabetic foot ulcers. *Journal of Cardiovascular Surgery* **50**, 275-291 (2009).

16 Albert, S. Cost-effective management of recalcitrant diabetic foot ulcers. *Clinics in Podiatric Medicine and Surgery* **19**, 483-491 (2002).

17 Dalla Paola, L. & Faglia, E. Treatment of diabetic foot ulcer: An overview strategies for clinical approach. *Current Diabetes Reviews* **2**, 431-447 (2006).

18 Brem, H. & Tomic-Canic, M. Cellular and molecular basis of wound healing in diabetes. *Journal of Clinical Investigation* **117**, 1219-1222 (2007).

19 Yerushalmi, N., Arad, A. & Margalit, R. MOLECULAR AND CELLULAR STUDIES OF HYALURONIC ACID-MODIFIED LIPOSOMES AS BIOADHESIVE CARRIERS FOR TOPICAL DRUG-DELIVERY IN

WOUND-HEALING. *Arch. Biochem. Biophys.* **313**, 267-273, doi:10.1006/abbi.1994.1387 (1994).

20 Li, H., Song, J. H., Park, J. S. & Han, K. Polyethylene glycol-coated liposomes for oral delivery of recombinant human epidermal growth factor. *International Journal of Pharmaceutics* **258**, 11-19 (2003).

21 Saddi, K. R. G. C., Alves, G. D., Paulino, T. P., Ciancaglini, P. & Alves, J. B. Epidermal growth factor in liposomes may enhance osteoclast recruitment during tooth movement in rats. *Angle Orthodontist* **78**, 604-609 (2008).

22 Nounou, M. M., El-Khordagui, L. K., Khalafallah, N. A. & Khalil, S. A. Liposomal formulation for dermal and transdermal drug delivery: Past, present and future. *Recent Patents on Drug Delivery and Formulation* **2**, 9-18 (2008).

23 Pierre, M. B. R. & Dos Santos Miranda Costa, I. Liposomal systems as drug delivery vehicles for dermal and transdermal applications. *Archives of Dermatological Research* **303**, 607-621 (2011).

24 Kim, M. K., Chung, S. J., Lee, M. H. & Shim, C. K. Delivery of hydrocortisone from liposomal suspensions to the hairless mouse skin following topical application under non-occlusive and occlusive conditions. *J. Microencapsul.* **15**, 21-29 (1998).

25 Mitkari, B. V., Korde, S. A., Mahadik, K. R. & Kokare, C. R. Formulation and evaluation of topical liposomal gel for fluconazole. *Indian Journal of Pharmaceutical Education and Research* **44**, 324-333 (2010).

26 Lopez-Pinto, J. M., Gonzalez-Rodriguez, M. L. & Rabasco, A. M. Effect of cholesterol and ethanol on dermal delivery from DPPC liposomes. *International Journal of Pharmaceutics* **298**, 1-12, (2005).

27 Touitou, E., Godin, B. & Weiss, C. Enhanced delivery of drugs into and across the skin by ethosomal carriers. *Drug Dev. Res.* **50**, 406-415, (2000).

28 Touitou, E., Dayan, N., Bergelson, L., Godin, B. & Eliaz, M. Ethosomes - Novel vesicular carriers for enhanced delivery: Characterization and skin penetration properties. *Journal of Controlled Release* **65**, 403-418 (2000).

29 Bhalaria, M. K., Naik, S. & Misra, A. N. Ethosomes: A novel delivery system for antifungal drugs in the treatment of topical fungal diseases. *Indian Journal of Experimental Biology* **47**, 368-375 (2009).

30 Vieira, D. B. & Carmona-Ribeiro, A. M. Cationic lipids and surfactants as antifungal agents: mode of action. *J. Antimicrob. Chemother.* **58**, 760-767, (2006).

31 Søren T. Larsen, H. V. a. G. D. N. Airway Effects of Inhaled Quaternary Ammonium Compounds in Mice. *Basic & Clinical Pharmacology & Toxicology* **110**, 537-543 (2012).

32 Colletier, J. P., Chaize, B., Winterhalter, M. & Fournier, D. Protein encapsulation in liposomes: Efficiency depends on interactions between protein and phospholipid bilayer. *BMC Biotechnology* **2** (2002).

33 Bennett, N. T. & Schultz, G. S. GROWTH-FACTORS AND WOUND-HEALING .2. ROLE IN NORMAL AND CHRONIC WOUND-HEALING. *Am. J. Surg.* **166**, 74-81, (1993).

34 Meibohm, B. & Derendorf, H. Basic concepts of pharmacokinetic/pharmacodynamic (PK/PD) modelling. *Int. J. Clin. Pharmacol. Ther.* **35**, 401-413 (1997).

CONCLUSIONS

The work accomplished in the present Thesis on the use of CO2-expanded solvents based methodologies for the production of nanovesicle-bioactive conjugates to be used as nanomedicines, has driven to the following conclusions:

- ✓ DELOS-SUSP methodology allows the easy and direct preparation of different liposome-biomolecule conjugates with good physic-chemical characteristics and homogeneous morphology in a reproducible and robust manner, which is crucial in the performance of a nanoconjugate as nanomedicine.

- ✓ The study of the interactions between the hydrophilic model protein BSA and quatsomes demonstrated that the protein produces changes in the morphology and the physicochemical characteristics of quatsomes after certain ratios BSA/CTAB. Therefore interaction studies between any negatively charge biomolecule and quatsomes are strongly recommended if encapsulation or functionalization experiments are going to be carried out.

- ✓ GLA loaded liposomes-RGD and rhEGF loaded quatsomes conjugates were prepared and applied in the treatment of Fabry disease and complexed wounds. h In both formulations it was observed the increase in the bioactivity when the protein/enzyme was associated to the vesicle which reinforces the importance of the nanostructuration in the efficacy of nanomedicines.

- ✓ The promising in-vitro and in-vivo results make this new methodology very attractive for the preparation of a second generation of protein therapeutics that will provide safer, more efficacious drugs, site-specific delivery, improved patient compliance, and favorable clinical outcomes.

Based on these conclusions we can say that this Thesis contributes to demonstrate the enormous potential of CF-based methodologies for the production of nanovesicle-bioactive conjugates to be used as nanomedicines.

EXPERIMENTAL SECTION

1. Materials

Cholesten-3*β*-ol (*cholesterol*; purity 95%) was obtained from Panreac (Barcelona, Spain), Cetyltrimethylammonium bromide (CTAB), Bovine Serum Albumin (BSA) protein, fluorescein sodium salt and bis (2-ethylhexyl) sulfosuccinate sodium salt were purchased from Sigma-Aldrich (Tres Cantos, Spain), 1,2-Dipalmitoyl-*sn*-glycero-3-phosphocholine was supplied by Avanti Polar Lipids (Alabaster, AL, USA). 1,1'-dioctadecyl-3,3,3',3'-tetramethyl-indodicarbocyanine perchlorate (*DiD oil*) was purchased from Invitrogen (Barcelona, Spain), Lysotracker Green DND-26 was obtained from Molecular probes (Eugene, Oregon) and Hoechst 33342 dye from Sigma-Aldrich. Cholesterol-PEG_{1000} and Cholesterol-PEG_{2000} were purchased from NOF corporation. The solvents ethanol and acetone of HPLC grade were purchase of from Teknocroma (Sant Cugat del Vallès, Spain)

Carbon dioxide (purity 99.9%) was supplied by Carburos Metálicos S.A. (Barcelona, Spain). The water used was pre-treated with the Milli-Q Advantage A10 water purification system (Millipore Ibérica, Madrid, Spain). TRIS buffer (pH = 7.5) with 20mM Tris-HCl and 5% in dextrose, and Acetic buffer 0.01 M (the pH=4.5 was adjusted with sodium acetate) were used for some vesicles preparation. PBS buffer (pH= 7.4) with a 100 mM concentration of salts (0.094M in NaCl, 0.0031M in Na_2HPO4, 0.0009M in NaH_2PO_4) was used in some in-vitro cell assays .

2. Preparation of nanovesicle-bioactive conjugates. Equipments and procedures

2.1 Preparation of nanovesicle-bioactive conjugates vesicles by DELOS-SUSP

2.1.1 Equipmet and procedure for preparation at lab-scale

2.1.1.1 Equipment

The equipment used for the preparation of nanovesicles-bioactive conjugates by DELOS-SUSP using a 7.5 mL reactor is schematized in Figure ES1. The configuration comprises a 7.5 mL reactor (*R*), whose temperature is controlled by an external heating jacket; a thermostated syringe pump (model 260D, ISCO Inc., Lincoln, US) (*P*) to introduce CO_2 inside *R* through valve *V1*; a depressurization valve (*V3*), from which the expanded liquid solution is depressurized into the aqueous phase placed in a collector (*C*) located after *V3*. N_2 can be introduced through *V2* directly from a pressurized reservoir. Two one-way valves are located before *V1* and *V2* to prevent contamination in the CO_2 and N_2 lines. There is also a pressure indicator (*PI*) and other one-way valve before the reactor.

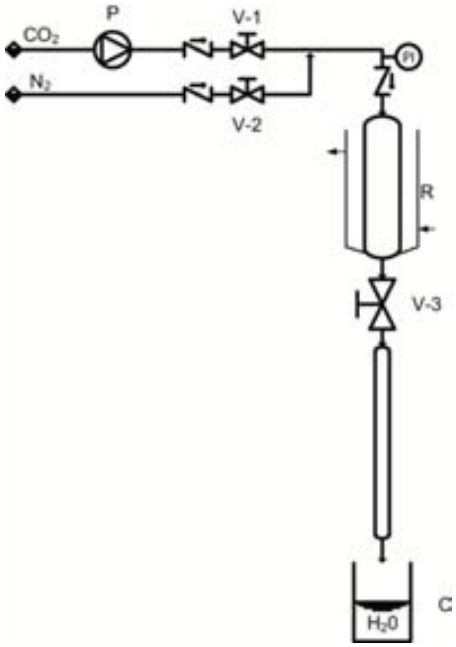

Figure ES1. Scheme of the lab-scale set-up used for the DELOS-susp experiments

2.1.1.2 Experimental procedure

For all DELOS-SUSP experiments a 2.88 mL of a solution of cholesterol in ethanol (in the case of quatsomes) or 1.2 mL of an ethanolic solution of a mixture of cholesterol and DPPC in the case of liposomes, was loaded into a high-pressure vessel at atmospheric

pressure and the working temperature (T_w = 308K). The solution was then volumetrically expanded with compressed CO_2 until achieving a molar fraction (X_{CO2}) of 0.60 for quatsomes and 0.85 for liposomes, reaching a working pressure (P_w) of 10 MPa. The system was kept at 308 K for approximately 1 hour to achieve a complete homogenization and to attain thermal equilibration. Afterwards the depressurization of the volumetric expanded organic phase was performed over 24 mL of an aqueous solution containing CTAB for cholesterol:CTAB vesicles (quatsomes), or 24 mL of a buffer or mQ water for cholesterol:DPPC vesicles (liposomes). In this step a flow of N_2 at the working pressure is used as a plunger to push down the CO_2−expanded solution and to maintain a constant pressure of P_w inside the vessel during the depressurization. In both vesicular formulations the biomolecules were dissolved in the organic or in the aqueous phase, depending on their solubility and their passive integration was produced during the depressurization step. The average time per experiment was around 2 hours and the nanovesicles obtained were stored at 4 °C until their characterization.

2.1.2 Equipmet and procedure for preparation at pilot plant scale

2.1.2.1 Equipment

To scale-up the nanovesicles-bioactive conjugates by DELOS-SUSP we used the system schematized in Figure ES2. In this configuration, CO_2 is pumped through a high pressure pump, *P1*, which head is cooled by a cooling unit. Before entering into the 315 mL reactor, *R*, CO_2 is heated to the working temperature, *Tw*, using a heat exchanger, *H*. The amount of CO_2 added to the reactor through valve *V1* is measured by a mass flowmeter, *F*. Inside *R* a variable speed stirrer *ST* warrants the homogeneity of the mixture in the volumetrically expanded phase. The vessel temperature is controlled using an external fluid heating jacket. *R* is connected through *V4* to a filter, *FL*, which has been previously pressurized with N_2 at the working pressure *(Pw)* through *V5* in order to separate the solid that could precipitate due to the antisolvent effect of CO_2 before the depressurization step. *FL* is connected to a T-mixer, where the depressurized solution is mixed with the aqueous phase after opening the depressurization valve V6. V6 is remotely controlled. During the depressurization step, the aqueous phase is pumped at a constant flow using *P2*. Vesicles are collected in *C* after their formation. The system is also equipped with pressure, *PI1, PI2, PIC*, and temperature, *TI, TI1*, indicators, as well as with safety devices like rupture disks, *RD1RD2*.

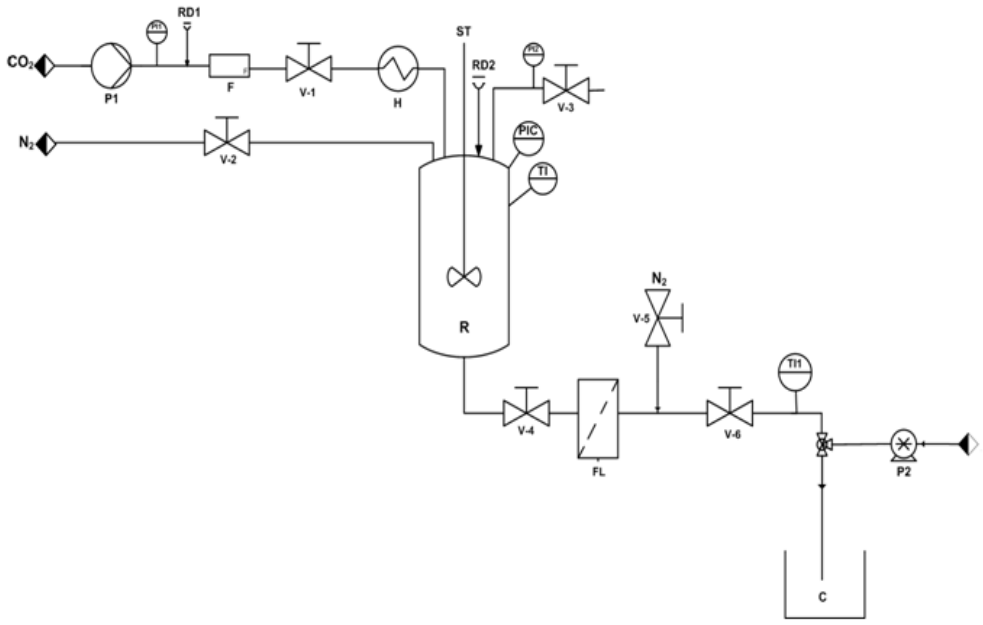

Figure ES2. Scheme of the 315 mL set-up used for the DELOS-SUSP experiments

2.1.2.2 Experimental procedure

For the scale-up experiment 3.8 g of cholesterol were dissolved in 144 mL of EtOH and introduced in a 315 mL reactor already warmed at 308K. After 15 min of thermal equilibration, CO_2 was introduced to achieve the desired P_w (10 MPa) and X_{CO2}(0.6). After at least 45 min, the CO_2-expanded solution was depressurized through a one-way automatic valve into a T mixer, to which 1200 mL of an aqueous solution containing 3.4 g of CTAB and BSA (16 μM) were pumped at 900 mL/min, to for the vesicles. Average time per experiment was 2 hours and the nanoconjugates prepared were stored at 4 °C until characterization

2.2 Differences between the equipment configurations for the small and large scale reactors

Apart from the capacity of the high pressure vessels (7.5 mL vs 315 mL), there are other differences between both equipment configurations (Figure ES3). One of the variations is in regard to the mixing of the alcoholic solution of cholesterol with CO_2 in the high pressure container. While unnecessary at small scale, a mechanical stirrer is used for a quicker achievement of the thermodynamic equilibrium of the CO_2-expanded solution in the 315 mL system. The depressurization configuration also changed at larger scale, where the manual depressurizing valve used in the 7.5 mL system is substituted by an automatic one, whose flow rate can be better controlled. Another important divergence

concerns the way in which the CO_2-expanded solution and the aqueous phase are mixed. Whereas the depressurization of the 7.5 mL container is performed directly over a vessel containing the aqueous phase, good mixing between the two solutions at larger scale is ensured by depressurizing the expanded solution into a T mixer to which the aqueous phase is simultaneously pumped. All this differences can explain the better homogeneity encountered when using the 315 mL reactor.

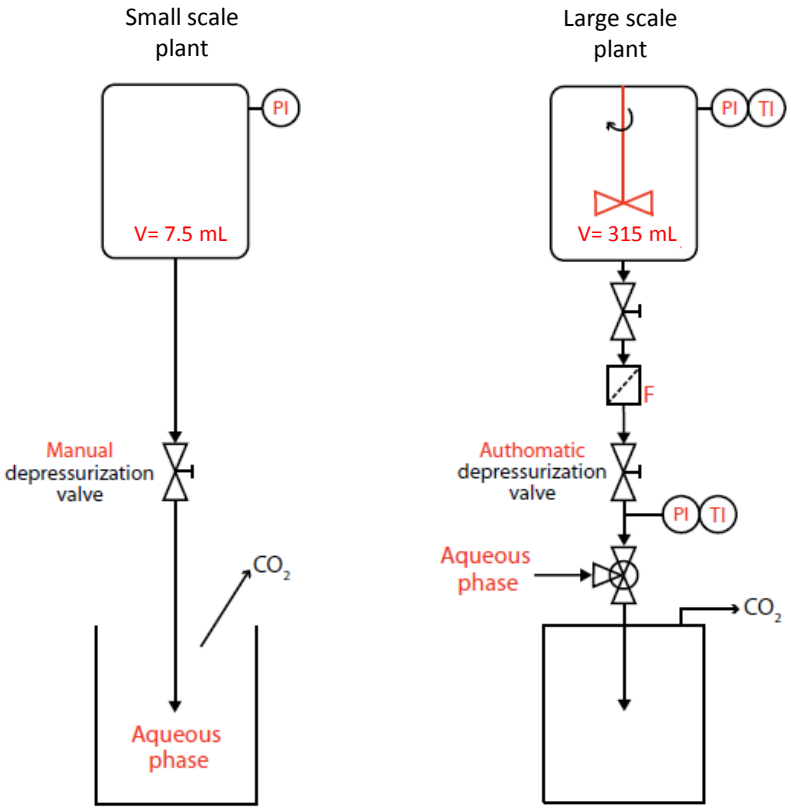

Figure ES3. Differences between the small scale and the large scale equipment configurations

2.2 Preparation of vesicles by thin film hydration (TFH)

The integration of cholesterol_PEG_{200}_RGD molecule in cholesterol-rich vesicles by hydration methodology was performed according to the following procedure. The appropriate quantities of the membrane components dissolved in chloroform are mixed in a glass vial and the solvent is slowly evaporated under a N_2 flow to create a lipid thin film. The glass vial is then placed in vacuum for at least 4 hours for removing the possible entrapped solvent. Once dried, the lipid film is hydrated overnight using the appropriate aqueous medium (water in our case), at room temperature. Next, the sample

are taken through 10 rounds of freeze/thaw cycles by transferring it between liquid nitrogen (77 K– 1 min) and water bath (313 K – 5 min) for finally being extruded through a polycarbonate filter with a pore size of 800 nm. A commercially available manual extruder (Avanti® Mini-Extruder, Avanti Polar Lipids, Alabaster, AL, USA), was used for that purpose (Figure ES4). The obtained vesicles were stored at 277 K until characterization.

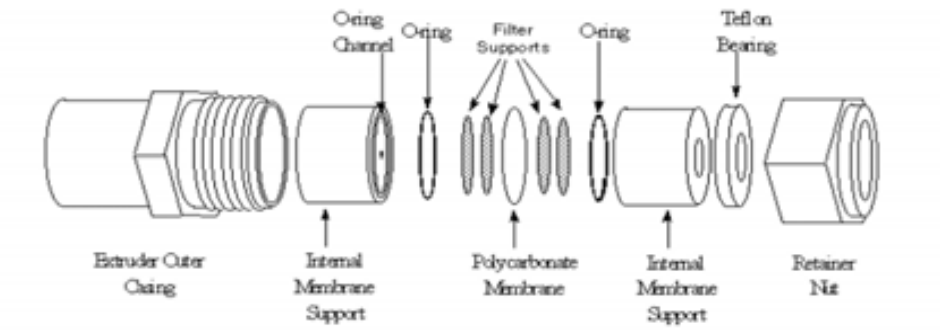

Figure ES4. Schematic representation of the parts forming the mini-extruder

2.2.1 Preparation of Liposome-RGD conjugates by TFH

Preparatio of liposome_RGD conjugates by thin film hydration was performed following the experimental procedure described above but with the incorporation Cholesterol-PEG_{200}-RGD molecules in the chloroform solution together with the other membrane components.

2.3 High pressure phase analyzer for solubility analysis

Solubility measurements in CO_2-expanded solvents were performed in a home-made high pressure analyzer, schematized in Figure ES5. The main components of this configuration are: a Jergusson liquid level gauge 16T-40 used as variable volume view cell (VC), which is equipped with two sapphire windows and is placed inside a thermostatic chamber (TC) with a range of working temperatures from 308 K to 453 K; a piston pump (model PU-158 from JASCO Inc., Easton, US) (P1) to introduce liquid solvents or solution through valve V1; a thermostated syringe pump (model 260D, ISCO Inc., Lincoln, NE, US) (P2) to introduce CO_2 using valve V6; and a recirculation pump (micropump serie 180) (P3) to ensure a good homogenization of the mixtures.

The variation of the cell volume from 50 to 75 mL is performed by means of a stainless steel piston (PI) introduced into the view cell and moved by a pneumatic system (SMSC CE2B63-200J) (C). The set up is equipped with a N_2 connection through valve V3, from which the gas is added when necessary. Solids (S) can also be introduced into the cell by placing them in a screw-on cap placed in the bottom of the cell. Valves V4 and V5 are used for evacuating the fluids from the cell.

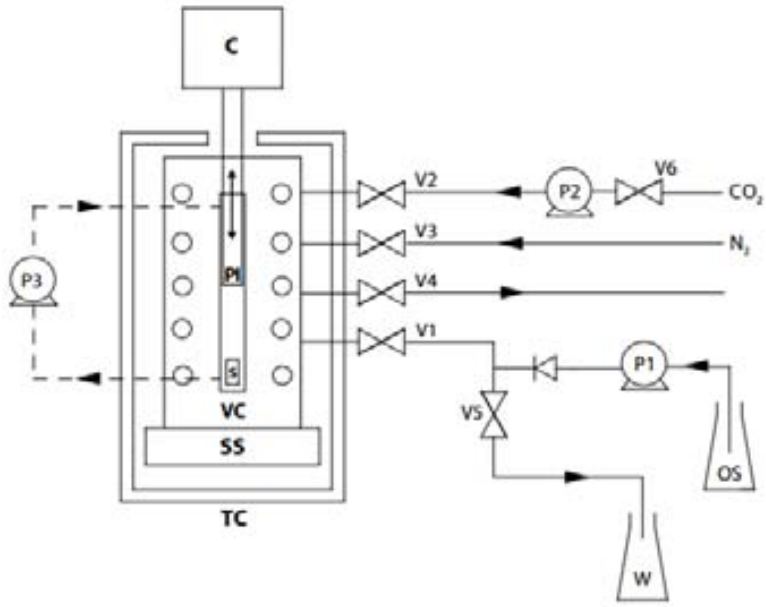

Figure ES5. Scheme of the high pressure analyser. C: pneumatic cilynder; PI: piston; VC: view cell; SS: stirring system; TC: thermostated chamber; P: pump; V: valve; S: solid sample; OS: organic solvent or solution; W: waste.

2.3.1 Solubility behavior DPPC in ethanol and CO_2

DPPC is not water soluble, presenting a solubility of 30 mg/mL in ethanol. In order to produce the liposomes by DELOS-SUSP, both cholesterol and DPPC have to be placed in the organic phase. A fundamental requirement to used DELOS-SUSP is that the components to be processed should be completely miscible in ethanol/CO_2at 10 MPa. Therefore the high pressure phase analyzer equipment was used to study the solubility behavior of cholesterol and DPPC in the ethanol/CO_2mixture. As DPPC is an expensive molecule, only a specific point corresponding to the CO_2 molar fraction used for the preparation of Quatsomes was study. At this molar fraction the cholesterol formed one

phase with ethanol and CO_2. 200 mg of DPPC was placed in the screw-on cap at the bottom of the phase analyzer (Figure ES6).

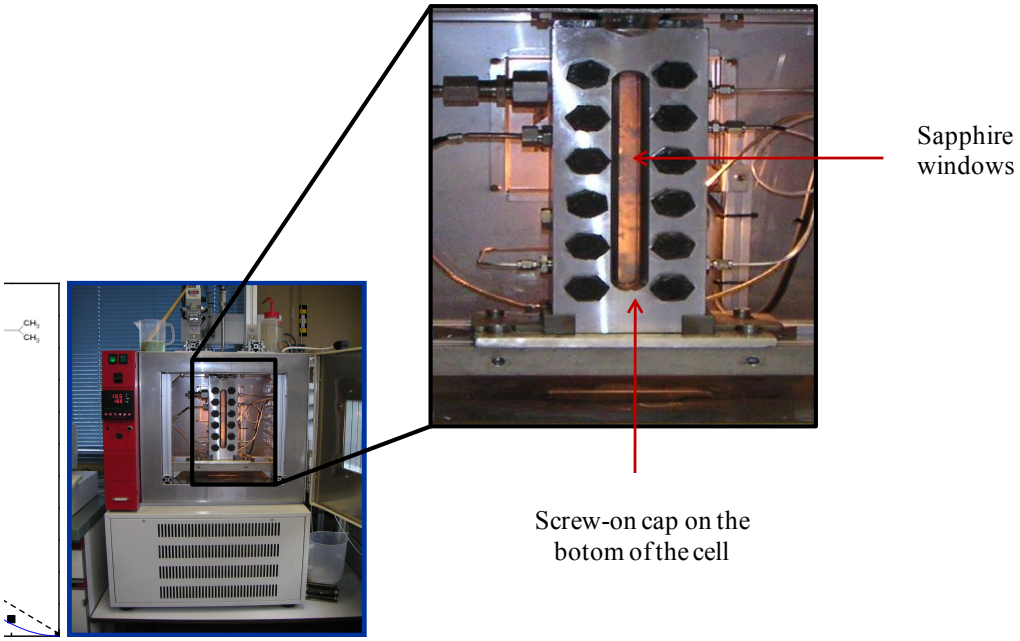

Figure ES6. Picture of the high pressure phase analyzer. A zoom of the cell is also shown for better details.

A volume of 23 mL of ethanol was added through a piston pump to the cell together with CO_2 until reach a preassure of 10 MPa. After 1 hour at 308 K, the depressurization was performed and the cap checked. No traces of DPPC were found which means that this phospholipid can be processes by DELOS-SUSP at a molar fraction around 0.6.

3. Physicochemical characterization of the nanovesicle-bioactive conjugates. Instruments, techniques and procedures.

3.1 Size, polydispersity index and Z potential

The size, polydispersity index (PdI) and Z potential of all the vesicle systems produced were measured using a dynamic light scattering analyser combined with non-invasive backscatter technology (NIBS) (Malvern Zatasizer Nanoseries, Malvern Instruments, U.K). The samples were analyzed one day after their preparation without any previous modification or dilution. All the values reported were the average result of 3 consecutive measurements on the same sample. The size and polidispersity index were measure by placing 1 mL of the sample in a cell, in the DLS equipment. In this work, size and particle size distribution have been presented in terms of scattered intensity. They provide information about the percentage of light scattered by particles, in this case vesicles, of each size in a sample. These are the most recommendable data when using dynamic light scattering, since they are the original data provided by the analyzer and no assumptions are involved for calculating particle size. The z potential was measure by placing 1 mL of the sample in a folded capillary cell, in the DLS equipment.

3.2 Morphology

The morphology of the systems was studied using cryogenic transmission electron microscopy (Cryo-TEM). The images were obtained with a JEOL JEM-2011 microscopy (JEOL LTD, Tokio, Japan) operating at 120 kV. The preparation of the frozen samples was performed in a vitrification system with controlled environment (CEVS) Leica, model EM-CPC (Leica Microsystems, Germany). A 4µl drop of sample was placed in a cupper grid coated with a perforated polymer film. Excess solution was removed by blotting with filter paper to obtain a thin film of 20-400 nm. Right after this the grid was plunged into a liquid ethane held at a temperature just above its freezing point (94 K). The vitrify sample was transferred to the microscope for analysis. To prevent sample perturbation and the formation of crystals, the specimens were kept cool (77 K) during the transfer and the viewing procedure.

3.3 Lamellarity

X-ray scattering experiments were performed on the beamline BM16 at the European Synchrotron Radiation Facility (ESRF) in Grenoble (France). The samples were exposed to polarized monochromatic X-rays of wavelength λ=0.979 Å (12.6 keV) for 120 s. The given scattering plot corresponds to an averaged over 5 identical sequences after verifying precise reproducibility. Small angle X-ray scattering (SAXS) and wide angle X-ray scattering (WAXS) patterns were simultaneously recorded using a MarCCD and a Princenton Instruments CCD camera detector, respectively. A sample to detector distance of 1.4 m was used for SAXS and of 0.37m was used for WAXS. Standard silver behenate and polyethylene samples were used for the calibration of SAXS and WAXSW diffraction spacing, respectively. Experiments were performed at 22ºC. A Julabo chiller (Julabo GmbH, Germany) with a mineral oil refrigerator was used for controlling the temperature with a ± 0.1ºC precision. Samples were loaded into a fixed temperature controlled flat cell with mica windows and a beam path thickness of 3mm. The background with the cell filled with buffer was measured in an identical manner and the corresponding background intensity of the buffer solution was subtracted.

3.4 Stability

The stability of all systems under storage conditions was evaluated by means of their Z potential and size using dynamic light scattering analyzer (Biomaterials, 24, 4283-4300, 2003). The measure of Z potential allows predicting the storage stability of a colloidal dispersion. The higher the Z potentials, the more stable a suspension will tend to be due to the electrostatic stabilization. From a practical point of view over |30| mV we can find good stability, reaching and optimum over |60|mV. Between |5| and |15| mV we are in the region of limited flocculation and incipient instability; and finally between |5| and |3|mV we find maximum flocculation. The size measurement is also another parameter that can indicate whether a system has reached the physical instability due to phenomena such as vesicle aggregation or vesicle growth.

3.4.1 Study of vesicles stability by their size evolution with time.

The stability of all systems under storage conditions was evaluated by means of their Z potential and size using dynamic light scattering analyzer. In general the Quatsome-

biomolecule nanoconjugates reminded stable for at least 5 months. The Liposome-biomolecule nanoconjugates stability was much lower and varied depending on the integrated biomolecule. The higher stabilities were achieved when stabilizing/targeting moieties were incorporated to the membrane, with storage stability times between 1 and 3 months. After this time not only phase separation and vesicle aggregation but also the oxidation of the lipids composing the membrane was observed. The size evolution with time for all systems prepared in Chapter 1 is showed in Table ES1 and Figure ES7.

Table ES1. Particle size evolution with time for the nanoconjugates.

System	Size	PdI	Time elapsed (months)	Size	PdI
Quatsome_PEG_{1000} (3)	67 ± 6	0.26 ± 0.01	5	71± 1	0.247 ± 0.002
Quatsome_PEG_{2000} (3)	84 ± 0.5	0.20 ± 0.03	5	126 ± 4	0.12 ± 0.01
Liposome_PEG_{1000} (3)	138 ± 10	0.40 ± 0.10	1	132 ± 1	0.25 ± 0.01
Liposome_PEG_{2000} (3)	135 ± 9	0.43 ± 0.02	1	133 ± 1	0.43 ± 0.01
Liposome_RGD (4)	144 ± 12	0.19 ± 0.01	1	159 ± 2	0.35 ±0.2
GFP loaded-Liposomes (2)	228 ± 8	0.42 ± 0.02	1 week	220 ± 1	0.410 ±0.01
BSA loaded-Quatsomes (3)	149 ± 12	0.26 ± 0.01	5	135 ± 10	0.22 ± 0.03
BSA loaded-Quatsome_PEG_{1000} (2)	82 ± 8	0.23 ± 0.01	5	118 ± 7	0.13 ± 0.01

The size distribution of the data presented in the table above is shown in Figure ES7.

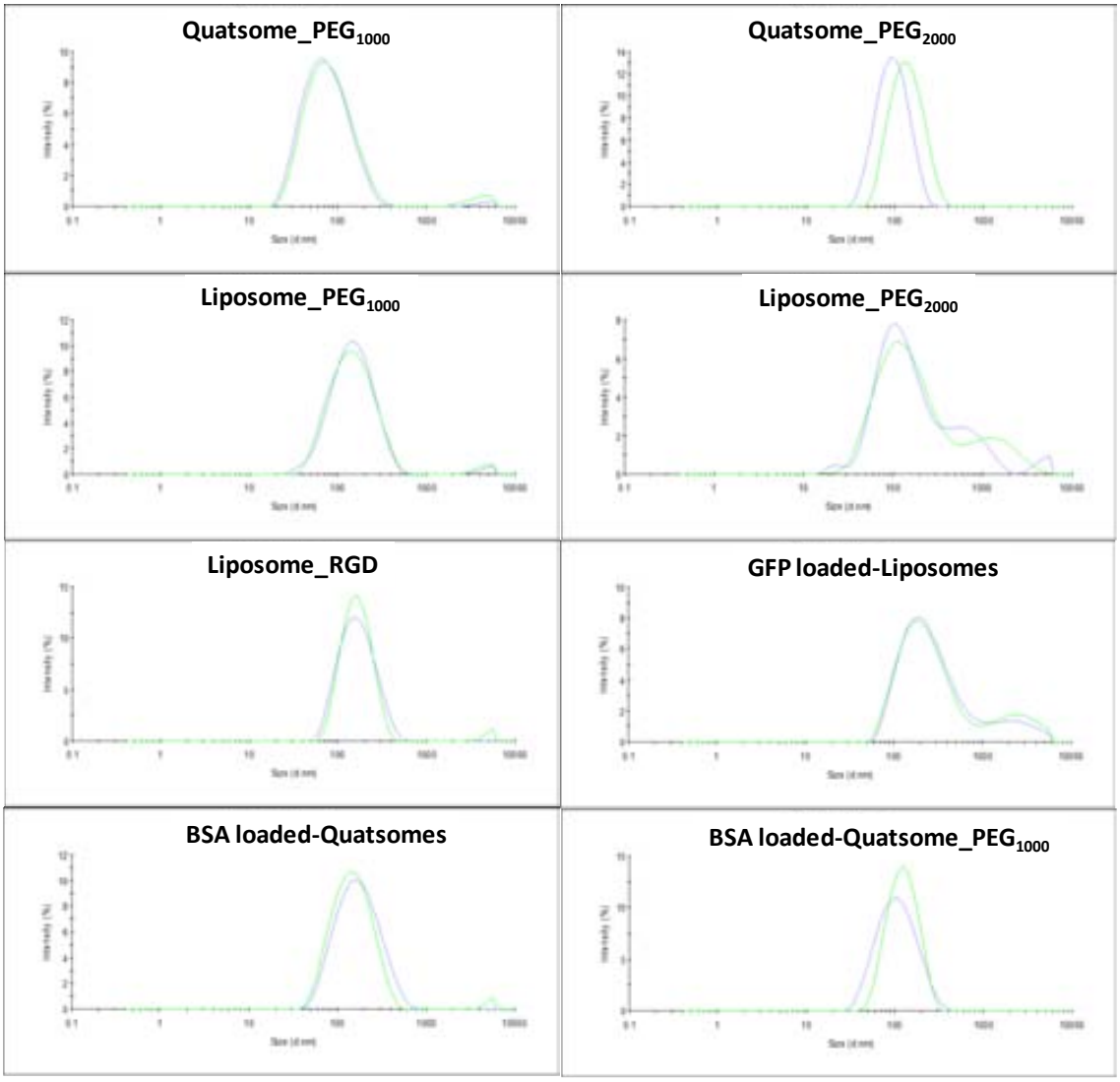

Figure ES7. Evolution of the particle size distribution of the systems. The blue curve is the size distribution right after the conjugates preparation. The green curve is the size distribution after the time elapsed reported in the Table ES1.

5. FT-IR determinations

Fourier Transform Infrared (FTIR) spectroscopy was carried out in a Spectrum One (PERKIN ELMER, USA) spectrometer. The solid samples were analyzed using an attenuated total reflectance (ATR) accessory (UATR accessory, PERKIN ELMER, USA), which allows sample analysis without further modifications. A small amount of the white solid formed at the end of the vesicles titration with BSA, was directly placed on the diamond disk and scanned in the range of 4000 to 650 cm^{-1} wave numbers at a resolution of 1 cm^{-1}.

The spectra of the solid formed in the titration of quatsomes with BSA were compared with pure cholesterol and pure CTAB. As observed in Figure ES8 there are two bands in the precipitate spectrum that are characteristics of pure cholesterol. Those are the one at 2969 (m), corresponding to C-H vibration from the cicloalkenes, and the bands between 1300 -1350(m) corresponding to the vibration between the carbon from a cicloalkane and the –OH. The big band at 3250 (s) belong to the vibration of the –OH present in the solvent (ethanol/water mixture).

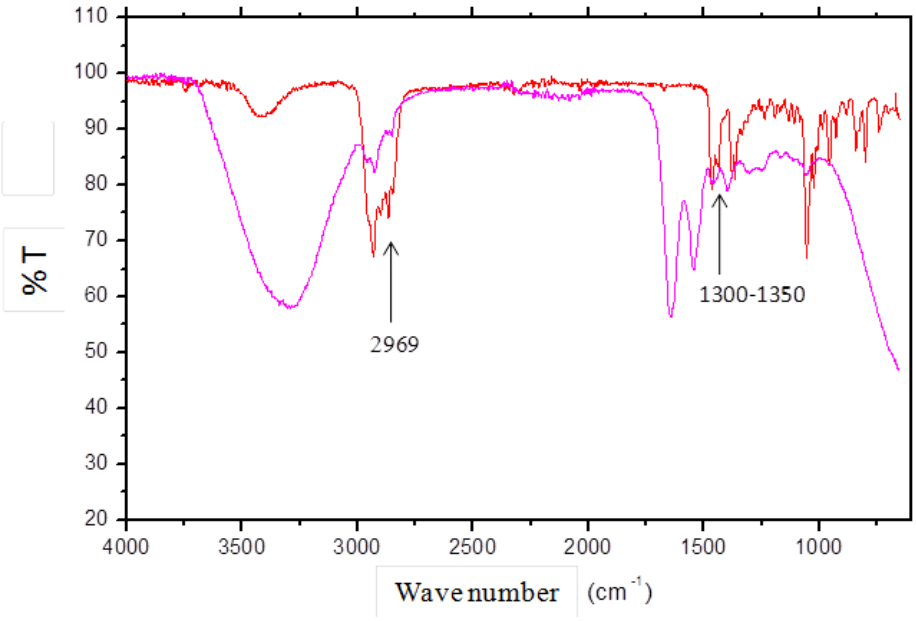

Figure ES8. Infrared spectrum of the white precipitate (pink curve) and pure cholesterol (red curve)

When the spectra of the white solid were compared with pure CTAB there were not coincident peaks which indicate that the solid is not composed by this surfactant (Figure ES9).

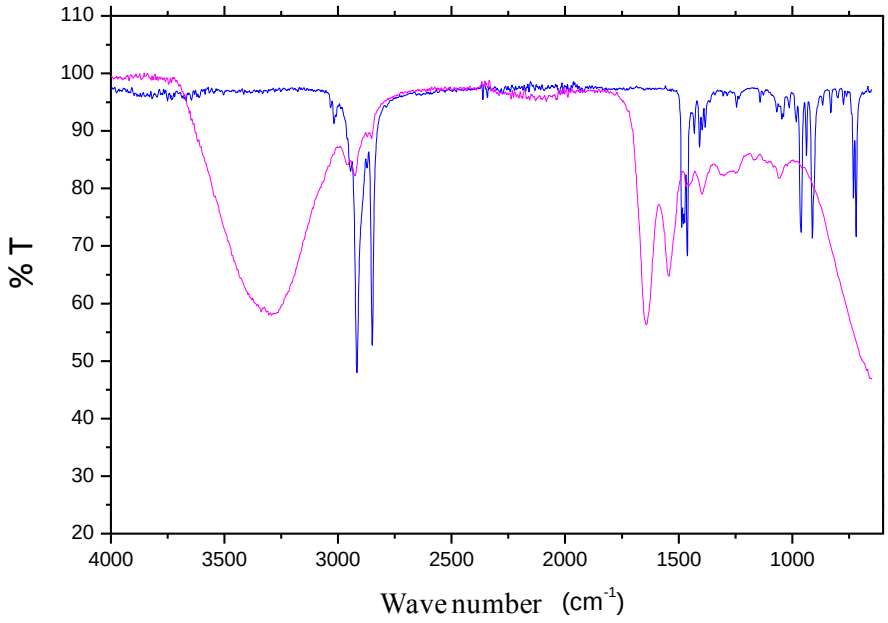

Figure ES9. Infrared spectrum of the white precipitate (pink curve) and pure CTAB (blue curve)

4. Determination of the degree of loading/functionalization of vesicles

The degree of loading/functionalization in the nanovesicle-bioactive conjugates was analyzed through the determination of the Entrapment Efficiency percentage (% EE). The analysis of the %EE comprises two steps: 1) the separation of non-integrated biomolecules from the loaded nanovesicles and 2) the quantification of the entrapped biomolecules using the appropriated technique.

4.1 Separation of non- integrated biomolecules from the nanovesicle-bioactive conjugates

4.1.1 Separation using centrifugal filter devices

Non-integrated actives were separated using centrifugal filter devices (Centricon, Merck Millipore) with different Nominal Molecular Weight Limit (NMWL) depending on the molecular weight of the biomolecules. Centricons of 30 and 100 KDa NMWL were equilibrated three times with the working buffer before using. The centrifugation velocities were 3500 and 6000 rpm, for 30 and 100 KDa centricons respectively. In all cases, 3 mL of sample were loaded into the Centricon and centrifugated until concentrated volume was 500 μL. The concentrate (vesicles loaded with biomolecule) was collected from the filter device sample reservoir using a pipette, while the ultrafiltrate with the free biomolecule was collected in the provided centrifuge tube. We used centricons to separate the following biomolecules from the loaded systems: Cholesterol-PEG_{200}-cRGDfk, GFP, BSA and EGF

4.1.2 Separation using a centrifugation procedure

For the centrifugation procedure firstly we put the sample in aliquots of 1,5 mL in eppendorfs tubes. Afterwards we centrifuge at 4 degrees increasing the centrifugation speed every 20 min and going from 6000 rpm, then 9000 rpm and finally 12 000 rpm for a total centrifugation time of 1h. The supernatant was separated from the pellets and the pellets were re-suspended until the desired volume. The two fractions (the supernatants and the pellets) were collected in pools. We used this procedure to separate GLA from the loaded vesicle system

4.1.3 Separation using a diafiltration equipment

In some cases we separate the non-incorporated active using the KrossFlo® Research IIi TFF System (KR2i) (Figure ES10). With this equipment an automatic diafiltration

processes can be performed using the different columns, depending on the size of the protein. The advantage of using it is that one can separate the non-encapsulate biomolecule, concentrate the sample and change the dispersant medium if desired. An image of the equipment is shown below:

1. **Peristaltic pump**
2. **Digital pressure monitor**
3. **Back pressure valve**
4. **Scales**
5. **Column (filter)**
6. **Sample container**
7. **Pressure transducer**
8. **Tubes**

Figure ES10. Configuration of the KrossFlo® Research IIi TFF System (KR2i)

In order to perform the diafiltration, a volume between 4 and 10 mL can be added to the sample reservoir, which is connected to the column and the buffer reservoir. Once the parameter has been set, the system can function automatically without the presence of an operator. In base on the experience, 6 cycles should be performed in order to eliminate the free biomolecules and the ethanol that is present in the sample. For example if the initial sample volume is 4 mL, then the equipment and with it the process will be stop when the filtrated waters volume is 24 mL. The same initial sample volume with the loaded vesicles and free of ethanol is collected from the sample reservoir. The process takes about 2 hours

4.14. Resume of methodologies used along this thesis work in order to separate the non-integrated biomolecules

Separation methodology	Duration (min)	Phases formed (number)	Efficiency of separation	Influence of the vesicle composition	Morphology after the separation
Centrifugation	60-120	Pellet and Supernatant (2)	+	Yes*	Is affected
Diafiltration (Centricons)	30-40	Diafiltrate and diafiltered waters (2)	++	No	Is **not** affected
Diafiltration (KR2i)	15-40	Diafiltrate and diafiltered waters (2)	+++	No	Is **not** affected

*If the system to be centrifuged is formed by vesicles containing a positively charge membrane, the pellet is not efficiently formed.

4.2 Quantification of the entrapped biomolecules

4.2.1 Quantification of cRGDfK in Liposome-RGD conjugates

First of all the fractions with free CHOL_PEG_{200}_RGD was separated from the peptide-loaded liposomes using centrifugal filter devices of 30 kDa (two replicates). Fractions containing the free peptide were hydrolyzed with HCl (6 M) during 16 h at 110 ^{0}C. Subsequently they were taken to dryness, dissolved in HCl (20 mM) and filtrated. An aliquot from this filtrated was derivatized following the AccQ –Tag method and analyzed using an HPLC with UV detection (λ= 254 nm). The equipment used was a gradient HPLC system, model WATERS 600 with WATERS 2487 detector and column Nova-Pack C18 (4 um) Waters (3.9x150 mm).

4.2.2 Quantification of GFP in liposomes

Amounts of SUV-encapsulated GFP-H6previously centrifuged using centrifugal filter devices (100 KDa) in order to separate free protein, were analyzed and quantified by SDS-PAGE and further Western-blot. For that, after SDS-PAGE proteins were blotted onto nitrocellulose membranes. GFP immunoreactive bands were developed by using a rabbit polyclonal anti-GFP serum from Santa Cruz Biotechnology, Inc. (sc-8334).

Amounts of GFP in each fraction (loaded liposomes and free protein) were estimated by comparison with known amounts of commercial GFP (Roche, 11814524001). Samples to be quantitatively compared were run in the same gel and processed as a set. Densitometric analysis of the bands was performed with the Quantity One software in order to associate the intensity of each band to the corresponding concentration.

4.2.3 Quantification of BSA in quatsomes

For this purpose we used a Micro BCA^{TM} Protein Assay Kit purchase from Thermo Scientific. The kit is based on the use of bicinchonicic acid (BCA) as the detection regent for Cu^{1+}, which is formed when Cu^{2+} is reduce by the protein in alkaline environment. The product of this reaction is a purple-soluble complex that presents a strong absorbance at 562 nm that is linear with the protein concentration. Due to the necessity of the basic environment for the chelating reaction, after the separation using Centricons, the fractions with free BSA were mixed with NaOH solution to obtain a final concentration of this reagent of 0.1 M. The samples, together with a calibration curve of BSA in NaOH (0.1 M), were mounted into a 96 well plated for further determination. Blanks of plain quatsomes and BSA in water samples (50 and 250 μg/mL) were also analyzed to check the good performance of the kit. As the plain Quatsomes interfered with the kit determination, the encapsulation efficiency percentage was determined using the fractions with the free BSA. The absorbance was measure in a UV-Vis Spectrophotometer **(**Labsystems iEMS Reader MF)

4.2.4 Quantification of GLA in liposomes

After the separation of non-encapsulated GLA from the loaded system, the amount of GLA in the different fractions was quantified. To estimate the incorporation of recombinant GLA into SUVs, samples from 1) initial GLA in water, 2) Total sample 3) purified SUVs and 4) water containing free, non-encapsulated GLA, were mixed with denaturing, loading buffer and analyzed by SDS-PAGE and further western-blot developed with a rabbit polyclonal anti-GLA serum from Santa Cruz Biotechnology (a-gal A H-104: sc-25823) and a goat anti-rabbit IgG HRP-conjugate (Bio-Rad Laboratories, Inc., cat.# 170-6515) as secondary antibody. Amounts of recombinant GLA within each of the above mentioned samples were estimated by comparison with known amounts (usually ranging from 25 to 125 ng) of a recombinant GLA previously produced, purified, and quantified in IBB laboratory. Samples to be quantitatively

compared were run in the same gel and processed as a set. Densitometric analyses of the bands were performed with the Quantity One software (Bio-Rad Laboratories, Inc). Percentage of encapsulated α-GAL was obtained by dividing the amounts of enzyme found in the loaded vesicles by the amount found in the total sample.

4.2.5 Quantification of EGF in quatsomes

Fractions with free EGF were analysed using an ELISA immune-assay. This is an inmuno-chemistry technique used mainly in immunology in order to detect the presence of an antibody or antigen. All ELISA determinations type sandwich using murin monoclonal antibodies, were performed following the protocol described below:

- The 96 well plate is covered by the antibody dissolved in the coating solution (Na_2CO_3, $NaHCO_3$, pH= 9.6) by adding 100 μL in each well and incubating at 50 ^{0}C during 40 minutes. Afterwards the plate is washed three times with a solution of Tween-20 in PBS.
- Different dilutions of the samples in solution 0.5 % BSA in PBS are required in order to have their concentration values in the range of the calibration curve of the assay. 100 μL of the sample is added to each well and incubated during 1 hour at 37 ^{0} C. Then the plate is washed 5 times with a solution of Tween-20 in PBS.
- 80 μL of the conjugation antibody is added and the plate is incubated during 1 h at 4 ^{0}C. The plate is washed 8 times with a solution of Tween-20 in PBS.
- 100 μL is of the substrate is added (a change in color is expected due to the enzyme action) and the plate is incubated 15 min at 25^{0}C
- Finally 50 μL of "stop" solution is added and the determination is performed in a spectrophotometer at 492 nm

5. Synthesis and characterization of bioactive compounds

5.1 Synthesis of Cholesterol-PEG_{200}-cRGDfk

This cholesterol-PEG_{200}-RGD derivative molecule was specially design and in collaboration with Miriam Royo group from the Combinatorial Chemistry Unit (Barcelona Science Park) for the preparation of liposome-RGD conjugates. The synthesis was performed in this lab following the procedure described below.

5.1.1 Synthesis of cRGDfK

The synthesis of peptide cRGDfK was carried out as described by Xuedong Dai et al. with minor modifications[1]. Briefly, the linear peptide was synthesized using standard SPPS on a 2-chlorotrityl chloride resin. After cleavage with Acetic Acid/TFE/DCM (1:1:3), peptide was cyclized by treatment of T3P in EtOAc in presence of TEA and DMAP. The final cyclic peptide was deprotected with a mixture of water and TFA (1:19) and purified by RP-HPLC obtaining peptide **D** (180.9 mg, 15%) as a white solid. Peptide content in 39 μg of crude: 20 μg of peptide.

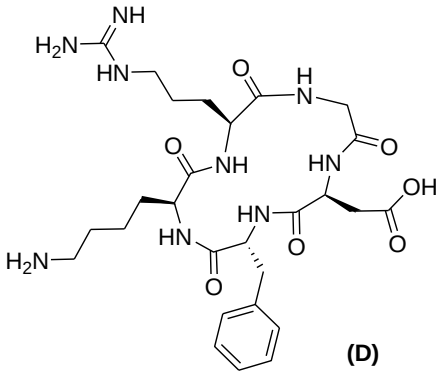

(D)

HPLC-MS: (C_{18}, 5-100 % B, 3.5 min (A: ACN B: NH_4HCO_3 20 mM), 1.6ml/min, λ=210nm) t_R: 2.47min, m/z= 604.3 $[M+H]^+$ (Calc.: 603,67) **MALDI-TOF(ACH):** m/z=604.24 $[M+H]^+$ (Calc. : 603,67). **AMINO ACID ANALYSIS:** Asp: 0.96, Gly: 1.05, Arg: 1.11, Lys: 0.97, Phe: 0.90

5.1.2 Synthesis of Cholesterol-cRGDfK

Cholesterol (2.60 mmol, 1.006g, 1.0 eq.) was dissolved in anhydrous Pyridine (12 ml). p-Toluenesulfonyl chloride (5.19 mmol, 1.004 g, 2.0 eq.) was added to the solution of cholesterol and the reaction mixture was stirred for 24 h at room temperature. After completion, H_2O (5 ml) was added to the reaction mixture and the aqueous solution was extracted with DCM (3x6 ml). To the organic phase was added Et_2O until a clear solution was obtained. The organic layer was dried over $MgSO_4$, filtered and concentrated under reduced pressure. The obtained crude was recrystallized from petroleum ether to afford compound **A** (0.969 g, 70%) as a white powder.

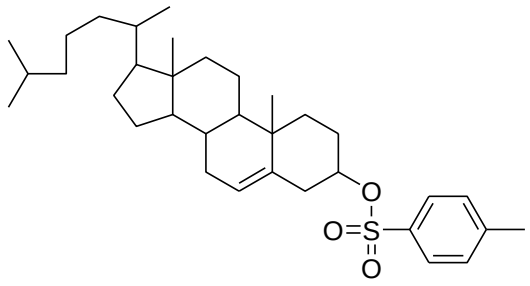

(A)

^{1}H-NMR: (400MHz, $CDCl_3$)**δ:** 0.656 (s, 3H); 0.852 (d,1.6 Hz, 3H); 0.869 (d, 2Hz, 3H); 0.901 (d, 6.8Hz, 3H); 0.965 (s, 3H); 2.446 (s, 3H); 4.3 (m, 1H); 5.3 (m, 1H).

^{13}C-NMr: (100MHz, $CDCl_3$) **δ:** 144.52 (C32), 139.00 (C4), 134.85 (C35), 129.87 (C34, C36), 127.77 (C33, C37), 123.65 (C7), 82.54 (C2), 56.79 (C11), 56.25 (C17), 50.05 (C10), 42.43 (C12), 39.80 (C22), 39.65 (C13), 39.01 (C3), 37.03 (C5), 36.49 (C20), 36.31 (C18), 35.89 (C6), 31.99 (C9), 31.89 (C8), 28.77 (C1), 28.33 (16), 28.15 (C15), 24.38 (C23), 23.95 (C21), 22.95 (C25), 22.70 (C24), 21.77 (C38), 21.13 (C14), 19.28 (C26), 18.84 (C19), 11.98 (C27)

HPLC-PDA: (C_{18}, 5-100 % B, 4.5 min (A: ACN 0.1% TFA B: MeOH), 2ml/min, λ=210nm) t_R: 2.7min

Finally to a solution of compound A (0.93 mmol, 0.503 g, 1.0 eq.) in 5 ml of anhydrous 1,4-dioxane was added tetraethyleneglycol (18.48 mmol, 3.591 g, 19.8 eq.). The reaction mixture was heated to reflux and was stirred for 4h under argon atmosphere. The solvent was removed under reduced pressure and the crude was dissolved in 20 ml of DCM. The organic layer was washed with sat. $NaHCO_{3\ (aq)}$ (2x20 ml), H_2O (3x20

ml), brine (1x20 ml). The combined aqueous phases were extracted with 20 ml of DCM. Finally, the combined organic phases were dried over $MgSO_4$, filtered and concentrated under reduced pressure. The crude was purified by column chromatography on basic Al_2O_3 (DCM/MeOH 0-5%) to afford compound **B** (Cholesteryl-tetraethyleneglycol, 0.260g, 50%) as a yellow oil.

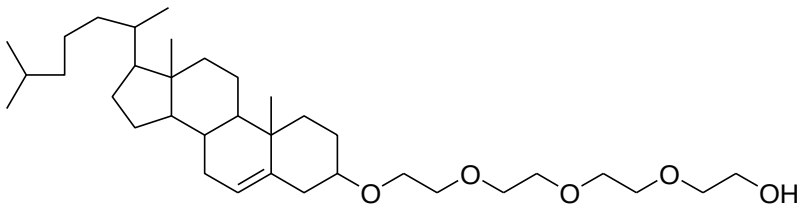

(B)

^{1}H-NMR: (400MHz, $CDCl_3$) **δ:** 0.674 (s, 3H); 0.856 (d, 1.6Hz, 3H); 0.876 (d, 1.6Hz, 3H); 0.913 (d, 6.4Hz, 3H); 0.994 (s, 3H); 3.183 (m, 1H); 3.668 (m, 16H).

^{13}C-NMR: (100MHz, $CDCl_3$) **δ:** 141.07 (C4), 121.71 (C7), 79.69 (C2), 72.82-70.40 (C30, C32, C33, C35, C36, C38), 67.36 (C29), 61.87 (C39), 56.93 (C11), 56.30 (C17), 50.33 (C10), 42.47 (C12), 39.93 (C22), 39.66 (C13), 39.11 (C3), 37.37 (C5), 37.01 (C6), 36.33 (C20), 35.92 (C18), 32.09 (C8), 32.04 (C9), 28.43 (C1), 28.37 (C16), 28.15 (C15), 24.43 (C23), 23.97 (C21), 22.96 (C24), 22.70 (C25), 21.21 (C14).

HPLC-PDA: (C_{18}, 5-100 % B, 4.5 min (A: ACN 0.1% TFA B: MeOH), 2ml/min, λ=210nm) t_R: 2.6 min

To a solution of Compound B (0.45 mmol, 0.260 g, 1eq.) in 9 ml of a mixture of DCM:ACN:DIPEA (1:1:1), was added DSC (1.07 mmol, 0.2746 g, 2.4 eq.). The reaction mixture was stirred under argon atmosphere for 16 h. Analysis by HPLC-MS showed full conversion of the starting material. The solvent was removed under reduced pressure and the crude was re-dissolved in 5 ml DCM. The organic layer was washed with 5 ml H_2O, dried over $MgSO_4$ and concentrated under reduced pressure. The crude was used without further purification (C)

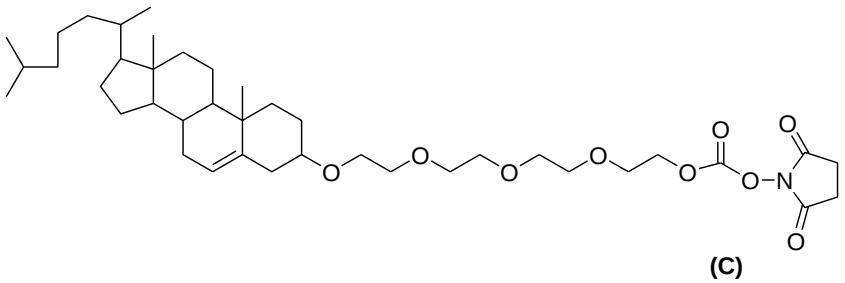

(C)

To a solution of compound **C** (0.09 mmol, 69.00 mg, 1.5 eq.) in 5 ml anhydrous DMF was added DIPEA (0.18 mmol, 32 µl, 2.0 eq.) and peptide **D** (0.11 mmol, 65.95 mg, 1.3 eq.). The reaction mixture was stirred for 16 h until peptide **D** (cRGDfK)was totally consumed(showed by HPLC-MS). The solvent was removed and the crude was precipitated with MTBE. After three precipitations compound **E** was obtained as a white solid (55.5 mg, 74%, purity (λ=210nm) 82%). Peptide content in 63 µg of crude: 62,7 µg of compound.

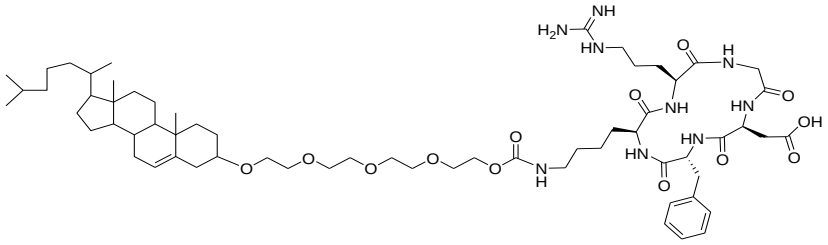

(E)

HPLC-MS: (Symmetry 300 C_4, 5-100% B, 30 min (A: ACN 0.07% HCOOH B: H_2O 0.1% HCOOH), 1ml/min, λ=210nm) t_R: 17.31min, m/z= 1192,8 $[M+H]^+$ (Calc. : 1192,53) **HPLC-PDA:** (C_4, 5-100% B, 30min (A: ACN 0.1% TFA B: H_2O 0.1% TFA), 1ml/min, λ=210nm) t_R: 20.1 min**. AMINO ACID ANALYSIS:** Asp: 0.93, Gly: 1.11, Arg: 1., Lys: 0.87, Phe: 0.99.

5.2 Production of the GFP-H6 protein

The protein was produced in the Institut de Biotecnologia i de Biomedicina (IBB), Universitat Autònoma de Barcelona. Details of GFP-H6 protein and its production in *Escherichia coli* Rosetta BL21(DE3) strain are given elsewhere[2]. GFP-H6 protein was purified by affinity chromatography in Ni^{2+} columns in an ÄKTA™ Purifier (GE healthcare) fast protein liquid chromatography. Positive fractions were pooled and dialyzed against the storage buffer (20 mMTris-HCl pH 7.5 plus 5% dextrose). The protein was finally aliquoted and kept at -80ºC until use.

5.3 Production of the α-GAL-HIS enzyme

The production of the protein was performed by the group of Dr. Antonio Villaverde in the IBB**.** The suspension-adapted cell line HEK (human embryonic kid-ney)

FreeStyleTM 293-F (Gibco, Invitrogen Corporation) was used to produce a recombinant, human GLA by means of polyethylenimine (PEI)-mediated transient gene expression. Details of GLA production and purification have been described elsewhere[3]. Briefly, human GLA monomer was produced with a hexahistidine tag fused to its C-terminus, allowing enzyme purification directly from the clarified supernatant, in a single affinity chromatography step, to a high degree of purity (>95% according to SDS-PAGE and Coomasie staining).

5.4 Production of rh-EGF

The production of EGF was performed in the Center of Genetic Engineer and Biotechnology (CIGB) located in Havana, Cuba. Soluble, extracellular-folded expression of rhEGF in yeast had been reported as an efficient strategy to obtain an rhEGF active pharmaceutical ingredient with high quality and yields[4]. The protein is expressed as a mixture of C terminal truncated forms of rhEGF1-51 and rhEGF1-52. Biological activity assay of rhEGF1-53, rhEGF1-52 and rhEGF1-51 gave almost identical thymidine uptake dose-response curves. In the same way, the assay of biological activity of different forms of EGF in vivo reduced gastric injury with no significant difference between forms[5] (Calnan et al., 2000)

6. Labeling of vesicles with dyes

6.1 Labeling with the sodium salt of fluorescein (FS)

For the labeling with FS, 5 mL of plain quatsomes were incubated with different amounts of FS in order to study a range of molar ratios FS:CTAB from 0.06 up to 8. The solutions were stirred during 30 minutes at 298 K.

6.2 Labeling with DiD dye

The first step was the preparation of a stock solution of the dye in ethanol (1 mM). For the labelling of the vesicles a volume of DiD from this stock solution was incubated with 500 μL of liposomes or quatsomes in order to have the desired final concentration of Did at 298 K and during 30 min. The final labelling concentration was 1nM or 50 nM, depending on the experiment.

After the labelling, the non-integrated dye was separated from the loaded vesicles by size exclusion chromatography using PD SpinTrap G-25. These mini-columns are designed for a rapid and convenient single use sample clean-up of proteins/biomolecules. It is critical to equilibrate the column to remove the storage solution completely, since UV absorbing stabilizers are used in column packing. So after placing the column in the appropriated size collection tube, the storage solution is removed by centrifugation for 1 min at 800 × g. 400 μL of equilibration buffer is added for centrifugation for another minute, the flow-through is discarding and the collection tube replaced. The procedure is repeated 5 times in total. The used collection tube is replaced by a new clean one and the sample is applied (100-180 μL) slowly in the middle of the packed bed. The elution takes place by centrifugation for 2 min at 800 x g. The sample with the incorporated dye is recovered in the collection tube.

7. Cellular uptake assays

7.1 Protocol established for the preparation of liposomal samples tested in cell assays.

Despite the properties of DELOS-SUSP method to allow sterile operation conditions, a protocol to prepare liposomal samples to be tested in cell assays was established. This protocol is explained in detail below and it was strictly followed in order to avoid cell contamination:

1. The working lab should be clean and organized before starting the experiment
2. All the lab material (micropipettes tips, eppendorf tubes, depressurization container, glass container to keep the sample, test tube, etc) should be clean and sterilized.
3. Once the sterilization process has finished the sterilized material should be covered in aluminium paper until used. Is highly recommended performed the sterilization process the day before the experiment
4. The reactor should be clean three times with the proper organic solvent and CO_2 at 100 bar before starting the experiment
5. The fume hood should be clean and the air extractor in on position (ideally the fume hood should have a laminar flux)
6. The compounds to be processed should be weighted in a clean analytical balance where no other compounds considered possible contaminants are weighted.

7.2 Cell culture

CDC/EU.HMEC-1 (HMEC-1) cells were provided by Centers for Disease Control and Prevention (CDC-NIDR*)*. HMEC-1 is an immortalized human microvascular endothelial cell line that retains the morphologic, phenotypic, and functional characteristics of normal human microvascular endothelial cells. HMEC-1 cells were maintained in MCDB 131 (Invitrogen) supplemented with 50 units ml^{-1} penicillin, 50 $\mu g\ ml^{-1}$ streptomycin, 10 mM L-glutamine and 10% fetal bovine serum (FBS) in a 37ºC humidified atmosphere with 5% CO_2. All the media, sera and antibiotics were purchased from Invitrogen.

7.3 Dual-color total internal reflection fluorescence (TIRF)-EPI microscopy

DiD-labeled nanovesicles were 10-fold diluted in phosphate buffered saline (PBS) solution and a volume of 200 µl was transferred to a glass coverslip mounted into a microscope chamber and put on the microscope stage. Imaging was performed on a home-built epifluorescence-TIRF setup arranged around an Olympus IX70 inverted microscope equipped with a 37ºC heated chamber. Samples were observed while illuminated in EPI/TIRF mode for 5 ms at 633 nm by a He-Ne laser and 514 nm by an Ar-Kr laser. The optical configuration adopted consists in an illumination area of 27×27 μm^2 with an excitation intensity of 1.35 $kW.cm^{-2}$. Fluorescence was collected with a 60×1.45 numerical aperture oil immersion objective (PLAPON 60XO TIRFM, Olympus) and guided into an intensified CCD camera (I-Pentamax, Princeton Instruments) through appropriate optics. Images were then recorded at a 10 Hz frame rate.

7.4 Cellular uptake of Liposomes assessed by laser scanning confocal microscopy (LSCM)

HMEC-1 cells were seeded onto Fluorodish culture plates (World Precision Instruments, Sarasota, FL) at a density of 2×10^5 cells per plate and allowed to grow for 36-48 hours. 50 µl of DiD-labelled Liposomes or DiD-labelled Liposome-RGD conjugates(1.5 mg/ml) were mixed with 200 µl MCDB 131 medium, added into the cells and incubated for 3 h at 37ºC in a humidified atmosphere with 5% CO_2. Subsequently, cells were washed with serum-free MCDB 131 and incubated at 37ºC for 5 min with Lysotracker Green DND-26 (50 nM, Molecular probes, Eugene, Oregon) to label the endosomal/lysosomal compartments. The nuclei in live cells were stained with Hoechst 33342 dye (Sigma). Cells were examined under an inverted Leica SP5 laserscanning confocal spectral microscope (Leica Microsystems Heidelberg GmbH, Mannheim, Germany) using a 60x 1.42 NA oil immersion objective. To visualize two colours of fluorescence simultaneously, we used the 514 nm line from Argon laser for Lysotracker green and the 630 nm line from a He-Ne laser for Did.

7.5 Flow citometry

HMEC-1 cells were seeded at densities of 2×10^5 cells ml^{-1} on Fluorodishculture plates (World Precision Instruments, Sarasota, FL) 36-48 h prior to experiment. Cells were

incubated with DiD-labelled Liposomes or DiD-labelled Liposome-RGD conjugates (0.3 mg/ml) resuspended into MCDB 131 supplemented with 10 mM L-Glutamine without FBS for 3 hours at 16ºC or 37ºC. Cells were subsequently washed twice with Dulbecco´s phosphate buffered saline (DPBS) solution, detached using trypsin and resuspended in cell culturing medium before subjecting to fluorescence-activated cell sorting analysis. Data acquisition and analysis was performed using FACScan (Beckton-Dickinson) and BD FACSDiva software. 10^4 viable cells were evaluated in each experiment.

8. Inmunomicroscopy

In order to find out the possible localization of proteins in the membrane inmunomicroscopy experiments were performed. The samples were prepared using the following general protocol:

- The grids are prepared with formvar 0.75 % (m/v) in dichloroethane
- Incubation of the samples (at the initial concentration) during 10-20 min
- The membranes are blocked with a solution containing PBS, BSA 0.1% (m/v) and Glicina 0.015% (m/v) during 5 minutes at room temperature
- Incubation with the first antibody during 30 min at room temperature
- The grids are washed 3 X 2 minutes with a solution of PBS and BSA 0.01% (m/v)
- Incubation with the gold nanoparticle linked to the second antibody (dilution 1/100 to 1/50) during 30 minutes at room temperature
- The grids are washed 3 x 2 minutes in PBS
- Then 3 X 2 minutes in mQ-water
- Addition of the contrast solution of Uranylacetate 2 % (m/v) during 1 min. The grids are blotted with whaltman paper to avoid the excess of contrast solution
- The samples are observed under a transmission electron microscope

8.1 Inmunomicroscopy of α-GAL loaded liposome_RGD conjugates

For the inmunomicroscopy of this nanoconjugates, it was used as first antibody commercial Anti-GLA, and as second an anti-rabbit antibody. Different dilutions of the first antibody were performed in order to adjust the best concentration and the images were taken in a JEOL JEM 1400 microscope operated at 100kV

8.2 Inmunomicroscopy of rh-EGF loaded quatsomes

For the inmunomicroscopy images taken to the Quatsomes-EGF nanoconjugates, we used as first antibody commercial AcM anti-EGF, and as second oro-IgG antibody (10 nm). Different dilutions of the first antibody were performed in order to adjust the best concentration and the images were taken in a JEOL 2000 EX microscope.

9. *In vitro* cell assays

9.1 Sterility

The sterility was measure following 2 different procedures. For the sterility experiment performed in collaboration with the Institut de Biotecnologia y Biomedicina (IBB) we used a 6 well plate and add 500 µL of water, PBS and culture mediafor duplicate. 100 µL of liposomes and quatsomes were placed in two different plates and incubated at 37 ^{0}C overnight. After 24 hours the formation of colonies was checked visually and byplacing a drop of the samples in the different media, into a glass slide and analyzing it using an optical microscope Olympus BX51 with a camera Olympus DP20 coupled.

For the sterility assays performed in Vall d'Hebron Hospital 100 µL of the nanoconjugate was placed in an agar plate without anthibiotic (by duplicated) and incubated over night at 37 ^{0}C. After this time the colonies forming units (CFU) were counted and 100 was set as the maximum number present in a sample to be considered sterile.

9.2 Cytotoxicity

The assays were carried out in Vall d'Hebron Hospital by the group of Prof. Simó Schwartz. The cytotoxicity was tested in HeLa and HMEC cells by a Sulforhodamine B colorimetric assay (SRB) established in this lab.

9.3 Hemolysis

This assay was carried out in Vall d'Hebron Hospital by the group of Prof. Simó Schwartz by incubation of the nanovesicles with RBC.

9.4 Biological activity

9.4.1 Assays performed by the group of Prf. Antonio Villaverde in IBB

The determination of biological activity in α-GLA conjugates, was performed in the Institut de Biotecnologia I Biomedicina (IBB). GLA enzymatic activity was assayed fluorometrically as described by Desnick et al.[6] with the modifications of Mayes et al.[7]. Basically, it was assayed by using 4-methylumbelliferyl-d-galactoside (4-MUG, Sigma Chemical) as substrate, at a concentration of 2.46 mM in assay buffer (0.01 M acetic acid, pH 4.5). A typical assay reaction mixture contains 100 µL of substrate and 25 µL of the sample. Enzymatic reactions took place in agitation (tubes placed in a rotator, set

at a rotation speed of 25 rpm), at 37 ^{0}C for 1 h, and were stopped with 1.25 mL of 0.2 M glycine-NaOH buffer (pH 10.4). The released product (4-methylumbelliferone or 4-MU) was determined by fluorescence measurement at 365 and 450 nm as excitation and emission wavelengths, respectively. Samples of commercial product 4-MU (from Sigma Chemical) ranging from 5 to 500 ng/mL in 0.2 M glycine-NaOH buffer, pH 10.4, were used to obtain a calibration curve in order to transform fluorescence readings into product 4-MU concentration. Enzymatic activity and specific activities are expressed as "ng 4-MU/mL/h" and "_mol 4-MU/mg GLA/h", respectively.

9.4.2 Assays performed by the group of Dr. Simó Schwartz in Vall d'hebron hospital

Primary cultures of mouse aortic endothelial cells (MAEC) of GLA deficient mice (Gla^{tmKul1}) were isolated following procedures previously described. Endothelial origin of isolated cells was confirmed by CD105 staining. For activity assays, cells in passages 2 to 5 were seeded in 24 well plates and maintained at 37ºC and 5% of CO_2. Twenty-four hours after seeding 8 μM of NBD-Gb3 (Matreya) was added to the cultures along with the specified concentrations of tested compounds (free enzyme, enzyme containing SUVs or empty SUVs). After 48 h incubation, cells were trysinezed and Gb3-NBD fluorescent signal was analyzed by flow cytometry (FacsCalibur, Beckton Dickinson). To calculate the percentage of Gb3-NBD signal, fluorescent signal in control cells (without treatment) was established as 100% and the rest of the values were normalized accordingly. Since alpha-galactosidase activity reduces those Gb3 deposits, the percentage of Gb3 loss (% Gb3 loss = 100 - % Gb3-NBD signal) was used to plot the results.

9.4.3 Assays performed by the Biological testing Laboratory in CIGB

The biological activity in quatsome-EGF conjugates was determined by the ability of the samples to induce cell proliferation in 3T3 mouse cells A31 and measurements were performed in the Department of Biological Assays of CIGB. The biological activity of the different vesicular suspensions was evaluated by applying an appropriate dilution of the suspension directly onto the test cells, so that the absorbance of the samples fell within the range of the curve of the working reference material, which was previously calibrated against the international reference material EGF 91/550, provided by the National Institute for Biological Standards and Control (NIBSC, United Kingdom).

The protocol was the following:

- 100 µL of a cellular suspension at 1.5 x 106 cells/mL is added to each well in a 96 well plate, which is incubated at 310 K, 5 % CO2 atmosphere and 95 % relative humidity during 24 hours.
- The plate is then wash twice with PBS buffer
- The seeded cells were incubated with DMEM media without serum and during 24 hours
- The dose-response curves of the reference material, the control and the samples are prepared and incubated for 24 hours.
- After the incubation the assay is revealed by adding 50 µL of crystal violet solution (0.5% m / v) to each well. Cells are then incubated 3 minutes at 298 K and then washed with water.
- Acetic acid at 10% is added in order to dissolve the dye and absorbance of all samples is read at 580 nm.

The biological activity was calculated using the program LOGIT / PROBIT, CIGB by the method of parallel lines. For each sample, the procedure is repeated several days or three replicas are made in one day, never less than three times, to get to 3-8 biological activity values. The value of the geometric mean is always reported.

9.5 Native electrophoresis experiments without SDS

These experiments were carried out in the Analytical Development Department of CIGB. The polyacrylamide gel electrophoresis (PAGE) was performed following the method described by Laemmli (Laemmli UK, 1970) in this case under native conditions. For this the gels, the assay buffer and the running buffer were prepared in the absence of SDS surfactant (Sodium dodecyl sulfate). Moreover, during the preparation of samples no heat was applied. A separator gel was used with a linear gradient of 10 to 20 polyacrylamida% (m / v). After the electrophoretic run, the proteins were visualized by staining using Coomassie brilliant blue G-250. Samples of Quatsome-EGF and Liposome-EGF conjugates were tested.

Two gradient gels were prepared (10% to 20% acrylamide) without SDS for each type of system; one gel in order to treat the samples with SDS and the other to treat them with Triton X-100. The solutions of the samples with Triton X-100 and SDS at different

concentrations (from 0 to 1 %) were incubated for 30 minutes at 298 K. Finally NATIVE sampler buffer is added to the samples prior application into to the gel.

9.6 Resistance to protease assay

For this assay, performed in the Formulations Development Department in CIGB, trypsin was used as a model protease. The enzymatic reaction was prepared in Tris buffer (pH 8.5, 20 mM), containing 0.5 µg/mL of trypsin. The final concentration of free EGF and EGF in the vesicle preparation was 125 µg/mL. Incubation of the samples was performed for periods of 4, 8, 16 or 24 hours at 310 K. To stop the enzymatic reaction trifluoroacetic acid (TFA) 0.1% (v / v) was used.

After stopping the reaction, samples were diluted in absolute methanol to a final concentration of 80% (v / v), vortexed and centrifuged at 10 000 rpm for 5 minutes. The supernatants waters were filtered through polycarbonate filters of 0.2 µm pore size and then applied to a HPLC system (Merck, Germany). The EGF standard and vesicle samples were analyzed using a C18 reverse phase column (Vydac, Hesperia, CA, USA) and detected at 226 nm. For this, a linear gradient from 20% to 40% B was used for 28 minutes. The mobile phase A consisted of 0.1% TFA in water and the mobile phase B consisted of a 0.05% TFA in acetonitrile. The injection volume was 5.0 mL and the flow rate used was 1.0 mL per minute. EGF concentration in the samples was quantified using a calibration curve. The percent of EGF remaining in each sample after incubation with trypsin, was calculated from the following expression:

$$\text{Residual EGF (\%)} = \frac{\text{EGF conc. after incubation withtrypsin (µg/mL)} * 100}{\text{EGF conc. before incubation with trypsin (µg/mL)}}$$

9.7 Antimicrobial activity

This activity was determined using the agar diffusion method (*Manual of Clinical Microbiology. 6th ed. Washington, DC: ASM; 1995*). The effectiveness of the different suspensions was assayed against Gram positive bacteria ((*Bacillus subtilis*, *Staphylococcus aureus*), Gram negative bacteria (*E. coli*, *Proteus mirabilis*), and against fungi (*Candida albicans*, *Aspergillus niger*) using the technique of wells in nutrient agar plates. These microorganisms were identified and provided by the microorganism

collection BCCM/LMG (Belgium). Bacteria were grown overnight at 37 °C in Tryptone Soy Broth (Oxoid), and fungi were incubated for 72 hours at 28 °C in Sabouraud Dextrose Broth (Oxoid). These suspensions were used as inocula. A final inoculum, using 100 µl of a suspension containing 10^8 colony forming units/ml of bacteria, or 10^4 spores/ml of fungus, was spread on Tryptone Soy Agar and Sabouraud Dextrose Agar (Oxoid) plates, respectively. The disk (6 mm in diameter) was impregnated with each of the different vesicle suspensions to be tested. Ciprofloxacin and fluconazole (100 µg/ml) were used as positive controls for bacteria and fungi, respectively. Assay plates were incubated at 37 °C for 24 hours for bacteria, and 28 °C during 72 hours for fungi, depending on the incubation time required for visible growth.

9.8 Pharmacodynamic effect of quatsomes loaded with rhEGF in animal models of wound healing.

To evaluate the pharmacological efficacy of the formulations listed below, an experimental model of chronic ulcer of total thickness was developed on the back of rats. Sprague Dawley rats of 250-270 grams weight, which were randomly assigned to form 3 experimental groups of 10 animals each were used. Rats were anesthetized intraperitoneally with a combination of ketamine/xylazine to extensively depilate their dorsal region. Two symmetrical bilateral retroscapular ulcers were made of 8 mm diameter and total thickness up to the upper fascia, which was spared. Immediate application of triamcinolone acetonide, as compresses was begun, once a day during the first three days, to stop healing and induce the characteristic changes of chronicity. After 7 days, the interruption of the healing process and chronicity of the ulcers were corroborated by the absence of granulation tissue and hypertrophy of the epithelial edges. From this moment, application of the studied treatments started as described below:

Group # 1: Treatment free, with a sterile physiological saline solution applied in a nebulized form.

Group # 2: Treated with a suspension of plain quatsomes.

Group # 3: Treated with a suspension of rhEGF loaded quatsomes with a concentration of 25 µg /ml.

Wounds were cleaned daily. After sanitizing them, each group was administered the suspension indicated in each case. The application of the suspensions was performed twice daily by nebulization for 14 days. All animals were subjected to autopsy and sampling 14 days after onset of the treatment assigned to each group. Samples were fixed in 10% neutral formalin, and 72 hours later were hemisected uniformly, for later inclusion in paraffin. The stains used were: hematoxylin-eosin, Mallory's trichrome reaction, Verhoeff's and Gomori's reticulum method. The samples were analyzed blindly by two independent researchers.

10. Experimental studies related to biomolecule-nanocarrier interactions

10.1 Isothermal Titration Calorimetry (ITC) measurements

All ITC measurements were carry out at the Laboratoire des Biomolécules- UMR 7203, Paris France. An isothermal titration calorimeter (TA Instruments, WATERS) was used to measure enthalpies of mixing at 310 K. The volume of the syringe and the cell was 250 μL and 983 μL respectively. For each experiment 25 aliquots of 10 μL of the ligand was injected sequentially into the cell. Each injection lasted 30 s with an interval of 300s between successive injections. The solution in the reaction cell was stirred at a speed of 300 rpm. Measurements were carried out in triplicate. Blanks were always subtracted to the main curves. The reaction cell was cleaned up after each experiment first with 100 mL of DECON detergent solution (10%) and then with 1000 mL of destilled water.

10.1.1 Determination of the micellization enthalpy in CTAB micelles

For determine the micellization enthalpy, a syringe containing CTAB at 10 mM was progressively diluted in water contained in the sample cell using Nano ITC equipment. The sample cell was always under agitation at 300 rpm and the temperature was settled at 37 ^{0}C. With this experiment what is calculated is ΔH demicelization which is equal in magnitude to ΔH micellization but with the opposite sign. The enthalpy of demicelization is defined as:

$$\mathbf{\Delta H_{demic} = \Delta H_{observed} - \Delta H_{micelles,\ dil} - \Delta H_{monomers,\ dil}}$$

From the calorimetric titration curve (Figure ES11), the ΔH demicelization is calculated by subtracting the enthalpy of micelle dilution and the enthalpy of monomer dilution, from the ΔHobs (calculated from the enthalpy difference of the two levels of the titration curve).

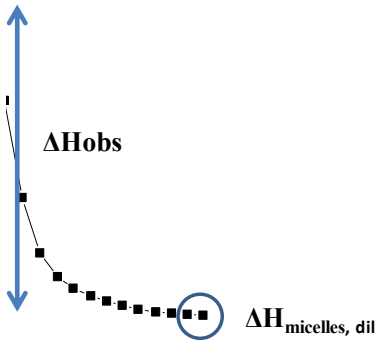

Figure ES11.. Calorimetric titration curve of CTAB 10 mM over water.

In practice $\Delta H_{observed}$ is calculated by subtracting the enthalpy value at the end of the curves (average enthalpy values from points 17 to 23) from the enthalpy value at the beginning (average enthalpy values from points 2, 5 to 11). The enthalpy of micelle dilution ($\Delta H_{micelles,\ dil}$) is taken from the last two points of the curve. The $\Delta H_{monomers,\ dil}$ is calculated by performing the titration of CTAB monomer over water by ITC. The value at 298 K and determined previously in our lab, was equal to -0.2 Kj/mol.

With all the values determined:

$\Delta H_{demic} = \Delta H_{observed} - \Delta H_{micelles,\ dil} - \Delta H_{monomers,\ dil}$

ΔH_{demic}= 2.54 Kj/mol – 0.02 Kj/mol – (-0.2 Kj/mol)

ΔH_{demic}= **2.7 Kj/mol**

$-\Delta H_{demic} = \Delta H_{mic}$ = -2.7 kJ/mol

10.2 Turbidity measurement

Turbidity measurements were carried out under conditions designed to mimic those used in the ITC experiments. Aliquots of 10µL of protein solution were added to a glass containing 1 mL of the macromolecule (monomers, micelles or quatsomes), at intervals of 300 s. The solutions were kept at 310 K and were stirred throughout the experiment using a magnetic stirrer. At the end of each injection period, the turbidity of the solutions was measured at 600 nm in an UV-Vis Spectrometer (UVIKON 931, Kontron Instruments.

10.3 Fluorescent measurements

Fluorescent measurements were carried out under conditions designed to mimic those used in the ITC experiments. Aliquots of protein solution were added to a glass containing 1 mL of the macromolecule (monomers, micelles or quatsomes), in order to achieved the desired BSA/CTAB molar ratios and at intervals of 300 s. The solutions were stirred throughout the experiment using a magnetic stirrer and the temperature was kept at 310 K. Intrinsic tryptophan fluorescence of BSA-CTAB solutions at the different molar ratios chosen were obtained at excitation wavelength of 295 nm. The excitation spectra were recorder from 300 nm to 450 nm.

10.4. DLS measurements

Fluorescent measurements were carried out under conditions designed to mimic those used in the ITC experiments. Aliquots of protein solution were added to a glass containing 1 mL of the macromolecule (monomers, micelles or quatsomes), in order to achieved the desired BSA/CTAB molar ratios and at intervals of 300 s. The solutions were stirred throughout the experiment using a magnetic stirrer and the temperature was kept at 310 K. The size and Z potential were measure after each injection using a dynamic light scattering analyser combined with non-invasive backscatter technology (NIBS) (Malvern Zatasizer Nanoseries, Malvern Instruments, U.K)

11. References

1 Xuedong Dai, Z. S. a. J. O. L. An improved synthesis of a selective a_vb_3-integrin antagonist *cyclo*(-RGDfK-). *Tetrahedron Letters* **41**, 6295-6298 (2000).

2 Vazquez, E. R., Monica; Diez-Gil, Cesar; et al. Protein nanodisk assembling and intracellular trafficking powered by an arginine-rich (R9) peptide. *Nanomedicine* **5**, 259-268 (2010).

3 José Luis Corchero, R. M., Julia Lorenzo, Victor Rodríguez-Sureda,Carmen Domínguez, Esther Vázquez, Neus Ferrer-Miralles and Antonio Villaverde. Integrated Approach to Produce a Recombinant, His-Tagged Human a-Galactosidase A in Mammalian Cells. *Biotechnol. Prog.* **00** (2011).

4 Valdés, J., Mantilla, E., Márquez, G., Bonilla, R., Proenza, Y., Díaz, M., Martínez, S., Frometa, W., Martínez, Y., Narciandi, E. Improving the expression of Human Epidermal Growth Factor in Saccharomyces cerevisiae by manipulating culture conditions. *Biotecnol.Apl* **26**, 1-9 (2009).

5 Calnan, D., Fagbemi, A., Berlanga-Acosta, J., Marchbank, T., Sizer, T., Lakhoo, K., Edwards, A., Playford, R. Potency and stability of C terminal truncated human epidermal growth factor. *Gut* **47**, 622-628 (2000).

6 Desnick, R. J. *et al.* Fabry's disease: Enzymatic diagnosis of hemizygotes and heterozygotes. α-Galactosidase activities in plasma, serum, urine, and leukocytes. *The Journal of Laboratory and Clinical Medicine* **81**, 157-171 (1973).

7 Mayes, J. S., Scheerer, J. B., Sifers, R. N. & Donaldson, M. L. Differential assay for lysosomal alpha-galactosidases in human tissues and its application to Fabry's disease. *Clinica Chimica Acta* **112**, 247-251 (1981).

PATENTS

Santana Milián, H.; Ventosa Rull, L.; Martínez Díaz, E.; Berlanga Acosta, J.A.; Cabrera Puig, I.; Veciana Miró, J. Vesicles comprising epidermal growth factor and compositions that contain them. Patent Application CU2012-0112 (**2012**)

Ventosa Rull, L.; Veciana Miró, J.; Cabrera Puig, I.; Elizondo Saez De Vicuña, E.; Melgarejo Diaz, M.; Royo Expósito, M.; Albericio Palomera, F.; Pulido Martinez, D.; Sala Vergés, S.; Corchero Nieto, J. L.; Schwartz Navarro, S.; Abasolo Olaortua, I.; Villaverde Corrales, A. Functionalized liposomes useful for the delivery of bioactive compounds PCT/EP2013/063646 (**2012)**

ARTICLES

Ingrid Cabrera, Elisa Elizondo, Olga Esteban, Jose Luis Corchero, Marta Melgarejo, Daniel Pulido, Alba Córdoba, Evelyn Moreno, Ugutz Unzueta, Esther Vazquez, Ibane Abasolo, Simó Schwartz Jr., Antonio Villaverde, Fernando Albericio, Miriam Royo, Maria F. García-Parajo, Nora Ventosa, Jaume Veciana. "*Multifunctional nanovesicle-bioactive conjugates as nanomedicine carriers prepared by a one-step scalable method"***.** *Nano Lett*, **2013**,13, 3766-3774

E. Elizondo, J. Larsen, N. S. Hatzakis, I. Cabrera, T. Bjørnholm, J. Veciana, D. Stamou, N. Ventosa, *Influence of the preparation route on the supramolecular organization of lipids in a vesicular system*. J. Am. Chem. Soc., **2012**, 134, 1918

BOOK CHAPTER

E. Elizondo, E. Moreno, I. Cabrera, A. Córdoba, S. Sala, J. Veciana, N. Ventosa. *Liposomes and other vesicular systems: structural characteristics, methods of preparation, and use in nanomedicine*. Progress in Molecular Biology and Translational Sceince, **2011,** *104*, Ed. A. Villaverde.